Forming of Novel Drug Carriers for Stimulated Encapsulation, Storage and Release

Dissertation submitted for the degree of

Doctor of Philosophy

Ming-Wei Chang

Department of Mechanical Engineering

University College London

09/2011

Declaration

I, Ming-Wei Chang, confirm that the work presented in this thesis is my own. Where information has been derived from other sources, I confirm that this has been indicated in the thesis.

Yours sincerely,

Ming-Wei Chang

Abstract

This research investigates the feasibility of using co-axial electrohydrodynamic atomisation (CEHDA) as a 'one-step' processing method to produce a new polymeric drug carrier. Moreover, a novel concept for stimuli-responsive drug encapsulation, storage and release from polymeric vehicles is demonstrated, using perfluorohexane (PFH) and polymethylsilsesquioxane (PMSQ).

Firstly, hollow polymeric microspheres with precise control over their diameter and shell thickness have been prepared using CEHDA, by integrating a simple mechanism to form core-shell structures without the need of surfactant, additives or templating in the forming process. In this study, the release characteristics of the hollow capsules presented a Fickian mechanism as the release rate was a function of the shell thickness of the hollow capsule.

Secondly, the feasibility of producing a hollow microsphere with a single hole in its shell by CEHDA has been explored. The diameters of the microspheres and of the single surface pore were controlled by using the CEHDA process. The process overcomes several of the key problems associated with existing methods of monoporous microsphere formation including the need for elevated temperatures, which utilize multiple processing steps. A major advantage of the micrometer-size opening on the hollow capsules allows one to directly and quickly load drug and other materials. The presence of different pore sizes provided varied encapsulation rates and also resulted in different release profiles.

Finally, it was possible to develop stimulated drug carrier by using CEHDA without relying on a smart polymer. The release rate can be regulated by external temperature and ultrasound stimulations. When the stimulus temperature was applied, controlled encapsulation of different amounts of drug in the capsules was achieved and also provided enhanced release with real-time response. In addition, the functionalities of ultrasound induced release have also been observed, depending on the exposure time, duty cycle, and applied intensity. These findings offer great potential for drug delivery applications and provide new generic insights into the development of stimuli drug release systems.

Awards and Publications

Publications

1. Chang, M.-W., Stride, E. & Edirisinghe, M., Ultrasound controlled release using volatile core-shell capsules, in preparation.
2. Chang, M.-W., Stride, E. & Edirisinghe, M. (2011) Nanoorganized microshells and their application in controlled release, *Therapeutic Delivery,* 2, 1247-1257.
3. Enayati, M., Chang, M.-W., Bragman, F., Edirisinghe, M. & Stride, E. (2011) Electrohydrodynamic preparation of particles, capsules and bubbles for biomedical engineering applications. *Colloids and Surfaces A: Physicochemical and Engineering Aspects*, 382, 154-164.
4. Chang, M.-W., Stride, E. & Edirisinghe, M. (2010) Controlling the thickness of hollow polymeric microspheres prepared by electrohydrodynamic atomization, *Journal of the Royal Society Interface,* 7, S451-S460.
5. Chang, M.-W., Stride, E. & Edirisinghe, M. (2010) Stimulus-responsive liquids for encapsulation storage and controlled release of drugs from nano-shell capsules, *Journal of the Royal Society Interface,* 8, 451-456.
6. Chang, M.-W., Stride, E. & Edirisinghe, M. (2010) A new method for the preparation of monoporous hollow microspheres, *Langmuir*, 26, 5115-5121.
7. Chang, M.-W., Stride, E. & Edirisinghe, M. (2009) A novel process for drug encapsulation using a liquid to vapour phase change material, *Soft Matter,* 5, 5029-5036.

Awards

- Old Students Association (OSA) Scholarship Award, UCL, 2010.
- Overseas Research Scholarship (ORS) Award, UCL, 2009.
- Old Students Association (OSA) Scholarship Award, UCL, 2009.

Patent Application

Edirisinghe, M., Stride, E. & Chang, M.-W. 'Layered bodies, compositions containing them and processes for producing them', UK 1102148.2, 2011.

Conference Presentations

1. Chang, M.-W., Stride, E. & Edirisinghe, M. (2011), Ultrasound controlled release using volatile core-shell capsules, The Stimuli-Responsive Particles and Particle Assemblies conference, Berlin, Germany.
2. Chang, M.-W., Stride, E. & Edirisinghe, M. (2008). A novel platform for controlled micro drug delivery capsule, Symposium on Encapsulation for Drug delivery & Microbubbling, University College London, UK.

Acknowledgements

Many individuals have supported the success and completion of the research presented in this thesis, without which this PhD thesis would not have been possible.

Firstly, I would like to thank my principal supervisor professor Mohan Edirisinghe, who devotes his life to create a scientific and pilot laboratory environment for pursuing outstanding research in science. I would like to give sincere gratitude to him for his unforgettable encouragement, inspiring guidance and financial support throughout the course of this research. I would also like to thank my co-supervisor Dr. Eleanor Stride for her continuous support and insightful guidance during my research. Besides, she sets an example of a world-class researcher for drug delivery and ultrasonography research. I was fortunate to have this precious opportunity to study and work with these two supervisors.

I am very grateful for the PhD ORS (Oversea Research Student) award from UCL without which this research program would not be possible. I also thank OSA (Old Students Association) award of UCL for providing me a research scholarship continuously, which enabled me to focus my time on this research. The committee members for my transfer defence have been advising me since 2010. I want to give thanks to them for their precious suggestions and time: Professor William Bonfield (Cambridge University) and Dr. Ben Hanson (University College London).

Mr. Kevin Reeves from the Department of Archaeology at UCL is thanked for all his tremendous help throughout my work with regards to obtaining good SEM images and particle sizing of my very challenging capsules.

I am also thankful to my colleagues in the Bio-material Processing Laboratory, especially Dr. Rafiq, Dr. Zeeshan, Dr. Farook, Dr. Anushini, and Zeynep Ekemen. I am privileged to have worked with so many talented people in the group. They have been very helpful during the long hours in the lab. They not only helped me in my research, but also offered great friendship. It was my pleasure to work with them.

Last, but definitely not the least, I would like to give my deepest thanks to the most important people in my life, my parents. All their unflagging support and encouragement are so much appreciated. They have never complained in spite of all the hardships in their life. More importantly, they make me look at the world differently. I am thankful that I have them in my life. Without these important people present in my life, I couldn't have had these achievements.

Contents

Declaration i

Abstract ii

Awards and Publications iii

Acknowledgements v

Contents vi

List of Tables xiii

List of Figures xiv

Glossary of Abbreviations xxii

Chapter 1 1

Introduction 1

1.1 Background 1

1.2 Aims and objectives 4

1.3 Structure of the thesis 6

1.4 Benefits of the research 9

Chapter 2 12

Literature review 12

2.1 Drug delivery 12

2.1.1 Drug delivery profiles and systems 12

2.1.2 Drug carrier materials 14

2.1.3 Drug release mechanisms 16

2.1.3.1 Diffusion controlled devices 16

2.1.3.2 Solvent controlled devices 17

2.1.3.3 Chemically controlled systems 18

2.2 Stimuli drug delivery system 18

2.2.1 Responsive materials 19

2.2.2 Temperature triggering.....20

2.2.3 Electro-sensitivity 21

2.2.4 pH sensitivity 22

2.2.5 Magnetic sensitivity 23

2.2.6 Light sensitivity.....24

2.2.7 Ultrasound triggering 25

2.2.8 Creating a stimuli-drug delivery system 26

2.3 Hollow microspheres 26

2.3.1 Fabrication of hollow microspheres.....28

2.3.1.1 Spray method 28

2.3.1.2 High temperature method.....29

2.3.1.3 Templating method 30

2.3.1.4 Self-assembly method 31

2.3.1.5 Polymerization 33

2.3.1.6 Emulsion processing 34

2.3.2 Fabrication of monoporous hollow microspheres.....34

2.3.3 Encapsulation of hollow microspheres 37

2.3.4 Challenges: forming hollow and monoporous spheres 38

2.4 Electrohydrodynamic atomisation 39

2.4.1 Historical development 41

2.4.2 Modes of electrohydrodynamic atomisation.....43

2.4.3 Mechanism of stable cone-jet mode.....44

2.4.3.1 Acceleration of the liquid in the liquid cone.....47

2.4.3.2 Jet break-up 47

2.4.3.3 Evolution of spray after droplet production.....49

2.4.3.4 Droplet evaporation.....50

2.4.4 The effect of liquid properties 51

2.4.4.1 Surface tension 51

2.4.4.2 Viscosity 52

2.4.4.3 Electrical conductivity 52

2.4.4.4 Density 53

2.4.5 Processing parameters 53

2.4.6 Scaling laws 54

2.4.7 Co-axial electrohydrodynamic atomisation 56

2.4.7.1 Concept of the driving liquid 57

2.4.7.2 Scaling law of co-flowing liquids 58

2.4.8 Microencapsulation by electrohydrodynamic atomisation 59

Chapter 3 63

Experimental details 63

3.1 Introduction 63

3.2 Materials 63

3.2.1 Polymethylsilsesquioxane 63

3.2.2 Perfluorohexane 64

3.2.3 Ethanol 65

3.2.4 Evans blue dye 66

3.2.5 Aspirin 66

3.2.6 Lactoflavin 66

3.2.7 Cyanocobalamin 67

3.3 Preparation of solutions 68

3.3.1 Polymer 68

3.3.2 Perfluorohexane 68

3.3.3 Evans blue dye and drugs 68

3.4 Characterisation of liquids and solutions 69

3.4.1 Density 69

3.4.2 Electrical Conductivity 69

3.4.3 Viscosity 70

3.4.3.1. Determination of viscosity using U-Tube viscometer 70

3.4.3.2. VISCOEASY rotational viscometer 71

3.4.4 Surface tension 72

3.5 Experimental set-up and equipment 72

3.5.1 Needle configuration and ground electrode 73

3.5.2 High voltage power supply 74

3.5.3 Infusion pumps 74

3.5.4 Data recording system 76

3.6 Thermal treatment 76

3.7 Ultrasound treatment 76

3.8 Characterization of capsules 78

3.8.1 Optical microscopy 78

3.8.2 Scanning electron microscopy 78

3.8.3 Characterization of material composition 79

3.8.4 Determination of the temperature of release medium 80

3.8.5 Determination of the amount of PFH in polymeric structure 80

3.8.6 Determination of ultrasound power 80

3.8.7 *In-vitro* drug release measurements 81

Chapter 4 84

Electrohydrodynamic atomisation as a novel approach for the preparation of hollow capsules 84

4.1 Characteristics of processing liquids 85

4.2 Parametric investigation 86

4.2.1 The encapsulation process 87

4.2.2 The influence of flow rate 88

4.2.3 The influence of needle-substrate distance 92

4.2.4 The influence of polymer concentration 93

4.2.5 The influence of applied voltage 96

4.3 Steady jetting region and D/t ratio 98

4.4 Characterization of composition 100

4.5 Mechanism of hollow capsule formation 102

4.6 Evaluation of characteristics of hollow capsules 103

4.6.1 Characterization of Evans blue dye 103

4.6.2 Size and shell thickness of hollow capsules 105

4.6.3 Effects of shell thickness on the storage capacity 108

4.6.4 Effect of dye concentration on the release capacity 110

4.6.5 Effects of shell thickness on the release behaviour 111

4.6.6 Effect of different temperatures on the release behaviour 114

4.6.7 Effect of release on the hollow structure 115

4.6.8 Effect of capsule diameter on the release behaviour 116

4.7 Summary 118

Chapter 5 120

Electrohydrodynamic atomisation as a novel approach for the preparation of monoporous hollow capsules 120

5.1 Characteristics of processing liquid and suspension 121

5.2 Parameters for the preparation of monoporous hollow capsules 122

5.2.1 Fabrication of monoporous hollow capsules 122

5.2.2 Effect of flow rate 123

5.2.3 Effect of needle-electrode distance 127

5.2.4 Effect of polymer concentration 129

5.2.5 Effect of applied voltage 132

5.3 Structural features and D/t ratio 132

5.4 Steady jetting region 134

5.5 Mechanism of pore formation 137

5.6 Evaluation of encapsulation and release behaviour of monoporous hollow capsules 138

5.6.1 The influence of different pore sizes 139

5.6.2 The influence of different diameters 140

5.6.3 The influence of β values 141

5.6.4 The influence of encapsulation time 142

5.6.5 Effect of the storage and release on the monoporous structure 144

5.7 Summary 145

Chapter 6 146

Study of stimuli-responsive drug carrier for encapsulation, storage and release 146

6.1 Design and development of stimuli drug delivery system 147

6.1.1 Temperature stimulus 147

6.1.2 Ultrasound stimulus 148

6.2 Evaporation in PFH-loaded capsules 149

6.3 Temperature stimulation 151

6.3.1 Effect of incubation time 151

6.3.2 Effect of temperature 152

6.3.3 Stimuli-enhanced release 155

6.3.4 Evaluation of surface morphology 155

6.4 Ultrasound stimulated drug delivery system 158

6.4.1 Effect of ultrasound on hollow capsules 158

6.4.2 Effect of ultrasound on hollow capsules with PFH 159

6.4.3 Effect of exposure time 161

6.4.4 Effect of duty cycle 162

6.4.5 Effect of ultrasound power 164

6.4.6 Effect of PFH content 164

6.4.7 Stimuli-enhanced release 166

6.4.8 Evaluation of surface morphology 168

6.5 Applications to drugs 174

6.5.1 Characterization of drugs 174

6.5.2 Stimuli-enhanced release 177

6.6 Summary 180

Chapter 7 181

Conclusions and Future work 181

7.1 Conclusions 181

7.2 Future work 190

References 198

List of Tables

Table 2.1 pH in various tissues and cellular compartments (adapted from (Bawa *et al*., 2009)) 23

Table 2.2 The advantages and the disadvantages of the fabrication methods (Wang *et al*., 2007, Gao *et al*., 2009, Zhu *et al*., 2005, Bertling *et al.*, 2004) 40

Table 2.3 Characteristic features of the fragments of liquid modes of electrohydrodynamic atomisation (Jaworek and Krupa, 1999a).....45

Table 2.4 Characteristic features of the modes of EHD Liquid jets (Jaworek and Krupa, 1999a).....46

Table 3.1 Properties of perfluorohexane (Kornmann *et al*., 2008, Couture *et al*., 2006) 65

Table 3.2 Properties of Evans Blue dye and other drugs 68

Table 4.1 Measured physical properties of the liquids used in experimental work (n=5) 86

Table 4.2 Measured properties from the hollow capsules (18, 27 and 36 in the first column refer to PMSQ concentration, n=50).....105

Table 5.1 Details of monoporous hollow capsules for encapsulation and release evaluations 139

Table 6.1 Microscopic images of polymer carriers subjected to treatment at various temperatures 157

Table 6.2 Surface morphology of the capsules subjected to ultrasound treatment at various conditions (Scale bar: 1μm) 172

Table 6.3 Properties of applied drugs 174

List of Figures

Figure 2.1 Different types of controlled release systems. (a) Simple diffusion and partition. (b) Sustained release. (c) Pulsatile release. (d) Release profile and drug conversion of the polymer-drug conjugate as a prodrug. (e) Temporally controlled. In all graphs the Y and X axes are drug plasma concentration and time, respectively (Kim *et al*., 2009) 14

Figure 2.2 Schematic drawings of two types of polymer-based diffusion controlled drug delivery devices (Kim *et al*., 2009) 17

Figure 2.3 Different types of stimuli-responsive materials (Ganta *et al*., 2008) 19

Figure 2.4 Structure and drug release from a thermoresponsive polymeric micelle (Klouda and Mikos, 2008) 20

Figure 2.5 Schematic representation of the electro-responsive effect in a polymer gel. The paths of the particles have been formed prior to application of the electric field (Shiga, 1997) 21

Figure 2.6 Schematic representation of the assembly and permeability of microcapsules embedded with gold-coated cobalt (Co@Au) nanoparticles under an oscillating magnetic field (Lu *et al*., 2005) 24

Figure 2.7 Scanning electron micrographs: (A) poly(ethyl methacrylate) / divinylbenzene composite particles produced by suspension polymerization, (B) cross sections of the composite particles (Okubo *et al*., 1998) 27

Figure 2.8 Flow chart of the process of spray drying (Wang *et al*., 2007) 29

Figure 2.9 Schematic representation of PS hollow microspheres prepared by the high temperature method (Wei *et al*., 2006) 30

Figure 2.10 Schematic illustration of the formation process of hollow microspheres using a templating method (Wang *et al*., 2007) 31

Figure 2.11 Schematic illustration of procedures for preparing inorganic and hybrid

hollow spheres using the layer-by-layer (LBL) technique based on PS colloidal templates (Caruso *et al*., 1998) 32

Figure 2.12 The formation mechanism of hollow polymer particles by polymerization (Itou *et al*., 1999).....33

Figure 2.13 Illustration of emulsion processing (Varde and Pack, 2004).....35

Figure 2.14 Scanning electron micrographs of dye-induced colloidal bucket, the colloidal buckets were made at 9200 rpm and heated to 65°C (Yow and Routh, 2008) 35

Figure 2.15 Fabrication procedure of dye-induced monoporous hollow microspheres (Yow and Routh, 2008).....37

Figure 2.16 Schematic illustration of drug encapsulation of hollow capsules (Matsusaki and Akashi, 2009) 38

Figure 2.17 Schematic representation of the electrohydrodynamic atomisation equipment rig (Jayasinghe and Edirisinghe 2003) 41

Figure 2.18 Forces of the liquid cone in the EHDA process (Hartman *et al*., 1999b)..48

Figure 2.19 Jet break-up modes: (a) the axisymmetric varicose break-up and (b) the lateral kink break-up (Hartman *et al*., 1999a) 49

Figure 2.20 Schematic representation of the conventional CEHDA setup (Loscertales *et al*., 2002). 57

Figure 2.21 Structures produced using precise control of electrospraying including (A) melded spheres, (B) tapered spheres, (C) porous surface, (D) fibres, (E) blood cell-shaped particles, (F) net, (G) smooth surface, and (H) distinct particles (Berkland *et al*., 2004) 60

Figure 3.1 Chemical structures of perfluorohexane liquid (Díaz-López *et al.*, 2010)..65

Figure 3.2 Schematic representation of the experimental set-up used for co-axial electrohydrodynamic atomisation 73

Figure 3.3 Dimensions configuration of the co-axial needle device.....75

Figure 3.4 Experimental set-up for temperature treatment 77

Figure 3.5 Experimental set-up for ultrasound treatment 77

Figure 4.1 Illustration of hollow capsule and its dimensions.....85

Figure 4.2 Illustration of dripping (a) and stable jetting (b) behaviour of PMSQ/PFH during CEHDA 88

Figure 4.3 Diameter and shell thickness of microspheres prepared as a function of varying flow rate of PMSQ and with PFH flow rate fixed at 150 μl min^{-1} (Error bars represent the standard deviation from three experiments) 89

Figure 4.4 Effect of PMSQ flow rate (μl min^{-1}) on geometry of the hollow microspheres, (a) 200; (b) 250; (c) 350; (d) 450; (e) 550; (f) 650.....91

Figure 4.5 Scanning electron micrograph of fractured hollow microsphere 92

Figure 4.6 Size and shell thickness of microspheres vs working distance with inner needle flow rates of 150 μl min^{-1} and outer needle flow rate of 450 μl min^{-1} (Error bars represent the standard deviation from three experiments) 93

Figure 4.7 Size and shell thickness of microspheres vs PMSQ concentration with the inner flow rate fixed at 150 μl min^{-1} and the outer needle flow rate kept at 300 μl min^{-1} (Error bars represent the standard deviation from three experiments).....94

Figure 4.8 SEM image of increasing the PMSQ concentration to 63 wt %.....95

Figure 4.9 Optical image of increasing the PMSQ concentration to 63 wt %.....96

Figure 4.10 Size and shell thickness of microspheres vs. applied voltage with an inner flow rate of 150 μl min^{-1} and an outer flow rate of 300 μl min^{-1} (Error bars represent the standard deviation from three experiments).....97

Figure 4.11 Mapping of applied voltage and flow rate of PMSQ at different PMSQ concentrations (a) 18 wt%, (b) 27 wt%, and (c) 36 wt% (Error bars represent the standard deviation from three experiments).....99

Figure 4.12 Variation of D/t ratio (α) with polymer concentration 100

Figure 4.13 FTIR spectra of PMSQ and dried hollow microspheres.....101

Figure 4.14 The UV-vis spectra of Evans Blue dye at different concentrations (0.06-0.018 mg/ml) 104

Figure 4.15 SEM images of cross-sections of the hollow capsules obtained at different PMSQ concentrations: (a) 18; (b) 27; (c) 36 wt% (inserted images are high-magnification, scale bar =100 nm) 106

Figure 4.16 Channel width in PMSQ hollow capsules for different shell thicknesses (Error bars represent the standard deviation from three experiments).....108

Figure 4.17 Effect of shell thickness on amount of dye loaded in capsules (Error bars represent the standard deviation from three experiments) 109

Figure 4.18 Release profile of dye from PMSQ capsules loaded with different doses of dye (Error bars represent the standard deviation from three experiments).....111

Figure 4.19 Effect of shell thickness (t) of PMSQ capsules on the release behaviour of dye at 37 °C (Error bars represent the standard deviation from three experiments)...112

Figure 4.20 Fitted Higuchi model: profile of cumulative dye release versus square root of time 114

Figure 4.21 Dye release behaviour from PMSQ capsules at 57 °C (Error bars represent the standard deviation from three experiments).....115

Figure 4.22 SEM images showing cross-section of the hollow capsules after release of dye. PMSQ concentrations: (a) 18; (b) 27; (c) 36 wt% (Inserted images are high-magnification, scale bar =100 nm) 117

Figure 4.23 Dye release behaviour from PMSQ capsules with different capsule diameters (D). Error bars represent the standard deviation from three experiments ..118

Figure 5.1 Illustration of monoporous hollow capsule and its dimensions.....121

Figure 5.2 Size of microspheres and pore vs. flow rate of PMSQ (Error bars represent

the standard deviation from three experiments).....124

Figure 5.3 Variation in the β ratio with flow rates of PMSQ and PFH (Error bars represent the standard deviation from three experiments).....125

Figure 5.4 SEM images of the one-hole microspheres obtained at different PMSQ flow rates: (a) 200; (b) 300; (c) 400; (d) 500; (e) 600 μl min^{-1}; (f) low-magnification of (e). Some spheres are aggregated to others which might be because of wetting and drying during sample preparation.....126

Figure 5.5 Size of microspheres and pore vs. flow rate of PFH (Error bars represent the standard deviation from three experiments).....127

Figure 5.6 Size of microspheres and pore vs. working distance (Error bars represent the standard deviation from three experiments).....128

Figure 5.7 Size of microspheres and pore vs PMSQ concentration (Error bars represent the standard deviation from three experiments).....130

Figure 5.8 Optical microscopy image showing the product obtained at 63 wt % PMSQ concentration.....130

Figure 5.9 Scanning electron micrograph of fractured electrospinning fibre.....131

Figure 5.10 Scanning electron micrograph of fractured electrospinning fibre without hollow cavity.....131

Figure 5.11 Diameter of microspheres and pores vs. applied voltage (Error bars represent the standard deviation from three experiments).....133

Figure 5.12 Scanning electron micrographs of (a) fractured monoporous microsphere; (b) cross section of monoporous microsphere; (c) cross section of hollow microsphere.134

Figure 5.13 Variation of the ratio of capsules to pore diameter (β) as a function of polymer concentration and voltage (Error bars represent the standard deviation from three experiments).....135

Figure 5.14 Stable jet mode map showing the relationship between the applied voltage

and PMSQ flow rate at PMSQ concentrations of (a) 18 wt%, (b) 27 wt%, and (c) 36 wt% (Error bars represent the standard deviation from three experiments).....136

Figure 5.15 Effect of different pore sizes on the release behavior (Error bars represent the standard deviation from three experiments).....140

Figure 5.16 Effect of capsule diameter on the release behavior (Error bars represent the standard deviation from three experiments).....141

Figure 5.17 Dye release behaviour of the capsules with the highest (β:12.3) and the lowest β values (β:3.7) (Error bars represent the standard deviation from three experiments).....142

Figure 5.18 A comparison of dye release behaviour with respect to different encapsulation times (Error bars represent the standard deviation from three experiments).....143

Figure 5.19 SEM images of the monoporous hollow capsules after release of dye: (a) $PMSQ_1$, (b) $PMSQ_2$, (c) $PMSQ_3$, and (d) $PMSQ_4$ 144

Figure 6.1 PFH loaded PMSQ capsules: (a) optical micrograph taken immediately after preparation, (b) scanning electron micrograph with typical cross-section in top RHS corner 149

Figure 6.2 Thermogravimetric trace showing the PFH content retained as a function of time at different temperatures (Error bars represent the standard deviation from three experiments).....150

Figure 6.3 Dye release at 37 °C from capsules originally incubated at 45 °C for different times (300, 1800, and 3600s). Error bars represent the standard deviation from three experiments 152

Figure 6.4 Release behaviour of capsules filled with dye at different temperatures (37, 45, and 57 °C) while being subsequently held in the release medium (a: 37 °C, b: 45 °C, c: 57 °C). Error bars represent the standard deviation from three experiments....154

Figure 6.5 Cumulative release of dye from capsules at 37 and 57 °C. Initial incubation was at 45 °C for 1500s. Error bars represent the standard deviation from three experiments 156
Figure 6.6 Release kinetics of dye from hollow capsule with and without exposed to ultrasound (20 kHz). Error bars represent the standard deviation from three experiments 159
Figure 6.7 The influence of ultrasound on release kinetics of dye from PFH capsules. Error bars represent the standard deviation from three experiments 160
Figure 6.8 Dependence of release enhancement on ultrasound for various time spans. Error bars represent the standard deviation from three experiments 162
Figure 6.9 Comparison of release rate at duty cycles: 30, 60, and 90%. Error bars represent the standard deviation from three experiments 163
Figure 6.10 The dependence of release rate on ultrasound treatment at various ultrasound intensities while maintaining a constant duty cycle (60 %). Error bars represent the standard deviation from three experiments 165
Figure 6.11 Dye released from capsules originally incubated at 37, 45 and 57 °C for 1500s and subjected to ultrasound treatment for 300s and a duty cycle 60%. Error bars represent the standard deviation from three experiments 166
Figure 6.12 Release of dye from capsules without and with ultrasound exposure for 300s at duty cycle 60%. Error bars represent the standard deviation from three experiments 167
Figure 6.13 The UV-vis absorbance spectra of aspirin with different concentrations (0.1-0.5 mg/ml) 175
Figure 6.14 The UV-vis absorbance spectra of lactoflavin with different concentrations (0.04-0.1 mg/ml) 176
Figure 6.15 The UV-vis absorbance spectra of cyanocobalamin with different

concentrations (0.02-0.1 mg/ml) 176

Figure 6.16 Cumulative release of aspirin from capsules without and with stimuli treatment. Error bars represent the standard deviation from three experiments 178

Figure 6.17 Cumulative release of lactoflavin from capsules without and with stimuli treatment. Error bars represent the standard deviation from three experiments 179

Figure 6.18 Cumulative release of cyanocobalamin from capsules without and with stimuli treatment. Error bars represent the standard deviation from three experiments 179

Glossary of Abbreviations

BSA	Bovine serum albumin
CEHDA	Co-axial electrohydrodynamic atomization
DDS	Drug delivery systems
EHDA	Electrohydrodynamic atomization
HFMF	High-frequency magnetic field
LBL	Layer-by-layer
LCST	Lower critical solution temperature
MCM	Mobile crystalline material
PEG	Poly ethylene glycol
PEO	Poly(ethylene oxide)
PDMS	Polydimethylsioxane
PFH	Perfluorocarbon
PGA	Polyglycolides
PLA	Polylactides
PLGA	Poly lactide-co-glycolic acid
PPO	Poly(propylene oxide)
PMSQ	Polymethylsilsesquioxane
PNIPAAm	Poly (N-isopropylacrylamide)
PS	Polystyrene
PVA	Poly vinyl alcohol
SaPSep	Self-assembling of phase separated polymer
SEM	Scanning electron microscope

Chapter 1

Introduction

1.1 Background

Pharmaceutical products utilizing advanced drug delivery technologies were projected to account for 39% of all pharmaceutical sales and annual U.S. prescription sales to raise $291 billion in 2008 (Aggarwal, 2007). For most of the industry's existence, a strong social desire to improve therapeutic efficacy and economic pressures confronting the pharmaceutical industry has cause the market to move rapidly towards advanced drug delivery formulations. Seeking better therapies that minimize harmful side effects and improving capabilities of early detection, both effective and inexpensive, are the main goals of the medical professional spheres. Faced with numerous expirations of drug patents, pharmaceutical companies now view advanced drug delivery technologies as a means not only of improving human health, but maintaining and protecting highly profitable drugs (DiMasi *et al.*, 2003).

During the past three decades, research and development activity in drug delivery systems has become increasingly common and complex. In parallel, recent breakthroughs in understanding of diseases and manipulations of material at the nano/ micro length scales, targeting of drug carriers, and improved intracellular stability offer tremendous promise in disease prevention, diagnosis, and therapy (Ganta *et al.*, 2008). Different polymers used as drug carriers exhibit prolonged-release properties, but their shape are usually irregular and drug storage capacity is relatively low due to the much space taken up by the carrier through the entire matrix. In addition, potencies and

therapeutic effects of many drugs are limited or otherwise reduced because of inhomogeneous distribution of the drug through the matrix, which can affect the release rate between different samples, and the polymer degradation that occurs before reaching a desired target site in the body, or through an area where healthy bone and tissue might be adversely affected (Langer, 1990, Vallet-Regi *et al.*, 2001). To overcome these disadvantages, Zhu *et al*. (2005) reported uniform hollow microspheres with significantly high loading capacities of drugs owing to its hollow core structure, which are able to transport from the inner confined core to the outside environment, attracting much attention for drug encapsulation, storage and release (Zhu *et al.*, 2005, Zhu *et al.*, 2009).

Recently, hollow monoporous microspheres (i.e. hollow microspheres with a single hole in their shells) have received much attention and been classified as a new category of particles on account of their higher effective diffusivity of drugs and available surface area compared with microporous spheres of the same size (Jeong *et al.*, 2007, Yow and Routh, 2008). These microspheres offer enhanced rates of encapsulation, as well as being suitable for other applications, e.g. catalytic carriers, thermal insulation, and targeting (Guan *et al*., 2007). Minami *et al.* (2005) reported that such particles can be prepared by the SaPSeP (Self-assembling of Phase Separated Polymer) method (Minami *et al*., 2005). This technique has since been refined and similar particles with a single regular hole on their shells were formed at temperatures below 0 °C (Im *et al.*, 2005, Jeong *et al.*, 2007). However, the design and preparation of hollow monoporous microspheres present significant challenges. Many of the current techniques used are complex and require highly specialized equipment and/or processing environments (Yin and Yates, 2008).

Drug delivery systems that can respond to change in environment are considered to be one of the most promising drug carriers and show potential applications in medicine and therapeutic applications (Ehrbar *et al*., 2008, Cai *et al*., 2009). The uses of stimuli-responsive carriers offer opportunities for delivery systems because they become an active participant rather than a passive vehicle. The ability of these polymeric carriers to encapsulate, protect and controllably release therapeutics and nutrients would improve the therapeutic efficacy. For example, Shenoy *et al*. (2005) and Devalapally *et al*. (2007) using pH-sensitive release have found significant enhancement in the treatment of tumor mass as compared to non-pH-sensitive carriers (Shenoy *et al*., 2005, Devalapally *et al*., 2007). Drug delivery systems incorporating responsive elements e.g., micellar, hydrogels, polymersomes, and biopolymer conjugates have been designed and can undergo shape or phase changes in response to variations in the environment providing controllable release of drug from the polymer matrix along with minimizing undesirable side effects (Dong *et al*., 2006).

Currently, development of stimuli- responsive drug delivery systems are heavily reliant on responsive polymeric materials (Nelson, 2008, Hest, 2009). Functionalization of polymers, both tunable and controllable in their operation and performance, can be achieved by applying stimuli including oxidation, pH, temperature, ionic strength, light, electric fields, magnetic fields, and ultrasound (Yang *et al*., 2009, Stuart *et al*., 2010). Owing to their unique sensitivities, these single stimulus-responsive properties would limit their potential for practical applications. For example, some of them (pH and oxidation) require chemical environmental changes, which may not be compatible during drug administration (Wang *et al*., 2008). The radiation of light may cause damage to organisms and normal cells, and its penetration depth is weak in tissues

(Geest *et al*., 2007). Furthermore, toxic by-products and the biocompatibility of responsive polymers may be a significant impediment to the development of these delivery systems and for patient use (Putnam, 2008, Kim *et al*., 2009). Therefore, a new stimuli- drug delivery system independent of the action of smart polymers, which could respond to more than one extracorporeal stimulus is very important to speedily enable their application in drug delivery (Rzaev *et al*., 2007).

Electrohydrodynamic atomisation (EHDA), also known as electrospraying or electrostatic atomisation, is one of the most promising approaches to manufacturing micro- and nano-capsules with a narrow size distribution (Pareta and Edirisinghe, 2006). In this process, liquid flowing out from a needle is subjected to an electric field, which causes a jet which subsequently breaks up into droplets. Using different combinations of needles provides versatile capabilities of encapsulation. Two immiscible liquids can be successfully encapsulated in a polymer in the absence of processing additives by using co-axial electrohydrodynamic atomisation, where two concentric needles are used (Farook *et al*., 2008). Compared to other current techniques of encapsulation, EHDA offers a range of advantages, such as low cost, simple apparatus, convenience, ambient temperature and pressure processing and a high degree of control over product characteristics.

1.2 Aims and objectives

This research is aimed towards the exploration of the use of electrohydrodynamic atomisation (EHDA) to produce a novel drug carrier for stimulated encapsulation, storage, and release. A fundamental understanding of electrohydrodynamic processing is important to prepare hollow, core-shell, microspheres without using surfactants or additives. Furthermore, the research also investigates at an in-depth study of the

diameter and size distribution of monoporous hollow microspheres that are influenced by the electrohydrodynamic process; an area which still has not been well documented in related studies. Finally, this research is to develop compatible stimuli-responsive elements in the hollow structure. Ideally, a drug delivery system should respond to on-demand requirements, and alter the encapsulation and drug release profile accordingly. To achieve these objectives, several studies in different stages are necessary, which will be arranged into three separate sections as follows.

The initial objective of this study is to investigate the feasibility of using EHDA to produce hollow capsules without using surfactant and other additives. The objective is to be able to easily and efficiently produce core-shell structures preferably using a 'single-step' processing method rather than the repetitive measures followed in the literature. Perfluorohexane will be used as the core material due to its variety of uses ranging from industrial to biomedical applications. However, whether perfluorohexane can be encapsulated into the polymer by EHDA and whether EHDA can be used to generate truly hollow microspheres with controllable diameter rather than the sponge like structures obtained in the literature will be elucidated. Therefore, a suitable spraying process needs to be optimized, and its ability to be electrosprayed will be investigated and modifications to the polymer solution will be carried out. To understand the capability of controlled release from the prepared hollow capsules, a study of wall thickness is needed in order to uncover the suitable influence for the drug delivery system as well as capsule morphology.

The EHDA technique has been used to produce spherical and non-spherical micro/nano drug carriers in the literature and most of the selected polymers used as a drug carrier provides electrical conductivity for electrospraying and offers a framework for the

incorporation of drug molecules. However, there has been no previously attempt to produce monoporous hollow capsules using EHDA. Therefore, the second objective of this research is to investigate the feasibility of using the EHDA method to produce core-shell structure with a monopore to perform as drug carriers at ambient temperature and pressure. The effects of the controlling parameters for the monoporous hollow capsule need to be investigated and the relationship between the processing parameters and the mean sphere diameter (D), pore size (d) and ratio $\beta = D/d$ will be determined. Furthermore, the validation and characterization of monoporous capsules used as a drug carrier will be carried out.

As afore-mentioned, although the stimuli drug release system can provide the controlled release pattern and improve the therapeutic efficacy, the development of electrosprayed drug carrier response to the environment is still limited. In addition, most stimulated drug delivery systems are based on synthetic polymers. Therefore, the investigation of EHDA spraying technique for stimulated drug carrier with different triggering elements is very important. Essentially, a suitable stimuli element for core-shell configuration of microspheres needs to be investigated. The fundamental mechanism of the responsive process and the effect of the stimuli-element for drug release will also be explored by using temperature control and ultrasound radiation, since both external triggers are considered as the most potential technique for remote responsive drug delivery systems.

1.3 Structure of the thesis

Chapter 1 briefly describes the background for this thesis. The chapter introduces the main drawbacks of the current drug delivery systems prepared using traditional techniques, the importance of hollow capsules and monoporous hollow capsules, a novel stimuli drug delivery system, and the concept of EHDA spraying, and states the

aims, the objectives and the scope of this research.

Chapter 2 is dedicated to a critical literature review where the basic physiology and properties of drug delivery systems are discussed. The hollow capsule design requirements, the preparation of core/shell structure, the use of drug and their different types are discussed. The reasons and methods used for the preparation of monoporous hollow capsules are explained. The concept of stimulated mechanism is also examined subsequently to clarify the motivation of the development and utilisation of new stimuli-elements. The preparation of smart drug carriers, the use of drug and their different types are discussed. To understand the mechanism of EHDA processing, various modes of this processing carried out by other researchers are reviewed, which is used for the experimental part of this thesis.

Chapter 3 describes the materials and the preparation of the investigation carried out in this research. Preparation of polymer suspension is described as well as the general equipment set-up used for electrohydrodynamic processing. Details of the designs for the electrohydrodynamic process development are also described. The sample characterisation methods used in this research are introduced.

Chapter 4 investigates the feasibility of using EHDA to produce hollow capsules for controlled release. The contents of the present work are divided into two parts including the preparation of hollow capsule and an *in-vitro* release study. The first part investigates the feasibility of using EHDA to produce hollow capsules with varied shell thickness in absence of surfactant and other additives. The experimental process has been optimized by changing EHDA parameters as well as the measurement of the dimension of the capsules produced by the stable jet. A comprehensive study is also

included in the section to uncover the mechanism of hollow structure formation and control of the core-shell structure. The second part of this chapter focuses on the study and analysis of the effect of core-shell carriers with varied shell thicknesses for drug delivery applications. The release characteristics of hollow shell drug delivery carriers are strongly dependent on the properties of the capsule shell, in particular its thickness and porous structure. The related release mechanism is elucidated in this chapter.

Chapter 5 investigates the possibility of using the EHDA technique for the processing of monoporous hollow capsules for drug delivery. The research in this part reveals pore formation is highly dependent on the properties of the volatile liquid (perfluorohexene) and the sprayed capsule size that is produced during electrospraying. The influence of the experimental parameters such as the polymer concentration, flow rate, applied voltage, and working distance on the control of pore size and outer diameter of capsule has been studied. Mode selection maps of EHDA have been plotted to determine the flow rate of PMSQ polymer and applied voltage for conducting the experiments. The surface topography of hollow structures with a single pore on its surface are also characterized using scanning electron microscopy and optical microscopy. Subsequently, the capsules obtained with various pore sizes and outer diameters are used as drug carriers to study their capability in drug delivery. The mechanism of pore formation and the advantages/disadvantages of the EHDA technique are also discussed in detail in this chapter.

Based on the results obtained in **Chapter 4**, it was observed that hollow, core-shell, capsules with sustained release could be prepared by electrospraying. **Chapter 5** demonstrates the possibility of improving the encapsulation rate via a hole formed on the hollow capsule by electrospraying. However, **Chapter 6** describes a new strategy:

How a temperature-responsive non-toxic, volatile liquid can be encapsulated and stored under ambient conditions and subsequently programmed for controlled drug release without relying on a smart polymer. When the stimulus temperature is reached, controlled encapsulation of different amounts of molecules in the capsules is achieved providing sustained release behaviour. Under different ratios of the liquid (perfluorohexane): drug in the capsules, enhanced controlled release with real-time response is provided. This research also presents a novel method for the remotely stimulated release of an encapsulated material from hollow capsules using ultrasound. The effects of subjecting the capsules to ultrasound and their effects on the enhanced release and capsule morphology are investigated. Finally, a variety of drugs with different molecular weight are performed to understand the new strategy and to investigate the influence of drugs on release behaviour and the structure-drug interaction.

Chapter 7 makes comprehensive conclusions based on the results and discussion of the investigations carried out in **Chapters 4, 5** and **6**. The findings from these investigations set out the future plan and suggestions that could be carried out for further exploitation of this interesting research for biomedical and pharmaceutical applications. It also addresses the need for further research in this particular field for commercial success.

1.4 Benefits of the research

This research provides contributions both to the scientific community by cementing knowledge with regards to the electrohydrodynamic processing and benefits the industrial community by demonstrating innovative, and low cost processing techniques to produce smart and stimuli-responsive capsules with improved response for biomedical and pharmaceutical applications. The information provided in this research

opens new insights to extend the capabilities of the EHDA technique and to institute an advanced drug delivery system.

In the first part of this research, polymethylsilsesquioxane (PMSQ) coated capsules of liquid perfluorohexene (PFH) were successfully prepared in the absence of additives using EHDA. The processing parameters for PFH capsules have been optimized and the structures of the core-shell capsules were examined by electron microscopy. The thickness of the polymeric coating was found to be uniform over individual capsules and to scale with the capsule outer diameter by a factor of ~6.8 to 10. It has been shown that the release profiles from hollow microcapsules represent a Fickian mechanism and can be regulated by controlling shell thicknesses. This is a crucial forward step in obtaining advanced capsules for drug delivery applications. Also, the processing technique proved to be simple, fast and economical and can be implemented for the controlled release of encapsulated materials with controlled release rates.

In the second section of the research, a new method for the creation of hollow capsules with a controllable single hole in its shell has been uncovered and its characteristics demonstrated. The diameters of the microspheres and of the single surface pore have been successfully controlled by varying the flow rate, the concentration of the PMSQ solution and the applied voltage in the EHDA process. Furthermore, an in-depth study of the effect of pore size on encapsulation and release has shown improvement in the encapsulation of a model drug. Primarily by increasing the pore size to 135 nm, high encapsulation rates have been achieved. This research has shown that EHDA is a promising technique and overcomes several of the key problems associated with existing methods of monoporous microsphere formation including the need for elevated temperatures, multiple processing steps and the use of surfactants and other additives.

A drug delivery system that allows remote real-time control of release dosage according to the therapeutic treatment is extremely important in clinical application. In the final section, the research presents a novel method for release of an encapsulated material from core-shell capsules based on temperature control and ultrasound cavitation. With a model system used for drug release studies, a new strategy of temperature-responsive carriers for drug encapsulation, subsequently programmed for controlled drug release without relying on a smart polymer has been developed. Controlled encapsulation of different amounts of drug in the capsules and subsequent enhanced release are achieved when the stimulus temperature is reached. Furthermore, “remote” controlled release from such novel capsules have been studied by using ultrasound. The release of encapsulated molecules can be precisely controlled; the magnitude of drug release being a function of power, duty cycle, and time of application of ultrasound. The collapse of hollow structures of polymer was also observed when high-power output levels of ultrasound were introduced, which offers an alternative mechanism for extracorporeal real-time remote release of an encapsulated therapeutic molecule from hollow capsules. Hence, this research offers great potential for drug delivery applications and provides new generic insights into the development of stimulated drug delivery systems.

Chapter 2

Literature review

Modern drug delivery systems have been made possible by the progress in polymer science and fabrication technology. These advances have resulted in drug delivery systems with unique properties. Initially, polymers were used as additives to stabilize drugs or as mechanical supporters for the sustained release of drugs. As new polymers were introduced, drug delivery systems with tailor-made properties were produced. Input from other research areas, such as biochemistry, physiology, and nanotechnology, has led to more effective drug delivery systems with well-defined structures. In this chapter, a brief history of drug delivery systems, hollow capsule generation and the development of stimuli-drug delivery systems are reviewed. This will help to specify the limitations of traditional drug delivery and encapsulation techniques, and therefore provide the motivation for the study of novel functional drug delivery systems. A number of techniques have been employed in the development of drug carriers with advanced functions and properties. However, the electrohydrodynamic atomisation (EHDA) technique offers advantages regarding this and therefore a discussion on the physical principles of the EHDA technique helps to provide a comprehensive understanding of the process to further investigate the optimized electrospraying conditions.

2.1 Drug delivery

2.1.1 Drug delivery profiles and systems

For conventional formulations, the plasma concentration of a drug is directly

proportional to the administrated dose. Controlled drug delivery can be used to achieve sustained constant concentration of therapeutically active compounds in the blood with minimum fluctuations and provide predictable and reproducible release rates over a long period of time. The protection of bioactive compounds which can have a very short half-life is important. The elimination of side-effects, waste of drug and frequent dosing have also needed to be considered. Furthermore, optimized therapy, better patient compliance, and better drug stability has to be obtained (Langer, 1990).

Figure 2.1a displays the typical profiles of plasma drug concentration as a function of time after oral or intravenous administration. The advantage of conventional formulations is low cost. Unfortunately, drug concentration is decreased for extended periods of time and high drug concentration in systemic circulation often induces adverse effects, usually requiring multiple administrations to obtain the desired therapeutic effect (Kim *et al*., 2009). **Figure 2.1b** shows sustained drug release, resulting in prolonged plasma drug concentration within a therapeutic window. Synthetic polymers or pumps deliver drugs at a constant rate so that the drug concentration in the blood stream is maintained at an optimal level of therapeutic effectiveness (Langer, 1990).

Figure 2.1c shows a therapeutic agent can be released only when it is required. As shown in **Figure 2.1d**, active drug can be generated by continuous degradation of linkers by which drugs and polymers are chemically conjugated. Polymer-drug conjugation has also resulted in an increase of the drug circulation time and drug stability in blood (Duncan, 2003). As an extension of the pulsatile release system, multiple drug release with temporally programmed release behaviour is an excellent solution to supply controllable doses of drug. In this system, multiple drug components

are supposed to be sequentially released only when they are demanded (**Figure 2.1e**).

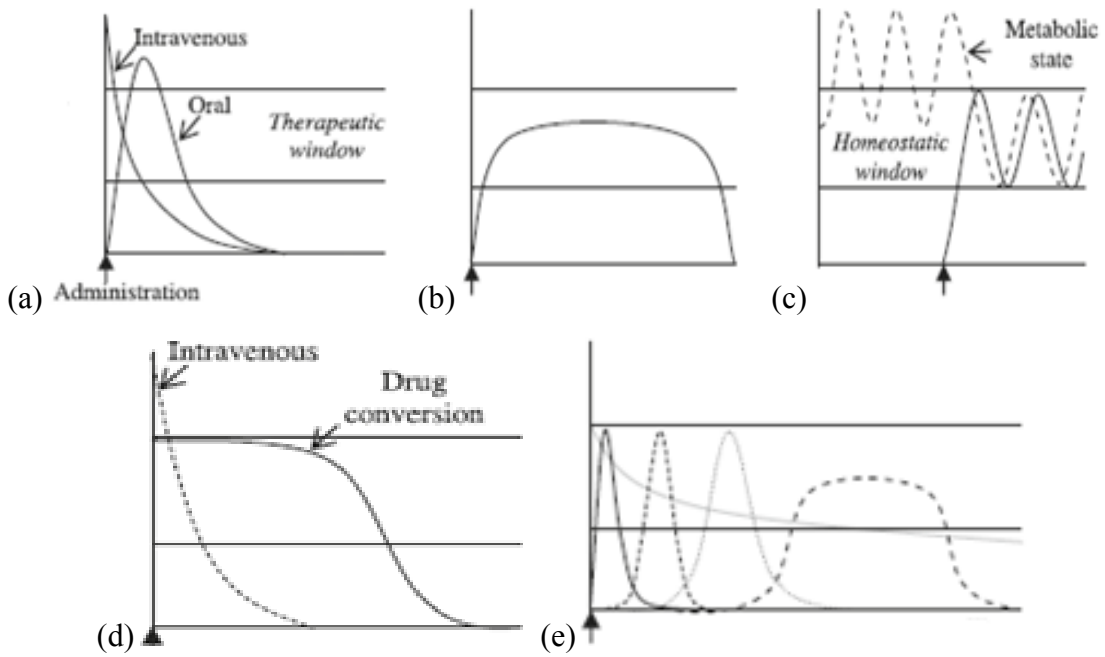

Figure 2.1 Different types of controlled release systems. (a) Simple diffusion and partition. (b) Sustained release. (c) Pulsatile release. (d) Release profile and drug conversion of the polymer-drug conjugate as a prodrug. (e) Temporally controlled. In all graphs the Y and X axes are drug plasma concentration and time, respectively (Kim *et al*., 2009)

2.1.2 Drug carrier materials

The development of materials for drug delivery systems, particularly controlled drug delivery systems, have been practical in recent decades, but within a short time they have had an impact on almost every sphere of medicine including cardiology, ophthalmology, endocrinology, oncology, and pulmonary medicine (Prestwich and Luo, 2001). The materials for drug delivery systems have to be involved with the

physiological environment when performing their functions in the human body. This situation requires non-toxicity and has to be considered with non-viable materials. Finally, the materials become a part of the body either temporarily or permanently or get eliminated by the natural functions of the living tissues or organs. Therefore, the proper function of the material is restricted by its long-term biocompatibility and the behaviour of the material in the host. Furthermore, drug delivery materials should provide an adequate combination of the desired biological agent against the inflammatory response and bioactivities (Tang and Eaton, 1995).

Biodegradable materials have been used as a route to achieve spatial and temporal release of therapeutics into the body for controlled release. The approach for controlling release rates is to embed the drug within a hydrolytically degradable material but normally the polymers erode in injection. The development of biodegradable materials for drug carriers can be achieved from a variety of polymers including polyesters, polyorthoesters, polyanhydrides and polycarbonates (Grayson *et al*., 2003, Zawaneh *et al*., 2006). Polyesters based on lactic acid and glycolic acids (PLGA) have been used as a primary material for degradable drug delivery because of their physical properties such as elasticity, physical strength, suspension capabilities, and controllability of the release profile. Eventually, these polymers are degraded within the body during circulation. However, such polymers usually lead to significant local inflammation because the by-products of degradable polymers are often acidic in nature (Brodbeck *et al*., 1999). This challenge associated with this paradigm limits the use of these polymeric materials for some diseases, such as myocardial infarction, tissue fibrosis, and diminished cardiac function (Putnam, 2008, Kim et al., 2009).

A variety of non-biodegradable polymers such as acrylic-based and polysaccharide-based polymer, and alkylsilicone resin have found wide application in the drug delivery systems or transdermal vehicles (Pillai and Panchagnula, 2001). Furthermore, silica-based systems have been extensively investigated and have shown a potential as a high-performance drug carrier in recent years (Chen *et al*., 2004, Zhao *et al*., 2008). Since MCM-41 (Mobile Crystalline Material) was first utilised as a drug delivery system, silica-based materials have been investigated as drug carriers (Lai *et al*., 2003) and the biocompatibility of silica capsules with cellular systems has been demonstrated (Kortesuo *et al*., 2000, Chia *et al*., 2000). Therefore, a set of biocompatible polymers modifies the drug-release kinetics and constitutes an advantage in bioactivity over currently used biodegradable polymer devices. Drug carrier materials that are handled in drug delivery systems include nano and micro sizes where the property is decided depending on the applications (Uhrich *et al.*, 1999, Jong and Borm, 2008).

2.1.3 Drug release mechanisms

It is known that drug concentration levels in the blood plasma depend on the quantity of drug released from the device as drug absorption is determined by its solubility in tissues and the availability of local blood flow in tissue (Bruck, 1983). According to the mechanism controlling drug release, delivery systems can be classified as diffusion controlled devices, solvent controlled devices, and chemically controlled devices (Heller, 1987, Ranade and Hollinge, 1996).

2.1.3.1 Diffusion controlled devices

There are two types of diffusion controlled systems, reservoir devices and matrix devices. A schematic representation is shown in **Figure 2.2**. Reservoir systems are

hollow devices in which an inner core can be in powdered or liquid form. The drug core is surrounded by a non-biodegradable polymeric material through which the drug slowly diffuses. The drug and membrane properties control the rate of release from such a system. The drug transport mechanism through the membrane is usually a solution-diffusion mechanism. The rate of drug release will depend on the solubility of the drug in the polymer and the thickness of the membrane (Rathbone *et al*., 2000). With matrix devices, the drug is either dissolved or dispersed randomly in the polymer. The drug is released from the matrix by diffusion. The proportion of matrix material and drug can influence the release mechanism and release rate. An inherent drawback of the matrix systems is the continuously decreasing release rate. This is due to the increasing diffusion length for the penetrating drug (Khan and Zhu, 1999).

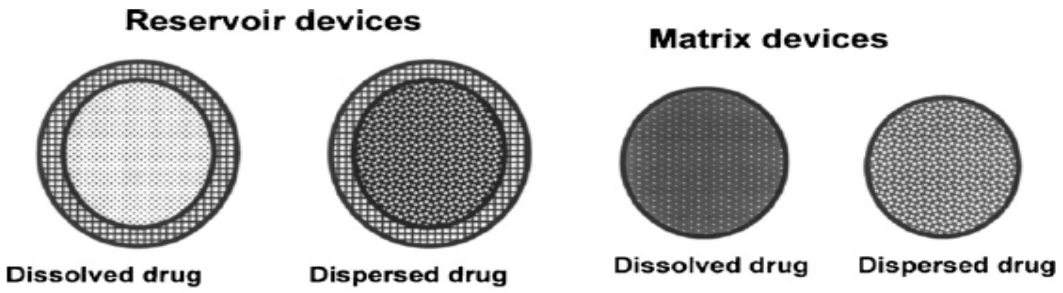

Figure 2.2 Schematic drawings of two types of polymer-based diffusion controlled drug delivery devices (Kim *et al*., 2009)

2.1.3.2 Solvent controlled devices

Solvent controlled release devices are based on the principle of solvent penetration. There are two types of solvent controlled systems - osmotic and swelling (Heller, 1987). Osmotic controlled systems involve an external fluid containing a low concentration of drug moving across a semi-permeable membrane into a region within the device

containing a high concentration of drug. In swelling controlled systems, a polymer which can hold a large volume of water is employed. When the device is placed in an aqueous environment water penetrates the matrix and the polymer consequently swells. As a result of the polymer swelling, chain relaxation takes place and the drug is able to diffuse through.

2.1.3.3 Chemically controlled systems

Chemically controlled devices can also be divided into two classes - “pendant-chain” systems and biodegradable (also known as bioerodible) systems. In pendant-chain systems, a drug molecule is chemically bonded to a polymer backbone. The rate of drug release is controlled by the rate of hydrolysis. Bioerodible systems are designed to have a drug which is dispersed throughout the polymer. The polymer erodes because of the presence of hydrolytically or enzymatically labile bonds. As the polymer erodes, the drug is released to the surrounding medium (Heller, 1987).

2.2 Stimuli drug delivery system

Research in polymer science and engineering has developed new polymers for advanced controlled delivery of therapeutic drugs. Stimuli-sensitive polymer also called smart polymer, which can actively respond to designed environmental signals and physicochemical changes are in demand. There are three groups of stimulus used for advanced drug delivery systems: Physical (temperature, ultrasound, light, electricity, magnetism), chemical (pH, ionic strength), and biological signals (enzymes, biomolecules). The signal can be either applied by ‘external’ sources or by the ‘internal’ environment of a certain pathophysiological condition. The following sections will discuss the application of the key responsive materials on stimuli-responsive carriers and their stimuli-behaviour for controlled release.

2.2.1 Responsive materials

Several families of molecular assemblies are used as stimuli-responsive carriers for either passive or active drug delivery. **Figure 2.3** shows main responsive materials such as liposomes, polymeric nanoparticles, block copolymer micelles and dendrimers. These colloidal molecular assemblies can undergo volume change in response to variation in environmental parameters (Ganta *et al*., 2008). The combination of these molecular assemblies can be considered as biomimetic and can be used as drug carriers with desired stimuli-responsive properties. The most fascinating features of using such materials for drug delivery system arise from versatility and tunable sensitivity. Numerous monomers can be tailored to respond to one stimulus signal as well as to copolymers answering multiple stimuli. The versatility of stimuli drug delivery systems makes it possible to tune up more accurate and programmable drug delivery with a means of regulating pharmacokinetics and improving therapeutic efficacy (Li and Keller, 2009).

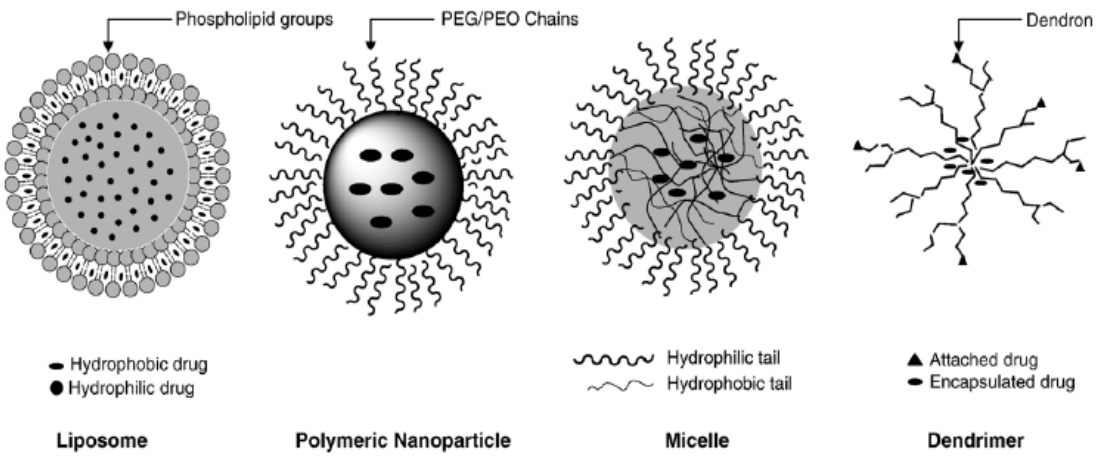

Figure 2.3 Different types of stimuli-responsive materials (Ganta *et al*., 2008)

2.2.2 Temperature triggering

Temperature-induced drug delivery is considered to be one of the most simple techniques of external trigger. Temperature sensitivity originates from the balance between hydrophobic and hydrophilic segments resulting in polymer chain aggregation via physical cross-linking. Kaneko *et al*. (1999) reported that poly (N-isopropylacrylamide) (PNIPAAm) is soluble in water in the ambient temperature range from 25 to 32 °C. Above the lower critical solution temperature (LCST), the solution becomes opaque and finally turns into gel (Kaneko *et al*., 1999). Jeong *et al*. (1997) also showed thermo-sensitivity can be obtained by using block copolymers of poly(ethylene glycol)/poly(lactic-co-glycolic acid) (PEG/PLGA, ReGel) and poly(ethylene oxide)/poly(propylene oxide) (PEO/PPO, Pluronic) (Jeong *et al*., 1997). This phenomenon has been used for thermo responsive drug carriers and the gelation occurs as depicted in **Figure 2.4** (Klouda and Mikos, 2008).

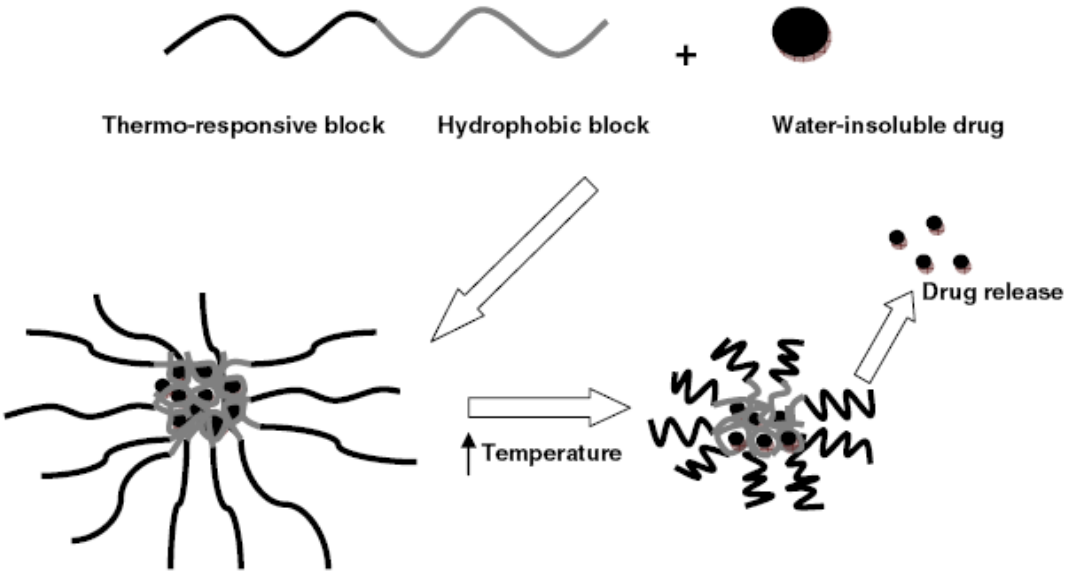

Figure 2.4 Structure and drug release from a thermoresponsive polymeric micelle (Klouda and Mikos, 2008)

2.2.3 Electro-sensitivity

An electro-stimulus also allows for precise control over the magnitude of the current, the duration of electrical pulses, and the interval between pulses. The electro-responsive concept is depicted in **Figure 2.5.** Shiga (1997) reported that delivery systems exploiting electro-stimulus are prepared from polyelectrolyte polymers, which contain a relatively high concentration of ionizable groups along the backbone chain. Under the influence of an electric field, hydrogels generally shrink or swell, depending on a number of conditions. For example, when electric potential is applied across both the anode and cathode electrodes of polyacrylamide hydrogels, a volume collapse can be observed after a minute. This is due to the electrostatic attraction between the anode surface and the negatively charged acrylic acid groups creating stress along the gel axis. Predictable release rates were modulated by altering the magnitude of the electric field between the electrodes (Shiga, 1997).

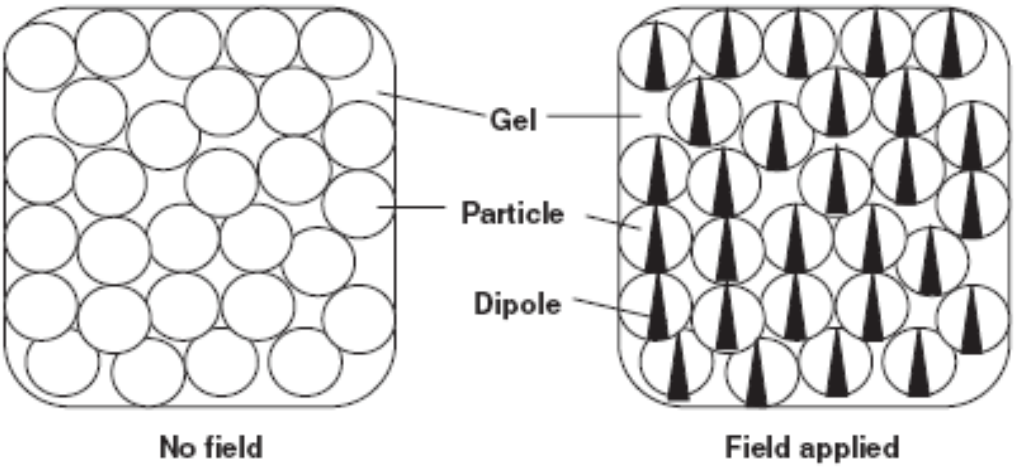

Figure 2.5 Schematic representation of the electro-responsive effect in a polymer gel. The paths of the particles have been formed prior to application of the electric field (Shiga, 1997)

2.2.4 pH sensitivity

pH sensitive polymers, which respond to pH changes in the surrounding environment, normally contain pendant acidic (e.g. carboxylic and sulfonic acids) or basic (e.g. ammonium salts) groups that are capable of either accepting or releasing protons, thus leading to conformational changes of the polymers (Gupta *et al.*, 2002). In a healthy human, pH of the body tissue is maintained around 7.4 and in the gastrointestinal tract the pH changes from, ~1-3 in the stomach and ~7 in the intestine (Phang *et al*., 2004). Each change has been utilized for the preparation of pH responsive drug delivery systems, which can exploit the biochemical properties at the diseased site for targeted delivery. Foss *et al*. (2004) reported that poly acrylic acid-g-PEG nanoparticles are stable for oral insulin delivery. At pH 6, the size of the nanoparticles becomes > 600 nm, thus expecting to avoid uptake by the intestinal Peyer's patch and provide treatment that plays a key role in intestinal immunization and in the removal of foreign substances (Foss *et al*., 2004). Lee *et al*. demonstrated that PEG-b-poly (L-histidine) (PEG-PHis) spontaneously loaded anti-cancer drug at high pH and eliminated multi-drug at pH 6.8, which might be expected to work *in-vivo* for breast tumor treatment (Lee *et al*., 2003). However, the pH-sensitive polymers used for anti-cancer drug delivery should have a narrow pH range for stimuli-release because more subtle pH changes occur within the various bodily tissues (**Table 2.1**). Otherwise, pH-sensitive drug carriers can induce either severe toxicity by drug burst or poor therapeutic efficacy.

Table 2.1 pH in various tissues and cellular compartments (adapted from (Bawa *et al*., 2009))

Tissue/cellular compartment	pH
Blood	7.35–7.45
Stomach	1.0–3.0
Duodenum	4.8–8.2
Colon	7.0–7.5
Early endosome	6.0–6.5
Late endosome	5.0–6.0
Lysosome	4.5–5.0
Golgi	6.4
Tumor, extracellular	7.2–6.5

2.2.5 Magnetic sensitivity

Magnetic targeting is based on the attraction of micro/nano magnetic particles to an external magnetic field source. In the presence of a magnetic field, a translational force will be exerted on the particle/drug complex (Bawa *et al*., 2009). Superparamagnetic iron oxide nanoparticles e.g. Fe_2O_3 or Fe_3O_4 with a diameter of <60 nm are encapsulated in organic or inorganic materials. These nanoparticles are capable of delivering drugs with desirable release rates at the intended site while an external magnetic field is applied. Lu *et al.* (2005) explored a magnetic field to modulate the permeability of polyelectrolyte microcapsules prepared by layer-by-layer self-assembly, as shown in **Figure 2.6** (Lu *et al*., 2005). As external magnetic fields were applied to the encapsulated magnetic particles, these nanoparticles disturbed and distorted the capsule

wall and drastically increased the permeability of the capsules. Hu *et al.* (2008) reported acceleration of drug release from magnetic-sensitive silica nanospheres can be manipulated by the use of a high-frequency magnetic field (HFMF). The HFMF rotated magnetic particles in the silica matrix subsequently generating heat and enlarged porous channels of the silica matrix which in turn enhanced drug release (Hu *et al*., 2008). The positioning, orientation and magnetic strength of the embedded magnetic materials have also been found to be important in tailoring release rate in these systems (Hu *et al*., 2007).

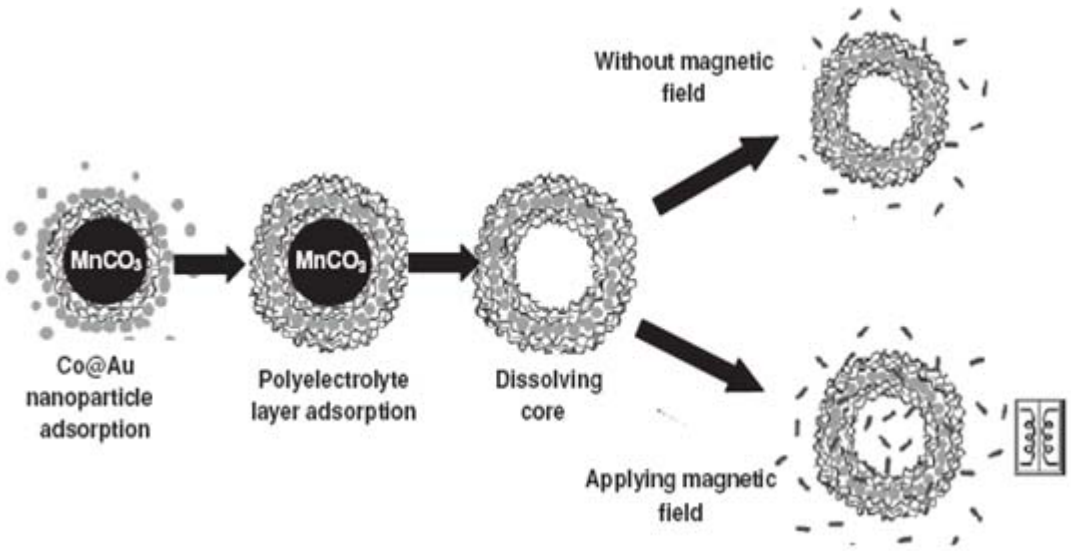

Figure 2.6 Schematic representation of the assembly and permeability of microcapsules embedded with gold-coated cobalt (Co@Au) nanoparticles under an oscillating magnetic field (Lu *et al*., 2005)

2.2.6 Light sensitivity

Light sensitive polymers can be manipulated under UV or visible light. Mamada *et al.* (1990) reported that hydrogels with Bis(4-dimethylamino)phenylmethyl leucocyanide in a polymer network can swell in response to UV irradiation but shrink when the UV

light is removed. The swelling is due to an increase in osmotic pressure within the gel and the cyanide ions formed by UV irradiation (Mamada *et al*., 1990). Susuki *et al.* (1990) demonstrated that visible light-responsive hydrogels can be synthesized by incorporating a light-sensitive element e.g. chromophore. When light is applied to the hydrogel, the chromophore is dissipated locally as heat by absorbing light, inducing an elevated temperature of the hydrogel. This increase in temperature alters the swelling behaviour of the hydrogel and paves a route for controlled release applications (Suzuki and Tanaka, 1990). However, visible light-responsive polymers and hydrogels are more desirable owing to being safe, inexpensive, readily available, clean and easily manipulated (Qiu and Park, 2001).

2.2.7 Ultrasound triggering

Ultrasound-induced drug delivery is considered to hold the most potential as an external trigger. The advantage of therapeutic ultrasound arises from the fact that it is relatively a non-invasive technique, broadly applicable to a variety of cells and to the interior of the body (Gao *et al*., 2005). Owing to its versatile and cost-effective modality in many clinical applications, various applications of drug delivery using ultrasound, especially in the frequency range from 20 kHz to 3 MHz, have been extensively investigated (Lin and Thomas, 2004, Lin and Thomas, 2003). Early studies have shown that acoustic cavitation is the primary effect to increase the degradation rate of biodegradable polymers and up to a 20-fold enhancement in the drug release rate was observed from polymer matrices, suggesting that low frequency ultrasound is more effective in enhanced release than high frequency (Kost *et al*., 1989, Leong *et al*., 1986, Schroeder *et al*., 2007). Moreover, synergistic therapeutic effects have shown that temperature-induced release and hyperthermia increases by ultrasound is beneficial for cancer treatment (Smet *et al*., 2011). On the other hand, cavitation

occurring through the collapse of microbubbles has also been used to enhance release of encapsulated materials by breaking up the polymer capsules (Geest *et al*., 2006).

2.2.8 Creating a stimuli-drug delivery system

In spite of extensive research in the development of smart polymers for stimuli drug delivery systems, it is not easy to find a commercialized product based on any smart polymer. The major challenge is caused by the biocompatibility issue. Bischoff (1972) reported the hydrolysis and free radical- or oxidation/reduction-mediated breakdown of implanted polymers. In addition, he demonstrated blood clotting, host-rejection, carcinogenesis, and phagocytosis by the reticuloendothelial system, which was induced by polymers inside living subjects (Bischoff, 1972). Currently, most of the research primarily focuses on how to design a polymer with more sensitivity, responding to a given stimulus *in-vitro*. There has been no significant advancement in the biocompatibility issue. In addition, the most significant weakness of all these external stumuli-sensitive polymer is that their response time is too slow (Qiu and Park, 2001). Therefore, questions about how to use existing biocompatible polymers and the incorporation of stimuli-elements to design a new stimulated drug delivery system with real-time response is an important and urgent challenge.

2.3 Hollow microspheres

Hollow microspheres are spherically symmetrical particles consisting of at least two phases with diameter between ~10 nm and 1000 μm. While the current need for hollow microspheres is gaining more and more attention in various disciplines, several colloidal synthetic methods have been used to prepare various hollow structures because of their high specific surface, low density, good heat-insulation and large pore volume (Wang *et al*., 2007). The typical thickness of the wall is in the range of 1 to 30

% of the diameter of the sphere. The wall material may be made from organic or inorganic materials. These features make the hollow structures a unique and promising candidate for multifunctional drug delivery vehicles including specific targeting, imaging, and controlled release (Zhang *et al*., 2009, Xiao *et al*., 2009, Bai *et al*., 2009). Typical scanning electron micrographs of hollow microspheres and their cross section are shown in **Figure 2.7** (Okubo *et al*., 1998). This section focuses on a critical literature review associated with the preparation of hollow microspheres. The basic principles and the processing techniques are also discussed in this section. In addition, the preparation and application of new monoporous hollow microspheres are also taken into account.

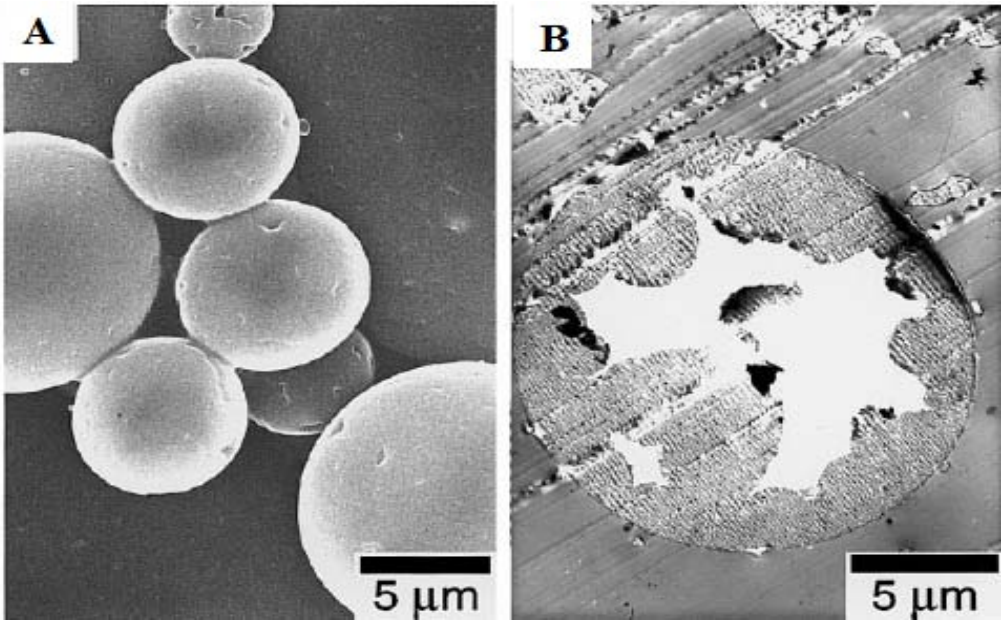

Figure 2.7 Scanning electron micrographs: (A) poly(ethyl methacrylate) / divinylbenzene composite particles produced by suspension polymerization, (B) cross sections of the composite particles (Okubo *et al*., 1998)

2.3.1 Fabrication of hollow microspheres

Colloidal particles with a hollow interior represent a special class of core-shell particles for drug delivery applications. Before 1998, most hollow particles were synthesized using spray-drying and gas-blowing methods for controlling structures on the micro-scale (Wilcox *et al.*, 1995). In the 1970s and 1980s, Matijevic and others primarily demonstrated core-shell colloids for the use in surface functionalization (Matijevic, 1993). These efforts heralded approaches for coating Au and Ag nanoparticles with silica by sol-gel processing (Ung *et al*., 1998, Liz-Marzán *et al*., 1996), and colloidal templating synthesis of hollow spheres (Caruso *et al*., 1998). These approaches gave rise to a new, more versatile, synthesis paradigm for the preparation of hollow structures based on hard-templating methods. Indeed, starting around 2001, there has been a large increase in research activity focused on preparation of hollow micro-/nano-structures using templates. The synthetic approaches to hollow sphere preparation are investigated in detail and can be categorised according to how the hollow structure is formed: spray method, high temperature method, templating, emulsion processing, and polymerization.

2.3.1.1 Spray method

Spray processes are the most widely used industrial technique. Droplets can be easily generated by capillaries, followed by the formation of the wall and the removal of the core material. In gas phase synthesis, pyrolysis was involved in spray drying to produce hollow particles (Chadda *et al*., 1991, Powell *et al*., 1997). The flow chart of the process of spray drying is shown schematically in **Figure 2.8**. In general, shell materials are dispersed in a suitable liquid and subsequently the solution is atomized by a capillary in the system. While the suspension is leaving the capillary, small droplets are formed due to gravitational and frictional forces (Bertling *et al*., 2004). The spray drying produces

one hollow or coated particle from one droplet. Therefore, the size and size distribution of particles are closely related to the dimensions of the droplet generators. However, the use of such systems is limited by the diameters of the technically available capillaries and solution viscosities. The smallest diameter achieved is about 50 μm if the dynamic viscosity does not exceed 500 mPa s.

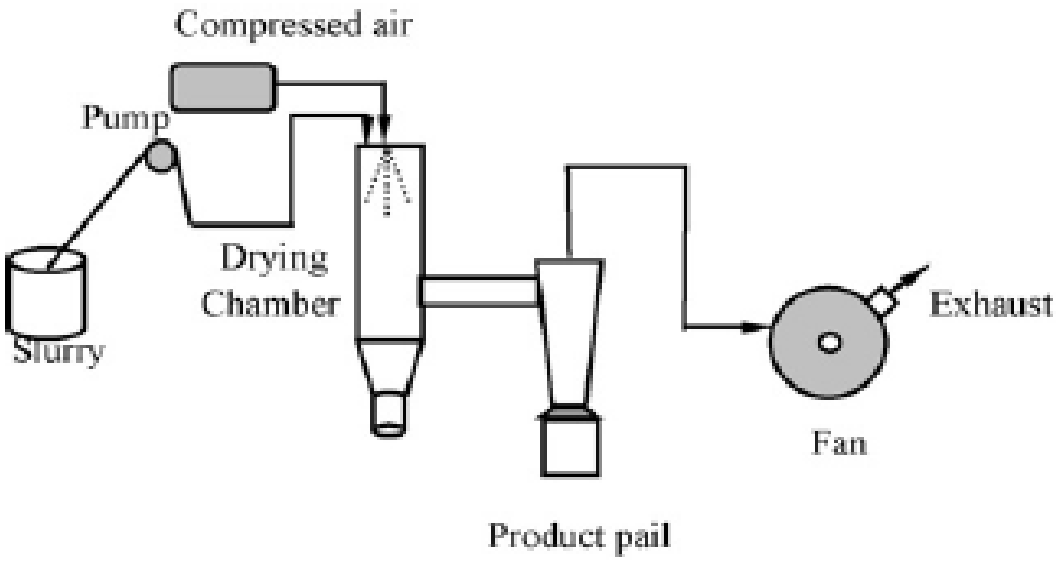

Figure 2.8 Flow chart of the process of spray drying (Wang *et al*., 2007)

2.3.1.2 High temperature method

The hollow polymer microspheres are formed by using equipment with multi-stage high temperature modules, which allow droplets to fall in the high-temperature furnace and institute the hollow microsphere structure (**Figure 2.9**). In general, when polystyrene (PS) droplets fall into the high-temperature vertical furnace (> 200 °C), they start shrinking due to the evaporation of the volatile solvent on the outer surface. With the gradual evaporation of the solvent, the condensation of PS on outer surface starts. This outer surface subsequently forms a thin film on the surface of the droplets, and the temperature of the droplets begins to rise because the evaporation of the inner

core is inhibited. When the droplets' temperature reach the boiling point of the organic solvent, bubbles can be observed in the droplets, and the spherical shell begins to expand. Finally when the expanded droplets fall into the low-temperature zone of the vertical furnace, hollow microspheres are obtained (Wilcox *et al.*, 1995). Dorogotovtsev *et al.* (1997) reported the influence of gas mixture in the furnace on the yield and quality of the hollow microspheres. The results suggested that with increasing concentration of gas mixtures of He and Ar, the yield rate of hollow microspheres increases, but with a variation of morphology (Dorogotovtsev and Akunets, 1997).

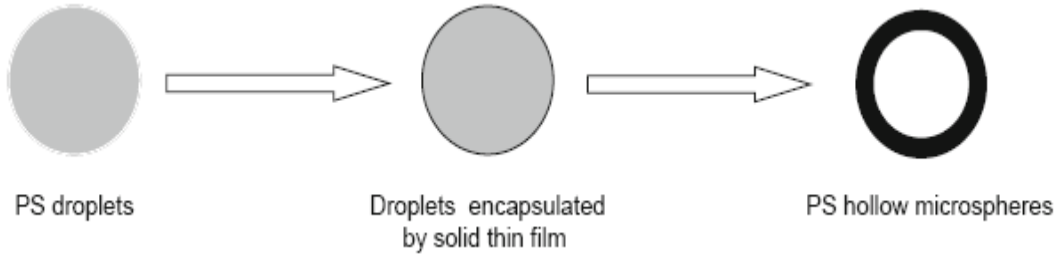

Figure 2.9 Schematic representation of PS hollow microspheres prepared by the high temperature method (Wei *et al*., 2006)

2.3.1.3 Templating method

Preparation of hollow structures by using a templating method can be described as follows: A polymer shell is formed on the surface of the prepared template due to the solute depositing or reacting on the surface of the dispersed templates and then the template particle is removed either by chemical solvent or high temperature calcination, and hollow shells are obtained (Sun *et al*., 2002). The templating method is often used to prepare hollow polymer microspheres, and has been proven to be a very successful method (Guan *et al*., 2007). However, despite being a simple process, the templating

method is limited because it requires a large amount of template, which needs a biocompatible material, resulting in high cost. In addition, the removal of the core template is critical, typically requiring special care to prevent collapse of the shells during the use of solvents or calcinations at high temperatures. For example, when using an organic solvent to dissolve template latex particles, swelling of the polymer can cause rupture of the hollow structure, subjecting the shell to uncontrolled shape change. The schematic illustration of preparation of hollow structure using the templating method is shown in **Figure 2.10** (Wang *et al*., 2007).

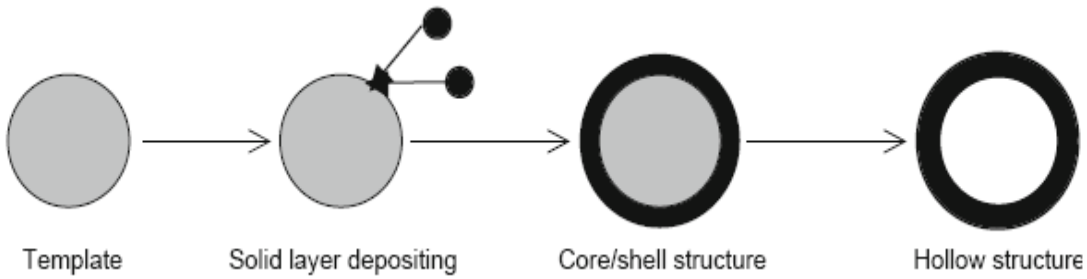

Figure 2.10 Schematic illustration of the formation process of hollow microspheres using a templating method (Wang *et al*., 2007)

2.3.1.4 Self-assembly method

Self-assembly, also known as layer-by-layer (LBL) technique, is the most suitable method to prepare hollow microspheres with controllable shell thicknesses. The formation mechanism of this technique is similar to that of the templating method. The shell is obtained through sequential deposition of oppositely charged polymer species on the core material and the hollow structure is obtained by removing the core materials (**Figure 2.11**). The versatility of LBL enables precise control over size and uniformity of the shell. Polymer capsules derived from this route facilitates the encapsulation of

diverse components (Zelikin *et al*., 2006). A large number of inorganic and polymer-based microspheres have been reported to form hollow microspheres by varying the mechanisms e.g. hydrogen bonding (Stockton and Rubner, 1997), hydrophobic interactions (Serizawa *et al*., 2002), and hybridization of DNA base pairs (Johnston *et al*., 2006). However, compared to the templating method, the LBL assembly procedure becomes quite tedious when many layers are required, normally involving surfactants or amphiphilic polymers to increase kinetic stability (Song *et al*., 2006, Daiguji *et al*., 2007). In addition, although hollow microspheres prepared by this method possess uniform shell thickness and good spherical morphology, the hollow structure generally lacks the mechanical robustness and tends to collapse irreversibly after drying (Liu *et al*., 2007).

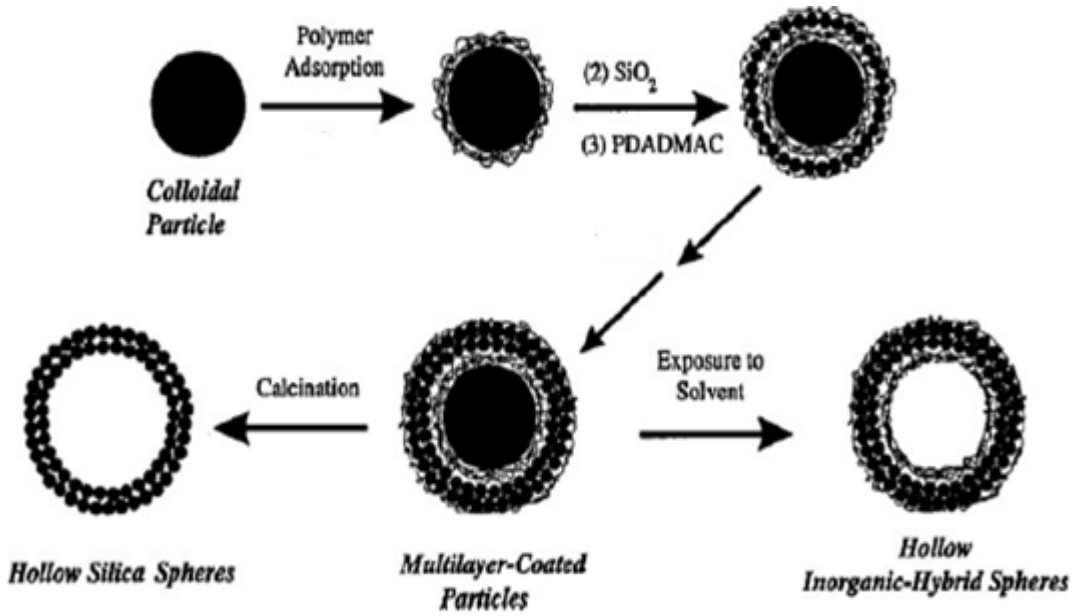

Figure 2.11 Schematic illustration of procedures for preparing inorganic and hybrid hollow spheres using the layer-by-layer (LBL) technique based on PS colloidal templates (Caruso *et al*., 1998)

2.3.1.5 Polymerization

The polymerization method was first studied by Kowalski and coworkers (1984) whereby they instituted a hard permeable polymer shell on latex seed. When the latex particles swells enough, the outer layer shrinks to form the hollow microspheres (Kowalski *et al*., 1984). Okubo and coworkers (1998) investigated the method of suspension polymerization to prepare hollow microsphere from different proportions of PS/DVB/toluene mixture solutions. They showed that the hollow structures were influenced by the concentration of PS and its molecular weight, indicating that PS plays an important role in the polymerization method (Okubo *et al*., 1998). The process also further studied by Itou *et al*., (1999), who showed that the polymerization occurs within highly swollen seed particles with a monomer. In addition, in order to form a small void the polymerization shrinkage must occur in the inside of the cross-linked polymer particle. Therefore, the void space is developed by the polymerization shrinkage, as shown in **Figure 2.12** (Itou *et al*., 1999).

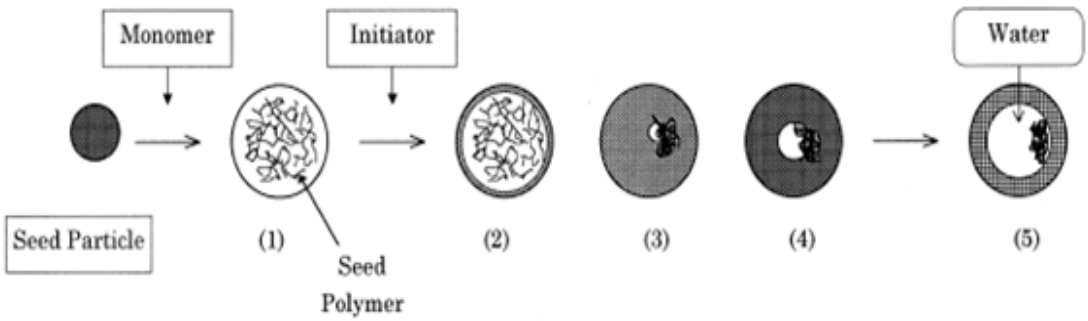

Figure 2.12 The formation mechanism of hollow polymer particles by polymerization (Itou *et al*., 1999)

2.3.1.6 Emulsion processing

In general, hollow microspheres can be produced as either oil-in-water or water-in-oil emulsions. Emulsions can be achieved when two immiscible liquids are mixed together via mechanical agitation (e.g., shaking, stirring, or ultrasound). Thus, liquid droplets of one phase can be dispersed in the other continuous phase. This status is thermodynamically unstable, therefore surfactants or amphiphilic polymers, which self-assemble at the interface between the droplets and continuous phase, are required to increase kinetic stability (Li *et al*., 2003). The typical process; water-in-oil (W/O) and water-in-oil-in-water (W/O/W) emulsions is shown in **Figure 2.13**. It should be noted that the emulsion acts as a microreactor, where the shell materials can initially institute in either the continuous phase or the droplets or both phases, depending on the chemical properties (Han *et al*., 2006). However, hollow structures with irregular morphologies will appear when the initial conditions of solutions are inappropriate. In addition, the size distribution of the products fabricated by this method is broad in the range of 1 to 100 μm.

2.3.2 Fabrication of monoporous hollow microspheres

Recently, hollow monoporous microspheres (i.e. hollow microspheres with a single hole in their shells, as shown in **Figure 2.14**) have received much attention and have been classified as a new category of particles on account of their higher effective diffusivity and available surface area compared with microporous spheres of the same size (Im *et al*., 2005). These microspheres offer enhanced rates of encapsulation, as well as being suitable for other applications, e.g. catalytic carriers, thermal insulation, and targeting (Guan *et al*., 2007). However, the design and preparation of hollow monoporous microspheres present significant challenges. Many of the current techniques used are complex and require highly specialized equipment and/or processing environments.

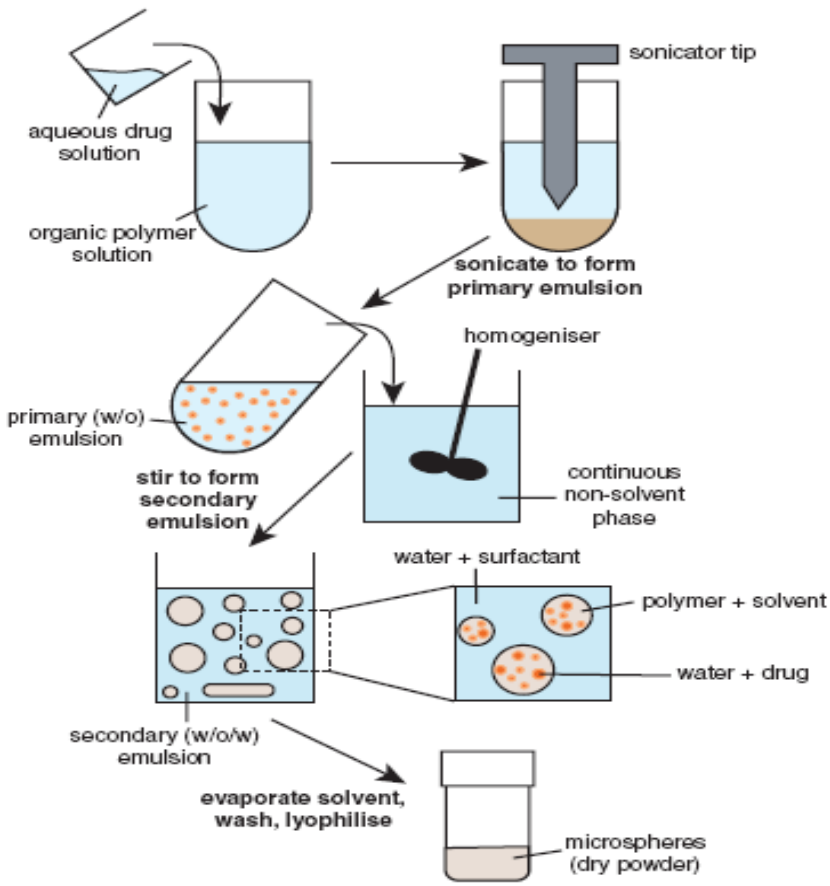

Figure 2.13 Illustration of emulsion processing (Varde and Pack, 2004)

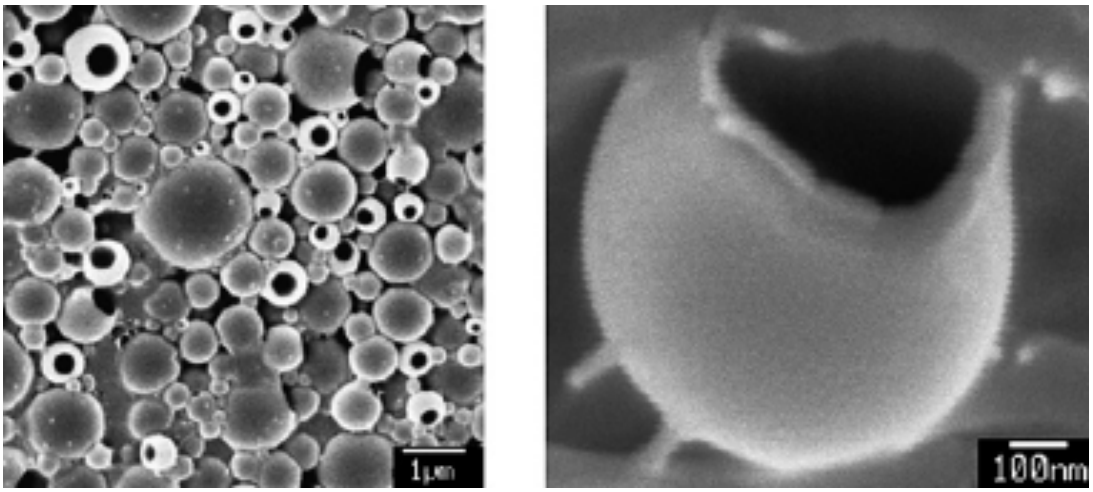

Figure 2.14 Scanning electron micrographs of dye-induced colloidal bucket, the colloidal buckets were made at 9200 rpm and heated to 65°C (Yow and Routh, 2008)

Much effort has been devoted in recent years to the development of monoporous microspheres. Minami *et al.* (2005) reported that such particles can be prepared by the SaPSeP (self-assembling of phase separated polymer) method. Particle characteristics can be controlled by altering the interfacial tension, surfactant and polymer concentration. The one-hole surface morphology of the hollow microspheres was achieved by heating them to 70 °C in a nitrogen atmosphere (Minami *et al*., 2005). This technique has since been refined and similar particles with a single regular hole on their shells were formed at temperatures below 0 °C (Jeong *et al*., 2007, Yin and Yates, 2008, Im *et al*., 2005). Yow and Routh (2008) fabricated colloidal "buckets" via a coacervation technique at 65 °C. Briefly, an oil core and a polymer were mixed with a volatile solvent. Subsequently, the mixture was emulsified in an aqueous solution and polymer precipitation occurred during evaporation of the volatile solvent. These microspheres were obtained by controlling the solvent evaporation rate and incorporation of a third component (precipitant) to alter the interfacial tensions between the different phases. The core was then removed by "washing" with a suitable solvent to obtain a hollow internal structure, as shown in **Figure 2.15** (Yow and Routh, 2008). In another interesting example, Guan and co-workers (2007) prepared monoporous hollow polymer microspheres and demonstrated high-capacity uptake of a target species. Polystyrene beads were used as the adsorption substrates for precipitation polymerization and then consecutive deposition and polymerization was carried out at 60 °C, followed by etching of the original beads (Guan *et al*., 2007).

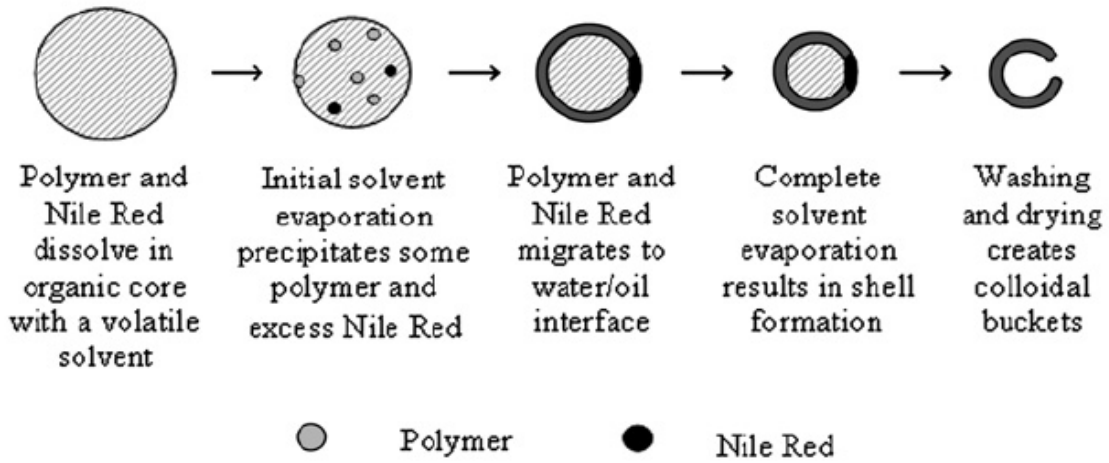

Figure 2.15 Fabrication procedure of dye-induced monoporous hollow microspheres (Yow and Routh, 2008)

2.3.3 Encapsulation of hollow microspheres

Various drugs and biomolecules can be loaded into the cavity and on the surface of a hollow microsphere through its porous shell and a typical sustained release pattern can be observed without any burst effect (Vasir *et al*., 2003, Gao *et al*., 2009). Up to now, the encapsulation of liquid drug into a hollow microsphere is mainly a post-process and uncontrollable. In general, two methods have been reported for the loading of therapeutic drugs into hollow capsules: Encapsulation in template with drugs or in hollow capsules (**Figure 2.16**). In the first method, drug macromolecules are well dispersed into the template particles during preparation. After forming the shell structure on the template, the template materials are dissolved, resulting in a relic drug in the hollow core. This method usually needs high selective etching process. Otherwise, the dissolution conditions for the core templates can destroy the encapsulated drug and shell structure (Volodkin *et al*., 2004). For the second method, the hollow carrier is first prepared, loading the drug molecules into the hollow capsules by immersing hollow

microspheres into the drug solution. The drug molecules are thereby physically adsorbed into the hollow microcapsules via porous channels of the shell, until reaching the gradient balance between core and sink (Nishiyam and Kataoka, 2006). However, in order to obtain the effective encapsulation and storage of drugs in hollow capsules, the size of drug molecules must be smaller than the diameter of their pore channels.

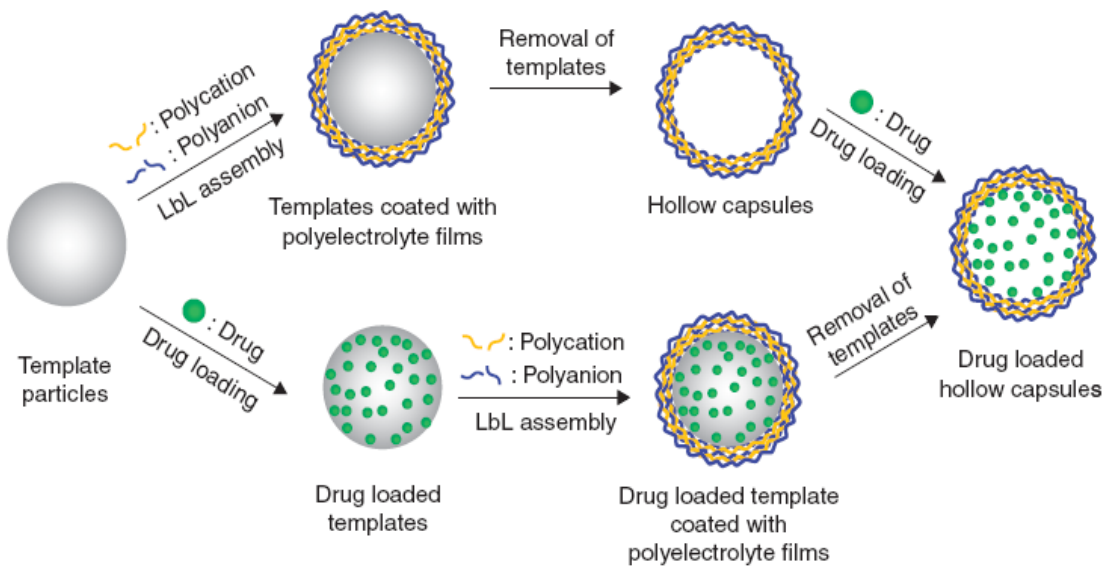

Figure 2.16 Schematic illustration of drug encapsulation of hollow capsules (Matsusaki and Akashi, 2009)

2.3.4 Challenges: forming hollow and monoporous spheres

Despite the versatility and growing popularity of hollow spheres, above mentioned methods suffer from three key shortcomings. First, the assembly procedure becomes quite tedious and time-consuming when many layers are required. Second, as-prepared polymer capsules are only stable in solution, once dried they tend to collapse irreversibly. Third, key applications of hollow structures, such as drug and therapeutic delivery, require facile access to the hollow interior space. With hard templates, refilling the

hollow interior with functional species is very challenging. In addition to these limitations, the synthetic process and post-treatment are necessary to involve surfactants and chemical additives to increase kinetic stability (Kim and Yoon, 2004). This in turn results in side effects and the introduction of impurities (Song *et al*., 2006). Furthermore, the wide spread applications of spherical hollow structures have been limited, mainly because of the disadvantages associated with the fabrication techniques. Therefore, some novel methods have prompted interest in simpler approaches for producing hollow shells that permit easy encapsulation and release of guest species. **Table 2.2** depicts both the advantages and the disadvantages of the fabrication methods mentioned above.

2.4 Electrohydrodynamic atomisation

Electrospraying- more generically described as electrohydrodynamic atomisation (EHDA)- covers the process of the splitting of a moving (dynamic) liquid (hydro) in an electric (electro) field (**Figure 2.17**). The "atomisation" of a liquid charged by primarily high electric potential, which includes both the acceleration of the liquid and subsequent disruption into tiny droplets, has lead to a total physical model of the cone, the jet and the droplets formed (Grace and Marijnissen, 1994, Hartman *et al*., 1999b). The droplets produced with uniform size distribution are electrically charged and neutralized by guiding these particles toward the ground electrode. The electrohydrodynamic processing technique has proved to be an effective and versatile method to prepare particles or fibres in the micrometre to nanometre scale range for a host of applications in optical sensor (Wang *et al*., 2002), membrane technology (Zong *et al*., 2003), tissue engineering (Raghunath *et al*., 2009), and drug delivery (Pareta and Edirisinghe, 2006). This section focuses on a critical literature review associated with this research. The basic stable cone-jet mode of electrohydrodynamic atomisation is most important. In

addition, the effect of the liquid properties, processing parameters, and other features developed affecting the EHDA process will be discussed.

Table 2.2 The advantages and the disadvantages of the fabrication methods (Wang *et al*., 2007, Gao *et al*., 2009, Zhu *et al*., 2005, Bertling *et al.*, 2004)

Methods	Advantages	Disadvantages
Spray method	Can be controlled easily	Particle size and polydispersivity is high
High temperature method	The efficiency is high	Needs high temperature
Templating method	Can be controlled easily	Needs excess template materials and is difficult for biological encapsulation due to the use of harsh solvents
Self-assembly method	The morphology and its shell thickness can be controlled accurately	Is time-consuming and only possible with low particle concentrations
Emulsion processing	Different compositions can be prepared with varied shell thickness and diameter	Fabrication difficult to control and needs use of organic solvents and chemical additives
Polymerization	Good control over shell composition and thickness	Risk of incomplete shell formation

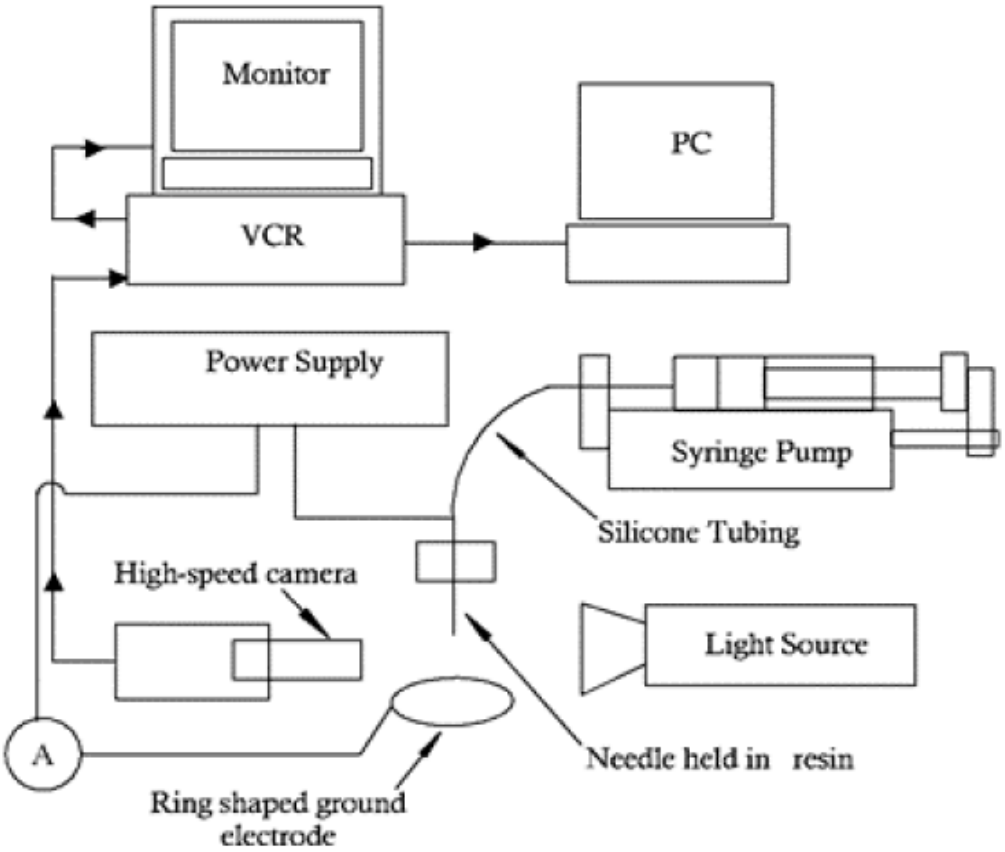

Figure 2.17 Schematic representation of the electrohydrodynamic atomisation equipment rig (Jayasinghe and Edirisinghe 2003)

2.4.1 Historical development

Electrohydrodynamic atomisation is a process of droplet generation by the imposition of a high electric field. Thus, a liquid flowing out from a needle under a high voltage subjects the elongation of its meniscus to form various modes. The liquid can deform into a stable cone-jet and disrupts into charged droplets due to the electrical force (Mora and Loscertales, 1994). However, the application of liquids via EHDA was noted and reported as early as 1600 by Gilbert, but Bose is the first to describe the EHDA process in 1745 (Ganan-Calvo, 1999). It was noticed that Rayleigh made the earliest observations of the instability of EHDA and analyzed the behaviour of jets and drops

under the influence of electric charges (Rayleigh, 1878). Rayleigh suggested that the unstable conditions for a drop or jet are dependent on the balance of forces between electrical stresses and surface tension (Rayleigh, 1879). The fission of liquids was further investigated by Gomez *et al*. (1994). They observed that charge of droplets reduced when a drop approached the Rayleigh limit, defined as the maximum amount of charge a liquid droplet could carry, resulting in a strain of a few smaller droplets (Gomez and Tang, 1994). The charge and size of the droplet can be controlled by adjusting the liquid properties and the liquid flow rate, applied voltage and needle geometry.

Zeleny (1914, 1995) used a needle injected with liquid and applied a high voltage between a top and "ground" electrode that marked the breakthrough into this exciting field of research and attracted considerable interest from a fundamental point of view (Zeleny, 1914, Zeleny, 1915). After 50 years, equilibrium between electric field and surface tension of liquid derived by Taylor (1964) showed the conditions for a meniscus to exist in a conical form under competing actions. He found that a conductive liquid could be kept stable with a conical shape by using glycerine and glycerine-water mixtures when an electric field was applied (Taylor, 1964).

Since then, this phenomenon has been used as a processing technique and has managed to attract a number of studies. Jones and Thong (1971) observed that the kerosene droplet size is almost independent of voltage and droplets could only be achieved within a certain range of applied voltage as a function of liquid flow rate (Jones and Thong, 1971). Later in 1980, Nagorynyi and Bezrukov (1980) found the decrease in droplet diameter can be obtained by increasing the applied potential, thus obtaining an important condition for processing fine droplets by electrostatic atomisation (Nagorynti

and Bezrukov, 1980). Furthermore, Smith (1986) published a general discussion on the effect of the liquid physical properties, such as electrical conductivity, surface tension and viscosity (Smith, 1986).

Electrospraying was investigated further, systematically and quantitatively, in the 1990s. Cloupeau and Prunet-Foch (1990) reported the classification of functional modes for electrohydrodynamic processing, according to the operating conditions. They showed that electrohydrodynamic processing presented several measurable differences by increasing applied voltage, while liquid properties and flow rate were kept constant. They also investigated the characteristics of each mode based on visual observation (Cloupeau and Prunet-Foch, 1990).

Later, Meesters *et al*. (1992) investigated cone-jet mode atomisation at high flow rates and observed a very high droplet production (Meesters *et al*., 1992). Thereafter, Jaworek and Krupa (1999b) further defined the modes of electrohydrodynamic processing and provided a route to produce droplets for engineering research (Jaworek and Krupa, 1999b). Jayasinghe and Edirisinghe (2002) demonstrated the effect of viscosity on the size of products produced by electrohydrodynamic processing. They suggested that increasing viscosity in the range 1-1340 mPa s had a significant effect on the mode of electrohydrodynamic processing and size distribution of relics (Jayasinghe and Edirisinghe, 2002).

2.4.2 Modes of electrohydrodynamic atomisation

The spraying modes were characterized by two principle categories based on the observations and photographic documentation. The first category comprises the modes; dripping, micro-dripping, spindle, multi-spindle, and ramified modes. The

characterization of the first category only shows fragments of liquid being ejected from the capillary without a continuous jet and these fragments can be in the form of regular large drops. The second category shows a long continuous jet which disintegrates into droplets of a few millimeters in size. The stable cone-jet, precession, oscillating-jet, and multi-jet modes are included in this category. The meniscus and the jet can be fine, stable, vibrate, and rotate spirally around the capillary axis (Jaworek and Krupa, 1999a). Different modes of electrohydrodynamic atomisation with their key characteristics were summarized by Jaworek and Krupa (1999). This has been reproduced in this thesis (**Table 2.3 and 2.4**) and the stable cone-jet mode used in this work is described in more detail.

2.4.3 Mechanism of stable cone-jet mode

As previously discussed, the cone-jet mode is crucial for the preparation of particles and capsules due to its near-monodisperse droplets production capability. The understanding of the fundamental mechanism of the cone-jet mode formation is therefore necessary in order to utilize EHDA for drug encapsulation. Hartman and coworkers (1999) established a physical model and described the phenomenon of the stable cone-jet mode of the electrohydrodynamic process (Hartman *et al*., 1999a). They divided the stable cone-jet mode into three stages: (1) Acceleration of the liquid in the liquid cone; (2) jet break-up (droplet production); (3) evolution of spraying after droplet production. In addition, the influence of droplet evaporation during the electrohydrodynamic process is also crucial to control droplet/ relic size and surface morphology. Therefore, the droplet evaporation will also be discussed later.

Table 2.3 Characteristic features of the fragments of liquid modes of electrohydrodynamic atomisation (Jaworek and Krupa, 1999a)

Mode of spraying	**Forms of liquid**	**Dynamics of meniscus/jet**	**Spray pattern**
Dripping 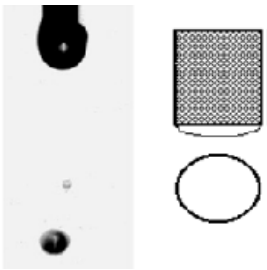	Meniscus: semi-spherical Drop: simple spherical	Axially vibrating	Single drop (with siblings)
Micro-dripping 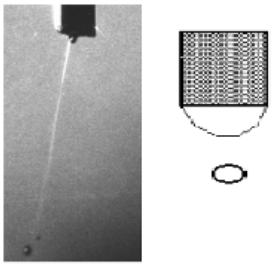	Meniscus: cone/hemispherical Drop: small, simple spherical (in some case with trailing/ leading thread)	Axially stable	Linear series of droplets (accompanied with fine mist)
Spindle 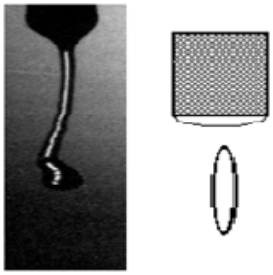	Meniscus: cone/semi-spherical Drop: elongated fragment of liquid (spindle) (with trailing thread)	Axially vibrating	Spindles disrupting into small droplets
Multi-spindle 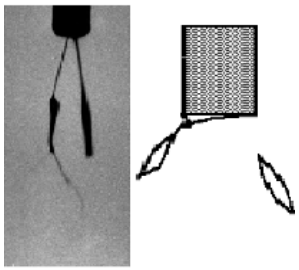	Meniscus: flat/multi-cone Drops: multiple spindles (with trailing thread)	Stable/lateral vibrating	Spindles around the axis disrupting into small droplets

Table 2.4 Characteristic features of the modes of EHD Liquid jets (Jaworek and Krupa, 1999a)

Mode of spraying	**Forms of liquid**	**Dynamics of meniscus/jet**	**Spray pattern**
Precession 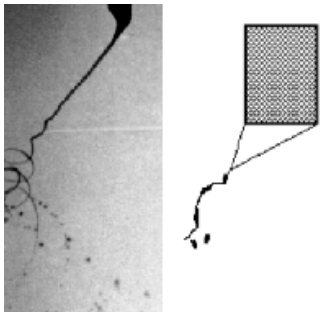	Meniscus: skewed, rotating cone Jet: spiral, rotating around the capillary axis	Rotating around the capillary axis, spiral instabilities	Fine aerosol sprayed in a regular cone
Cone-jet 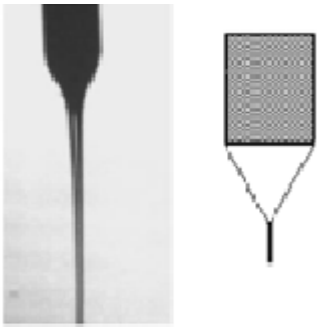	Meniscus: cone (linear, concave, convex, skewed) Jet: simple straight linear	Axially stable, varicose or kink instabilities	Fine aerosol sprayed in regular cone
Multi-jet 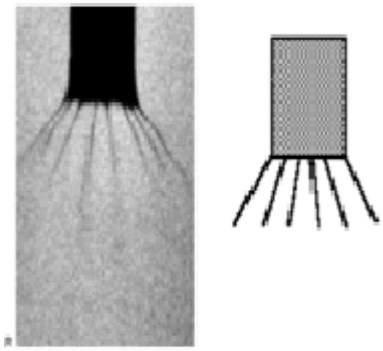	Meniscus: flat, with small cones on the rim Jet: linear, multiple	Stable (usually with kink instabilities)	Fine aerosol sprayed in distinct directions

2.4.3.1 Acceleration of the liquid in the liquid cone

A stable liquid cone is formed when the liquid pressure is optimized, and its relies on successfully balancing the forces such as liquid surface tension, gravity and electric stresses in the liquid surface, as shown in **Figure 2.18**. Taylor (1964) was the first to analyze the conical shape and suggested that there are various forces acting on cone formation when the outward stress (applied electric field) balances the inward stress (liquid surface tension) (Taylor, 1964). Electric force is the main driver of cone-jet mode formation. Therefore, in order to achieve a relatively stable jet, the electrical potential needs to penetrate the injected liquid and its electric field tangential to the liquid surface has to act on the surface charges, to be able to create a force which drives the liquid and accelerates the jet downstream (Cloupeau and Prunet-Foch, 1990). It was also noted by Hartman and co-workers (1999) that this acceleration process and the shape of the liquid surface are a result of the balance of the stress and surface tension of the liquid, gravity and electric stresses of the liquid surface and of the inertia and viscosity of the liquid (Hartman *et al*., 1999a).

2.4.3.2 Jet break-up

Each liquid has a certain range of flow rate in which the stable cone-jet mode is achieved. Jet break-up occurs in the stable cone-jet mode due to instabilities. This is also named as the droplet production process (Hartman *et al*., 1999a). There are two mechanisms that lead to the emission of liquid from the tip of a stable jet. In one mechanism, ions, neutral atoms and droplets are emitted from the liquid surface by applying an intense electric field at the tip. This emission results in instabilities. The other is that the liquid is ejected via the formation of the cone-jet which breaks into tiny droplets after some length due to surface instabilities (Rulison and Flagan, 1994). The latter is more commonly observed.

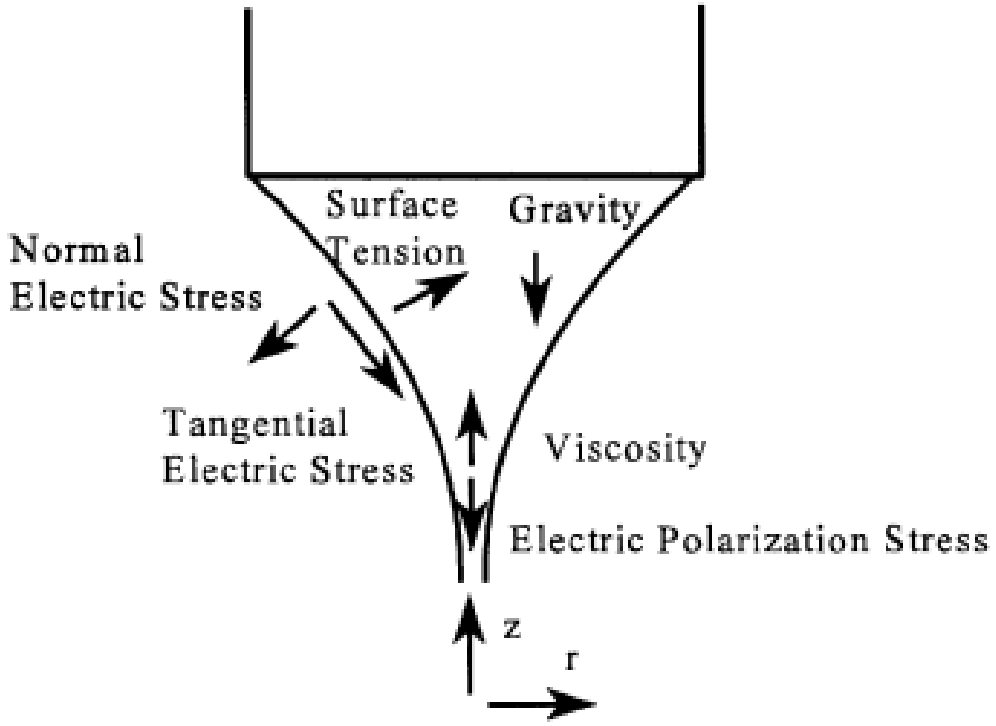

Figure 2.18 Forces of the liquid cone in the EHDA process (Hartman *et al*., 1999b)

When a jet breaks up into droplets, different flow rates can result in different instabilities. Axisymmetric instabilities cause jet break-up and can be observed at low flow rates. These instabilities are also named varicose instabilities. In the varicose instabilities, waves are generated on the surface of the jet and contract in the nodes. The jet disintegrates into uniform fine droplets due to electrical and inertial forces. At higher flow rates, the current through the liquid cone increases which in turn increases the surface charge on the jet. Above a certain surface charge, jet break-up will also be influenced by the lateral instabilities in the jet. These instabilities are called "kink" instabilities (Hartman *et al*., 1999a). The kink instabilities are sometimes also known as a whipping motion of the jet and the jet moves irregularly off the axis of the capillary,

as shown in **Figure 2.19**. The size distribution of the main droplets become broader if the influence of these kink instabilities increases (Cloupeau and Prunet-Foch, 1989). However, in the cone-jet mode of EHDA, the process not only involves the electric field, but also the acceleration of the liquid in the jet. Such characteristics establish that the stable cone-jet mode can only be achieved at a certain flow rate range for a specific liquid, beyond which other electrohydrodynamic modes will be present.

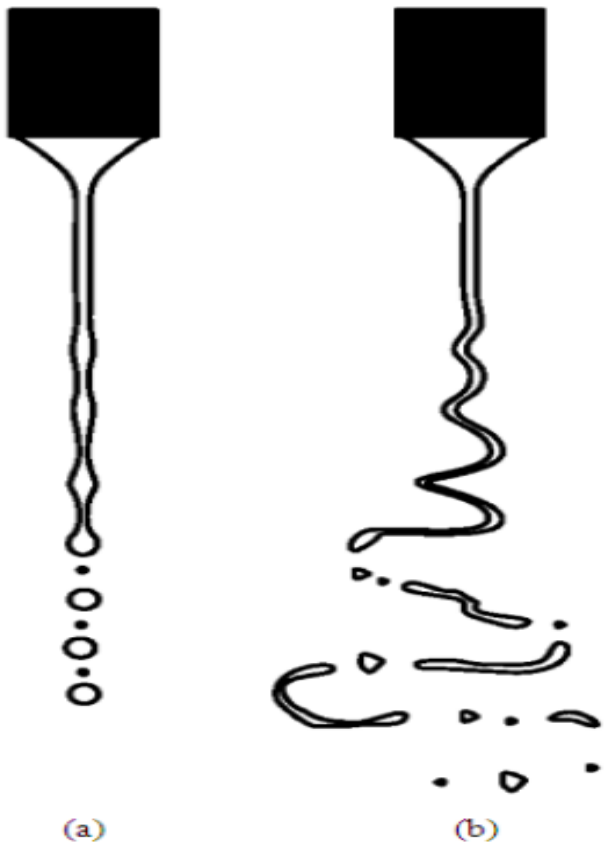

Figure 2.19 Jet break-up modes: (a) the axisymmetric varicose break-up and (b) the lateral kink break-up (Hartman *et al*., 1999a)

2.4.3.3 Evolution of spray after droplet production

When the jet becomes unstable, it will eventually disintegrate into droplets, which was catalogued as the third process of the stable cone-jet mode (Hartman *et al*., 1999a).

Segregation of tiny droplets can be attributed to highly charged droplets under electrical interaction, causing a high mobility. The smaller droplets (called satellite droplets) are found at the edge of the spray while the larger sized droplets (called main droplets) are found at the centre of spraying (Ganan-Calvo *et al.*, 1994, Hartman *et al.*, 1999a, Hartman *et al.*, 1999b). The distance between main droplets and secondary droplets is approximately half of the distance between main droplets. Different droplet diameters possess variable electric forces due to the difference in droplet charge. A big droplet has a higher inertia than a small droplet, which results in a smaller acceleration. As a result, the distance between the main droplet and the secondary increases and the small droplet possesses a higher radial velocity.

2.4.3.4 Droplet evaporation

While evaporation does not alter droplet transport significantly after the jet break-up, it is another key factor in the forming process and can drastically change the morphology and size of droplet and relics, depending on the solvent properties, environment humidity, and environmental temperature (Wilhelm *et al.*, 2003, Xie *et al.*, 2006). Rayleigh (1978) showed the relationship between the droplet radius and Rayleigh limit (**Eq. 2.1**). The size of the droplet will decrease and the Rayleigh limit for the droplet charge can be reached if evaporation of highly charged droplets occurs. Therefore, droplet fission can take place which subsequently changes the size distribution again.

$$Q_R = 8\pi(\gamma\varepsilon_0 r_d^{\ 3})^{1/2} \qquad \textbf{(Eq. 2.1)}$$

Where Q_R is the Rayleigh charge limit (C), γ is the surface tension (Nm^{-1}), r_d is the droplet radius (m) and ε_0 is the permittivity constant of free space, 8.85 x 10^{-12} F/m.

However, when the electrical charge decreases below the original charge of the droplet, droplet fission occurs to reduce the charge of the individual droplets, resulting in a smaller droplet size and distribution. This is because the Rayleigh charge limit of the charged droplet decreases accordingly. Therefore, when a liquid with specific physical properties such as surface tension and dielectric constant (relative permittivity) is considered, the liquid droplet radius (r_d) decreases during the evaporation process. Changing the properties of the solvents with different evaporation rates can also result in varied morphologies of the final droplets. Berkland *et al*. (2004) showed that specific structural types, such as tapered shapes, porous surfaces, and blood cell-shaped particles could be achieved by varying the solvents and polymer properties (Berkland *et al*., 2004).

2.4.4 The effect of liquid properties

As mentioned above, despite the processing parameters, the modes of EHDA are also influenced by the liquid properties such as surface tension, viscosity, electrical conductivity, relative permittivity, and density (Ganan-Calvo *et al*., 1997, Hartman *et al*., 1999b). The following sections are devoted to the effect of these key physical properties of the liquid on the electrohydrodynamic processing.

2.4.4.1 Surface tension

In order to form the stable cone-jet mode, the electric stresses need to overcome the surface tension (Mora and Loscertales, 1994). Higher surface tension requires a larger electric field in order to electrospray. Once the electric field is higher than the critical value, electrical discharge occurs due to the surrounding air. According to the experimental results obtained by Smith (1986) the onset applied voltage for the stable jet spray increased with increased liquid surface tension (Smith, 1986). However, if the

liquid surface tension is too high, stable electrospraying may not be established because the electric field breaks down in the surrounding gas (Gomez and Tang, 1994).

2.4.4.2 Viscosity

Viscosity is another vital liquid property which plays a significant role in the jet break-up process and its size distribution. Weber (1931) suggested that high viscosity led to increase of droplet size in electrohydrodynamic processing (Weber, 1931). During droplet formation, the high viscosity enhances the damping of the initial oscillations and retains the solution meniscus at the capillary. In addition, viscosity plays a key role in maintaining the primary droplet near spherical shape as detaches from the capillary. Further investigations were carried to study the effect of viscosity on the relic size generated in electrohydrodynamic processing. It was found that increasing the viscosity by over three orders of magnitude in electrohydrodynamic processing has a dramatic effect on droplet and relic sizes (Jayasinghe and Edirisinghe, 2002).

2.4.4.3 Electrical conductivity

Among the properties of liquid, electrical conductivity is the most important physical property for generating the cone-jet mode (Cloupeau and Prunet-Foch, 1989). Sufficient electrical conductivity of the liquid is required to form a conical shape. If the electrical conductivity is too low, the stable cone-jet mode cannot be achieved because there is not enough charge in the liquid. If the electrical conductivity is too high, electrohydrodynamic processing will be impossible due to the corona discharge before attaining the required applied voltage for the stable cone-jet mode formation (Hartman *et al*., 2000). Jones *et al.* (1971) suggested the maximum liquid electric conductivity for a stable electrospray was 10^{-3} Sm^{-1} (Jones and Thong, 1971). Later, Mutoh *et al*.

(1979) found that the stable cone-jet mode could also be achieved when the liquid conductivity was above 10^{-5} Sm^{-1} (Mutoh *et al*., 1979). Cloupeau and Prunet-Foch (1989) suggested that a liquid with too low electrical conductivity cannot be atomized due to lack of tangential electrical stress (Cloupeau and Prunet-Foch, 1989).

2.4.4.4 Density

The viscous force depends on the density of the liquid (Ganan-Calvo *et al*., 1997). Therefore, the density of the liquid also plays a role in determining the jet diameter in electrohydrodynamic processing. When the viscosity and the electrical conductivity of the liquid are high enough, the electrical charge is transmitted efficiently across the jet by viscous forces. However, the liquid density influences the cone shape due to the gravitational force. Especially, if the diameter of capillary is > 1mm, the gravitational force influences the shape of the cone significantly (Hartman *et al*., 1999b).

2.4.5 Processing parameters

The outcomes of electrohydrodynamic processing can be controlled by a range of processing parameters, such as flow rate, applied voltage and the needle-substrate distance. The eventual droplet size and its distribution are directly influenced by flow rate, which may also result in the instability of the cone-jet mode (Hartman *et al*., 1999a). The higher liquid flow rate results in an increase in the diameter of the composite dropt/ relic sizes. In addition, the applied voltage determines the magnitude of the driving force of the EHDA process. It's crucial to change the mode and achieve the stable cone-jet mode. It is also possible to decrease droplet size and size distribution by increasing the applied voltage. However, the distance between needle and ground electrode is also a key factor when a high electrical potential is applied. The change of the needle-substrate distance influences electrical field and the "free

fall" travel distance. Furthermore, the droplet size and morphology can be altered by changing needle-substrate distance due to the degree of the evaporation of the liquid.

2.4.6 Scaling laws

Scaling laws are established to define a relationship of mean droplet size and the parameters involved in electrohydrodynamic processing. It provides better understanding of the mechanisms correlated to liquid physical properties (electrical conductivity, density, viscosity, surface tension and dielectric constant) and liquid flow rate in the process. Initially, for classical EHDA to occur, the hydrodynamic time ($t_h=LD^2/Q$) must be higher than the electrical relaxation time ($t_e=\beta\varepsilon_0/K$) as a condition that should be satisfied to have a steady state cone-jet shape (Ganan-Calvo *et al*., 1997). The electrical relaxation time (t_e) is the time required to smooth a perturbation in the electric charge (Loscertales *et al*., 2002).

$$t_h >> t_e \qquad \textbf{(Eq. 2.2)}$$

$$\frac{LD^2}{Q} >> \frac{\beta\varepsilon_0}{K} \qquad \textbf{(Eq. 2.3)}$$

where L and D are the axial length and the diameter of the jet, respectively, Q is the flow rate, β is the relative permittivity, K is the electrical conductivity and ε_0 is the permittivity of free space (8.854×10^{-12} F m^{-1}) (Ganan-Calvo *et al.*, 1997).

The size of droplets in the electrohydrodynamic processing is of fundamental and practical importance. The size of the droplets produced in the cone-jet mode can be estimated through theoretical analysis. For example, by assuming that the jet diameter

is much smaller than that of the needle (valid for a liquid with relatively high conductivity, 5×10^{-5} Sm^{-1}), Fernandez reported a scaling law for droplet size as a function of the flow rate and liquid properties in the cone-jet mode (Mora and Loscertales, 1994):

$$d = \alpha_1 \left(\frac{Q\varepsilon_0\varepsilon_r}{\gamma_1}\right)^{1/3} \qquad \textbf{(Eq. 2.4)}$$

where α_1 is a constant depending on spray conditions, γ_1 is the liquid conductivity, ε_0 is the permittivity of the free space, ε_r is the dielectric constant of the liquid and Q is the liquid flow rate.

Ganan-Calvo *et al.* (1997) experimentally obtained an equation for droplet size generated in the cone-jet mode:

$$d = \alpha_2 \left(\frac{Q^3\varepsilon_0\rho_1}{\pi^4\sigma_1\gamma_1}\right)^{1/6} \qquad \textbf{(Eq. 2.5)}$$

where γ_1 is the liquid conductivity, ε_0 is the permittivity of the free space, Q is the liquid flow rate, ρ_1 is the liquid density, σ_1 is the surface tension of the liquid and α_2 was assumed to be 2.9.

These scaling laws are widely accepted for a simple prediction of EHDA processing and provide a better understanding of the mechanisms involved in the process. The use of scaling laws for the prediction of relic size is, however, still controversial.

Ganan-Calvo *et al*. (1997) for example, subsequently obtained a different equation for the size of a droplet generated in the cone-jet mode (Ganan-Calvo *et al*., 1997). This is partly because the experimental uncertainty in the analysis of different relics can be very high but also due to the inherent interdependency of the processing variables. In addition, Mei *et al*. (2007) showed that scaling laws cannot fit in because increasing the flow rate of the inner liquid resulted in an increase in capsule size, but the capsule size remained constant for a certain value of the flow rate. However, capsule diameter has also been shown to decrease with an increase in the magnitude of applied voltage, electrical conductivity, viscosity, density and surface tension of the sprayed solution (Mei and Chen, 2007).

2.4.7 Co-axial electrohydrodynamic atomisation

Co-axial electrohydrodynamic atomisation (CEHDA) is an extension of EHDA. A schematic experimental set-up of CEHDA is shown in **Figure 2.20.** Two immiscible liquids or suspensions (T1 Outer Liquid, T2 Inner Liquid) are injected through two concentrically placed needles. These needles are connected to the same electrical potential. Once under a certain voltage and flow rate, a stable cone-jet can be achieved at the exit of needles. The inner liquid is surrounded by the outer liquid concentrically. A liquid thread is issued from the vertex of each one of the two menisci, giving rise to a compound jet of two co-flowing liquids or suspensions. The two concentric liquid threads break-up resulting in an aerosol of relatively monodisperse compound droplets with the outer liquid encapsulating the inner one. However, to obtain a structured cone-jet, electrohydrodynamic forces must act on at least one liquid, either the inner or the outer, although they may act on both (Loscertales *et al*., 2002).

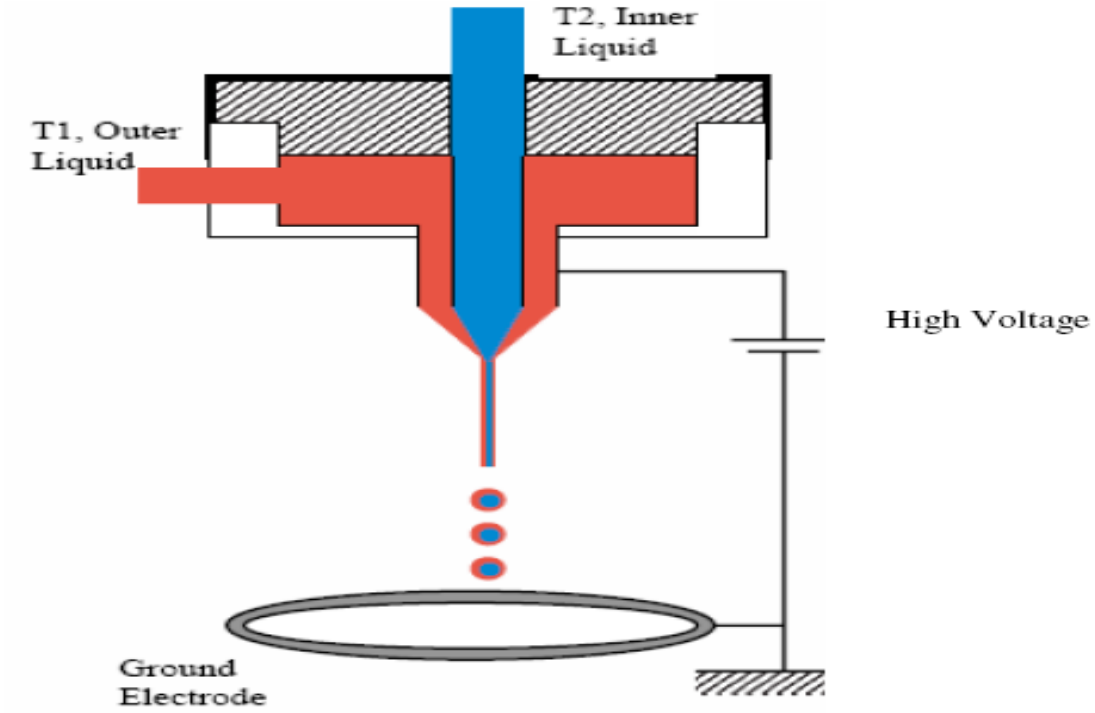

Figure 2.20 Schematic representation of the conventional CEHDA setup (Loscertales *et al*., 2002).

2.4.7.1 Concept of the driving liquid

As mentioned above, theories on cone-jet mode from single-liquid electrospray are particularly important and possesses advantages for micro/nanoscale droplet formation. However, according to the study of Loscertales *et al.* (2002), co-axial electrospraying is influenced by the driving liquid, on which the electrical forces act, i.e. either the inner or outer liquid to form the stable jet (Loscertales *et al*., 2002). This is a steady mode, just as in single-liquid electrospraying. The driving character of the liquids can also be explained by a comparison of its electrical relaxation times ($t_e = \beta\varepsilon_0/K$). If the electrical relaxation time of the inner liquid is much higher than that of the outer one, charges are located at the outer interface and they are supplied to the outer interface much more efficiently from the outer liquid bulk than from the inner one (Loscertales

et al., 2002).

Therefore, co-axial electrospraying can also be divided into two types: the driving liquid is outside and the driving liquid is inside of the jet. When charges are located at the outer interface, the tangential electrical stresses which point towards the vertex of the conical interface must be efficiently transmitted throughout the liquid bulk by viscous force at the liquid-liquid interface. This suggests that the viscosity of the either outer or inner liquid plays an important role in the liquid motion. Moreover, the electrical forces only act on the free surface of the meniscus and lead to the establishment of the stable jet. Then, the jet breaks into droplets with a small standard deviation. Both liquids, outer and inner, flow steadily with the same velocity due to intense re-circulations in the electrified meniscus. However, different mechanisms lead to the formation of cones for outer and inner liquid, which are electric shear stresses and viscous stress, respectively. In forming the jet, artificial additives can be used to increase viscosity and electrical conductivity of the liquids in order to satisfy the formation of a stable jet of the driving liquid (Lopez-Harrera *et al*., 2003).

2.4.7.2 Scaling law of co-flowing liquids

Several pairs of liquids have been used to explore the influence of liquid properties on the co-axial spraying process. Basically, the theory mentioned in **Section 2.4.6** that governs EHDA also applies to the co-axial system. As same as in single-liquid electrospraying, when two immiscible liquids are injected at appropriate flow rates through two co-axial needles, the menisci of both liquids adopt conical shapes with an outer meniscus surrounding the inner one. The liquid threads which issue the concentric layered jet eventually break up into an aerosol with the outer liquid encapsulating the inner one. However, the flow rate used in the equations must be that

of the driving liquid. Droplet size is dependent on the liquid viscosities and on the ratio of the liquid flow rates (Lopez-Harrera *et al*., 2003).

2.4.8 Microencapsulation by electrohydrodynamic atomisation

EHDA processing is an attractive method for preparing particulate polymeric drug carriers with sizes ranging from several tens of nanometres to ~100 micrometres. A variety of materials such as BSA, paclitaxel, taxol, insulin, lysozyme, or human antibodies were used as core material encapsulated within a polymeric matrix (e.g. polyethylenoxide, dextrose, starch, sucrose, PLGA, PCL, PEO, or lactose). Berkland *et al.* (2004) showed that specific structural types, such as tapered shapes, porous surfaces, and blood cell-shaped particles, could be achieved by varying the properties of the polymer solution (e.g. PCL, PLGA, and PLA) and solvents, as shown in **Figure 2.21** (Berkland *et al*., 2004). Ding *et al.* (2005) reported that monodispersed taxol-loaded PLA and PCL was prepared by EHDA and showed this method is a potentially suitable technique to prepare near- monodisperse drug particles (Ding *et al*., 2005). Xie *et al.* (2006) reported that biodegradable polymers encapsulating paclitaxel as an anticancer drug carrier can be prepared using EHDA. The shapes of polymer carriers such as spheres, doughnut shapes, silk, and corrugated shapes with different sizes for controlled release applications were generated in this way (Xie *et al*., 2006).

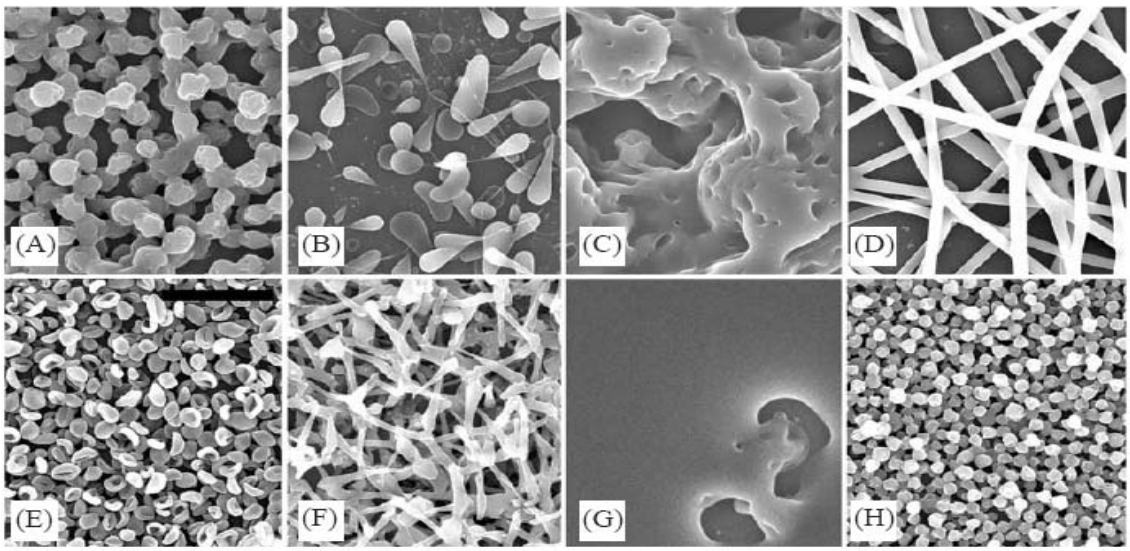

Figure 2.21 Structures produced using precise control of electrospraying including (A) melded spheres, (B) tapered spheres, (C) porous surface, (D) fibres, (E) blood cell-shaped particles, (F) net, (G) smooth surface, and (H) distinct particles (Berkland *et al*., 2004)

Co-axial electrohydrodynamic atomisation (CEHDA) was recently further developed as an encapsulation technique for biomedical applications. It facilitates encapsulation of sensitive core materials, for example, cells, enzymes or drugs in a protective shell. A range of polymeric materials including polyurethanes, polysiloxanes, polylactides (PLA), polyglycolides (PGA), poly(lactide-co-glycolides) (PLGA) have been used as the encapsulating shell on account of their desirable physical properties such as elasticity, electrical insulation, physical strength, and freedom from leachable impurities. Pareta and Edirisinghe (2006) showed that starch/bovine serum albumin (BSA) microspheres coated with polydimethylsiloxane (PDMS) can be prepared using CEHDA for sustained controlled release (Pareta and Edirisinghe, 2006). Work by Xie *et al.* (2008) reported the preparation of particles encapsulating BSA and lysozyme in a biodegradable polymer with diameters in the range of 1-10 μm. Significantly, the bioactivity of released

lysozyme reached higher levels than those previously reported using other preparation methods (Xie, 2008). Similarly, Farook *et al.* (2008) reported in-situ preparation of liquid-filled polymer microspheres. The microbubbles were collected in a vial of distilled water and they rapidly converted into polymer-shelled microspheres for liquid drug encapsulation (Farook *et al*., 2008). In addition, co-axial electrospraying producing oligodeoxynucleotide encapsulated lipoplex nanoparticles for either intravenous injection or pulmonary delivery has been demonstrated. The diameter of particles was about 190 nm and the particles provided an efficient medium for gene delivery (Wu *et al*., 2009).

Electrohydrodynamic atomisation (EHDA) is an attractive method for preparing particulate polymeric carriers with sizes ranging from several tens of nanometers to ~100 μm for the pharmaceutical, cosmetic and food industries, as well as several other technological fields. However, despite its versatility and growing popularity, the question as to whether EHDA can be used as a 'one-step' forming technique to produce new polymeric drug carriers (e.g. hollow and monoporous hollow capsule,) with predetermined characteristics remains unanswered. Moreover, the development of stimuli-responsive drug delivery system by using EHDA without relying on a smart polymer is limited.

Therefore, the objectives of this study were to demonstrate the fabrication of hollow and monoporous hollow polymeric capsules by EHDA and to determine the effect of individual processing parameters upon the capsules characteristics. In addition, a new responsive drug delivery systems independent of the action of smart polymers based on both temperature and ultrasound stimuli was investigated. A drug delivery system that allows real-time of release dosage according to the therapeutic treatment is extremely

important in clinical applications. However, compared with other methods described in the literature, this research offers a novel forming mechanism for capsule production, which not only makes the process of hollow polymer capsule generation more efficient, but also avoids the need for subsequent template removal by calcination or chemical solution. Similarly, the method proposed here does not require a separate shell-forming step, which further avoids the use of surfactants or other additives. Hence this work opens new insights to extend capabilities of the EHDA technique and offers significant potential benefits for drug delivery applications and the design of stimuli-responsive systems.

Chapter 3

Experimental details

3.1 Introduction

This chapter describes the details of materials, apparatus, equipment, software and methodologies used in this research. The characterization of materials is described appropriately. A detailed description about the accessories and equipment used in co-axial electrohydrodynamic processing is also given. Finally, the experiments conducted to characterise the capsules obtained are also discussed.

3.2 Materials

The main materials used in the experiments were polymethylsilsesquioxane and perfluorohexane. Other subsidiary materials used were ethanol and distilled water, while Evans Blue dye and other drugs were used as markers to study the capabilities of the drug carriers.

3.2.1 Polymethylsilsesquioxane

Polymethylsilsesquioxane, PMSQ, (MK powder, density 1240 kg m^{-3}, Wacker Chemie AG, Germany), was used as a main ingredient in this investigation. This polymer is a preceramic polymer and can be pyrolysed directly to make ceramic (SiO_C) (Nangrejo *et al.*, 2008). One reason for using PMSQ is that it is a basic material for a variety of biomedical applications, such as particle, fibre, and film fabrication (Colombo, 2008, Ahmad *et al*., 2009). Its inherent properties, e.g. non-toxicity, hydrophobicity, chemical stability and inactivity, and desirable physical properties such as high degree of thermal

stability and good forming properties have also gained PMSQ wide pharmaceutical applications in drug delivery matrices (Ye *et al*., 2010). In addition, this material has been used *in-vivo* on account of its bio durability and biocompatibility for several decades (Zhuo *et al.*, 2005).

3.2.2 Perfluorohexane

Perfluorohexane, PFH, ($C_6F_{14,}$ F2 Chemicals Ltd., Lea, UK.) is a fluorinated aliphatic compound and is considered biologically inert and chemically stable (Díaz-López *et al.*, 2010). Perfluorocarbon physical properties are determined by the length of the perfluorinated carbon chain wherein all hydrogen atoms in the molecule are replaced with fluorine atoms (Babiak *et al.*, 2008). Small chain species are gases, while these containing larger chains are liquids denser than water (**Figure 3.1**). Carbon-fluorine linkage provides unique properties (**Table 3.1**) that make it attractive for *in-vivo* medical applications such as burnt lung treatment, drug targeting (Lehmler *et al*., 1999, Riess, 2002). Among these, its low boiling point is ~57 °C, and it is odourless and colourless. It possesses high oxygen solubility, low surface tension, hydrophobicity and lipophobicity, inertness and absence of metabolism and these are the most interesting characteristics for their use in clinical applications (Riess and Kra, 1998).

However, as perfluorohexane has low solubility in water, biological fats and lipids, surfactants and other additives are indeed involved in all stages of preparing stabilized droplets. However, presently a number of challenges, such as uniformity of the emulsion droplets and toxicity issues associated with the use of stabilizing surfactants prevail (Heuschkel *et al*., 2007, Sivakumar *et al*., 2009).

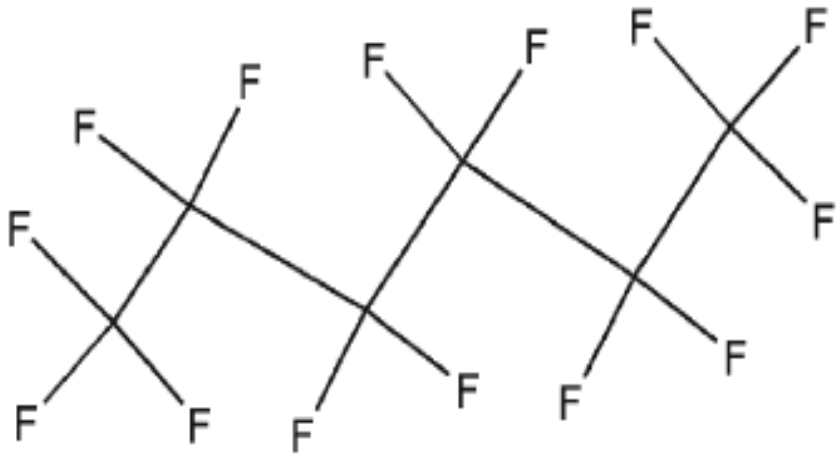

Figure 3.1 Chemical structures of perfluorohexane liquid (Díaz-López *et al.*, 2010)

Table 3.1 Properties of perfluorohexane (Kornmann *et al*., 2008, Couture *et al*., 2006)

Low surface tension (12 mNm^{-1})
Low viscosity (1.1 mPa s)
High density (1.76 g/ml)
Stable
Low diffusion rate
Low solubility in water, biological fats and lipids
Inert
High gas (O_2 and CO_2) solubility

3.2.3 Ethanol

Ethanol (research grade, C_2H_5OH, density 790 kg m^{-3}, molecular weight 46, electrical conductivity $3.4x10^{-5}$ Sm^{-1}, viscosity 1.3 mPa s, surface tension 23 mN m^{-1}, BDH Laboratory Supplies, UK) was used as the solvent medium for the preparation of polymer solutions. In addition, ethanol was also used to calibrate the characterization apparatus and as a cleaning liquid for the capillary needles which were the vital components of the experimental set-up.

3.2.4 Evans blue dye

Evans Blue dye (dye content 85%, molecular weight 960.81, Sigma-Aldrich, Poole, Dorset, UK) is a soluble marker and its UV absorption (λ_{max}) has a peak of ~607 nm. Evans Blue dye was used as a model marker to study the capability of the drug carriers in the investigations described in **Chapters 4, 5 and 6** as experimentally verified release profiles in previous studies have shown it to be in accordance with established drug release models (Pancholi *et al*., 2009). In addition, Evans Blue dye is also known as a relevant marker *in-vivo* to studies of permeability in a hepatoma of a rat and vascular extravasation in excised tissue (Bekeredjianlow *et al*., 2007, Böhmer *et al*., 2010).

3.2.5 Aspirin

Aspirin (≥99%, molecular weight 180.16, Sigma-Aldrich, Poole, Dorset, UK), also known as acetylsalicylic acid, is a typical anti-inflammatory drug, often used as an analgesic to relieve minor aches and pains and as an antipyretic to reduce fever (Das *et al.*, 2005). Aspirin is a soluble drug, which is widely available and cost-effective. Aspirin was used in the characterization of stimuli-drug release systems to help examine the influence of different molecular weights on release behaviour in the investigations described in **Chapter 6**. It is one of the series of drugs used to accommodate a range of molecular weights depicted in **Table 3.2**.

3.2.6 Lactoflavin

Lactoflavin (≥98%, molecular weight 376.36, Sigma-Aldrich, Poole, Dorset, UK), also known as Vitamin B2, plays important roles in energy metabolism and is required by the body to use oxygen and in the metabolism of amino acids, fatty acids and

carbohydrates. Lactoflavin is used for red blood cell formation, antibody production and cell respiration and growth. In humans, symptoms of lactoflavin deficiency include cracked and red lips, inflammation of the lining of mouth and tongue, mouth ulcers, cracks at the corners of the mouth, sore throat etc (Graham *et al.*, 2005). Lactoflavin was used in the characterization of stimuli-drug release systems to help recognize the influence of different molecular weights on release behaviour in the investigations described in **Chapter 6**. It is one of the series of drugs used to investigate a range of molecular weights, as depicted in **Table 3.2**.

3.2.7 Cyanocobalamin

Cyanocobalamin (≥98%, molecular weight 1355.37, Sigma-Aldrich, Poole, Dorset, UK) is a water-soluble drug; its primary functions are the formation of red blood cells and the maintenance of a healthy nervous system. Cyanocobalamin is an important micronutrient for therapeutics and is necessary to process folic acid. Deficiency of cyanocobalamin can lead to pernicious anaemia due to failure of red blood cell formation (Marley *et al.*, 2009). Bacteria, fungi, algae and virtually all types of meat and dairy products are found to be important resources of cyanocobalamin. Cyanocobalamin was used in the characterization of stimuli-drug release systems to help recognize the influence of different molecular weights on release behaviour in the investigations described in **Chapter 6**. Once again, it was one of the series of drugs used in the molecular weights investigation (**Table 3.2)**.

Table 3.2 Properties of Evans Blue dye and other drugs

Drug and material	Molecular fomula	Molecular weight (Da)	UV abs. peak (nm)
Evans Blue dye	$C_{34}H_{24}N_6Na_4O_{14}S_4$	960.81	607
Aspirin	2-$(CH_3CO_2)C_6H_4CO_2H$	180.16	270
Lactoflavin	$C_{17}H_{20}N_4O_6$	376.36	361
Cyanocobalamin	$C_{63}H_{88}CoN_{14}O_{14}P$	1355.37	445

3.3 Preparation of solutions

3.3.1 Polymer

For the investigations described in **Chapters 4, 5, and 6**, a polymethylsilsesquioxane solution of 63 wt. % polymer was prepared in a conical flask by dissolving it in ethanol at the ambient temperature (22 °C) via magnetic stirring to ensure full miscibility of the polymer. This parent-solution was subsequently diluted to prepare solutions containing 36, 27 and 18 wt. % polymer. The contents of polymer and ethanol in the remaining solutions were calculated just before diluting the solution by further addition of ethanol.

3.3.2 Perfluorohexane

For the investigations described in **Chapter 4, 5, and 6**, a perfluorohexane solution was used as received.

3.3.3 Evans blue dye and drugs

The Evans blue dye solutions were prepared by adding 0.005, 0.01, 0.015, 0.02, 0.025, and 0.04g of Evans blue dye to 200 ml of distilled water to give concentrations of 0.025,

0.05, 0.075, 0.1, 0.125, and 0.20 mg/ml, respectively. Similarly, high concentration of Evans blue dye and other drugs such as of aspirin, lactoflavin, and cyanocobalamin were prepared by following the same protocol by dissolving in distilled water separately to give different concentrations for investigation of controlled release.

3.4 Characterisation of liquids and solutions

3.4.1 Density

The densities of the liquid/polymer solutions were determined by using a 25 ml standard density bottle (VWR International, Lutterworth, UK) at ambient temperature and pressure conditions. The mass of the empty bottle and the mass of the bottle filled with liquid/polymer were obtained using an electronic balance (A&D - GR-300 - Analytical Balance, Leicester, UK) which was capable of giving precise values of up to four decimals. The mean value of the density of liquid/polymer solution was taken from five consecutive calculations as reported in this thesis. The density bottle and procedure was calibrated using ethanol. The density was calculated by equation 3.1.

The density of liquid/solution (D) = $(W_2-W_1) / V$ (**Eq. 3.1**)

Where W_1 is the weight of the empty density bottle, W_2 is the weight of the density bottle filled with liquid/solution, and V is the bottle volume.

3.4.2 Electrical Conductivity

HI-8733 (Hanna Instrument, USA) conductivity probe, which consists of a control panel and a conductivity probe, was used to measure electrical conductivity. The control panel provides selection of suitable measurement ranges and the probe with two electrodes is used to measure liquid conductivity. The measuring range of this

meter is 0.0 to 1999 / 0 to 19990 μS/m and 0.00 to 199.9 / 0.0 to 1999 mS/m, respectively. The measurements were performed using 30 ml of liquid in a beaker and the electrode was kept immersed in the solution up to the correct length of the electrode for 300s and the reading shown on the control panel was recorded. All measurements were carried out at the ambient temperature and the probe was always cleaned with distilled water and dried before measurement. The mean value of five consecutive readings was taken as the electrical conductivity of the sample.

3.4.3 Viscosity

For the determination of viscosity of different concentrations of polymer solutions, different methods were appropriately used. A U-tube viscometer (BS/U type, Schott Instruments GmbH, Germany) was used to determine dynamic viscosity of less viscous fluids such as ethanol etc, while the VISCOEASY rotational viscometer (CamLab Ltd, Cambridge, UK) was used for "thicker" fluids such as a high concentration of polymer solution etc. The dynamic viscosity was determined using the instructions provided in the operation manual of this equipment.

3.4.3.1. Determination of viscosity using U-Tube viscometer

U-tube viscometer (size C, nominal constant 0.03) was used to determine viscosity of 18, 27, and 36 wt. % polymer suspensions. This was determined by measuring the time (t) taken by the samples to pass through from upper region to the lower region in the U-tube viscometer. The time was recorded using a stop watch with 0.01 second accuracy and the mean value of the time (s) was calculated from five experiments. The kinematic viscosity is calculated by multiplying the viscometer constant (C) with the time (t).

$$\nu = Ct \qquad \textbf{(Eq. 3.2)}$$

Then, the dynamic viscosity (η) was then calculated by multiplying the kinematic viscosity by the density (ρ) of the suspension:

$$\eta = \nu\rho \qquad \textbf{(Eq. 3.3)}$$

If equations (3.2) and (3.3) are combined,

$$\eta = Ct\rho \qquad \textbf{(Eq. 3.4)}$$

Ethanol was used to calibrate the viscometer. The mean value of five readings was taken as the dynamic viscosity of the sample. The calibrated value is also essential for U-tube viscometers as the viscosity value cannot be calculated without comparison with another liquid. However, due to the high concentration of polymer suspension, it was not possible to use the U-tube method to determine viscosity of 63 wt. % polymer solution as the suspension seemed to block the fine capillary.

3.4.3.2. VISCOEASY rotational viscometer

For the determination of viscosity of 63 wt. % polymer solution, a VISCOEASY rotational viscometer was used. An appropriate spindle was selected and viscosity measurement was obtained with reference to the rotational speed of the spindle inside the suspension, which also gives an estimate of its accuracy based on torque required to turn an object in a fluid. At a rotational speed of 100 rpm, the viscosity of the polymer solution was measured. Five consecutive readings were taken and a mean value was obtained in each case.

3.4.4 Surface tension

Kruss Tensiometer K9 (Standard Wilhelmy's plate method) was used to measure surface tension of the liquids and polymer solutions. The probe (a plate) was hung on the hook and the beaker containing the sample was placed on the stage. The probe was completely immersed into the sample and was gradually lifted. The surface tension value was directly measured as the probe was just about to detach from the liquid surface, which provide a maximum force referred to the surface tension. Generally, 100 ml liquid was used for this measurement using a 150 ml beaker, which is sufficient to fully immerse the probe. In order to minimize errors, the "lifting force" was applied gradually and the probe was cleaned thoroughly and dried in a drier before each measurement. The mean value of five readings was taken as the surface tension of the sample.

3.5 Experimental set-up and equipment

The basic experimental set-up used for electrohydrodynamic atomisation processing consists of a co-axial needle, infusion pump, power supply and electrode, as shown in **Figure 3.2**. The experimental designs and the specification of each facility used are given below in detail. The co-axial needle is connected to the power supply and also connected to a syringe, which is fixed on a syringe pump to control the flow rate. 10 ml and 5ml volume capacity syringes were separately connected to the inner and outer needles using silicone tubing. The inner stainless steel needle was supplied with perfluorohexane, whilst polymer solution was introduced through the outer needle. The distance from the exit of the outer needle to the ground electrode (the working distance) was set at a range of values to achieve a size distribution in the studies. A high speed camera (600 frames per second) equipped with an optical light source was used to observe the jet and record the data of the spraying region. The applied voltage on the

needle was adjusted and the flow rate was controlled in order to achieve a stable jet during electrohydrodynamic spraying. At a specific flow rate, the stable jet was achieved within a range of applied voltage. Thus, the relationship between the applied voltage and flow rate for the suspension jetting was studied to investigate the optimized processing conditions.

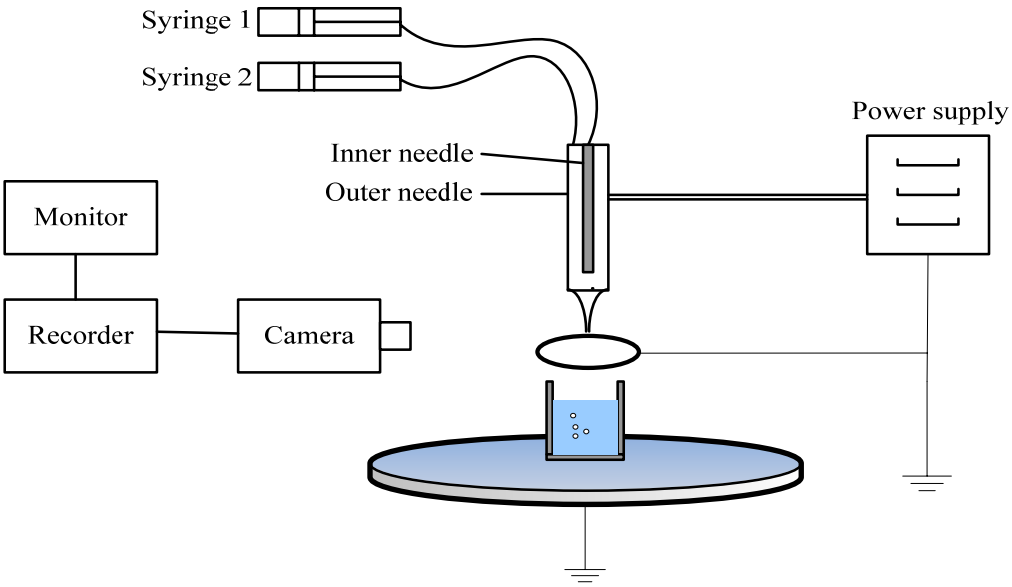

Figure 3.2 Schematic representation of the experimental set-up used for co-axial electrohydrodynamic atomisation

3.5.1 Needle configuration and ground electrode

The co-axial needle used for novel capsule generation was made up of an inner stainless steel needle (inner diameter 150 μm and outer diameter 300 μm) carrying the perfluorohexane flow (Liquid 1) surrounded by an outer stainless steel needle (inner diameter 685 μm and outer diameter 1100 μm) carrying the polymer solution (Liquid 2) (**Figure 3.3**). Both needles were designed with screw and thread type in order to prevent leakage of solution during the application of high pressure. The tip of the inner

needle was positioned ~2 mm inside the outer needle in order to allow the perfluorohexane to be encapsulated by polymer solution. A ring electrode (inner diameter 15 mm and outer diameter 20 mm) was placed below the tip of the outer needle as shown in **Figure 3.2.** The electric stress is determined by the electric field between the co-axial needle and the ground electrode configuration.

3.5.2 High voltage power supply

The needles and the ground electrode were connected to a high voltage DC power supply unit (FC30 P4, Glassman Europe Limited, Bramley, UK) using a high voltage power cable. The output voltage range of the power supply is 0-30 kV and the range of output current is 0-4 mA. The minimum resolution of output control is 0.1 kV. The operating temperature can vary from -20°C to 50°C. However, in this study, the work was carried at ambient temperature at all times.

3.5.3 Infusion pumps

In all the electrohydrodynamic experiments carried out in this thesis, the inner needle and the outer needle were connected to plastic syringes (BD Plastic^{TM}, VWR, Lutterworth, UK) containing the liquid or polymer solution. The flow rates of the liquid and the polymer solution through the needles were controlled by high precision Harvard syringe pumps (Infuse/withdraw PHD 4400 programmable syringe pump, Harvard Apparatus Ltd., Edenbridge, UK). Basically, it is a microcontroller that can provide a precision displacement. The motor drives a lead screw and a pusher blocker. Several operations, which include the infuse/defuse mode transformation, the syringe mode selection and the flow rate value, can be selected via the operation keypad. The capacity of the syringes used for the inner liquid and the outer solution were 10 ml and 5 ml, respectively.

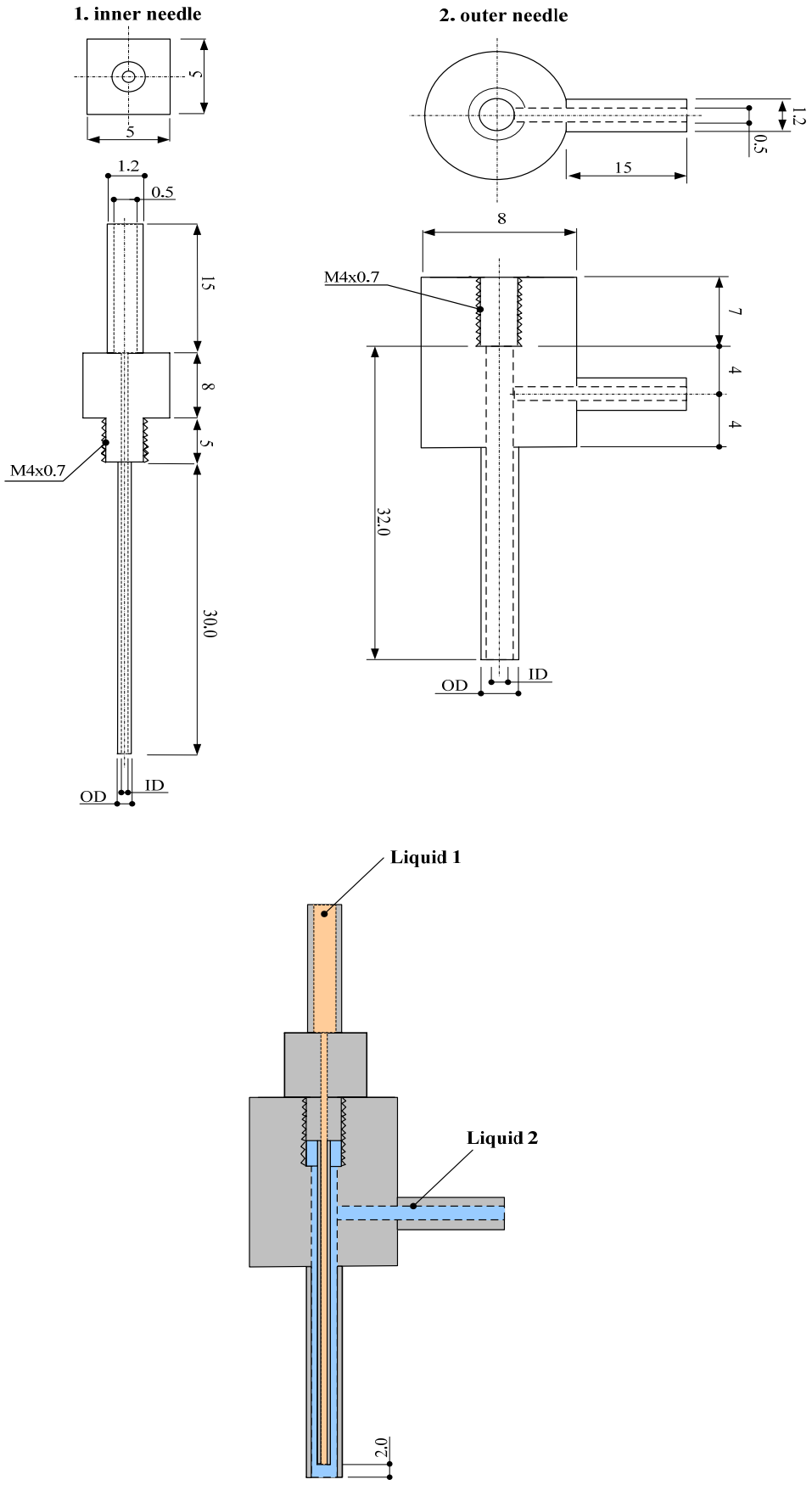

Figure 3.3 Dimensions configuration of the co-axial needle device

3.5.4 Data recording system

A LEICA S6D JVC-colour video camera was used to observe the spraying region and the flow of liquids exiting the needles. The camera contains a high-end CMOS sensor which can record ultra-high-speed frames. The lens on the camera allows focusing on objects down to a few micro meters from a distance of approximately 50 mm. The captured signal passes through a data DVD video recorder MP- 600 using a CDV Recorder/Editor DN-100 with a video screen for real time monitoring.

3.6 Thermal treatment

Temperature stimulated encapsulation and release were carried out using a hot plate (RCT basic IKAMAG®, Staufen, German) which could go up to a maximum temperature of 330°C, as shown in **Figure 3.4**. The heat-treatment programme of the capsules was followed throughout the thesis and was monitored using a thermometer, indicating precision resolution at 0.1°C. The capsules were stored in 20 ml of distilled water/ phosphate buffer solution and heated to a predetermined temperature (37, 45, 57 and 75 °C) for various time intervals (300, 1800, and 3600s) for controlled encapsulation and release.

3.7 Ultrasound treatment

Figure 3.5 schematically illustrates the set-up of ultrasound treatment experiments. The capsules were subjected to ultrasound treatment using a 20 kHz low-frequency ultrasonic processor (S-250A, Branson Ultrasonics Corporation, Danbury, USA) set at different controlling parameters. Ultrasound irradiation was conducted at varying exposure durations (from 0 to 600 s), duty cycles (from 30 to 90 %), and output levels. The ultrasonic probe (13 mm in diameter) was immersed in a glass vial containing 20 ml of the capsule suspension. The distance between the ultrasound probe and the bottom of

the vial is 35 mm. A custom-made ice bath was fitted on the wall of the vial in order to reduce the possible effect of heat-induced by absorption of ultrasonic waves in the aqueous medium. The temperature was monitored throughout the experiment.

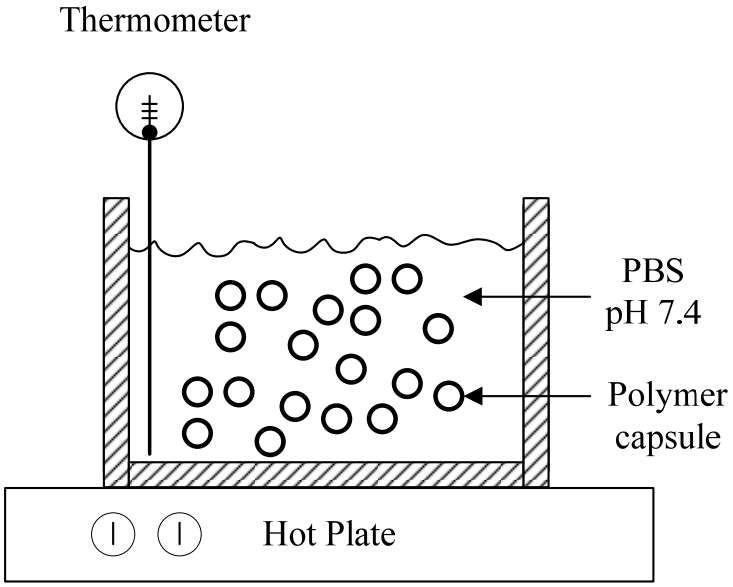

Figure 3.4 Experimental set-up for temperature treatment

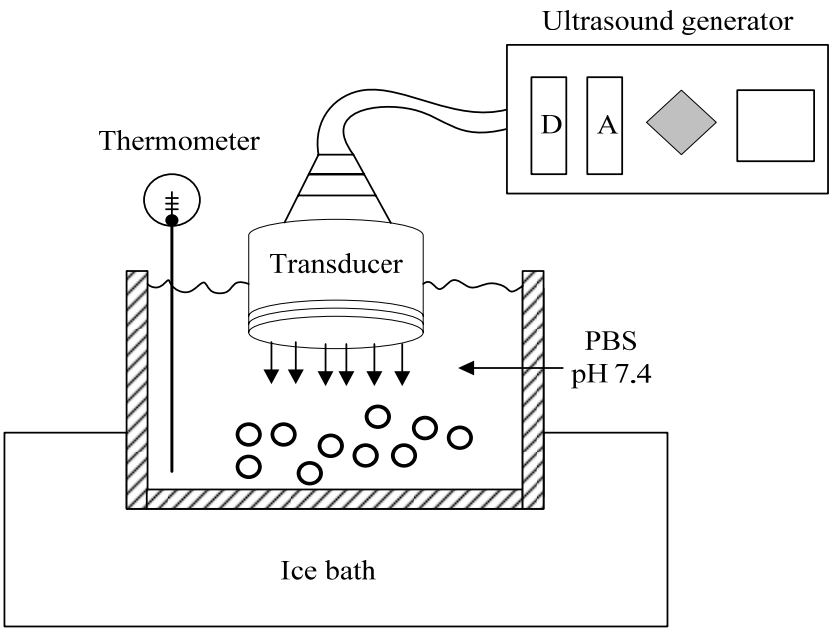

Figure 3.5 Experimental set-up for ultrasound treatment

3.8 Characterization of capsules

To gain insight or specific information of the system various techniques are needed. The capsules prepared during investigations described in **Chapters 4, 5 and 6** were analyzed using a combination of the optical microscopy, scanning electron microscopy, fourier transform infrared spectroscopy and UV-Vis measurements. Some methods give surface and morphology information, while other methods allow an in depth study of the system. Combining the knowledge gained from all the measurements with one another gives a better understanding of the whole system. The principles and layout of the methods used in this work are described in the following sections.

3.8.1 Optical microscopy

The optical microscope (Nikon Eclipse ME 600, Nikon, Japan) was extensively used for all investigations described in the following chapter. In each observation, shape and size of the relics collected from a 1 ml sample of capsules/ hollow suspensions were taken on a microscopic glass slide. The microscope is equipped with an incident light illuminating unit in which the light can come from either side of the specimen with variable optical strengths. There are five objectives equipped in this microscope (5×, 10×, 20×, 50× and 100×). The sizes of the obtained structure from optical microscopy were measured using standard Image-Pro Plus software (Media Cybermatics, L.P.Del Mar, CA, USA).

3.8.2 Scanning electron microscopy

Scanning Electron Microscopy (SEM) is an important method of capsule characterisation. It provides an overall picture of capsule size and morphology (as-formed products). A field emission scanning electron microscope (FE-SEM, JEOL

Ltd., Herts, UK) was used to characterize the surface morphology and shell thickness of the microcapsules. This instrument is equipped with an emitter that can achieve a resolution of ~ 1.5 nm. In all experiments, the accelerating voltage and the working distance between the emitter and the sample were kept at 5 kV and 19 mm, respectively. 1 ml samples of the microsphere were collected and put on glass slides for drying for 48 hours in a desiccator under ambient conditions before SEM analysis. In order to get the thickness and morphology of the capsule shells the dried microspheres were sectioned using a scalpel blade (No. 21, VWR International Ltd) at ambient temperature without embedding in any polymer. Since the polymer used for the microcapsules is an insulator, the glass slides with dried capsules were gold coated for 90s using a sputtering machine (Edwards sputter coater S150B). The sample was then fixed on a conductive stub using a carbon sticker and was placed in the SEM chamber to prevent charging of the sample surface during analysis. All measurements on the micrographs were carried out using IMAGE-PROPLUS software (Media Cybernetics, L.P. Del Mar, CA, USA).

3.8.3 Characterization of material composition

The compositions of the prepared capsules were evaluated by Perkin Elmer System 2000 Fourier transform infrared (FTIR) spectrometer (PerkinElmer Life and Analytical Sciences, Inc., Wellesley, USA). Fourier transform infrared spectra were obtained using the standard KBr pellet technique. Microcapsules were milled with potassium bromide in the ratio of 1:5 to form a very fine powder. This powder is then compressed into a thin pellet by a hydraulic press to give a hard clear white disc. The resulting disc was then placed carefully (to avoid cracking or breaking of the disc) in a holder which was subsequently positioned in the sample compartment of the infrared spectrometer. KBr is also transparent in the IR. All spectra were obtained after KBr background subtraction.

Each spectrum was collected by cumulating 30 scans.

3.8.4 Determination of the temperature of release medium

In order to examine the temperature of release medium, a thermometer was used in all experiments throughout the thesis. The temperature or temperature gradient is recorded when the value of the measurement of temperature is stable. The temperature range is from 0.0 to 90 °C with a accuracy of ±0.1°C.

3.8.5 Determination of the amount of PFH in polymeric structure

In order to evaluate the perfluorohexane loading, a sample of perfluorohexane loaded microcapsules were sprayed onto glass slides and weighed using an analytical balance (A&D - GR-300 - Analytical Balance, Leicester, UK). The analytical balance has a high resolution of 0.0001g and a standard deviation of 0.0001g. This sample was then heated to 75 °C for 1800s to evaporate the encapsulated PFH and was re-weighed after cooling to the ambient temperature when no further mass loss (evaporation) was noted. The PFH content was defined as the ratio of actual amount of PFH encapsulated in PMSQ and the actual weight of the capsules.

$$\text{PFH content (\%)} = \frac{\text{actual weight of PFH loaded into the capsules}}{\text{actual weight of capsules}} \times 100 \qquad \textbf{(Eq. 3.5)}$$

3.8.6 Determination of ultrasound power

The total power of the ultrasound was determined as described by Fay and Binker (1996). Theoretical analysis shows that temperature increase induced by absorption and scattering is precisely proportional to the power of the incident ultrasonic wave, and the absolute value of the ultrasonic power can be determined when the heat

conductivity and acoustic absorption coefficient of the absorber material used are known in the frequency range up to 14 MHz (Fay and Binker, 1996). Therefore, a commonly used calorimetric method was performed to calculate the power delivered by the sonicators based on the change of temperature in water although output level can be controlled by the processor used (Liu et al., 1998). The rate of increase of liquid temperature was measured and used to calculate the intensity using the equation described below (**Eq. 3.6**). Assuming that all of the temperature change of a liquid exposed to the ultrasound was due to incident acoustical power, and all the acoustical power was converted into heat. The following equation can be used to relate power to temperature rise:

$$I = \frac{mC_p}{A}\frac{\Delta T}{\Delta t} \qquad \textbf{(Eq. 3.6)}$$

Where I is the ultrasound intensity, m is the mass of medium exposed, C_p is the specific heat, $\Delta T/\Delta t$ is the rate of temperature change, and A is the transducer area.

3.8.7 *In-vitro* drug release measurements

UV/Vis Spectroscopy is a class of spectroscopy that can be used to measure drug release by assessing the absorbance of a substance in the UV/Vis range. The absorbance (A) is defined as the log of the intensity of incident light (I_0), divided by the intensity of the light after passing through the sample (I). The concentration (C) of the substance and the pathlength (l) through the sample and the molar extinction coefficient (ε) are related by the Beer-Lambert law, as shown in equation **3.6**. For each species and wavelength, ε is a constant known as the molar absorptivity or extinction coefficient.

$$A = \log_{10} \frac{I_0}{I} = Cl\varepsilon \qquad \textbf{(Eq. 3.7)}$$

Typically, the drug release study was carried out in 20 ml of phosphate buffer (pH 7.4) while stirring at 100 rpm in a flask. The temperature of the suspension was kept at 37 ± 0.5 °C. At designated time intervals, the vial was taken out and centrifuged at 4000 rpm for 1800s. The resulting supernatants were directly analyzed by UV spectroscopy at a wavelength corresponding to maximum absorption. The quantities of drug in the capsules were estimated by determining the difference in drug concentration in the suspension before and after release using an ultraviolet spectrometer (UV-2401PC spectrophotometer, Shimadzu, Japan). The concentration of drug in the supernatant was determined by UV absorption referred to a standard curve. After each measurement, the release medium was replaced using fresh solution to maintain ideal sink conditions. Calculation of the corrected concentration of released molecules is based on the following equation (Fisher *et al*., 2003):

$$C_{tcorr} = C_t + \frac{v}{V}\sum_{0}^{t-1} C_t \qquad \textbf{(Eq. 3.8)}$$

Where C_{tcorr} is the corrected concentration at time t, C_t is the apparent concentration at time t, v is the volume of sample taken and V is the total volume of dissolution medium. The loading efficiency was defined as the ratio of the actual to the theoretical amount of molecules encapsulated in the polymer shell:

$$\text{Loading efficiency (\%)} = \frac{\text{actual amount of drug loaded in the capsules}}{\text{theoretical amount of drug loading in the capsules}} \times 100 \quad \textbf{(Eq. 3.9)}$$

The kinetics of the release from polymeric carriers has been examined by using the Higuchi model (Peppas, 1985). According to this model, the release of a drug from an insoluble, porous carrier could be described as a square root of a time-dependent process based on Fickian diffusion. The release data were evaluated using the Higuchi model, which could be described by the following equation:

$$Q = K_H\, t^{1/2} \quad \textbf{(Eq.3.10)}$$

Where Q is the amount of dye released in time t and K_H is the Higuchi dissolution constant. Error bars represent the standard deviation from three experiments for all release experiments.

Chapter 4

Electrohydrodynamic atomisation as a novel approach for the preparation of hollow capsules

Hollow capsules play an important role in microencapsulation and have been used in medical, biological, pharmaceutical and other industrial applications. The importance and preparation of hollow capsule were discussed in the literature review. However, as discussed in the literature review, the processing methods currently used to produce hollow capsule involve complicated and multiple manufacturing steps, normally requiring surfactants or amphiphilic polymers to increase kinetic stability. This chapter investigates the feasibility of using the co-axial electrohydrodynamic atomisation (CEHDA) process to produce hollow capsules for controlled release applications. The aims of this investigation were: firstly to determine whether hollow capsules could be successfully fabricated in the absence of processing additives by using co-axial electrohydrodynamic atomisation; secondly, to assess the feasibility of controlling the diameter (D) and shell thickness (t) of the capsules and ratio D:t (α) in order to achieve an understanding of the effect of individual processing parameters (**Figure 4.1**); thirdly, to examine the capability of hollow capsules made by CEHDA for controlled release applications. This study forms the foundation for the further development of stimuli drug delivery techniques described in **Chapters 5 and 6.**

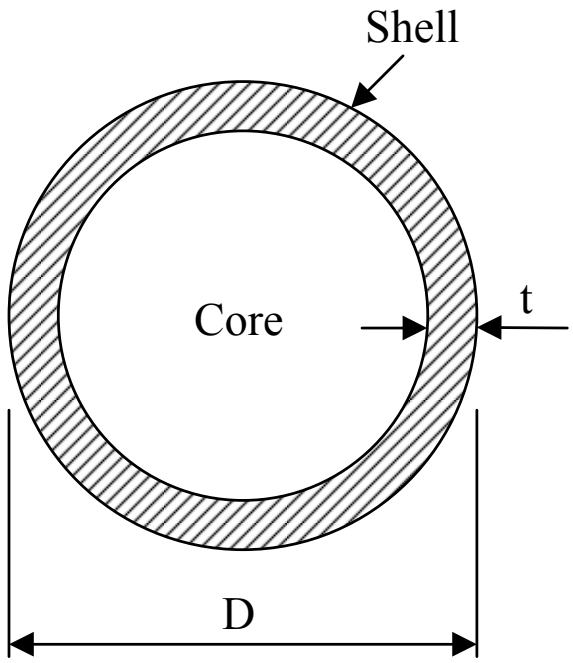

Figure 4.1 Illustration of hollow capsule and its dimensions

4.1 Characteristics of processing liquids

It is known that the size of the capsules obtained via CEHDA is influenced by the viscosity, density, electrical conductivity and surface tension of the encapsulated and encapsulating materials, as well as the processing conditions. Ethanol is a well known liquid to achieve a stable jet in electrohydrodynamic atomisation (Grace and Marijnissen, 1994), and its properties such as surface tension, electrical conduction and viscosity are key parameters in the process. However, ethanol was added for preparation of polymer solutions with polymer concentrations of 18, 27, 36, and 63 wt%. The physical properties such as density, viscosity, surface tension and electrical conductivity of polymer solutions and the PFH are shown in **Table 4.1**. All experiments were performed at ambient temperature and pressure and ethanol was used to calibrate each of the instruments mentioned above. As shown in **Table 4.1,** by increasing the polymer concentration to 36 wt%, the viscosity can be increased by five

times compared to the PFH liquid. The electrical conductivity of the polymer solutions has been dramatically decreased by increasing the polymer concentration. This is due to the large amount of entangled dielectric polymer chains in the solution.

Table 4.1 Measured physical properties of the liquids used in experimental work (n=5)

Material	Density kgm^{-3}	Viscosity mPa s	Surface tension mNm^{-1}	Electrical conductivity μSm^{-1}
Perfluorohexane	1710	1.1	12	$< 1 \times 10^{-5}$
PMSQ 18 wt %	805±0.5	1.8±0.1	23±0.2	9±0.2
PMSQ 27 wt%	834±0.5	2.9±0.1	23±0.2	8±0.2
PMSQ 36 wt%	861±0.5	5.2±0.1	23±0.2	6±0.2
PMSQ 63 wt%	993±0.5	53±0.5	26±0.2	1±0.2

4.2 Parametric investigation

It is the objective of this investigation to obtain hollow capsule with core-shell structures as a function of electrohydrodynamic processing parameters. Thus, the optimisation of the experimental parameters as well as a suitable mapping to create hollow structures needed to be investigated. The equipment used for co-axial electrohydrodynamic atomisation is shown in **Figure 3.2.** The co-axial needle dimensions were selected, as it seemed suitable and would enable suspensions of high viscosity to be electrosprayed without the blockages which would affect needles of finer diameters. In addition, it has been reported by Jayasinghe *et al* (2004) that using smaller inner diameters enables the use of lower flow rates. Such flow rates can produce much finer droplets (Jayasinghe and Edirisinghe, 2004). The investigation of

hollow preparations using the CEHDA process includes four subsections which are: the influence of flow rate, the influence of needle-substrate distance, the influence of polymer concentration, and the influence of applied voltage, as described below.

4.2.1 The encapsulation process

In this study, the outer PMSQ solution acted as the driving liquid because of its lower electrical relaxation time (Lopez-Harrera *et al*., 2003) and higher viscosity compared to PFH. The stable jet was not observed in the absence of the PMSQ solution, indicating that the inner liquid (PFH) cannot produce a stable jet because of its low electrical conductivity. **Figure 4.2** shows electrospraying of both the PMSQ solution and PFH at different applied voltages. The gravity driven dripping mode of PMSQ/PFH was observed at zero voltage, while the flow rates of syringe 1 (PFH solution) and syringe 2 (36 wt% PMSQ solution) were fixed at 150 μl $min^{-1}$and at 300 μl min^{-1}, respectively (**Figure 4.2a**). In this experiment the dripping mode can be approximately divided into two parts (upper and lower), in which the upper part is PMSQ polymer while the lower part consists of the PFH droplets surrounded by a thin layer of PMSQ because of the higher density of the inner liquid.

With increasing electric field strength (applied voltage), the dripping mode changed to stable jetting which was reached at 4.2 kV (**Figure 4.2b**). Normally, in this mode the cone volume is largely occupied by the inner liquid with the outer liquid flowing in a very thin film on the outside of the cone (Loscertales *et al*., 2002). In **Figure 4.2b**, however, it can be seen that there is a liquid interface inside the cone and the inner liquid does not fill the cone volume. This observation can be ascribed to the high density, low electrical conductivity and low miscibility of the PFH liquid and the high polymer concentration. However, once the cone-jet is formed, concentric droplets can

be generated as the jet breaks up into smaller highly charged droplets which are then neutralized by the presence of the ground electrode during collection.

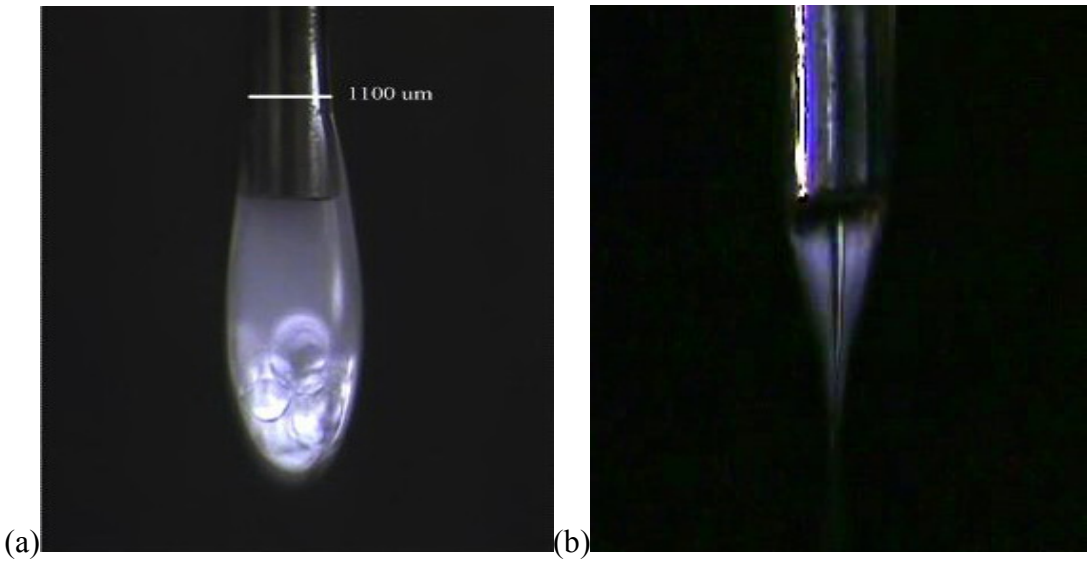

Figure 4.2 Illustration of dripping (a) and stable jetting (b) behaviour of PMSQ/PFH during CEHDA

4.2.2 The influence of flow rate

The liquid flow rates are often the key controlling parameters during preparation of hollow microspheres by CEHDA. To identify the influence of the driving liquid, the flow rate of syringe 2 (PMSQ solution 18 wt%) was varied between 200 and 650 μl min^{-1} while the flow rate of syringe 1 (PFH solution) was fixed at 150 μl min^{-1}. The distance from the exit of the outer needle to the ground electrode (the working distance) was fixed at 12 mm. **Figure 4.3** shows the effect of increasing the PMSQ solution flow rate on capsule mean diameter (D) which increased from 420 nm at 250 μl min^{-1} to 1000 nm at 650 μl min^{-1}. However, at a flow rate of 200 μl min^{-1}, irregular microspheres with a porous surface were generated instead of the spherical microspheres (**Figure 4.4a**). This can be attributed to the outer liquid (PMSQ solution)

being unable to provide sufficient driving force to encapsulate the PFH liquid. This kind of hollow microspheres with a porous surface have been reported and classified as a new particle on account of their higher effective diffusivity of drugs and available surface area compared with microspheres of the same size ((Im et al., 2005).

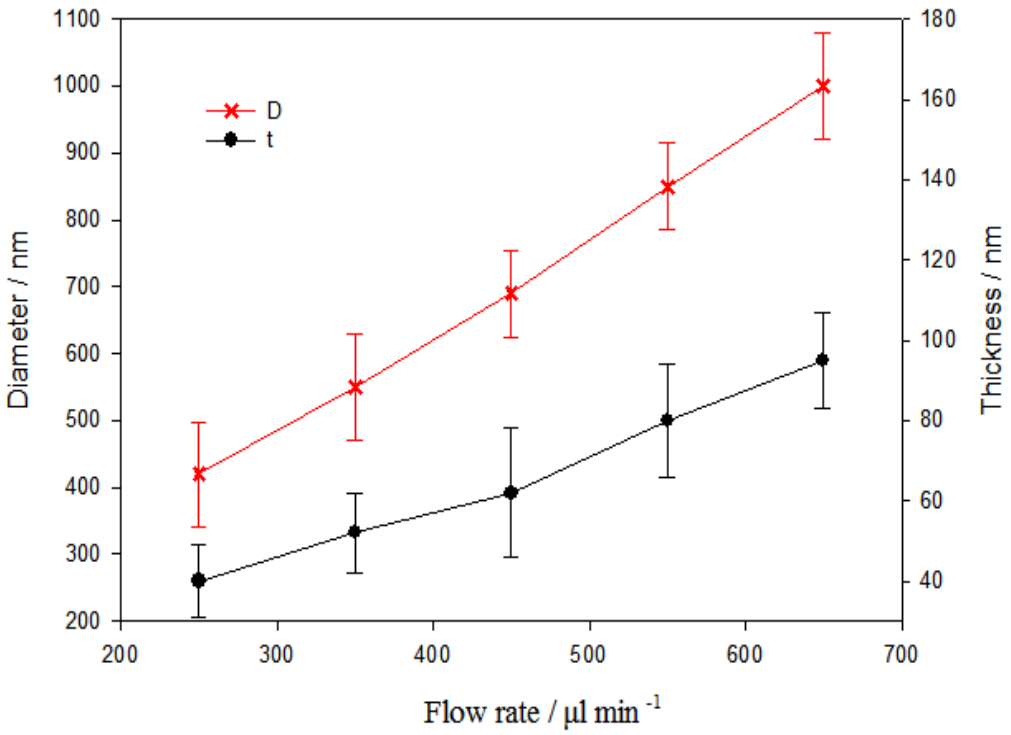

Figure 4.3 Diameter and shell thickness of microspheres prepared as a function of varying flow rate of PMSQ and with PFH flow rate fixed at 150 µl min^{-1} (Error bars represent the standard deviation from three experiments)

Panels a-f of **Figure 4.4** show SEM images of the hollow PMSQ microspheres fabricated at flow rates of PMSQ at 200, 250, 350, 450, 550, and 650 µl min^{-1},

respectively. As above, for liquid flow rates < 200 μl min^{-1}, microspheres of irregular morphology with a porous surface were generated (**Figure 4.4a**). When the flow rate was fixed > 250μl min^{-1}, the microspheres were spherical with smooth surfaces and a narrow size distribution. However, some of these microspheres were also seen to be interconnected. This is thought to have occurred as a result of water seeping out from the microspheres taken out of distilled water prior to being dried in a desiccator.

The mean shell thickness (t) was also influenced by increasing PMSQ flow rate and similarly increased with increasing flow rate (**Figure 4.3**). Typical cross sections are presented on the upper RHS of **Figure 4.4** panels b-f. The cross section of microsphere was obtained by a destructive method. The cutting force can result in some deformation and therefore these appear non-circular. **Figure 4.4** panels b-f indicate that hollow microspheres with a single cavity were successfully formed and that the shell thickness varied from 40 nm for a mean diameter of 420 nm to 95 nm for a mean diameter of 1000 nm. Furthermore, the D/t ratio (α) showed a slight increase from 10.5 at 250 μl min^{-1} to 10.7 at 650 μl min^{-1}. However, the ratio was kept almost constant by adjusting the flow rate under these processing conditions. **Figure 4.5** shows a microsphere with its shell cracked open and this is further evidence to indicate that the microspheres are not solid capsules but consist of a single internal cavity, which was previously occupied by PFH. If the spheres had been solid with a sponge like structure then this would have indicated the PFH liquid had not been successfully encapsulated.

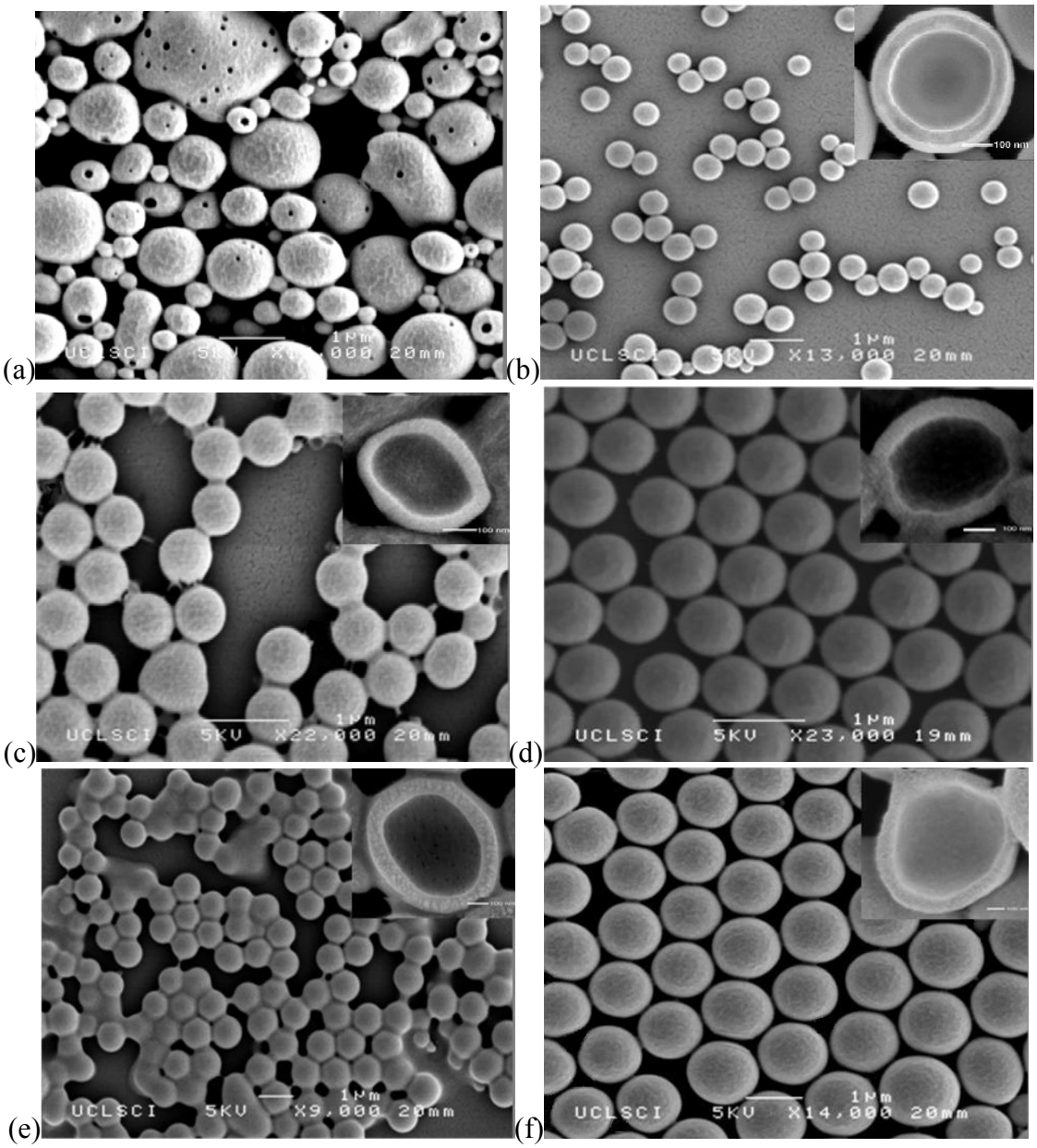

Figure 4.4 Effect of PMSQ flow rate (μl min^{-1}) on geometry of the hollow microspheres, (a) 200; (b) 250; (c) 350; (d) 450; (e) 550; (f) 650

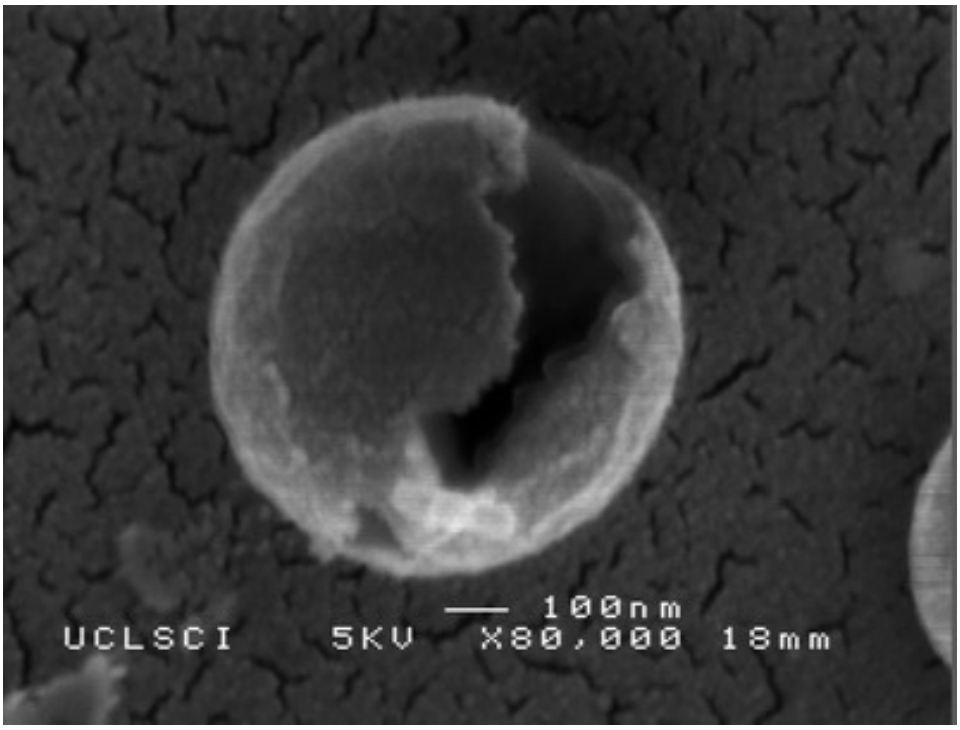

Figure 4.5 Scanning electron micrograph of fractured hollow microsphere

4.2.3 The influence of needle-substrate distance

As the needle-substrate distance plays an important role in influencing the liquid droplet dimensions during electrohydrodynamic processing, it is necessary to study the effect of the needle-substrate distance on the size of hollow capsule obtained. In this investigation, 18 wt% PMSQ was syringed to the outer needle at a flow rate of 450 μl min^{-1} while the flow rate of syringe 1 (PFH solution) was fixed at 150 μl min^{-1}. The size of hollow capsules made by varying the needle-substrate distance from 8 to 16 mm is shown in **Figure 4.6**. At a short distance (8 mm), the size of diameter and shell thickness showed a broad size distribution. With the increase of the distance, the diameter and shell thickness became smaller and this is due to the increasing evaporation of solvent during particle formation. However, when the distance was varied from 8 mm to 16 mm, the core-shell structure of the capsule was not affected.

The reason for that is because there was sufficient driving force for the core-shell formation during spraying.

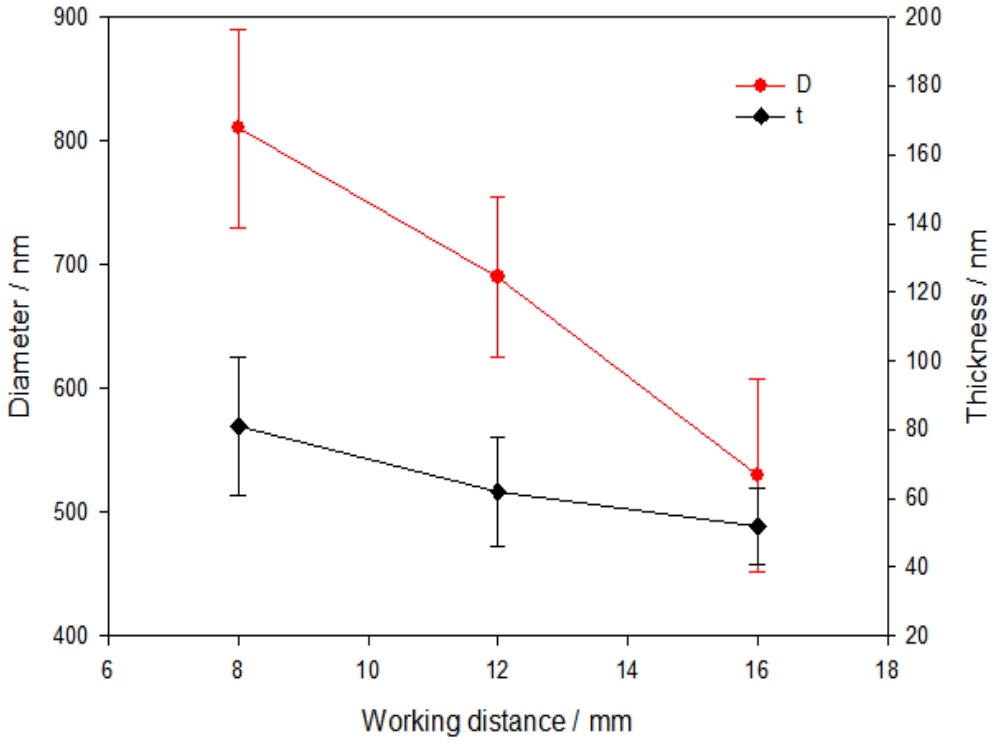

Figure 4.6 Size and shell thickness of microspheres vs working distance with inner needle flow rates of 150 μl min^{-1} and outer needle flow rate of 450 μl min^{-1} (Error bars represent the standard deviation from three experiments)

4.2.4 The influence of polymer concentration

The effect of PMSQ concentration on the preparation of hollow microspheres was studied for 18, 27, 36 and 63 wt% PMSQ in ethanol while the working distance was fixed at 12 mm. With increasing PMSQ concentration, the viscosity of the solutions increases due to increasing polymer chain entanglement, whilst electrical conductivity decreases because of the insulating characteristics of PMSQ (**Table 4.1**). Both parameters would be expected to affect the morphology of the microspheres. The

microspheres generated were spherical except at 63 wt% PMSQ. However, increasing the polymer concentration resulted in an increase in mean microsphere diameter (D) from 460 nm at 18 wt% PMSQ to 630 nm at 36 wt% (**Figure 4.7**). The increase in capsule size may be attributed to the high surface tension and viscosity and low electrical conductivity of the higher concentration solutions. The mean shell thickness of the microspheres varied from 45 nm at 18 wt% PMSQ to 95 nm at 36 wt% (**Figure 4.7**). In addition, the ratio α showed a decrease from 10.2 at 18 wt% to 6.6 at 36 wt%. These effects may similarly be attributed to the higher viscosity and higher surface tension (Hartman *et al*., 1999b).

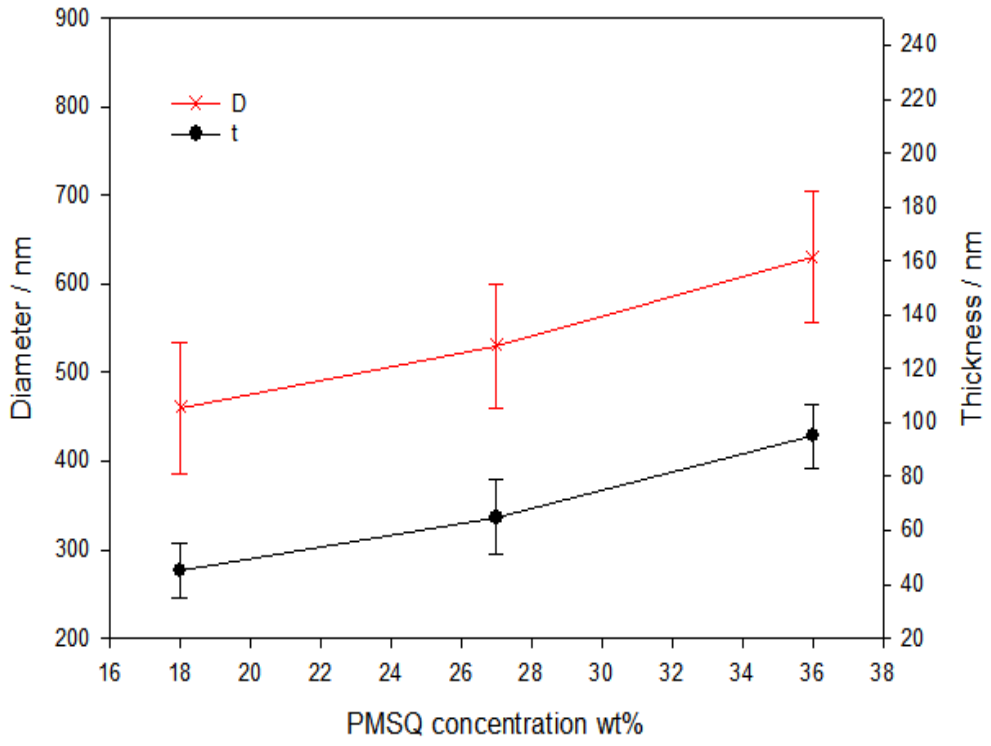

Figure 4.7 Size and shell thickness of microspheres vs PMSQ concentration with the inner flow rate fixed at 150 μl min^{-1} and the outer needle flow rate kept at 300 μl min^{-1} (Error bars represent the standard deviation from three experiments)

As the polymer concentration was increased to 63 wt%, a transition from electrohydrodynamic spraying to electrospinning was observed. Also, the polymer began to solidify and it became difficult to obtain hollow microspheres by adjusting the applied voltage. Instead, composite fibers were formed as shown in **Figure 4.8 and 4.9**. **Figure 4.8** shows a SEM image of an electrospun fiber prepared at 9.7 kV, whose surface shows both wrinkled and smooth features which are thought to be due to solvent evaporation during collection (Berkland *et al.*, 2004, Loscertales et al., 2002). **Figure 4.9** shows an optical image of the same fiber and provides more detailed internal information. The PFH liquid droplets with diameters of ~7 μm were encapsulated in a PMSQ fiber of ~10 μm diameter. This type of structure could potentially be used as a functional material e.g. for textiles (Sun *et al.*, 2003) and drug delivery applications (Sill and Recum, 2008).

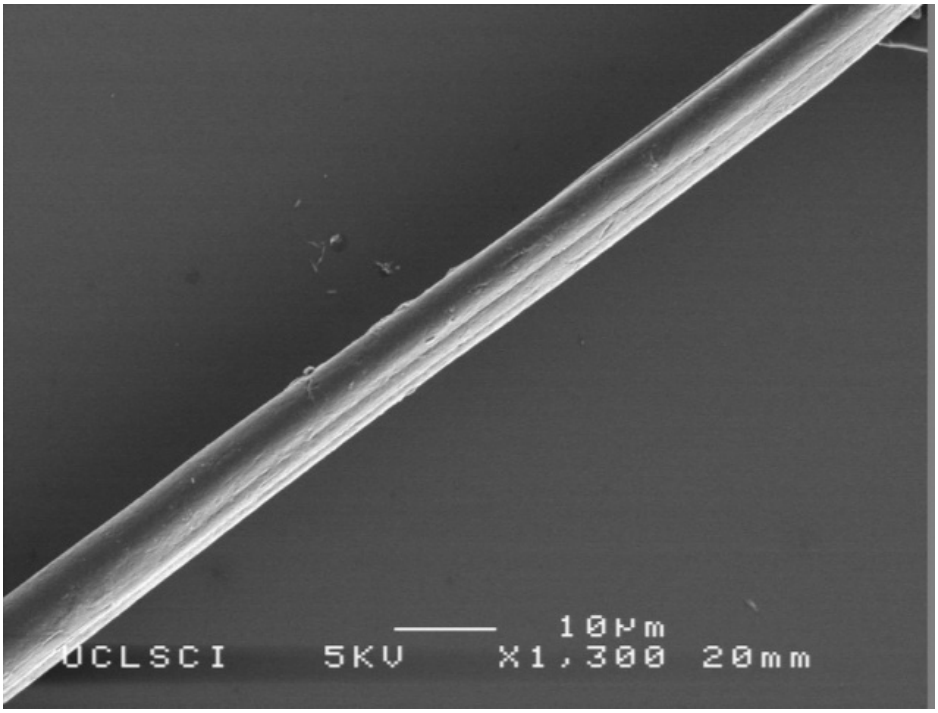

Figure 4.8 SEM image of increasing the PMSQ concentration to 63 wt %

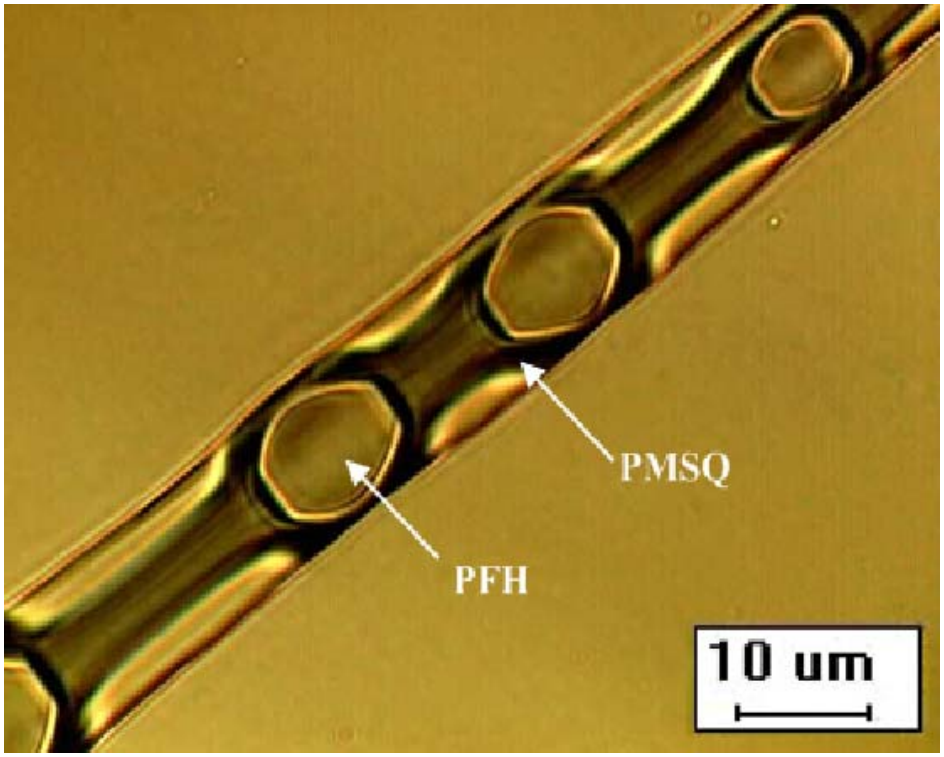

Figure 4.9 Optical image of increasing the PMSQ concentration to 63 wt %

4.2.5 The influence of applied voltage

The applied voltage between the needles and the ground electrode is the other key process control parameter (Lopez-Harrera *et al*., 2003). In this study, the effects of applied voltage on hollow microsphere geometry and shell thickness at different voltages of 3.4, 3.8, 4.2 and 4.6 kV were investigated, while the polymer concentration was fixed at 36 wt%, and the flow rates in the inner and outer needles were kept at 150 and 300 μl min^{-1}, respectively. It was found (**Figure 4.10**) that increasing the applied voltage resulted in a reduction in the mean microsphere diameter (D) from 810 nm at 3.4 kV to 370 nm at 4.6 kV. Thus, these results demonstrate that by increasing the applied voltage, microspheres with diameters of about four orders of magnitude smaller than the size of outer needle can be produced. However, when the applied

voltage was increased, the cone angle becomes larger and the acceleration distance to the exit of outer needle becomes correspondingly shorter, so there will be a maximum voltage above which it is difficult to reach steady state jetting. The mean shell thickness of hollow microspheres was 119 nm at 3.4 kV. By increasing the applied voltage to 3.8 kV, the mean thickness became smaller, reducing to 84 nm at 4.2 kV and 53 nm at 4.6 kV. The ratio α was almost constant at ~ 6.8.

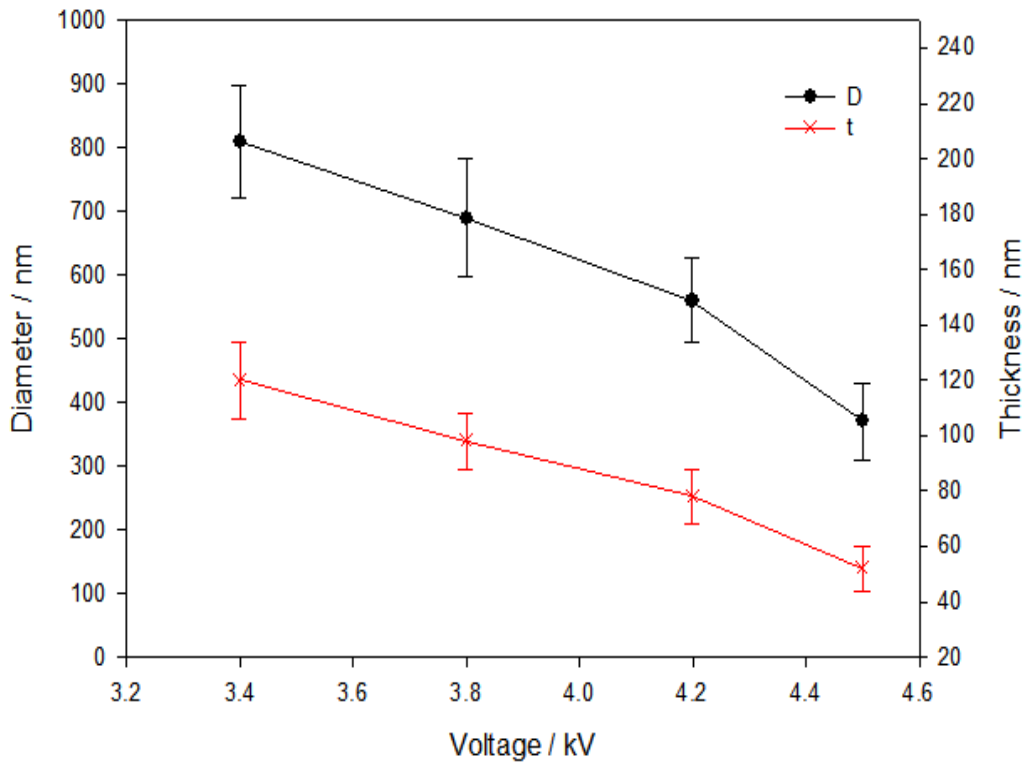

Figure 4.10 Size and shell thickness of microspheres vs. applied voltage with an inner flow rate of 150 μl min^{-1} and an outer flow rate of 300 μl min^{-1} (Error bars represent the standard deviation from three experiments)

4.3 Steady jetting region and D/t ratio

The driving liquid, which has high viscosity and electrical conductivity, plays an essential role in the preparation of hollow microspheres and the spray phenomenon is mainly determined by properties of the driving liquid (Loscertales *et al*., 2002). The relationship between applied voltage, flow rate, and the onset of stable jetting at PMSQ concentrations of 18 wt%, 27 wt%, and 36 wt% was investigated (**Figure 4.11 a-c**). In each stable jet region, with all other parameters fixed, the applied voltage increased with increasing PMSQ flow rate. In addition, by increasing the PMSQ concentration from 18 to 36 wt%, the applied voltage needed to prepare hollow microspheres becomes higher and the magnitude between upper and lower voltages of stable jetting decreases with the increase of the PMSQ concentration.

In this study, the ratio α provides important information as this determines the mechanical properties and transportation behaviour of the encapsulated bioactive agents (Qiu *et al*., 2001, Rachik *et al*., 2006, Dong *et al*., 2005). In addition, the ratio of diameter to wall thickness produced by different processes is in the range of 5 to 30. It is clear that the production of a thinner shell thickness will decrease the overall stiffness of the capsule wall (Rachik *et al*., 2006), and simultaneously increase the inner core volume while the outer diameter (D) is fixed. Over the entire parameter space, the largest value of α achieved (by a factor of ~10) was at 18 wt% PMSQ while the smallest value of α (6.6) was obtained by increasing polymer concentration to 36 wt% PMSQ (**Figure 4.12**). These hollow particles with a low D/t ratio are less prone to fragmentation but have a smaller core volume.

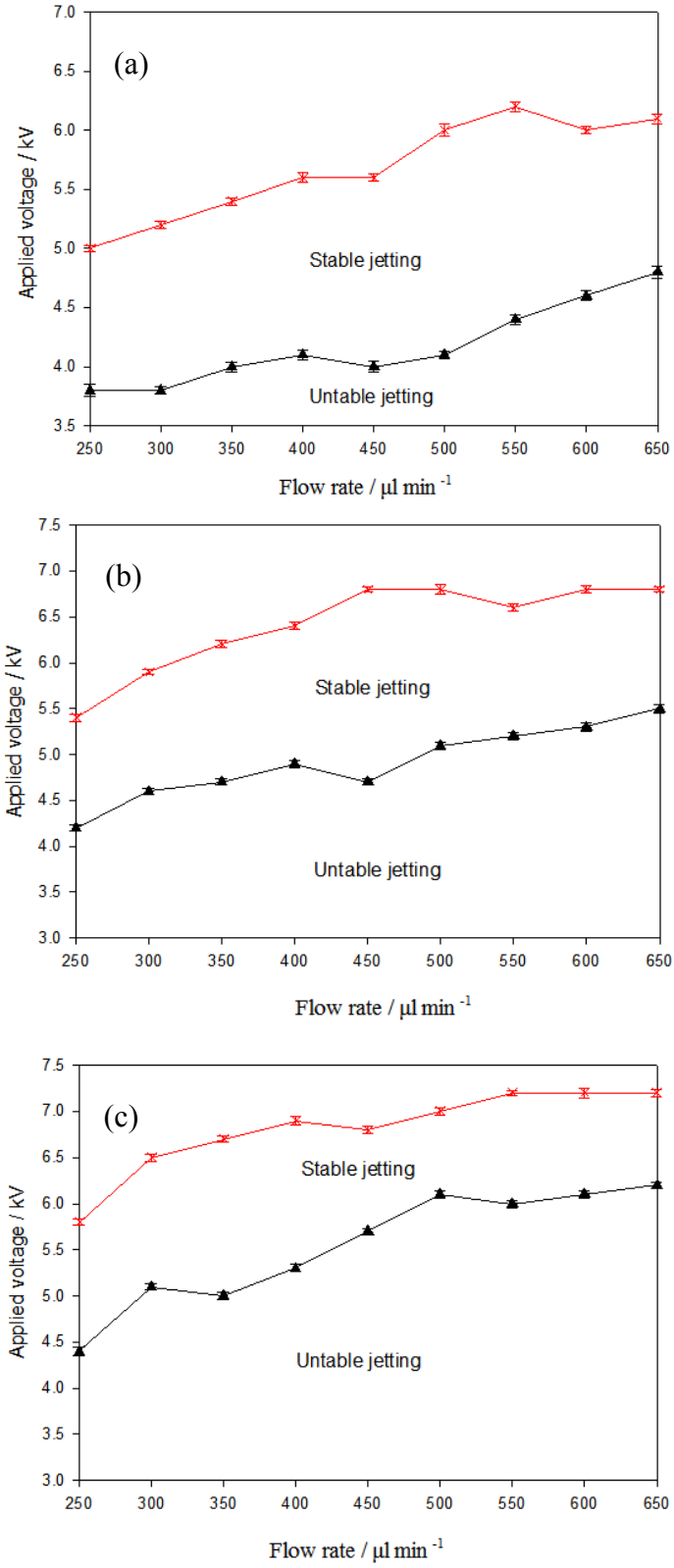

Figure 4.11 Mapping of applied voltage and flow rate of PMSQ at different PMSQ concentrations (a) 18 wt%, (b) 27 wt%, and (c) 36 wt% (Error bars represent the standard deviation from three experiments)

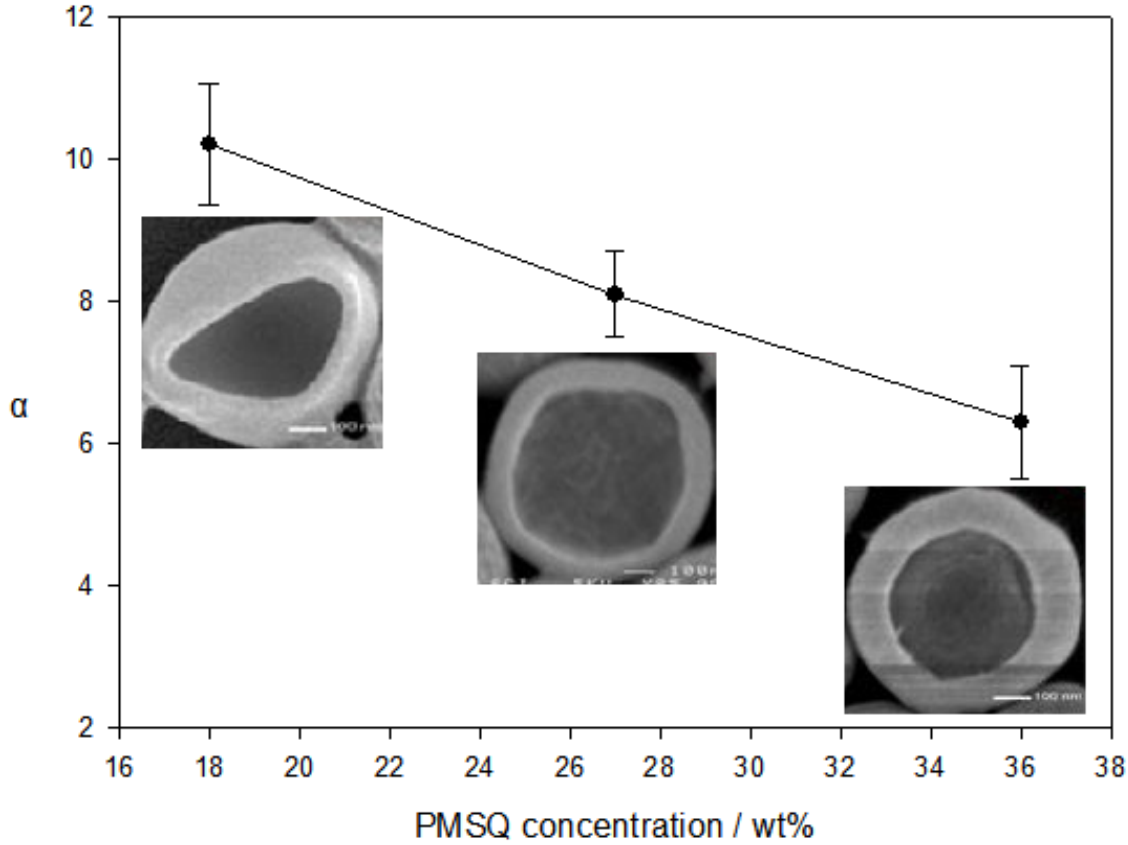

Figure 4.12 Variation of D/t ratio (α) with polymer concentration (Error bars represent the standard deviation from three experiments)

4.4 Characterization of composition

FTIR spectra were obtained to confirm the composition of the hollow microspheres. **Figure 4.13** shows infrared spectra of samples of native PMSQ powder and the microspheres over the wave number range 400 to 4000 cm^{-1}. C-H vibrations of –CH, $–CH_2$, and $–CH_3$ groups showed absorption bands at around 2900 cm^{-1}. Carbon dioxide was observed at 2359 cm^{-1} due to residual carbon dioxide not purged from the FTIR spectrometer (C-O asymmetrical stretching vibration) (Bogart *et al.*, 1995). The methyl groups (CH_3) were also observed at absorption bands of 1410 cm^{-1} and 1275 cm^{-1}, respectively. The typical absorption band of polysilsesquioxane at 1130

cm^{-1} was observed in both spectra (Ma *et al*., 2002a). The two spectra are almost identical except for an additional absorption in the spectrum of 'dried hollow microsphere' at 1119 cm^{-1}. This is attributed to C_2F_6 (Eapen *et al*., 1994) and suggested that the PFH provide a volume for shell formation, after which it evaporated. Thus, the polymer is stable and not reactive with the PFH during processing although PFH relics existed in the hollow PMSQ polymer. It should be noted that apart from being non-toxic, PFH is able to dissolve and deliver oxygen to several tissues (Riess, 2001), and also be used as an external phase of emulsion to entrap lipophilic drugs into hydrophilic or lipophilic polymers (Mana *et al*., 2007), thus providing a superior encapsulation rate after filtering the suspension and drying under ambient conditions.

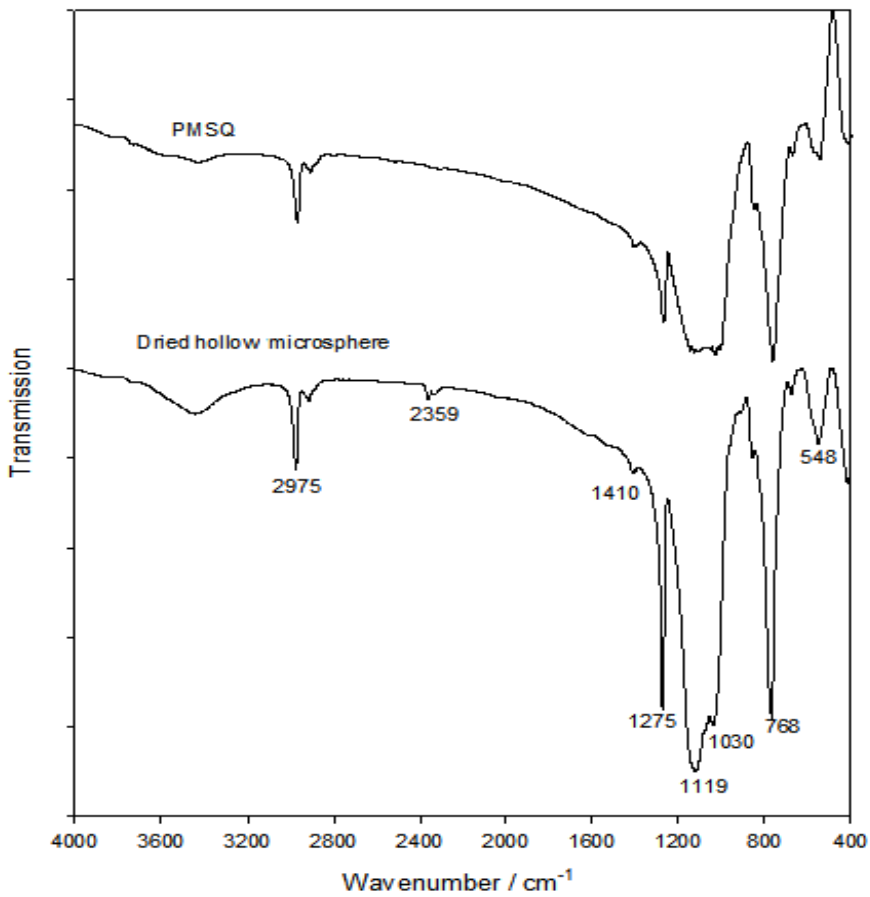

Figure 4.13 FTIR spectra of PMSQ and dried hollow microspheres

4.5 Mechanism of hollow capsule formation

Perfluorohexane (PFH), which is a liquid at the ambient temperature is non-toxic and has been used in the preparation of multifunctional microspheres for medical and pharmaceutical applications (Giesecke and Hynynen, 2003). The mechanism for the preparation of hollow microspheres takes advantage of its properties of immiscibility and volatility (Pisani *et al*., 2006). PFH and PMSQ were injected at appropriate flow rates under an applied voltage, in which the electrical forces acted on the driving liquid (PMSQ) and lead to the establishment of the stable cone. The PMSQ solution was accelerated by the electrical field, while the flow of PFH was dominated by viscous stresses. Hence, the electrical forces acting on the PMSQ film drives the inner viscous liquid and make both liquids flow steadily with the same velocity. Therefore, concentric droplets can be obtained with PMSQ around the PFH, these are stable and retain their integrity due to their immiscibility.

The core material (PFH) can change phase from liquid to air at ambient temperature due to its low boiling point. The thin PMSQ layer containing nano-pores and channels allow small molecules and ions to pass through the shell. However, after shell formation, the core liquid can be easily exiled by gentle evaporation in an ambient environment due to its volatility, leaving a single hole inside. Moreover, the use of PFH liquid droplets in this technique paves the way to incorporating functional oils or oil-soluble compounds inside the particles. Furthermore, PFH is biocompatible against other solid templates and may allow facile and efficient introduction of functional liquid cores, drug and DNA molecules inside the capsule, which is particularly attractive in drug delivery and pharmaceutical applications.

4.6 Evaluation of characteristics of hollow capsules

Hollow microspheres made by several techniques have been extensively studied to generate a variety of characteristics for drug delivery applications as described in **Chapter 2**. However, the question as to whether hollow microspheres made by the electrohydrodynamic processing method can be used as drug carriers with predetermined characteristics remains unanswered. Characteristics such as particle diameter, shell thickness, release mechanism and uniformity are very important in many cases for both fundamental research and practical applications and are not well documented.

The aim of this investigation was to conduct a detailed study of the relationship between: capsule processing parameters, the resulting shell characteristics and subsequent release of an encapsulated liquid with a view to addressing this lack of data. Hollow spherical capsules of ~1μm outer diameter were prepared using electrohydrodynamic processing and the shell thickness of the capsules was varied between 100-150 nm. To investigate the effect upon the release characteristics the capsules were loaded with a water soluble dye of molecular weight ~ 961 and release profiles were determined using ultraviolet spectroscopy. The release data were evaluated using the Higuchi model which describes drug release mechanisms based on Fick's law (Peppas, 1985). Finally, the core-sell structures prepared in this way were investigated as drug carriers in particular the influence of the hollow structure.

4.6.1 Characterization of Evans blue dye

Evans Blue dye (Mw: 961) was used as a marker to examine the loading, encapsulation, and release processes. Evans blue dye has been shown in previous studies to generate

experimentally verified molecule release profiles which agree with established drug release models (Pancholi *et al*., 2009). The calibration curve of Evans blue dye was determined by taking absorbance versus dye concentration measurements between 0.06 and 0.018 mg ml^{-1}. **Figure 4.14** shows the UV absorption spectra of Evans Blue dye solution analyzed by UV spectroscopy from 350 nm to 750 nm. The concentration of dye in supernatant was determined by UV absorption at the wavelength of 607 nm. The calibration curve fits Lambert and Beer's law and leads to **Eq. 4.1**.

$$A = 0.1259 \times C + 0.0056 \qquad \textbf{(Eq. 4.1)}$$

Where A is the absorbance value and C presents the dye concentration (mg ml^{-1}) in the release medium.

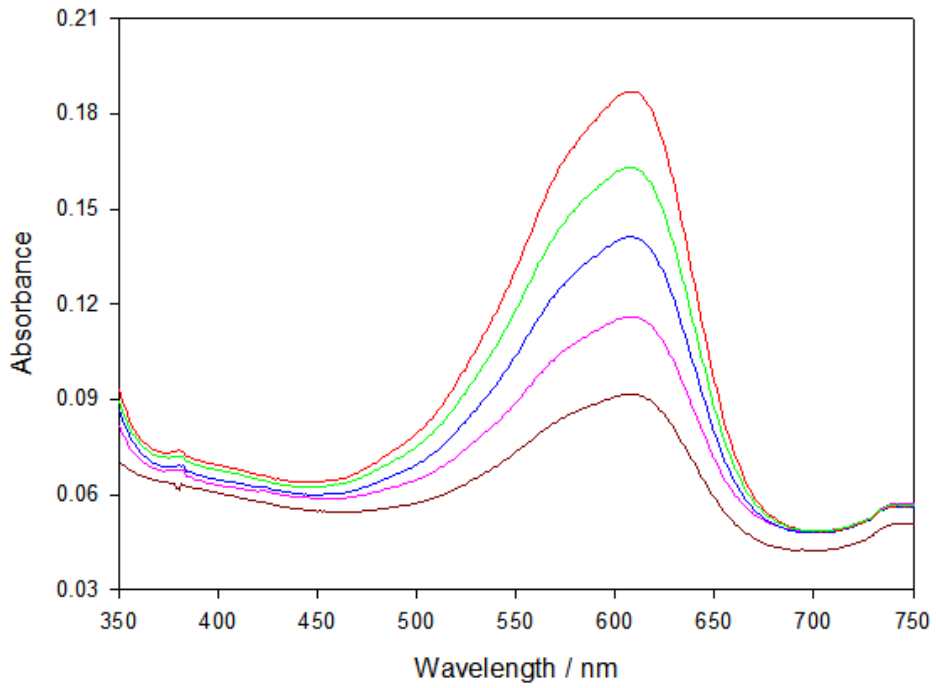

Figure 4.14 The UV-vis spectra of Evans Blue dye at different concentrations (0.06-0.018 mg/ml)

4.6.2 Size and shell thickness of hollow capsules

SEM images of the hollow capsules produced with various shell thicknesses are shown in **Figure 4.15**. The capsules appear spherical and the capsules have uniform shell thickness. The capsule dimensions depend on the polymer concentration used as shown in **Table 4.2**. The average outer diameter of the hollow capsules is fixed at ~ 1μm and, depending on the processing conditions, the mean inner diameter is in the range 650-840 nm (i.e. the shell thickness is in the range 100-150 nm). This illustrates that this PFH-based processing route can be used to control the spherical core volume.

Table 4.2 Measured properties from the hollow capsules (18, 27 and 36 in the first column refer to PMSQ concentration, n=50)

Sample	Diameter (nm)	Shell thickness (nm)	Inner diameter (nm)	Core Volume (m^3/kg)
PMSQ 18	1014±65	102±12	796±21	1.24×10^{-3}
PMSQ 27	1021±61	125±15	752±23	0.86×10^{-3}
PMSQ 36	1017±75	150±14	709±38	0.61×10^{-3}

For the PMSQ capsules shown in **Figure 4.15 (a)**, the shell thickness is approximately 100 nm, obtained with a concentration of the PMSQ solution of 18 wt%. PMSQ with different thicknesses of ~120 nm and ~150 nm were prepared by increasing the PMSQ concentration to 27 and 36 wt%, respectively, as shown in **Figure 4.15** (b) and (c). The shell remains spherical as its thickness increased. In addition, when the higher polymer concentrations were used, the shell was found to be more robust, and buckling and crumbling of the capsules could be avoided during removal of the core material (Cui *et al*., 2010). Thus, the polymer concentration is an important parameter that can be used to fine-tune the shell thickness and consequently the strength of the capsules.

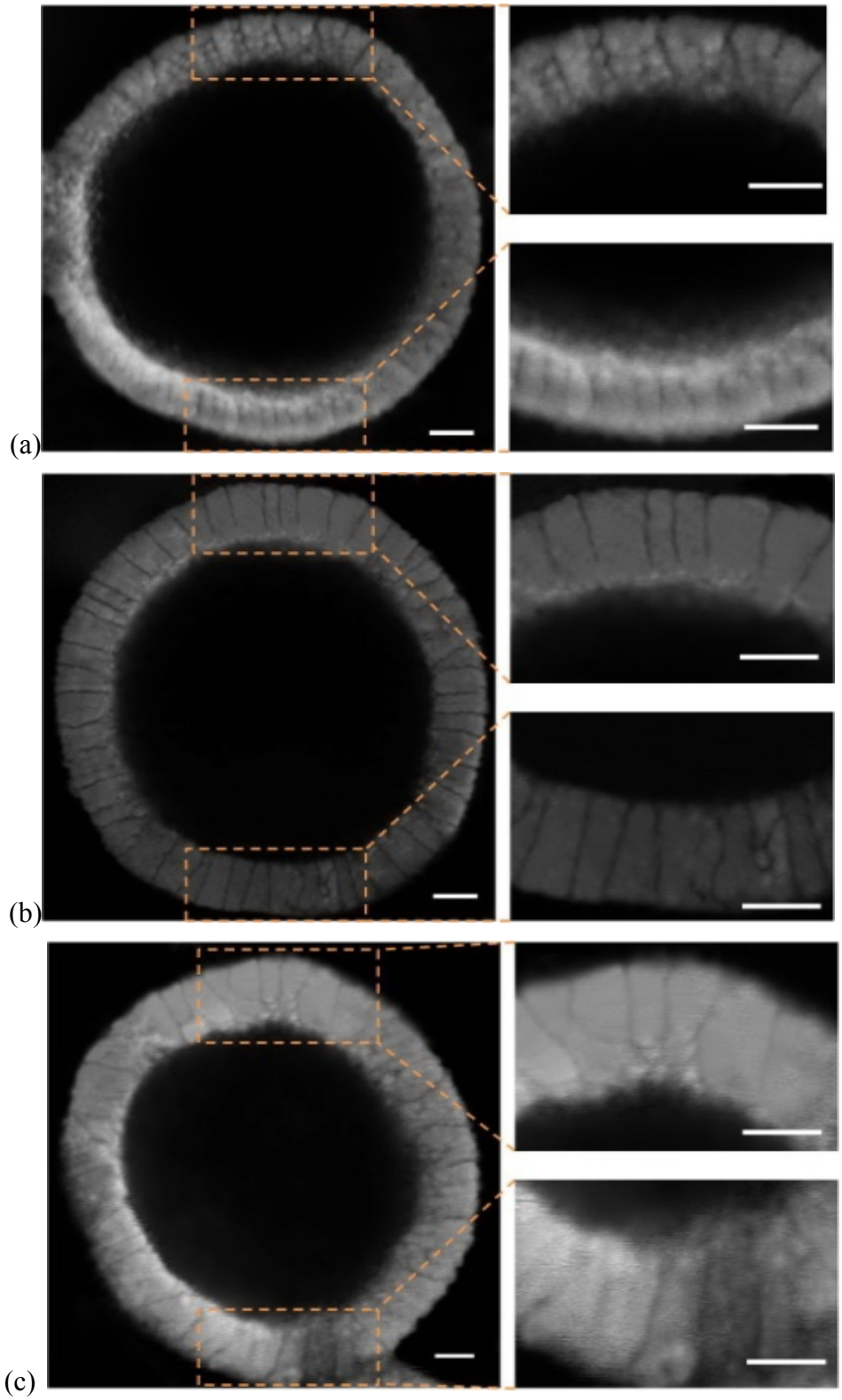

Figure 4.15 SEM images of cross-sections of the hollow capsules obtained at different PMSQ concentrations: (a) 18; (b) 27; (c) 36 wt% (inserted images are high-magnification, scale bar =100 nm)

In this work, investigation of the morphology of porous channels in the shell was also made using SEM. As shown in the inserts in **Figure 4.15**, the SEM images demonstrate the existence of mesoporosity, and this is the first time it has been possible to distinguish pore channels in the polymer shell of the hollow microsphere made by an electrohydrodynamic method. The dark lines in the cross-sections of the shells show some curvature and reveal that the porous channels are quite uniformly distributed in the shell. It also demonstrates that the pore shape is independent of the polymer concentration. It is interesting that although these hollow capsules were prepared by electrohydrodynamic spraying, they show a similar porous channel shape to those obtained by other methods, and this may be attributed to the chain structure of polysilsesquoxanes, e.g. ladder-like structures with branches (Jr *et al*., 1960, Ma *et al*., 2002b). The pore size distributions for various shell thicknesses are given in **Figure 4.16**. The pore size distribution was narrow and most of the pores had a width of ~5 nm, showing that different shell thicknesses have no significant effect on the pore size distribution. In addition, the porous channels in the wall traverse across the shell of the capsules with a radiating pattern from the core to the outer diameter.

The ability to control the core volume may be highly desirable for drug delivery applications as it can be used to control the quantity of drug loaded into the cavity. Also, if the pore size is larger than the size of the drug molecules, it allows drug molecules to be encapsulated in the carriers via its porous channel (Caruso *et al*., 2000). As the outer diameter of the hollow capsules is fixed at ~ 1μm, the core volume of the PMSQ capsule for shell thicknesses of 100, 125 and 150 nm was 1.24×10^{-6}, 0.86×10^{-6}, and 0.61×10^{-6} m^3/g, respectively, and this also means that inner PMSQ capsule surface area decreases with the increase of the shell thickness as a result of increasing polymer concentration. Factors such as pore shape and size of capsule prepared via this method

are clearly determined by the nature of the polymer and the concentration of the polymer. It has been reported that a "finger-like" structures (with straight pore channels throughout the whole thickness of the microcapsule membrane) can be obtained by a dense skin layer (Young and Chen, 1995). Therefore, to obtain a desired core volume, the properties of the polymer should be carefully selected in a given range of processing parameters.

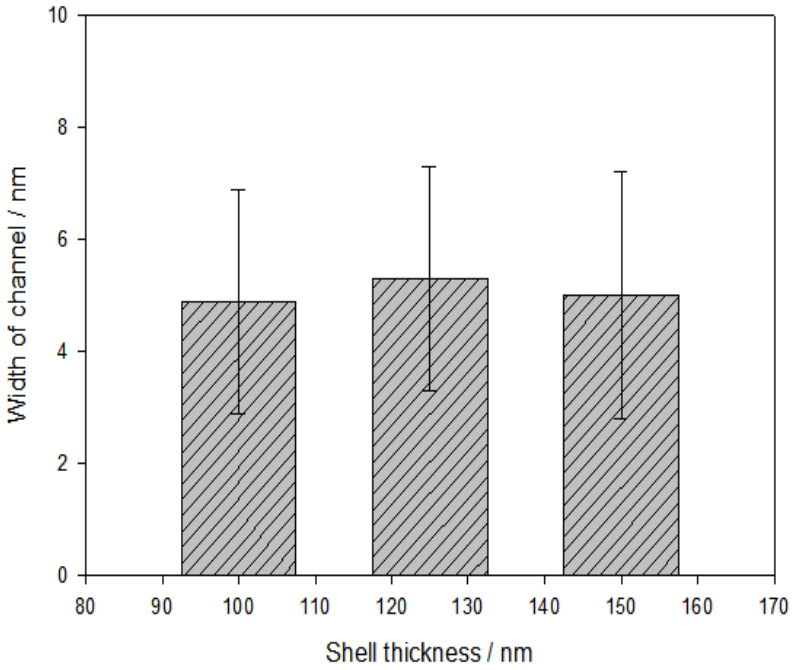

Figure 4.16 Channel width in PMSQ hollow capsules for different shell thicknesses (Error bars represent the standard deviation from three experiments)

4.6.3 Effects of shell thickness on the storage capacity

The effect of shell thickness on the amount of dye loaded in hollow PMSQ capsules is shown in **Figure 4.17**, which illustrates that dye was loaded in to the hollow capsules as a result of the concentration gradient between the reservoir (hollow core) and sink (release medium), and the amounts of dye loaded in hollow capsule for shell

thicknesses of 100, 125, and 150 nm were 5.2, 4.4 and 3.4 mg, respectively. This reveals that the loading amount decreased with the increase of shell thickness. An explanation could be simply that an increase in the shell thickness for a fixed outer diameter, causes a reduction of the core volume of the hollow volume as well as its surface area, leading to a decrease in the loading amount of dye.

Taking into account that the thickness of the polymeric layer with different sizes of approx. 100, 125, 150 nm, the dye storage in hollow polymer shell can be increased by increasing the surface area and cavity volume of the polymer shell. However, the hollow core provides more volume for storing dye molecules than the extended volume of the penetrating pore channels in the shell. Therefore, such a core-shell system is more desirable for control of core space than control of pore channels or porosity, in comparison with other methods such porous matrix, which provide much less space for molecule storage not providing hollow core volume (Li *et al*., 2003).

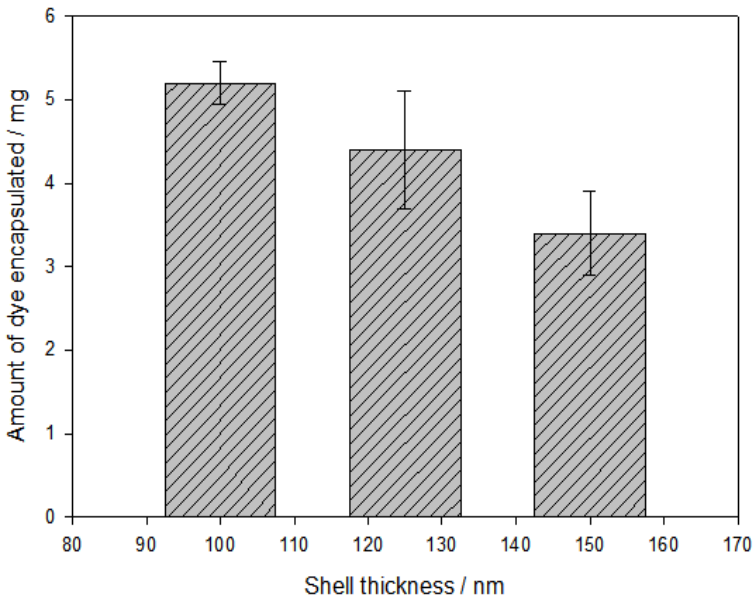

Figure 4.17 Effect of shell thickness on amount of dye loaded in capsules (Error bars represent the standard deviation from three experiments)

4.6.4 Effect of dye concentration on the release capacity

In the preparation of advanced drug delivery systems, varying doses of drug may be incorporated into the device as required for different lengths of treatment. Analysis of the release behaviour for different drug concentrations is an important factor for assessing the effectiveness of the system. Dye solutions having concentrations in the range 5.0 to 15.0 mg/ml were loaded into PMSQ capsules. The entrapped dye was released into a medium. **Figure 4.18** shows the release rate of dye from the hollow capsules for different dye concentrations. It shows that the release rate slightly increases with the increase of the dye concentration, from 0.53 mg at the dye concentration of 5 mg ml^{-1} to 0.60 mg at the dye concentration of 15 mg ml^{-1}. The highest dye released reaches 0.62 mg from per gram of PMSQ capsules with a dye concentration of 15 mg ml^{-1}. The observed increase in the release rate may be attributed to the fact that a higher loading of dye in the PMSQ capsules facilities a faster movement of the medium and dye molecules that penetrate the surface of PMSQ shell.

On the other hand, the results also suggest that the amount of dye loaded increases with increasing percent of dye concentration and the storage amount can be adjusted over a broad range. It should be pointed out that there are various other alternatives for prolonging the period of release: for example, simply by incorporating a higher dose of a pharmaceutical agent. However, in contrast, in matrix-type drug delivery devices, the release rate and burst release would significantly increase once a higher amount of drug is adsorbed due to the variation of effective area in matrix channels, which results in the a greater value for the drug release flux and this can cause adverse effects (Xie *et al*., 2006, Greenblatt, 2006). Therefore, hollow capsules can be effective in controlling treatment duration and can avoid a high drug release flux. In addition, the release rate

from a reservoir-type polymeric delivery device seems less dependent on the drug loading dose as long as the hollow cores can reach the maximum storage capacity and the drug molecules can transport into the hollow cores.

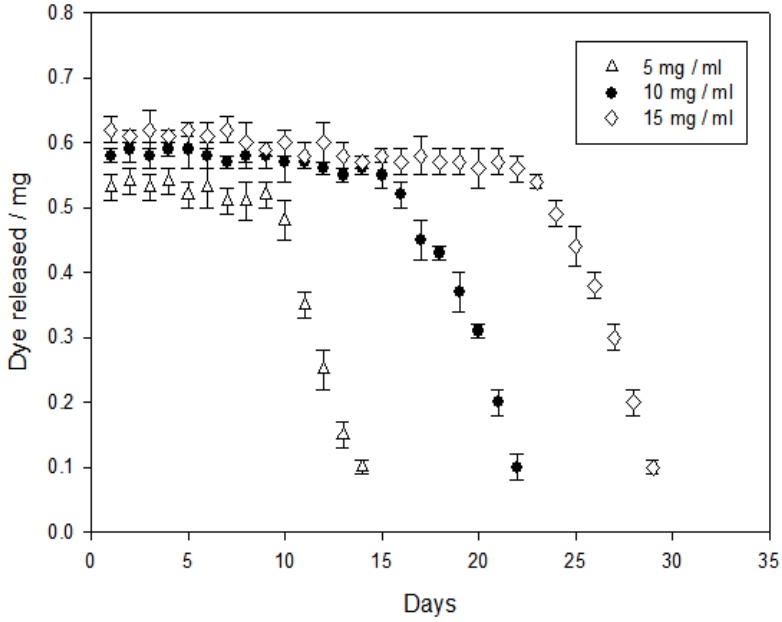

Figure 4.18 Release profile of dye from PMSQ capsules loaded with different doses of dye (Error bars represent the standard deviation from three experiments)

4.6.5 Effects of shell thickness on the release behaviour

The effect of shell thickness on the dye release behaviour from the PMSQ capsules is illustrated in **Figure 4.19**. The release of the dye stored in hollow capsules starts after the medium penetrates into the pore channels. It is observed that the release profiles of all samples follow a sustained release behaviour. The sustained release of dye is attributed to the presence of the shell membrane between the core and sink. The release rate then became significantly decreased after a period of time, and this is due to the amount of dye in the inner core of the PMSQ reaching a concentration balance

(equilibrium) between core and medium.

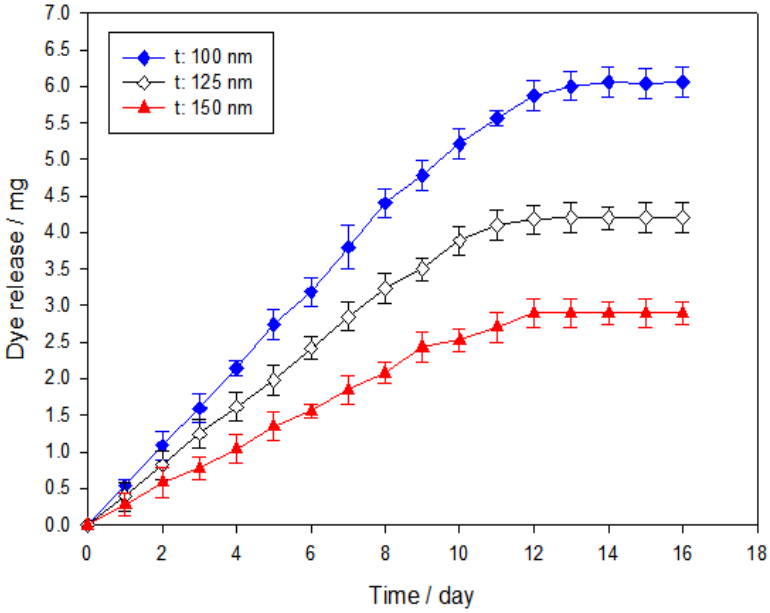

Figure 4.19 Effect of shell thickness (t) of PMSQ capsules on the release behaviour of dye at 37 °C (Error bars represent the standard deviation from three experiments)

It is observed that the dye released from a capsule with a shell thickness of 100 nm is slightly higher than for thicknesses of 125 and 150 nm, reaching the value 0.53 mg for 100 nm, 0.39 mg for 125 nm, and 0.28 mg for 150 nm per day (**Figure 4.19**). An increase in the thickness of the polymer membrane resulted in reduced relative release rates due to the increased length of the diffusion pathways and, thus, enhanced resistance to dye diffusion across the pore channels and increased dye concentration gradients. As diffusion is known to play a major role in the control of drug release from the capsules, the presence of an increased diffusion pathway length of polymer membrane is effective in the case of membrane controlled drug delivery systems and also provides the possibility of altering the release rate.

On the other hand, it should be pointed out that even though the dye released is different with varying shell thicknesses, the actual release period is similar. The different amounts of dye adsorbed by the polymer in each case leads to different quantities being delivered to the surroundings. As an example, after 12 days of release, capsules of 100 nm shell thickness have delivered about 5.87 mg of their total content, while this amount is reduced to 4.18 mg for 125 nm, and < 2.89 mg in the case of 150 nm. From this point of view, it would be possible to choose the amount of drug to be delivered on the availability of free space inside the hollow capsule.

The linear profiles of the release amount versus $\sqrt{time}$ are shown in **Figure 4.20**. A straight line of released dye generally does not apply beyond 0.6 of the total content, indicating that the first 60% of the fractional release can be characterized by some constant multiplied by the square root of time (Peppas, 1985). All fitted dye release graphs from the PMSQ system confirmed that the mechanism of dye release from core to the sink is primarily controlled by Fickian diffusion. Since dye molecules in the core space and the pore wall do not interact with PMSQ polymer, dye molecules can be relatively easily released from the carriers. Besides, PMSQ shows both physical and chemical stability under the experimental conditions used in this work (Ye *et al*., 2010). Therefore, the diffusion of dye through the channels in the shells is the controlling process for dye release. These findings indicated that the dye release from the hollow capsules prepared by electrohydrodynamic processing represents a Fickian mechanism and the release rate is a function of the shell thickness of the hollow capsule. Therefore, the release rate from a capsule can be regulated by shell thickness control as shown in **Figure 4.19**, indicating that the controlled release rate was determined by the diffusion from the polymeric shell. However, Fickian diffusional release from a thin film is

regulated by a barrier dependence of the length of shell thickness. The amount of dye released from such hollow capsules is inversely proportional to the shell thickness, suggesting that a small thickness (100 nm) is valid for the fast release rate while a thick value (150 nm) is suitable for the slower release rates.

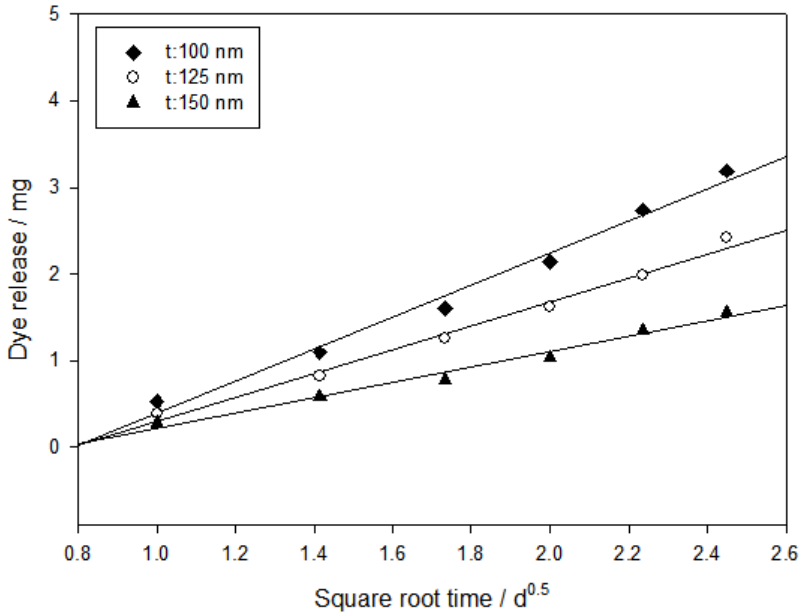

Figure 4.20 Fitted Higuchi model: profile of cumulative dye release versus square root of time

4.6.6 Effect of different temperatures on the release behaviour

The effect of increasing the temperature of the medium on the dye's release behaviour was also studied at 57 °C. The medium was kept at pH 7.4 and the capsules were stirred at 100 rpm. As shown in **Figure 4.21**, under these conditions, no apparent difference can be observed in the dye release, which also follows Fickian diffusion (compare with **Figure 4.19**). This can be explained by the stability of PMSQ capsules, which were collected in a cross-linker (distilled water) and possess good mechanical properties and chemical durability (Ye *et al.*, 2010). The PMSQ polymer can be

pyrolyzed into ceramic at only a very high temperature of ~1000 °C (Narisawa *et al*., 2010), and the glass-transition temperature of PMSQ polymer is in the range from 80 to 120 °C (Huang *et al*., 2003). Therefore, a moderate temperature increase above 37 °C has little or no effect. In contrast, it has been reported that some encapsulated molecules can show an increased release rate by increasing the temperature (Faisant *et al*., 2006). This is because the increased mobility of the polymer chains (different polymer to PMSQ) and drug molecules at elevated temperature, results in increased diffusion rates. In contrast, the PMSQ carriers are stable in the temperature range 37-57°C.

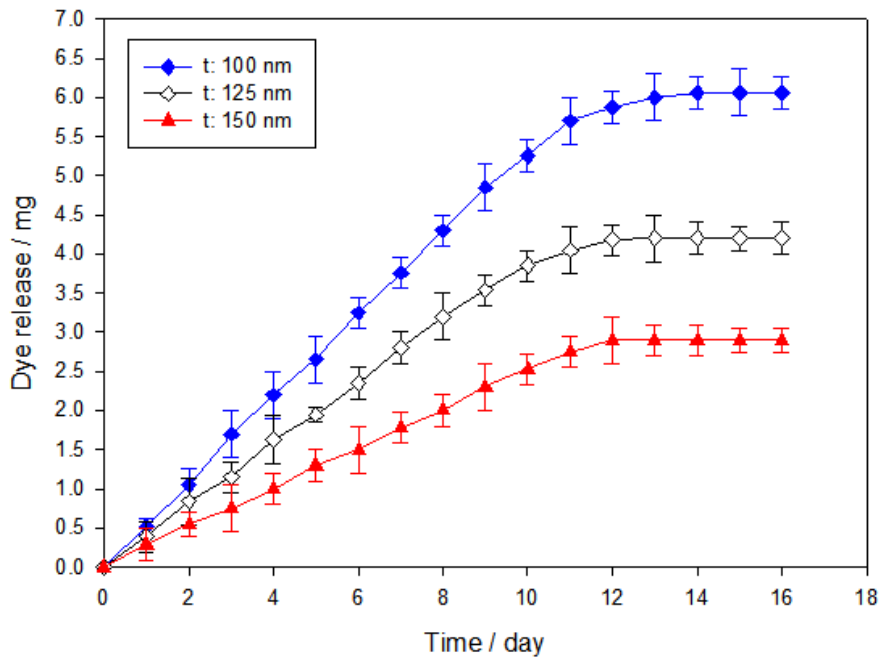

Figure 4.21 Dye release behaviour from PMSQ capsules at 57 °C (Error bars represent the standard deviation from three experiments)

4.6.7 Effect of release on the hollow structure

The SEM images of the pore channel before storage and release of dye are shown in

Figure 4.15 (a), (b) and (c). The width of pore channel is ~ 5 nm regardless of different shell thicknesses. However, after the storage and release of dye via pore channels, the structures still retain their textural symmetry. **Figures 4.22** (a), (b) and (c) show the SEM micrographs of PMSQ shells after the release of dye molecules. After the release of dye molecules, no apparent difference can be observed compared with the starting hollow capsules (**Figure 4.15**), and the highly ordered mesoporous structure of the shell also remains. The pore size distribution and polymer wall thickness also remain intact within the time span investigated in this work. In addition, there is no obvious change in the outer and inner diameters compared with those of the starting hollow capsules.

4.6.8 Effect of capsule diameter on the release behaviour

Dye-loaded hollow capsules having a wide range of sizes (i.e. 420 nm, 700 nm, and 1000 nm outer diameter) were produced to study influence of capsule size on release behaviour of dye. **Figure 4.23** shows the results of the dye release profile as a function of the capsule size. The dye release rate of the capsule was decreased by increasing the size from 420 to 1000 nm. It showed approximately 85% of the dye released after 12 days for the 1000 nm to release, whereas the same amount of the dye release for the 700 nm took less than 10 days. In addition, for the 420 nm capsules, the dye was released at a faster rate than that for the 700 nm. This phenomenon was due to the fact that as capsule size decreased the surface area-to-volume ratio of the capsules increased. As a result, the release rate of the capsule increased with decreasing capsule diameter. In addition, dye penetrating through smaller capsules may be quicker due to the shorter distance of shell thickness (t). Furthermore, the decrease in capsule size may lead to an increased release rate, because the shell thickness decreases with decreasing size, and drug release rates will be faster for smaller capsules. The effect of capsule size can be very significant for controlled release in drug delivery system.

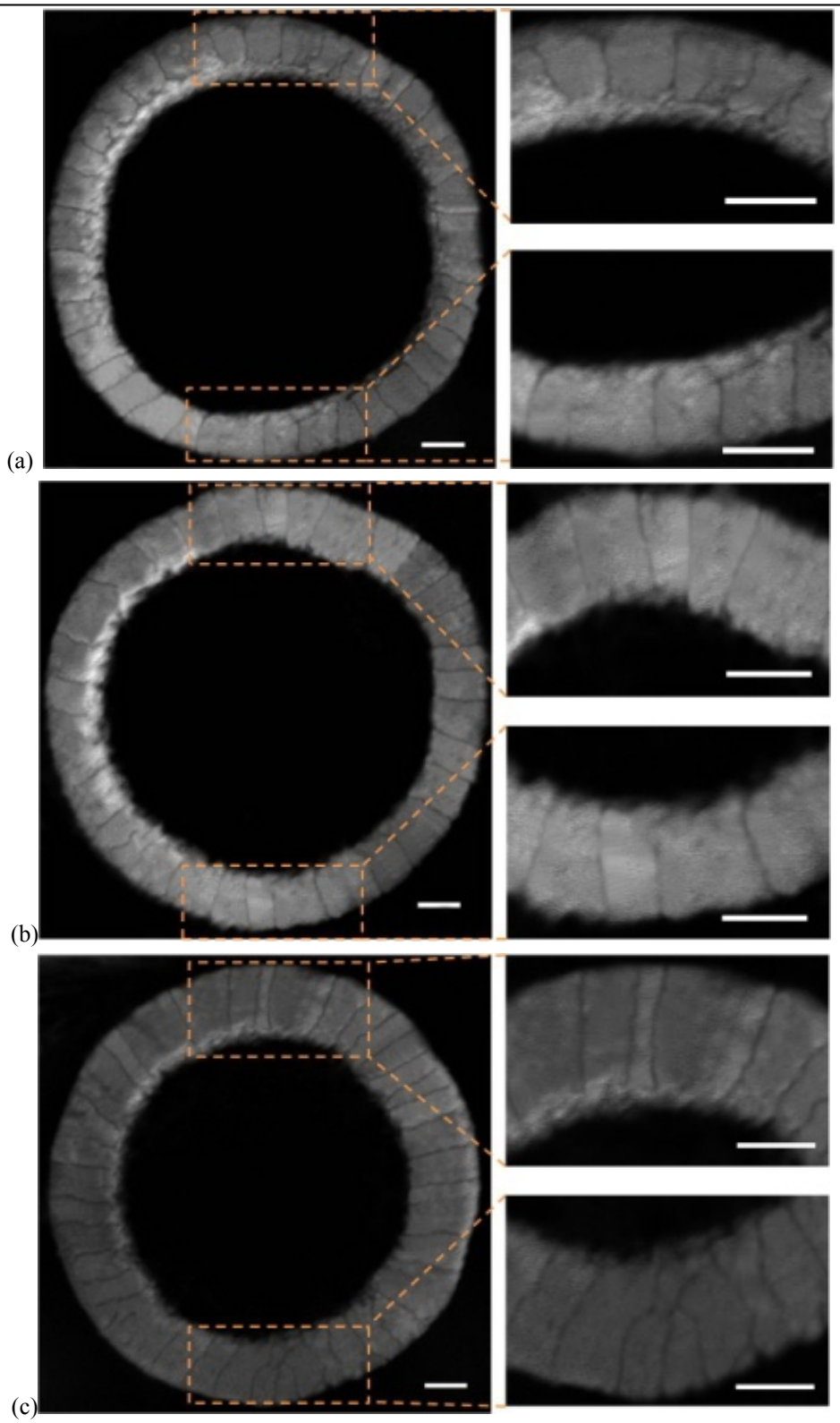

Figure 4.22 SEM images showing cross-section of the hollow capsules after release of dye. PMSQ concentrations: (a) 18; (b) 27; (c) 36 wt% (Inserted images are high-magnification, scale bar =100 nm)

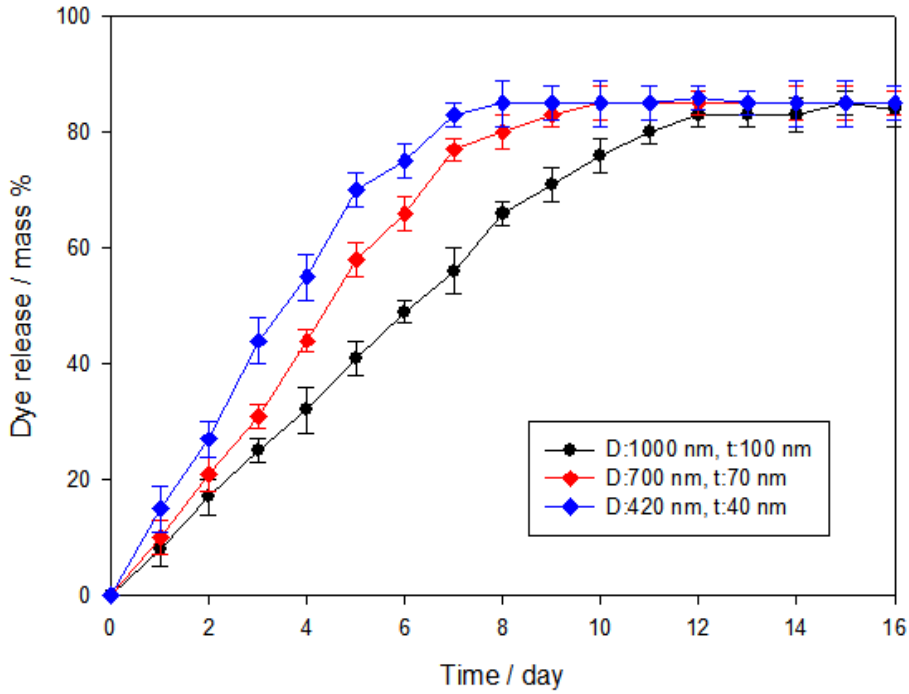

Figure 4.23 Dye release behaviour from PMSQ capsules with different capsule diameters (D). Error bars represent the standard deviation from three experiments

4.7 Summary

This work described in this chapter demonstrates that electrohydrodynamic atomisation provides a means of preparing hollow polymeric microspheres with excellent control over their diameter and shell thickness. This method provides a simple mechanism to integrate the forming of a core-shell structure in one step and offers a simplified route avoiding complex procedures involving templating. It also eliminates the use of surfactants or additives in the forming process. In this study, controlling the surface morphology, shell thickness, and diameter of hollow microspheres were investigated in-depth and results showed that the mean diameter of the hollow microsphere could be varied in the range from 310 nm to 1000 nm by adjusting either the flow rate, polymer concentration, or applied voltage. The shell thickness can be controlled by varying the

polymer concentration, as it is related to the outer diameter by a factor of ~10 at polymer concentration of 18 wt%, a factor of ~8 at 27 wt%, and ~7 at 36 wt%. However, at 63 wt% hollow microsphere cannot be achieved but PMSQ fibres with PFH liquid encapsulated in the fibres can be generated. A dye with a molecular weight of ~ 961 was used to simulate release. The prepared polymeric capsules provided a high storage capacity of dye molecules due to their hollow core space, and the storage capacity was also adjustable by changing the initial concentration of the dye. The release behaviour demonstrate that the PMSQ capsules show a sustained-release behaviour without any burst effect and the release rates increased with the decreasing of shell thickness. The Higuchi model confirmed that the release mechanism from the hollow capsules was diffusion dominated.

Chapter 5

Electrohydrodynamic atomisation as a novel approach for the preparation of monoporous hollow capsules

Monoporous hollow capsules play an important role in microencapsulation and have been extensively studied for drug delivery and biomedical applications due to their higher effective diffusivity and available surface area when compared to microporous capsules of the same size (Peng and Zhang, 2005, Im *et al.*, 2005). They are most commonly prepared by coating colloidal precursor onto the surface, after which the template or seed material is removed by etching. However, the design and preparation of hollow monoporous capsules presents significant challenges. Many of the current techniques used are complex and require highly specialized equipment and/or processing environments, as discussed in the literature review.

This research chapter investigates the feasibility of using co-axial electrohydrodynamic atomisation (CEHDA) to produce monoporous hollow capsules. Polymethylsilsesquioxane (PMSQ) was used as a shell material encapsulating a core of a volatile liquid, perfluorohexane (PFH), which was subsequently evaporated to produce the monoporous hollow microspheres. The influence of solvent properties and processing parameters (flow rate, working distance, the polymer concentration and applied voltage) on the formation of monoporous capsules using CEHDA was investigated in detail. The relationship between the processing parameters and the mean

capsule diameter (D), pore size (d) and ratio β = D/d was also investigated (**Figure 5.1**). Lastly, this chapter examined the capability of monoporous hollow capsules in controlled release applications and the advantages of this method over other techniques are discussed. Briefly, this method enables microspheres with a single surface hole to be easily prepared at ambient temperature and pressure. In addition, this "greener process" does not require the use of surfactants or other additives and so does not entail a template-removal step during the preparation.

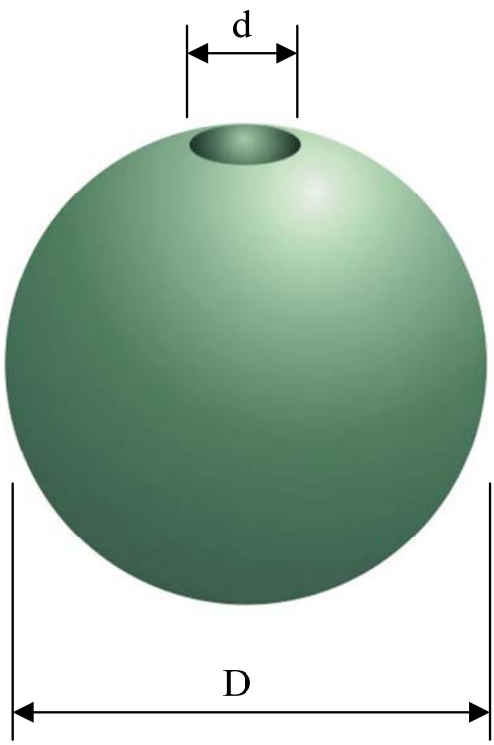

Figure 5.1 Illustration of monoporous hollow capsule and its dimensions

5.1 Characteristics of processing liquid and suspension

It is known from work described in **Chapter 4** that the size and morphology of the microspheres can be influenced by the viscosity, density, electrical conductivity and surface tension of the liquids from which they are formed as well as the processing

conditions, i.e. liquid flow rates, working distance and applied voltage. Polymer solutions with 18, 27, 36, and 63 wt% polymer concentration used in **Chapter 4** were also used in these investigations. The physical properties such as density, viscosity, surface tension and electrical conductivity of polymer suspensions and the PFH are shown in **Table 4.1** (page 85). All experiments were performed under ambient temperature and pressure and ethanol was used to calibrate each of the instruments mentioned in **Chapter 3**.

5.2 Parameters for the preparation of monoporous hollow capsules

The objective of this investigation was to obtain monoporous hollow capsules by varying the electrohydrodynamic processing parameters. The experimental parameters such as flow rate, working distance, the polymer concentration and applied voltage, as well as a suitable parametric mapping to create monoporous hollow structure, play an important role in preparation. The influence of electrohydrodynamic processing parameters on the preparation will be described in the following section.

5.2.1 Fabrication of monoporous hollow capsules

Electrohydrodynamic atomisation has been previously shown (in **Chapter 4**) to provide an advantageous means of preparing particulate polymeric carriers with a narrow size distribution at ambient temperature and pressure with a low number of fabrication steps. The experimental setup used shown in **Figure 3.2** (Page 73), consists of a pair of concentric needles, with the inner needle raised by 2 mm inside the outer needle. The outer and inner needle had an outer and inner diameters of 1100 μm and 685 μm and 300 μm and 150 μm, respectively. The two immiscible liquids, PFH and PMSQ, were injected with different flow rate combinations and under different applied voltages to determine the effect upon microsphere formation.

In this study, the microspheres were only produced when a stable jet mode was achieved with both liquids flowing. In the absence of the PMSQ solution no microspheres were produced which indicated that the inner liquid (PFH) cannot produce a stable jet on its own because of its lower electrical conductivity. This also confirmed that the polymer solution was the driving liquid due to its lower electrical relaxation time (Lopez-Harrera *et al*., 2003) and higher viscosity compared to PFH. The electrospraying modes of both the solution (18 wt % PMSQ) and PFH are shown in **Figure 4.2**. As before (**Chapter 4**), with increasing applied voltage, the dripping mode changed into a stable jet mode which was reached at 3.7 kV while the flow rates of PMSQ and PFH were kept constant at 300 μl min^{-1}, respectively. Once the jet was formed, it broke up into smaller highly charged droplets. These small droplets were neutralized by the presence of a grounded electrode during collection.

5.2.2 Effect of flow rate

In order to obtain monoporous capsules, the flow rates in the inner and outer needles are key control parameters. To identify the influence of the PMSQ flow rate, the flow rate of syringe 1 (PFH solution) was fixed at 300 μl min^{-1}, while the flow rate of syringe 2 (PMSQ solution 18 wt %) was varied between 50 and 600 μl min^{-1}. The effect of increasing the liquid flow rate on the capsule size and the distribution is shown in **Figure 5.2**. It shows that the mean diameter (D) of the capsules increased with increasing flow rate of PMSQ solution from 275 nm at 200 μl min^{-1} to 660 nm at 600 μl min^{-1}. However, if the liquid flow rate was not sufficiently high (< 200 μl min^{-1}), a stable jet could not be achieved since the PMSQ solution cannot provide sufficient driving force to encapsulate the PFH liquid. The ratio $\beta = D/d$ also showed a slight increase from 5.2 at 200 μl min^{-1} to 6.8 at 400 μl min^{-1} indicating that a higher

available surface-volume ratio could be achieved (Im *et al*., 2005). However, the value remained almost constant for flow rates > 400 μl min^{-1} (**Figure 5.3**). The high-magnification SEM images in **Figure 5.4a-e** show that the capsules were spherical with smooth surfaces and the low contrast of the core indicates that they had a hollow structure. Some spheres are aggregated to others might because of wetting and drying during sample preparation. By increasing the flow rate of the PMSQ solution, the mean size of the pore (d) on the shell of the microspheres increased from ~45 nm at 200 μl min^{-1} to ~100 nm at 600 μl min^{-1}. **Figure 5.4f** shows low-magnification SEM image of the monoporous hollow capsules. Some of holes cannot be observed only because the rest position of the microspheres generated, where the direction of hole points downwards after drying in a desiccator.

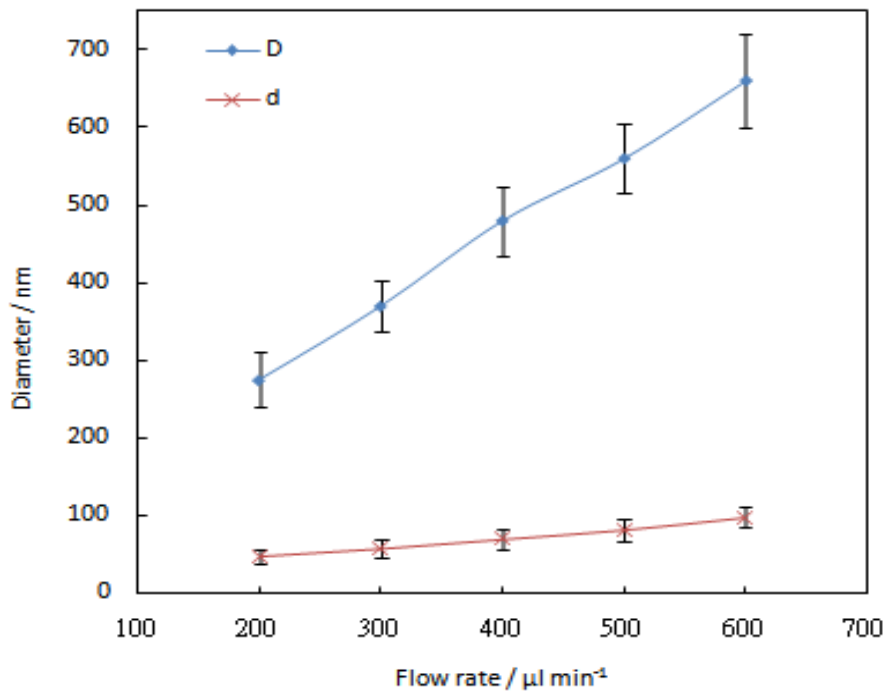

Figure 5.2 Size of microspheres and pore vs. flow rate of PMSQ (Error bars represent the standard deviation from three experiments)

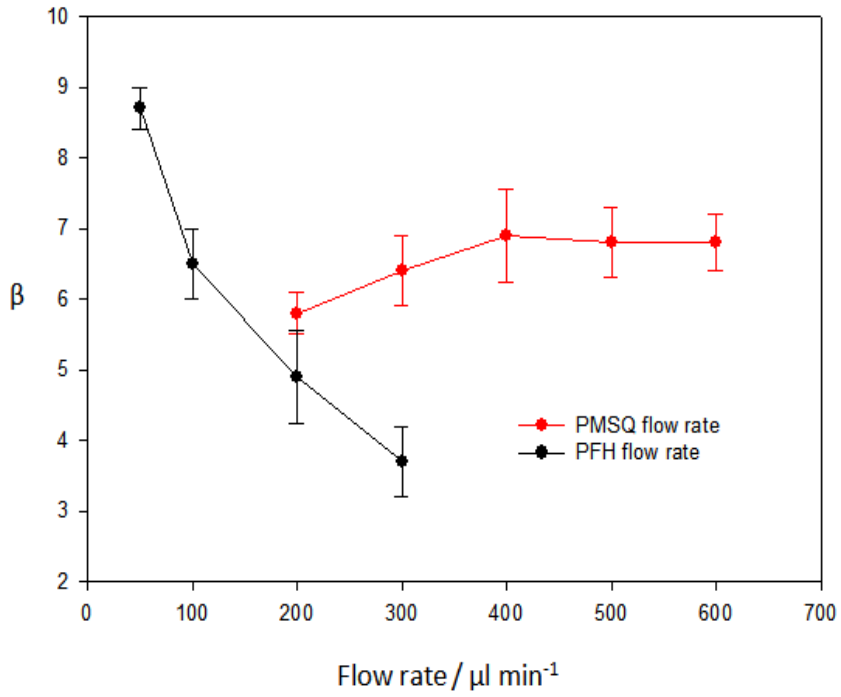

Figure 5.3 Variation in the β ratio with flow rates of PMSQ and PFH (Error bars represent the standard deviation from three experiments)

Figure 5.5 shows the relationship between the mean diameter of the microspheres and the flow rate of the PFH solution. The flow rate of syringe 1 (PFH solution) was varied between 50 and 300 μl min^{-1}, while the flow rate of syringe 2 (PMSQ solution) was fixed at 400 μl min^{-1}. It shows that increasing the flow rate of the PFH solution resulted in an increasing mean diameter and standard deviation. The diameter (D) varied from 420 nm at 50 μl min^{-1} to 505 nm at 300 μl min^{-1}. However, PFH is a highly volatile liquid with a relatively low electrical conductivity which can result in unstable jetting and so a stable jet could not be formed for PFH flow rates > 400 μl min^{-1}. In fact, the influence of the PFH flow rate on capsule diameter was smaller than that of the PMSQ solution (**Figure 5.2**), confirming that in this experiment the driving liquid with the lower electrical relaxation time dominated the formation of the microspheres.

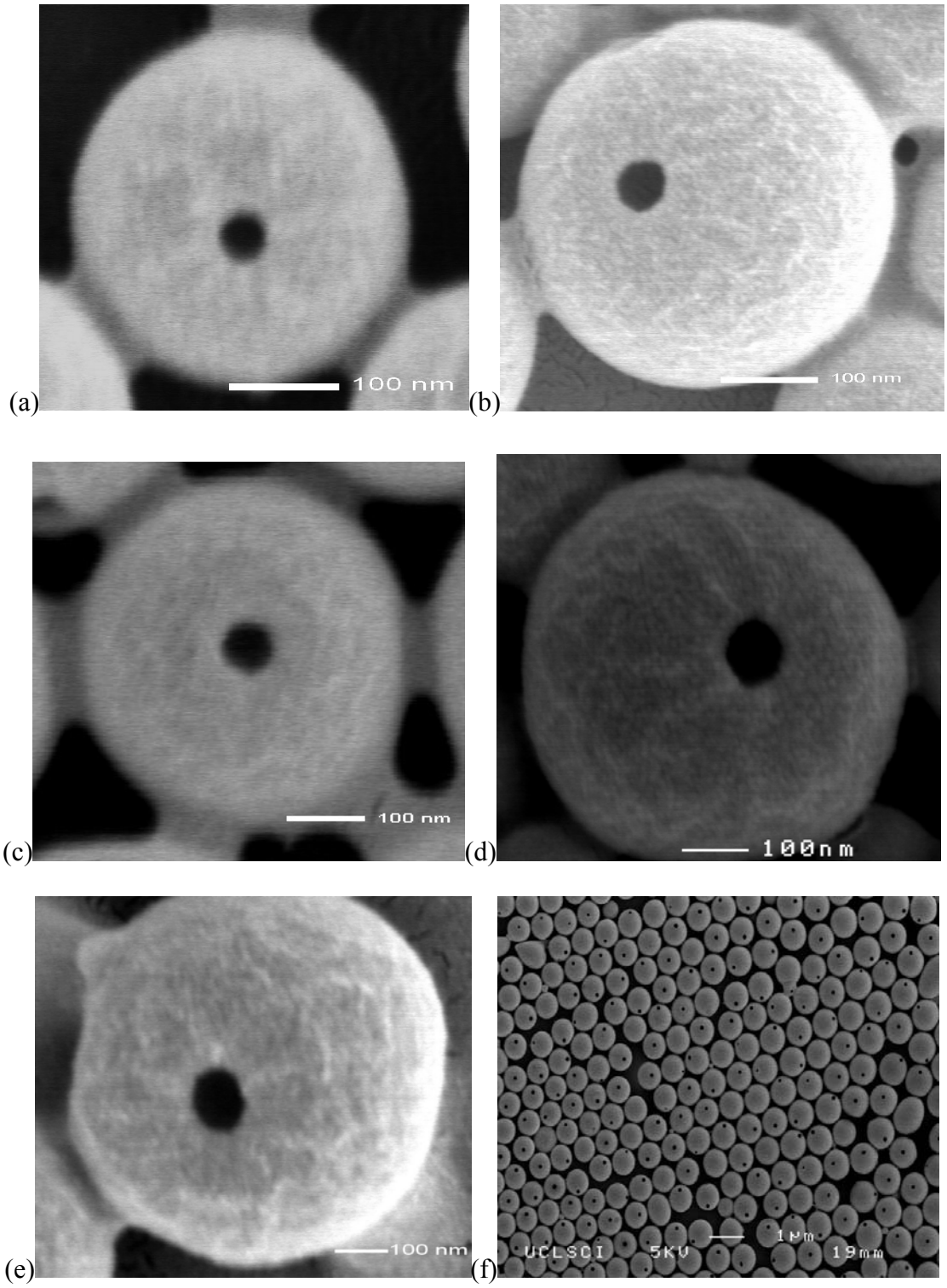

Figure 5.4 SEM images of the one-hole microspheres obtained at different PMSQ flow rates: (a) 200; (b) 300; (c) 400; (d) 500; (e) 600 μl min^{-1}; (f) low-magnification of (e). Some spheres are aggregated to others which might be because of wetting and drying during sample preparation

The mean diameter of the pore (d), however and its standard deviation again increased with increasing PFH flow rate, varying from ~50 nm for a mean sphere diameter of 420 nm to 135 nm for a mean sphere diameter of 505 nm. β was decreased from 8.7 at 50 μl min^{-1} to 3.7 at 300 μl min^{-1} (**Figure 5.3**). This suggested that the PFH flow rate had significantly influenced pore formation although its influence upon diameter (D) was relatively small.

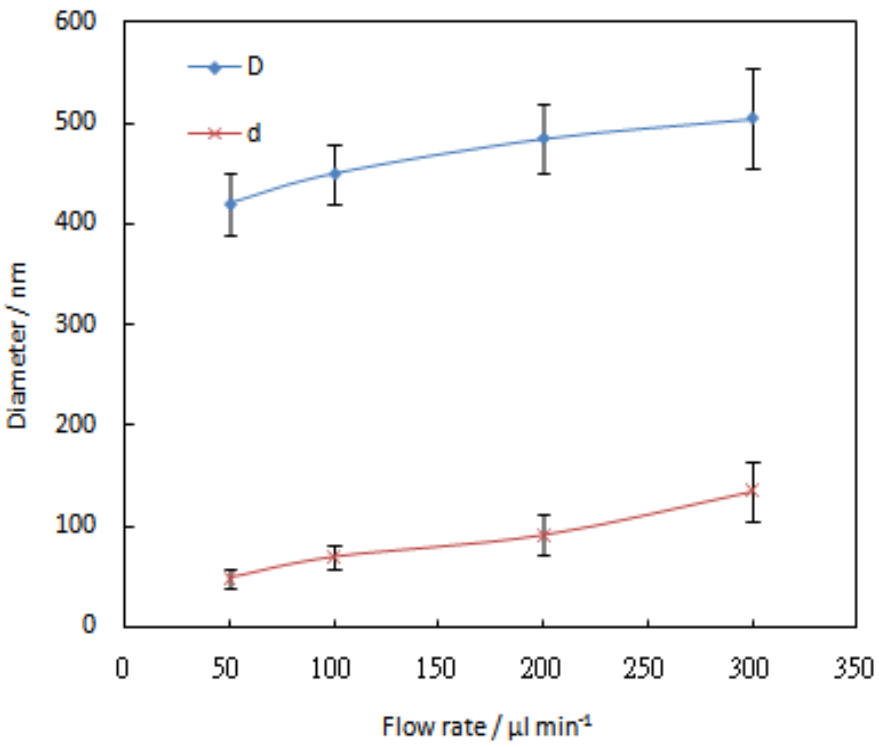

Figure 5.5 Size of microspheres and pore vs. flow rate of PFH (Error bars represent the standard deviation from three experiments)

5.2.3 Effect of needle-electrode distance

In order to understand the influence of needle-electrode distance on the size of monoporous hollow capsule, the needle-substrate distance was varied from 8 to 16 mm.

During this investigation, 18 wt% PMSQ was syringed to the outer needle at a flow rate of 300 μl min^{-1} while the flow rate of syringe 1 (PFH solution) was fixed at 300 μl min^{-1}. The size of hollow capsules made by varying distance between the needle and grounded substrate is shown in **Figure 5.6**. It shows that the mean diameter (D) of the microspheres decreased with increasing needle-electrode distance from 480 nm at 8 mm to 300 nm at 12 mm. The ratio β = D/d also showed a slight increase from 6.2 at 8 mm to 6.9 at 16 mm. This is because the evaporation of solvent increased with increasing distance (Xie *et al.*, 2006).

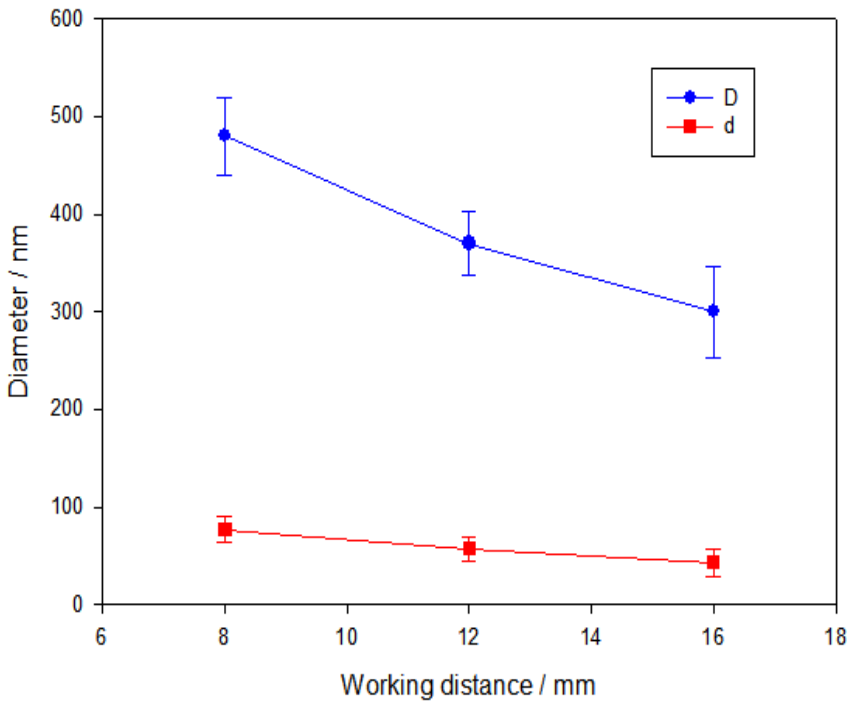

Figure 5.6 Size of microspheres and pore vs. working distance (Error bars represent the standard deviation from three experiments)

5.2.4 Effect of polymer concentration

The effect of the PMSQ concentration on the preparation of monoporous microspheres was studied at different concentrations of 18, 27, 36 and 63 wt%. In terms of shape, the microparticles generated were spherical except at 63 wt%. The concentration of PMSQ affected both the electrical conductivity and viscosity of the solution (**Table 4.1,** page 85), which increased and decreased, respectively, and the observed changes in mean capsule diameter (D) may be attributed to the variation in these properties (Hartman *et al*., 1999b, Jayasinghe and Edirisinghe, 2004). The mean diameter of the pore (d) was constant (~ 65 nm) for concentrations between 18 and 36 wt% (**Figure 5.7**). However, at a PMSQ concentration at 63 wt%, the transition from electrohydrodynamic spraying to electrospinning was observed. **Figure 5.8** shows that at 63 wt% fibres were spun and these consisted of PFH liquid droplets with a diameter of ~7 μm encased in a PMSQ strand of diameter ~10 μm. **Figure 5.9** shows a fibre with its shell cracked open and this is further evidence to indicate that the PFH previously occupied in the internal cavity and subsequently evaporated to form the hollow structure, while **Figure 5.10** shows an electrospinning fibre without a hollow cavity due to the absence of PFH. Thus, it may be concluded that low PMSQ concentrations can be used to prepare monoporous micropsheres whilst high PMSQ concentrations are suitable for preparing functional fibres, e.g. for protective textiles and drug delivery applications (Zong et al., 2003). However, varying the PMSQ concentration did not appreciably affect the pore size (d) although it did increase the mean diameter of the particles (D).

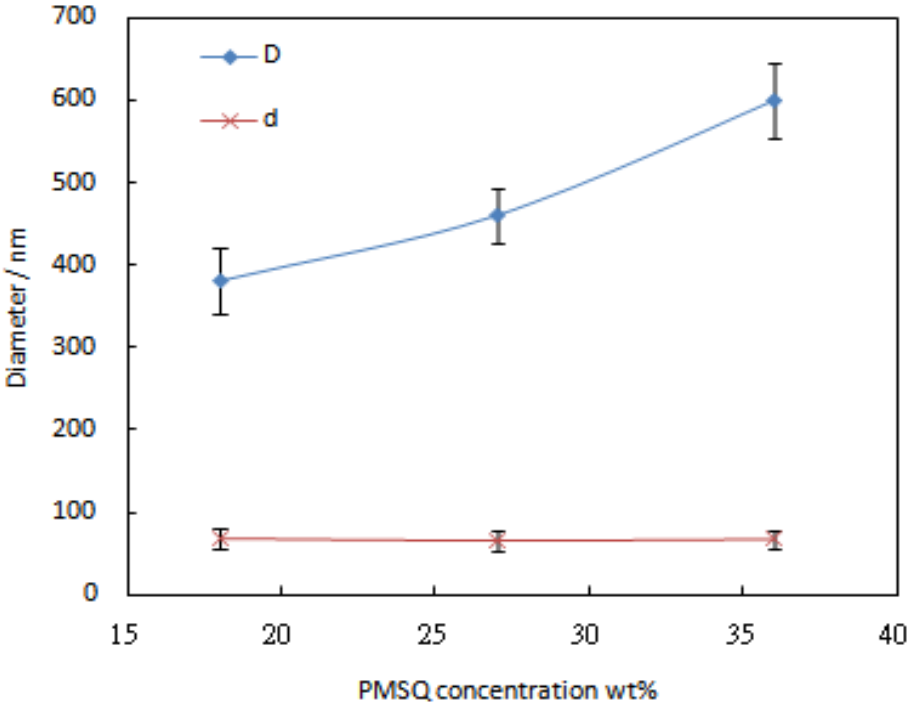

Figure 5.7 Size of microspheres and pore vs PMSQ concentration (Error bars represent the standard deviation from three experiments)

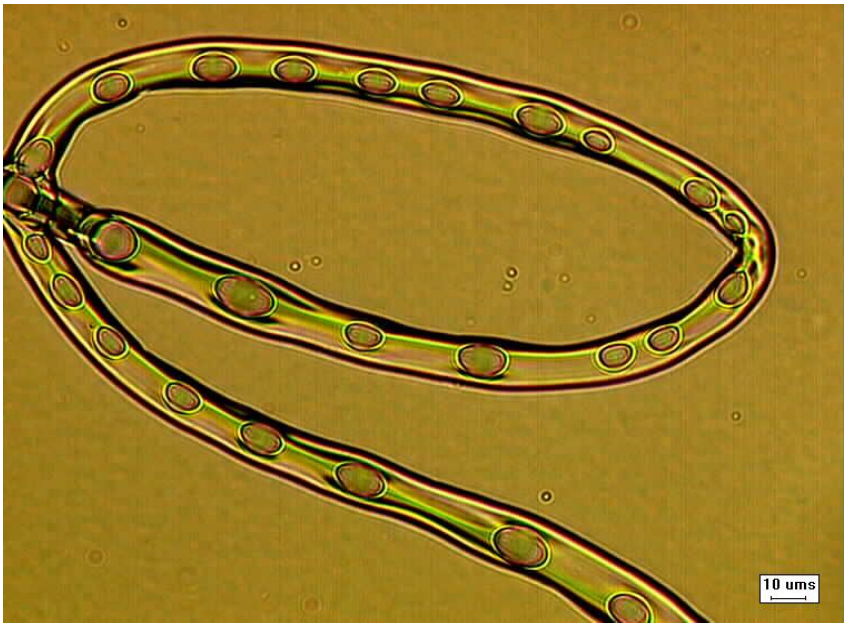

Figure 5.8 Optical microscopy image showing the product obtained at 63 wt % PMSQ concentration

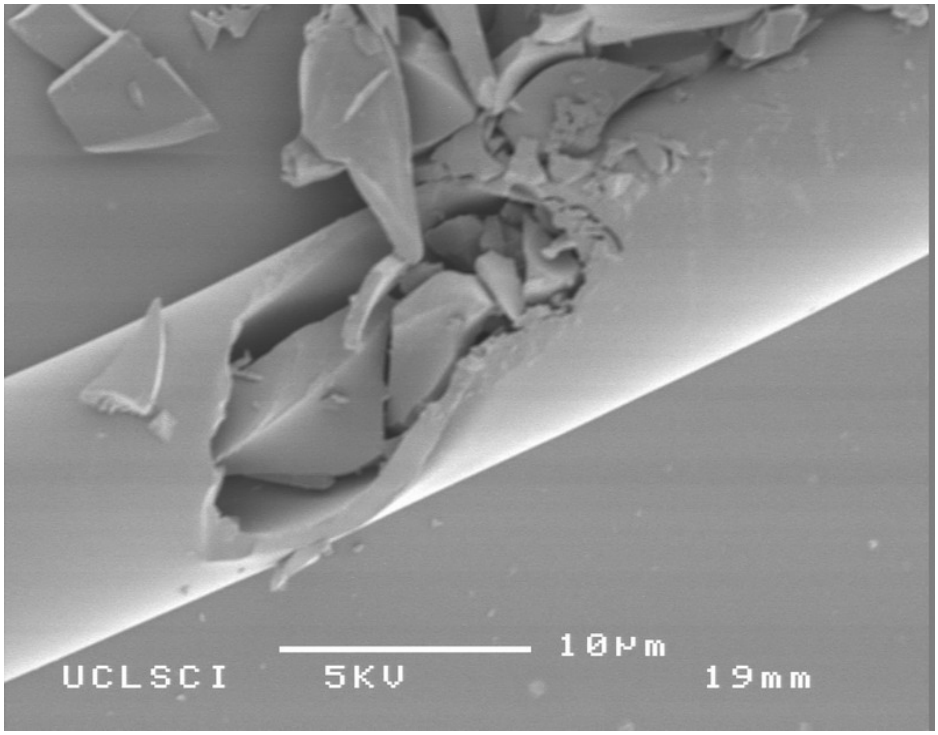

Figure 5.9 Scanning electron micrograph of fractured electrospinning fibre

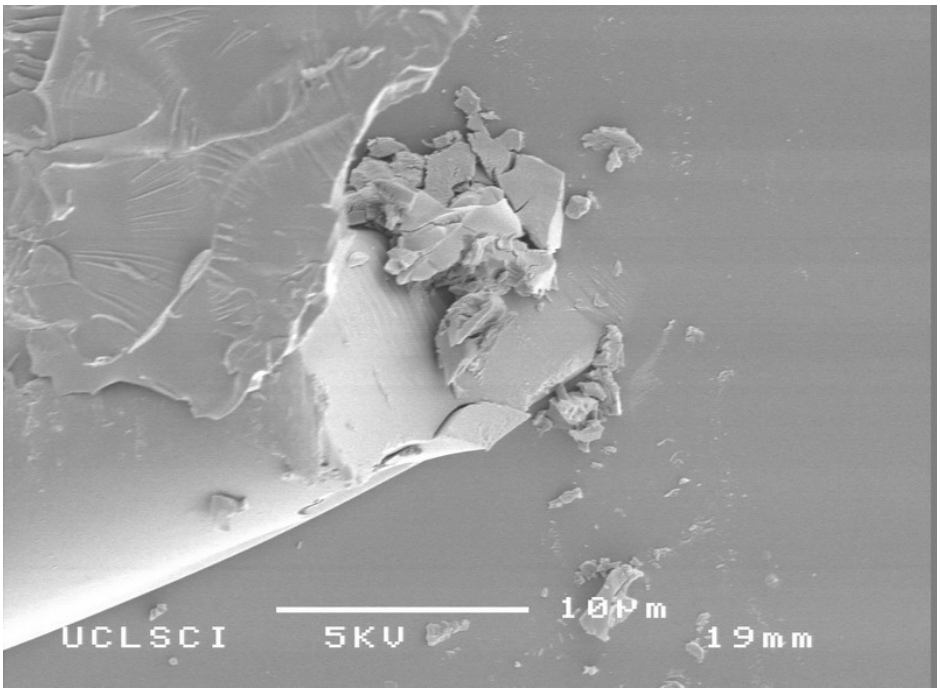

Figure 5.10 Scanning electron micrograph of fractured electrospinning fibre without hollow cavity

5.2.5 Effect of applied voltage

The voltage between the needles and the ground electrode is obviously a critical parameter in achieving different electrospraying modes (Lopez-Harrera *et al*., 2003). The effect of applied voltage on the formation of monoporous capsules at different voltages of 3.5, 3.8, 4.1 and 4.5 kV was investigated, while the polymer concentration was fixed at 36 wt%, and the flow rates in the inner and outer needles were kept at 300 and 300 μl min^{-1}, respectively. It was found that the mean diameter (D) of the microspheres decreased significantly with increasing applied voltage (**Figure 5.11**). Furthermore, as the applied voltage increased, the jet angle became larger and the acceleration distance became shorter. The diameter (D) varied from 860 nm at 3.5 kV to 350 nm at 4.5 kV, while the diameter of the pore (d) varied from 110 nm at 3.5 kV to 36 nm at 4.1 kV but the pore could not be observed at an applied voltage above 4.5 kV. This can be attributed to the smaller microsphere diameter and correspondingly smaller amount of PFH in the polymer shell whose evaporation flux may not be enough to create the hole in the surface. This hypothesis is supported by the fact that with increasing PFH flow rate, not only the capsule diameter but also the pore size increased (**Figure 5.5**).

5.3 Structural features and D/t ratio

Scanning electron micrographs of fractured microspheres were used to investigate their internal structure. In **Figure 5.12a**, fracture reveals a single cavity within a polymer shell, the cavity was occupied by PFH. **Figure 5.12b** shows the cross section of a monoporous microsphere prepared at 4.1 kV which has a varying shell thickness that becomes lowest in the vicinity of the pore (as marked by arrow). On the other hand, in **Figure 5.12c**, the cross section of a microsphere prepared at 4.5 kV without a hole on

its surface is shown, having a diameter of 360 nm and a relatively uniform shell thickness of 40 nm. It is interesting that although these monoporous microspheres were prepared by CEHDA, they show a similar internal morphology to those obtained by other methods (Jeong *et al*., 2007, Im *et al*., 2005). This may be attributed to phase separation caused by the low miscibility between PFH and the PMSQ solution.

In this study, the highest value of β (12.3) was obtained by increasing the applied voltage (**Figure 5.13**). In contrast, the smallest value of β (3.5) was obtained by increasing the PFH flow rate (**Figure 5.3**). The ability to control the ratio of sphere to pore diameter may be highly desirable for drug delivery applications as this can be directly used to load functional materials into the cavity and also be used to control encapsulation and release behaviours (Jeong *et al*., 2007, Guan *et al*., 2007).

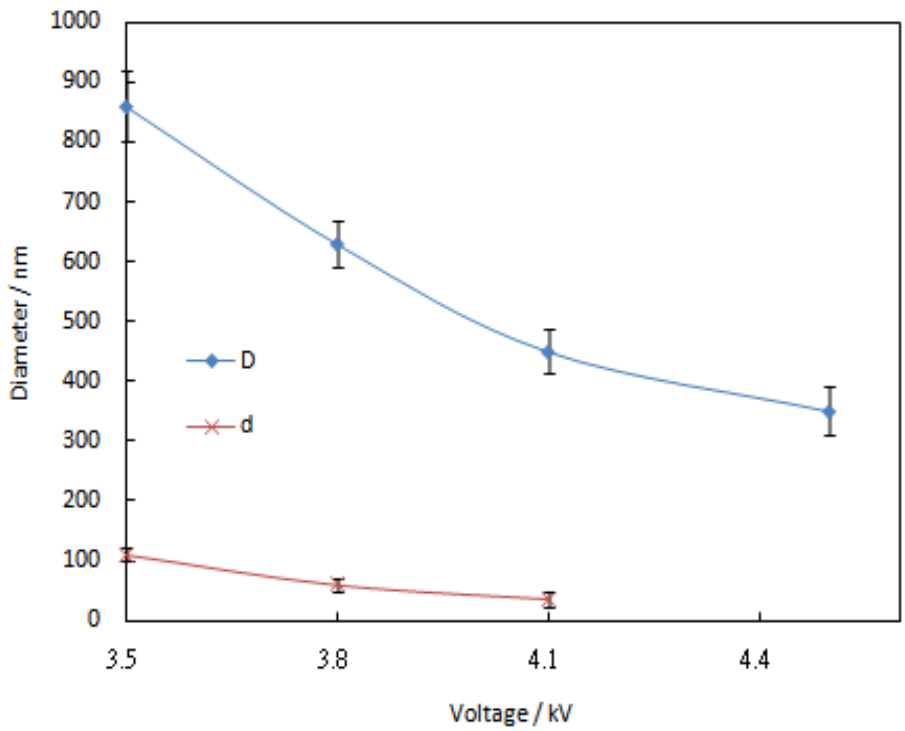

Figure 5.11 Diameter of microspheres and pores vs. applied voltage (Error bars represent the standard deviation from three experiments)

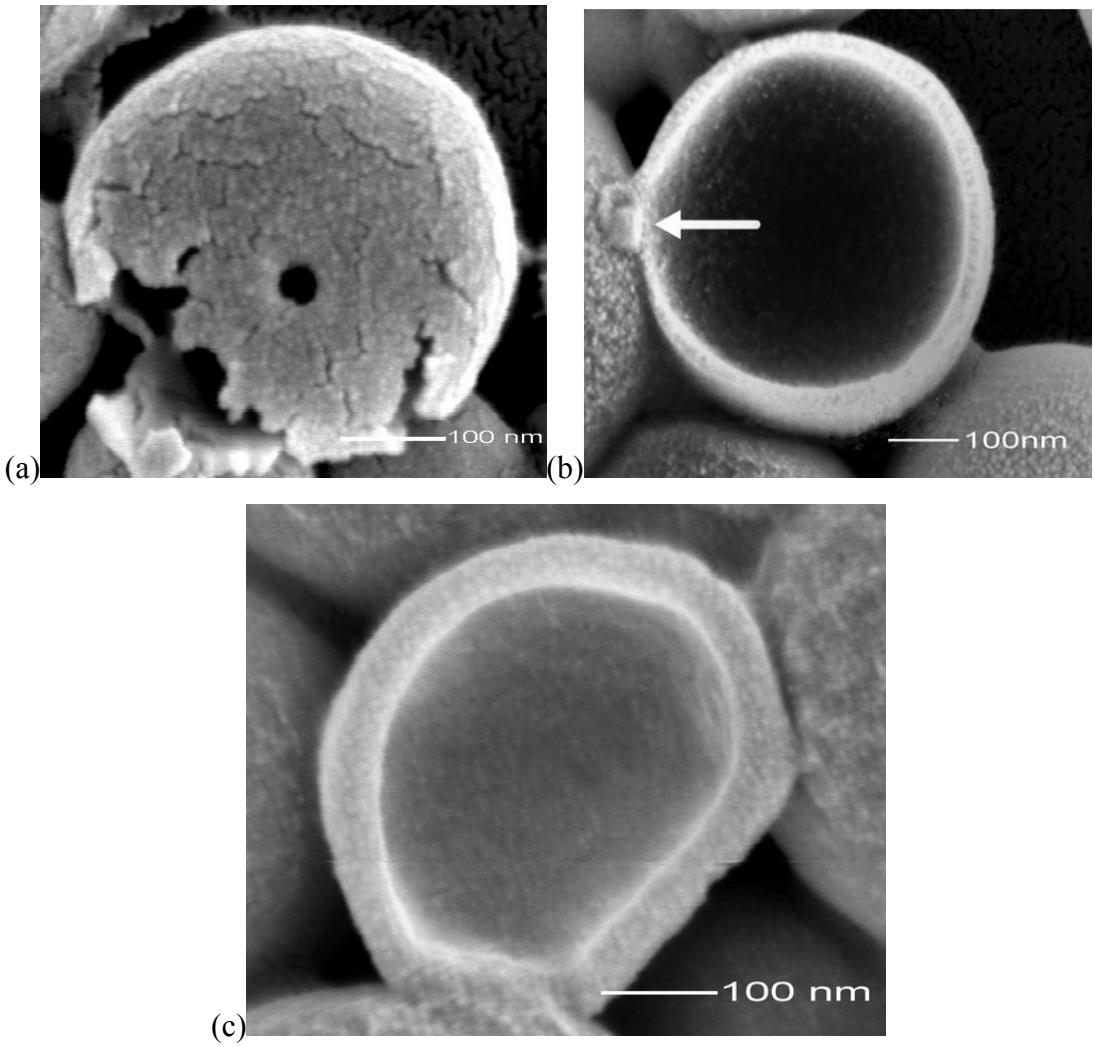

Figure 5.12 Scanning electron micrographs of (a) fractured monoporous microsphere; (b) cross section of monoporous microsphere; (c) cross section of hollow microsphere

5.4 Steady jetting region

Previous published work, has shown that capsule size and shape can be controlled by changing the flow rate, polymer concentration, working distance and applied voltage in electrohydrodynamic processing (Xie *et al*., 2006, Berkland *et al*., 2004). In this study, the influence of flow rate, PMSQ concentration, and applied voltage upon the mean microsphere diameter and pore size was investigated. The stable jet mode parametric

space for the preparation of monoporous microspheres at 18 wt%, 27 wt%, and 36 wt% PMSQ concentration is shown in **Figure 5.14 a–c**. With all other parameters held constant, the applied voltage required for the stable jet mode increased with increasing PMSQ flow rate. Furthermore, when the PMSQ concentration was increased from 18 to 36 wt%, the applied voltage required to achieve the stable jetting also became higher, which indicates that the difference between the upper and lower critical voltages for stable jet mode spraying decreases with increasing PMSQ concentration.

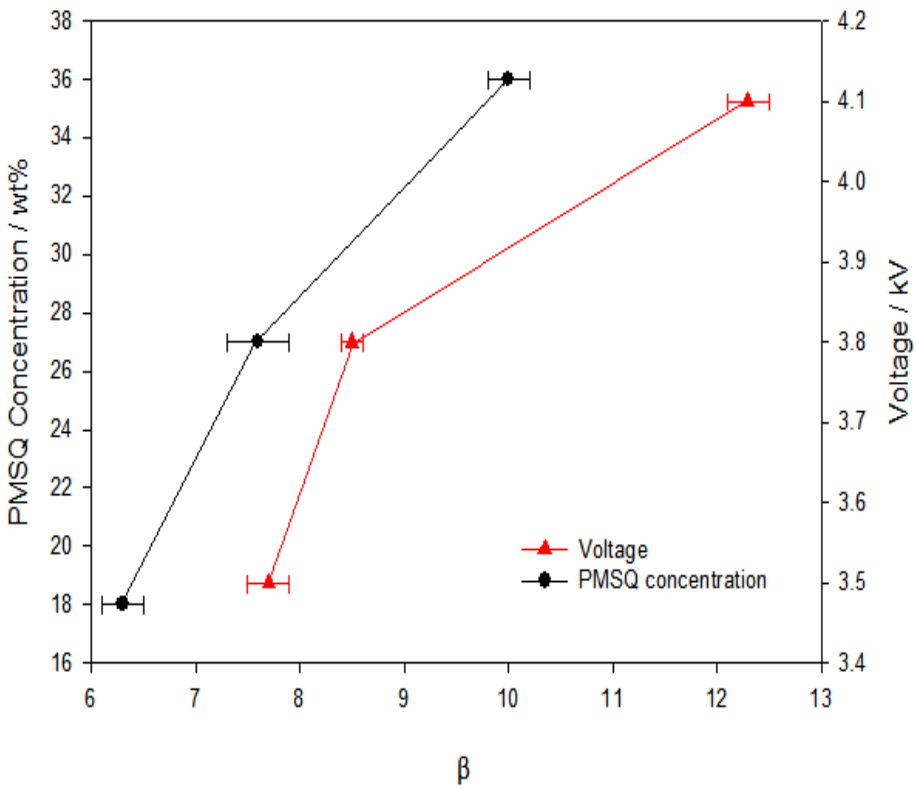

Figure 5.13 Variation of the ratio of capsules to pore diameter (β) as a function of polymer concentration and voltage (Error bars represent the standard deviation from three experiments)

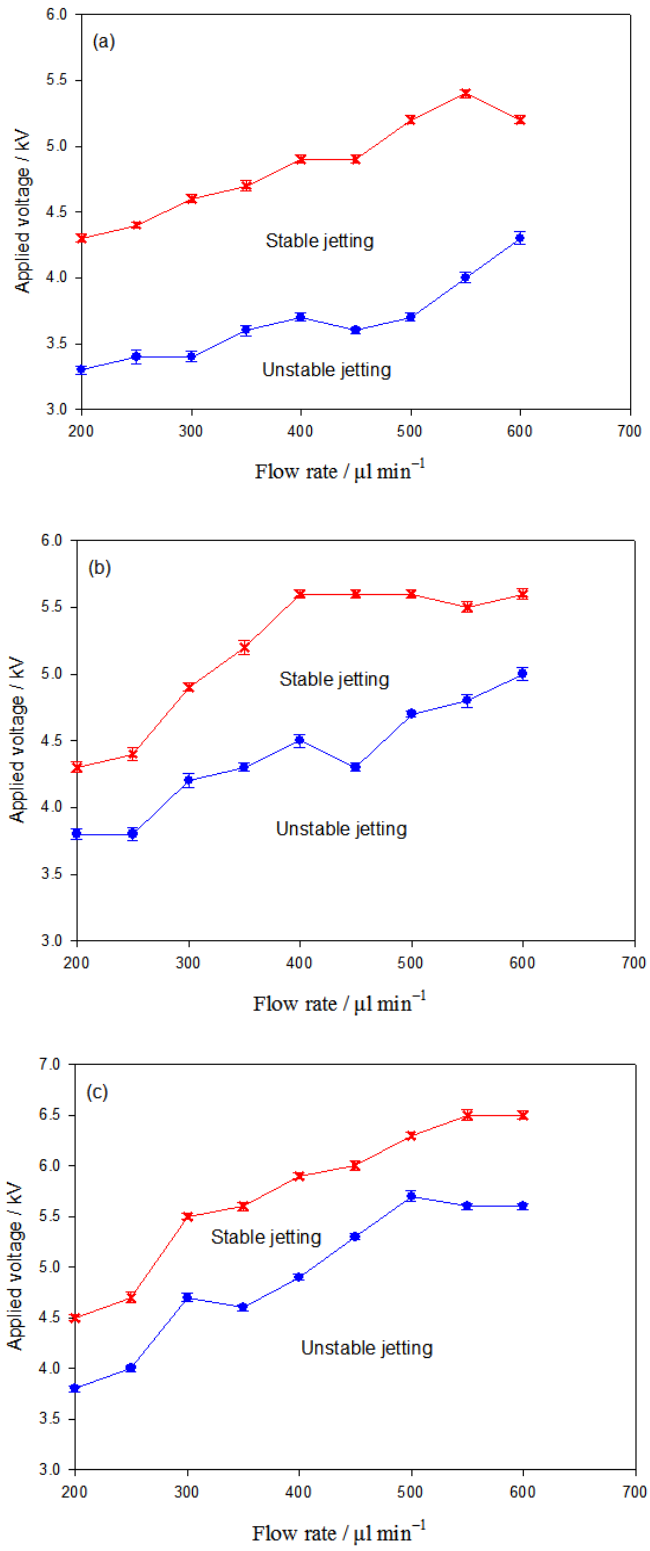

Figure 5.14 Stable jet mode map showing the relationship between the applied voltage and PMSQ flow rate at PMSQ concentrations of (a) 18 wt%, (b) 27 wt%, and (c) 36 wt% (Error bars represent the standard deviation from three experiments)

5.5 Mechanism of pore formation

The formation of the surface pore may be attributed to a number of factors. First of all, PFH is a volatile liquid with very low miscibility with organic solvents (Giesecke and Hynynen, 2003, Pisani *et al*., 2006). Indeed, PFH is crucial to achieving a hollow spherical shape. The creation of the pore on the surface of microsphere may be simply due to the evaporation flux of the solvent. The fact the pore size was found to be related to the PFH flow rate supports this. The fact that the core (PFH liquid) can be removed at ambient temperature via evaporation and without using chemical solutions avoids the need for template-removal steps which provides distinct advantages in terms of processing time, cost and preventing contamination. Some PFH may remain in the microspheres but since PFH is considered to be non-toxic and unreactive this is not problematic. It is also able to dissolve and deliver oxygen to several tissues (Riess, 2001) and is also used as an external phase of emulsion and provides a promising tool for the entrapment of lipophilic drugs into hydrophilic or lipophilic polymers.

A second possibility relates to the fact that the electrical conductivity of PFH is very low. In the present study, the PMSQ solution was the driving liquid as its electrical conductivity was substantially higher than that of PFH. When the polymer solution and PFH passed through the needles and were exposed to the electrical field, the PMSQ solution will have been accelerated by the electrical field, but the flow of the PFH would have been dominated by viscous stresses (Lopez-Harrera *et al*., 2003). Therefore, whilst the polymer solution underwent breakup to produce small diameter microspheres, the PFH was directed to the ring electrode (grounded) by the shear motion because the electrical stress was transferred to PFH. Thus, the formation of monoporous microspheres may realise before a complete PMSQ shell is achieved due

to the discrepancy in driving velocities. However, besides the factors mentioned above, the final morphology can have a strong dependence on the kinetic factors including polymerization, air resistance, and surface tension during the electrohydrodynamic atomisation process.

5.6 Evaluation of encapsulation and release behaviour of monoporous hollow capsules

In order to have effective storage and release of a drug in a hollow capsule, the size of drug molecules must be smaller than the pore channels of the shell thickness. Thus, the presence of a monopore in the shell of a hollow capsule enables enhanced encapsulation by allowing direct diffusion of drug into the carrier. Furthermore, their use can be found in other applications such as catalytic carriers, thermal insulation, and targeting (Moon and Jeong, 2008, Yow and Routh, 2008, Guan *et al*., 2007). The aim of this section was to conduct a detailed study of the relationship between capsule outer diameter and pore size in terms of loading and releasing capacity of encapsulated material. To investigate encapsulation and release, Evans Blue dye (Mw: 961) was used as a marker to examine the characteristics of four sets of monoporous hollow capsules denoted as $PMSQ_{(n)}$ (**Table 5.1**). They were dispersed in 20 mL of distilled water with Evans Blue dye. After the dye was absorbed over predetermined time intervals, the resulting capsules containing the dye were retrieved by centrifugation. The carrier particles were then dispersed in 20 ml of phosphate buffer solution (pH 7.4) and stirred at 100 rpm in a vial in order to perform release investigations. Typically, the temperature of the suspension was kept at 37 ± 0.5 °C. At designated time intervals, the vial was taken out and centrifuged. The supernatants were directly analyzed by UV spectroscopy at the wavelength of 607 nm. Finally, the capsule morphology was investigated after the encapsulation and release studies.

Table 5.1 Details of monoporous hollow capsules for encapsulation and release evaluations

Sample No.	Diameter (D), nm	Pore size (d), nm	β = D/d
$PMSQ_1$	450	69	8.7
$PMSQ_2$	450	36	12.3
$PMSQ_3$	505	135	3.7
$PMSQ_4$	630	60	8.5

5.6.1 The influence of different pore sizes

Dye-loaded capsules having a similar outer diameter and a wide range of pore sizes (i.e. 36 and 69 nm) were investigated to understand the effect of pore diameter on release behaviour. Different pore diameters led to a difference in the release rate of dye, where larger pore sizes exhibited high release rates, as shown in **Figure 5.15**. The burst release of $PMSQ_1$ is attributed to the rapid release of the dye, which is readily accessible in the buffer medium. Following the burst release of dye, a slower steady release of dye can be observed. On the other hand, the dye release rate of $PMSQ_2$ was significantly slower when compared to the $PMSQ_1$. It takes approximately two days for $PMSQ_2$ to release 40% of the dye, whereas it only takes one day for the $PMSQ_1$ to do likewise. After 4 days, ~75% of dye was released from $PMSQ_1$, compared to 80% released for $PMSQ_2$. Therefore, the difference in the release profiles of these two systems is attributed to the effect of pore size of $PMSQ_1$ and $PMSQ_2$. The higher pore diameter in the monoporous capsule can result in an increased release rate.

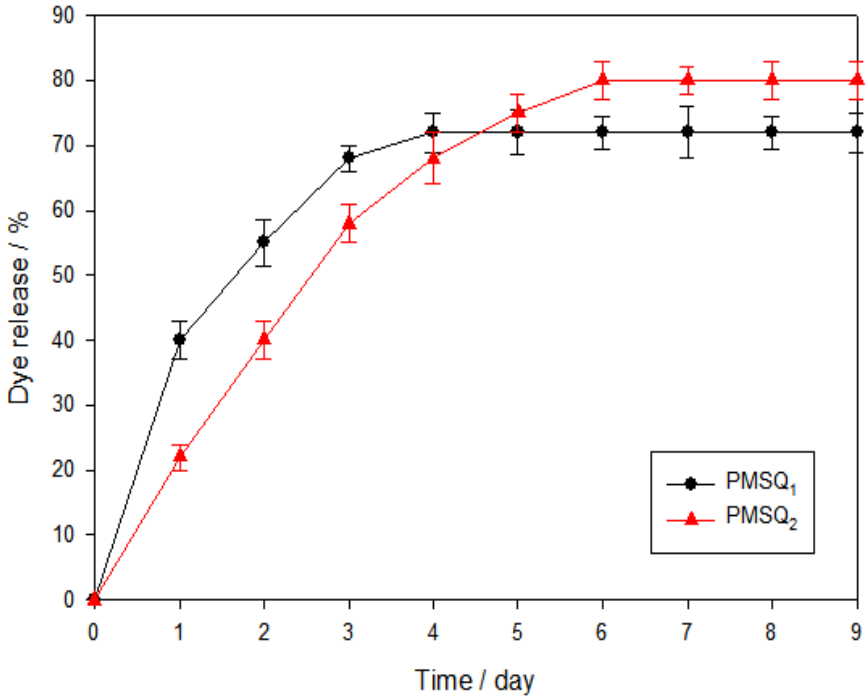

Figure 5.15 Effect of different pore sizes on the release behavior (Error bars represent the standard deviation from three experiments)

5.6.2 The influence of different diameters

The effect of monoporous capsules having different diameters on the release behaviour are shown in **Figure 5.16**. Both samples ($PMSQ_1$ and $PMSQ_4$) had similar pore diameters (~60 nm) and different outer diameters ranging from 450 nm to 630 nm. It can be seen that the release profiles of the two samples were similar with a high release rate at beginning stage, followed by sustained release of dye. In the first day, 40 % of amount dye was released from the two samples, and then 70 % of dye was released in the three days. A similar release behaviour is attributed to the presence of the same diameter mono pore on the hollow capsules, which provided a certain amount of dye to be released to the sink. In addition, although $PMSQ_4$ had a bigger diameter compared to $PMSQ_1$, the release rate of dye was not remarkably different. Therefore, these results suggested that the release rate is mainly controlled by the diffusion of dye molecules

through the mono-pore on the hollow capsule regardless of capsule diameter.

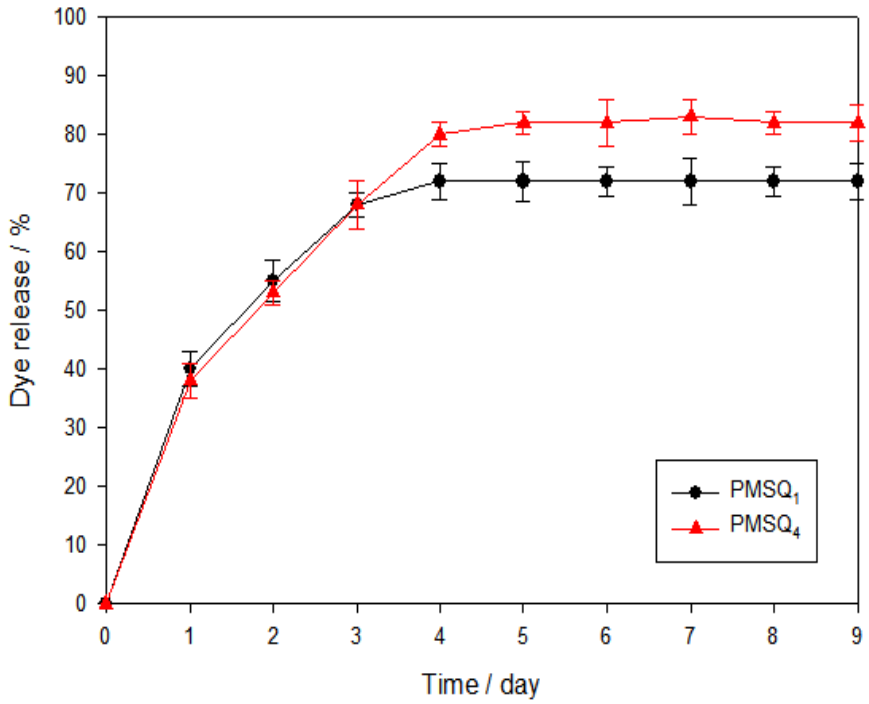

Figure 5.16 Effect of capsule diameter on the release behavior (Error bars represent the standard deviation from three experiments)

5.6.3 The influence of β values

The wide variation in the dye release as a function of the β value is presented in **Figure 5.17**. This is due to the combined effect of the pore and capsule diameters. Importantly, the release rate of the highest β value (12.3) is slower than that of the lowest β value (3.7). The latter released dye faster and reached a plateau at 35 % in one day, and then no noticeable release was observed. The high release rate of dye was thought to be due to the relative large pore diameter (~135 nm) in the capsules. In contrast, the dye release from the higher β value (12.3) showed a slower steady release because of the decrease in the pore diameter. In addition, it can be noted that the amount of dye released from the lower β value (3.7) sample was significantly decreased, despite the sample ($PMSQ_3$)

having a bigger capsule diameter compared with $PMSQ_2$, which should have provided a higher encapsulation rate. However, the amount of dye released from $PMSQ_3$ was limited to 35% which is attributed to the leakage of dye from the carrier during sample preparation.

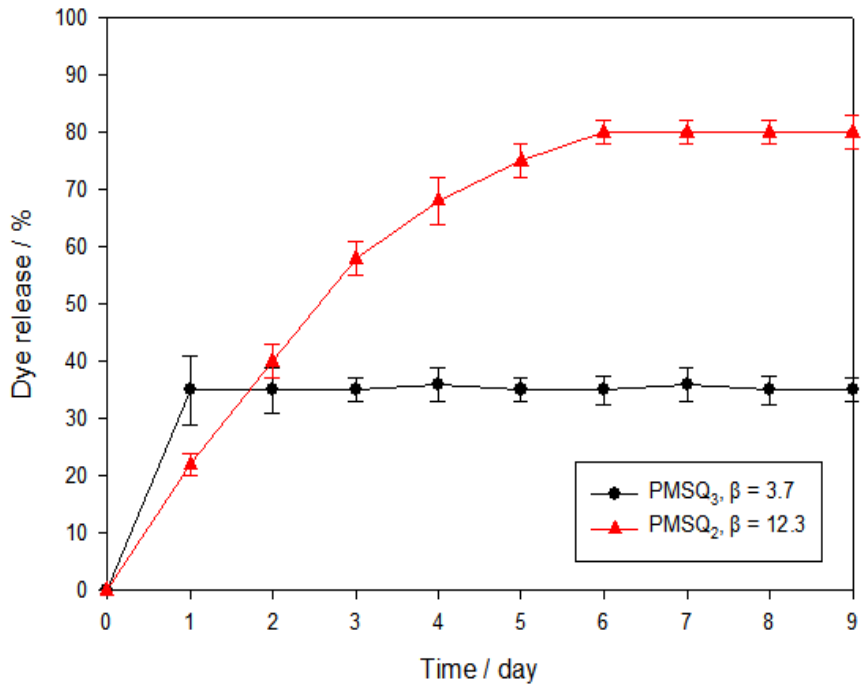

Figure 5.17 Dye release behaviour of the capsules with the highest (β:12.3) and the lowest β values (β:3.7) (Error bars represent the standard deviation from three experiments)

5.6.4 The influence of encapsulation time

Two samples of monoporous hollow capsules with different β values (**Table 5.1**) were used to investigate the effect of encapsulation capacity on the monoporous hollow capsule by incubating $PMSQ_1$ and $PMSQ_2$ in distilled water with Evans Blue dye for 360 and 3600s, respectively. The dye release behaviour from the two samples is shown in **Figure 5.18**. An increase in the dye loading was observed by increasing

encapsulation time from 360 to 3600s. The total amount of dye released from incubated $PMSQ_1$ in 360s was only 11 %, while 52 % of dye was released from incubated $PMSQ_1$ in 3600s. On the other hand, 7 % dye release was observed from $PMSQ_2$ in 360s and upon increasing incubation time to 3600s, the maximum dye content released reached 37 %. In addition, $PMSQ_1$ with a pore diameter of 69 nm had higher encapsulation capacity than that of 39 nm pore diameter of $PMSQ_2$ capsules. Therefore, the results indicated that despite similar particle diameters (450 nm), the existence of a pore on the surface of hollow capsules allows direct loading of dye. The bigger monopore size provided a higher loading capacity because of an easier absorption and quicker transport of dye molecules into the polymeric capsules.

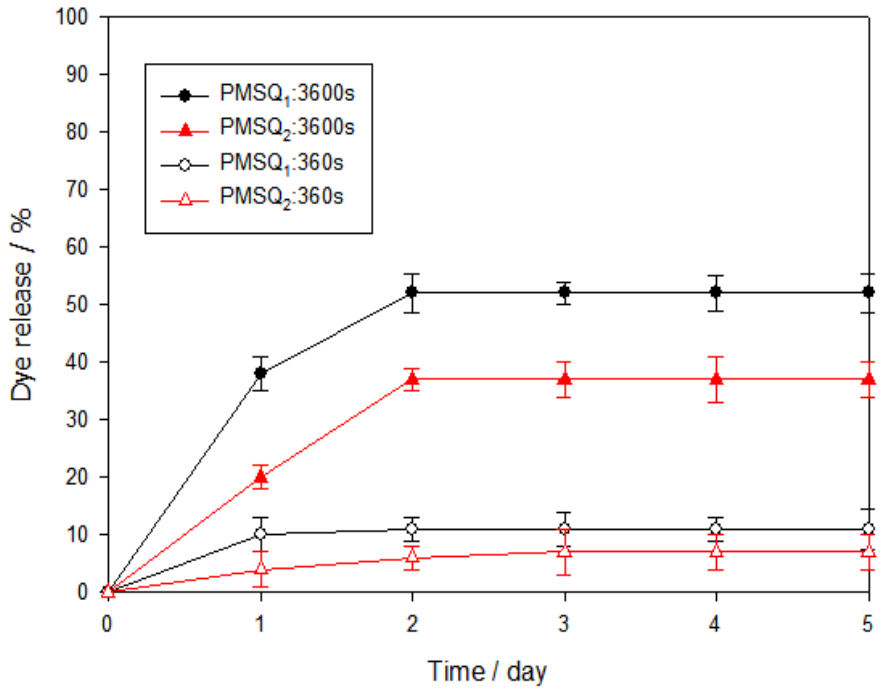

Figure 5.18 A comparison of dye release behaviour with respect to different encapsulation times (Error bars represent the standard deviation from three experiments)

5.6.5 Effect of the storage and release on the monoporous structure

The effect of the storage and release of dye on the structure of monoporous hollow capsules can be examined by microscopic images of the capsules after the encapsulation and release studies. These SEM images of monoporous hollow capsules after the storage and release of dye are shown in **Figures 5.19**. There is no apparent difference in the surface morphology compared to the monoporous hollow capsules before dye release. The pore on each hollow shell remained intact, and its pore size (d) and outer diameter (D) was unchanged. This result suggested that PMSQ drug carriers present desirable mechanical properties and stability for drug delivery and biomedical applications.

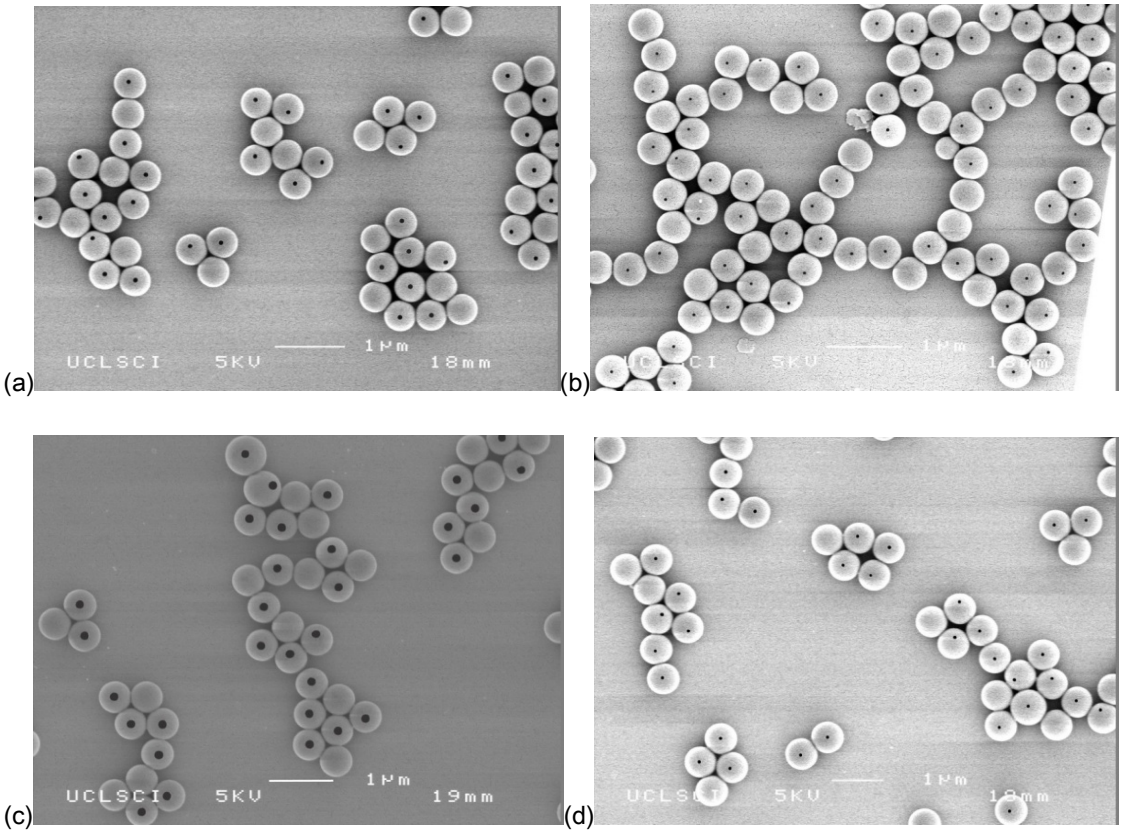

Figure 5.19 SEM images of the monoporous hollow capsules after release of dye: (a) $PMSQ_1$, (b) $PMSQ_2$, (c) $PMSQ_3$, and (d) $PMSQ_4$

5.7 Summary

In this chapter the feasibility of producing a hollow microsphere with a single hole in its shell by co-axial electrohydrodynamic atomisation (CEHDA) is demonstrated. The diameters of the microspheres and of the single surface pore were controlled by varying the flow rate of the components, the working distance, the concentration of the PMSQ solution, and the applied voltage used in the CEHDA process. The capsules were characterized by scanning electron microscopy and the range of the microsphere diameter was varied between 275 to 860 nm and the pore diameter was changed between 35 to 135 nm. This process overcomes several key problems associated with existing methods of monoporous microsphere formation including the need for elevated temperatures, multiple processing steps and the use of surfactants and other additives. The effect of the pore diameter and outer diameter of the capsules on the encapsulation and release was investigated. Analysis using UV-vis spectrophotometer suggested that monoporous hollow capsules fabricated by CEHDA could find use in the encapsulation and controlled release of drugs. As a major advantage over previously demonstrated particulate capsules, the micrometer-sized opening on the hollow capsules allowed direct and quick loading of dye molecules. The presence of different pore diameter provided different encapsulation rates and also resulted in different release profiles. It should be also noted that leaking is possible from capsules with low β values after sample preparation. This can result in contamination for capsule preparation. However, the approach and mechanism described here will help to provide a better understanding of the CEHDA processing technique and allow new opportunities in the applications involved in the uptake of target species and the encapsulation of drugs.

Chapter 6

Study of stimuli-responsive drug carrier for encapsulation, storage and release

Drug delivery systems with a unique capability to respond to a given stimulus can improve therapeutic efficacy and hold great promise for drug delivery and controlled release applications (Ehrbar *et al*., 2008, Cai *et al*., 2009). Development of such systems is currently heavily reliant on polymeric materials (Bajpai *et al*., 2008, Hest, 2009) that are responsive, for example, to enzymes, light, temperature, calcium, and ultrasound (Yang *et al*., 2009, Stuart *et al*., 2010). However, some crucial disadvantages are linked with the use of responsive polymers and these can limit their utility in biomedical applications. Furthermore, toxic by-products and the biocompatibility of responsive polymers may be a significant impediment to the development of these delivery systems for patient use (Putnam, 2008, Kim *et al*., 2009). Thus, design and development of new biophysically-friendly stimuli capsule systems are very important to speedily enable their application in drug delivery.

In **Chapters 4 and 5**, it has been clearly demonstrated that hollow capsules and monoporous hollow capsules can be successfully prepared in a single step by using electrohydrodynamic atomisation. Unlike the previous investigations, the study in this chapter was to uncover a new stimuli-drug delivery system independent of the action of smart polymers. The background to this study was briefly introduced in the first section of this chapter. The novel mechanisms behind stimuli-effects for different triggering methods and the enhanced release behaviour are described in the following sections.

The phenomena of enhanced release and surface morphology of the polymeric drug carrier are discussed subsequently. Finally, remote real-time control of release dosage according to triggering conditions for different drugs were investigated, which were found to have a significant potential for stimuli-drug delivery applications.

6.1 Design and development of stimuli drug delivery system

New strategies of external temperature and ultrasound stimulation on stimuli-responsive drug delivery system were investigated. The temperature and ultrasound-responsive drug carriers were prepared by electrohydrodynamic processing and stored under ambient conditions and subsequently "programmed" for controlled drug release without relying on a smart polymer. In a new stimuli drug delivery system, perfluorohexane (PFH), a volatile liquid, is used as the responsive element. Such a non-toxic, biocompatible fluorinated compound has been used in clinical applications such as liquid ventilation and exchange encapsulation (Spieth *et al*., 2007). PFH is a low surface tension (12 mNm^{-1}) biologically inert liquid at normal ambient temperature and can be easily transformed into the gaseous phase on account of its high volatility and high oxygen solubility (Mana *et al*., 2007). The new stimuli drug delivery system developed in this work integrates PFH into a core-shell structure. The stimuli effects were then investigated by controlling temperature and ultrasound treatment to provide new generic insights into the development of stimuli drug release systems.

6.1.1 Temperature stimulus

Temperature responsive drug delivery systems are one of the simplest and in this research the change in temperature is controlled by an external hotplate, which can trigger drug delivery according to a thermal change. A temperature-sensitive liquid, PFH, is encapsulated in the polymer shell to form the system. A major feature of the

temperature-responsive liquid is the phase change occurring according to temperature. Generally, when the stimuli temperature threshold is reached, controlled encapsulation of different amounts of drug in the capsules can be achieved and subsequent sustained release of drug can be obtained. With different triggering conditions, enhanced controlled release with real-time response can be provided. However, in order to investigate temperature stimuli effects on PFH capsules, different amounts of PFH existing in capsules were evaluated at 37, 45, and 57 °C to evaporate the encapsulated PFH. The PFH content is defined as the ratio of the actual amount of PFH encapsulated in PMSQ and the actual weight of the capsules (**Eq. 3.5,** page 79). The capsules with different amounts of PFH were subjected to aforementioned temperatures at different conditions to study the effect of incubation time, the effect of sink temperature and the effect of real-time enhanced release. The experimental details of the temperature treatment were illustrated in **Chapter 3.6** (page 75).

6.1.2 Ultrasound stimulus

Ultrasound-induced drug delivery is considered as a potential technique of external trigger of drug release. This research presents a method for remote release of an encapsulated material from hollow capsules using ultrasound treatment. The ultrasound treatment induces heat, cavitation, or a mixing effect and these combined effects, cause the capsule cores to exhibit significant instability of PFH liquid, triggering enhanced release. However, in order to study the influence of ultrasound stimuli effects, capsules with different amount of PFH in them were subjected to a 20 kHz low-frequency processor at different controlling parameters and the resulting scenarios were analyzed. The release of encapsulated material was conducted at various ultrasound exposure durations, duty cycles, and output levels. The experimental details of the ultrasound treatments were illustrated in **Chapter 3.7** (page 75).

6.2 Evaporation in PFH-loaded capsules

In this study, core (PFH)-shell particles (PMSQ) were prepared. The polymer spheres with PFH in the core are stable and sediment in water due to their relatively high density. **Figure 6.1a** shows an optical micrograph of these particles in suspension, while **Figure 6.1b** shows the dried microspheres. A hollow cavity is obtained after PFH evaporation. The PFH capsules are ~1 μm in diameter with a narrow size distribution. In this work, the shell thickness of the capsules was kept at ~100 nm. Both capsule size and shell thickness can be varied by the processing method used.

(a)

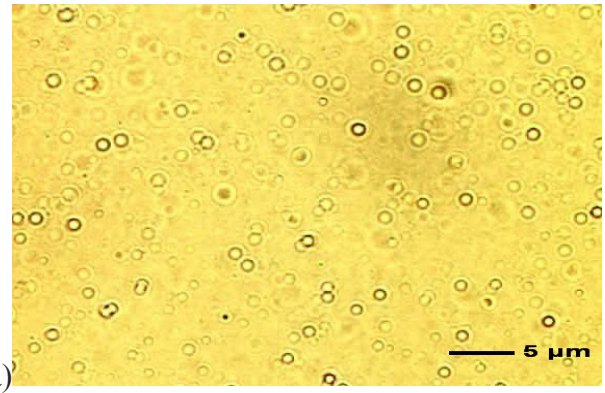

(b)

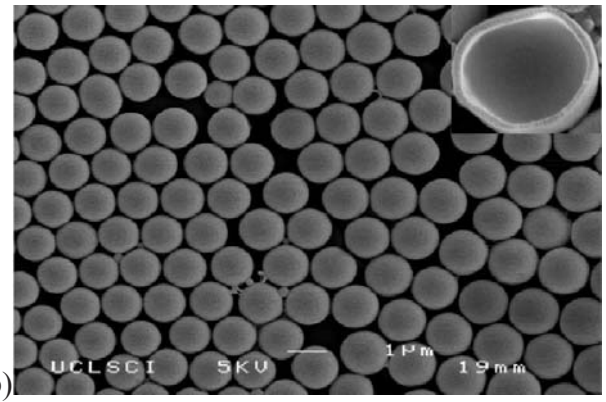

Figure 6.1 PFH loaded PMSQ capsules: (a) optical micrograph taken immediately after preparation, (b) scanning electron micrograph with typical cross-section in top RHS corner

In order to first establish the influence of temperature on the PFH capsules, samples were sprayed onto glass slides and incubated at 37, 45, and 57 °C to evaporate the encapsulated PFH. The capsules were re-weighed at regular intervals, as shown in **Figure 6.2**. At 37 °C the amount of PFH was constant for 1800s and then slightly decreased. In contrast, at 45 °C, the percentage of PFH remained constant for 600s and was fully released after 3000s. At 57 °C, all the PFH was lost in 1500s.

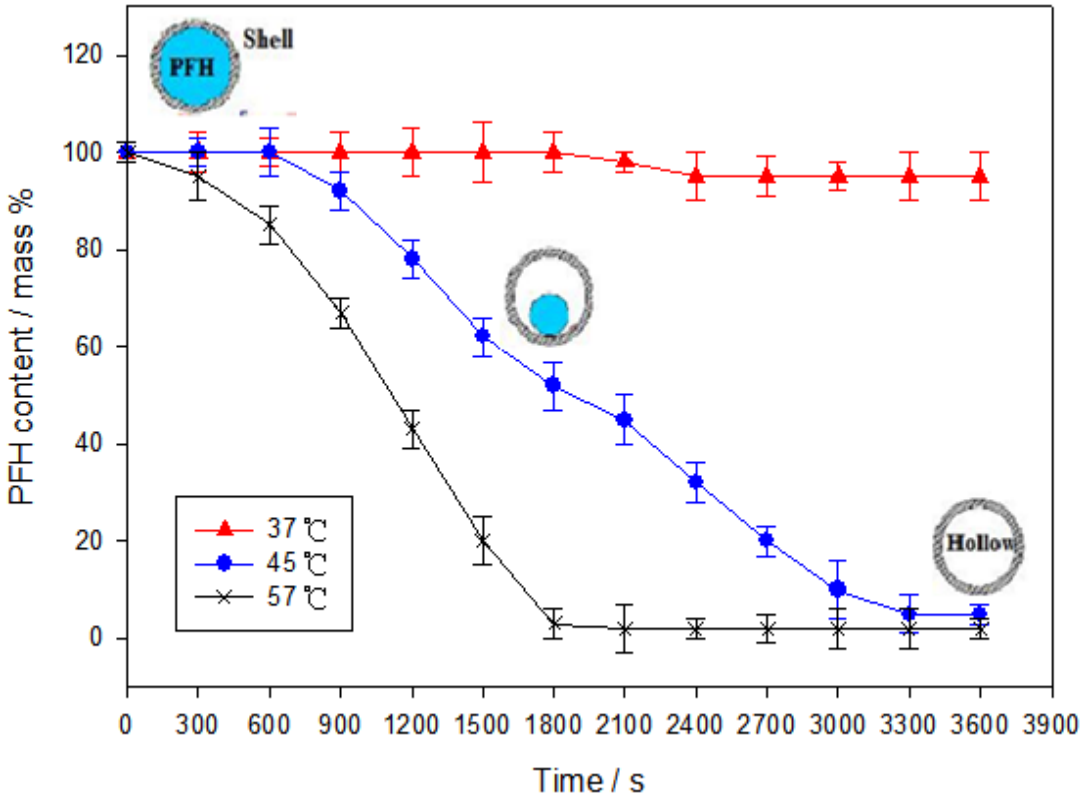

Figure 6.2 Thermogravimetric trace showing the PFH content retained as a function of time at different temperatures (Error bars represent the standard deviation from three experiments)

6.3 Temperature stimulation

6.3.1 Effect of incubation time

A suspension of hollow capsules in a solution of the material to be encapsulated results in the spontaneous filling of the capsules (Zhu *et al*., 2005, Im *et al*., 2005) and different amounts of drug encapsulation can be obtained by varying the size of the hollow spheres (Shchukin *et al*., 2003, Still *et al*., 2008). In addition, with capsules prepared this way, the capacity for filling depends on the PFH content retained in the capsules. *In vitro* dye release at 37°C from capsules after undergoing different incubation times (t_i) at 45 °C is shown in **Figure 6.3**.

For t_i= 300s, no dye release was observed because encapsulated PFH is stable in the polymer shell and the liquid medium. On increase of t_i to 1800s, a sustained release behaviour can be observed accompanied by a steady decrease in the release rate and only 40% of the dye was released. At t_i=3600s, after sustained release at a higher rate over 12 days, the amount of total dye release reached 82%. These results are in overall agreement with **Figure 6.2** but also show that the dye content incorporated into capsules is lower than the predicted values which, for example, suggests that dye in the capsules can reach ~ 48% when heated at 45 °C for 1800s. The 8% discrepancy is probably due to the evaporation rate of PFH under ambient conditions being faster than that in solution. In addition, oxygen concentration in the ambient environment can have a significant influence on the evaporation rate of PFH (Spieth *et al*., 2007). However, this system exhibited temperature-responsive controllable encapsulation, and therefore offers the ability to incorporate high or low doses of a drug in the capsule. In addition, as discussed before (**Chapter 4**) PMSQ is stable at 37, 45, 57°C and does not react with the PFH during the loading and the releasing process. The temperatures used here are much lower

than the critical temperature needed to affect the PMSQ shell. Therefore, the dye loading and release processes are dominated by the concentration difference between the core and the sink.

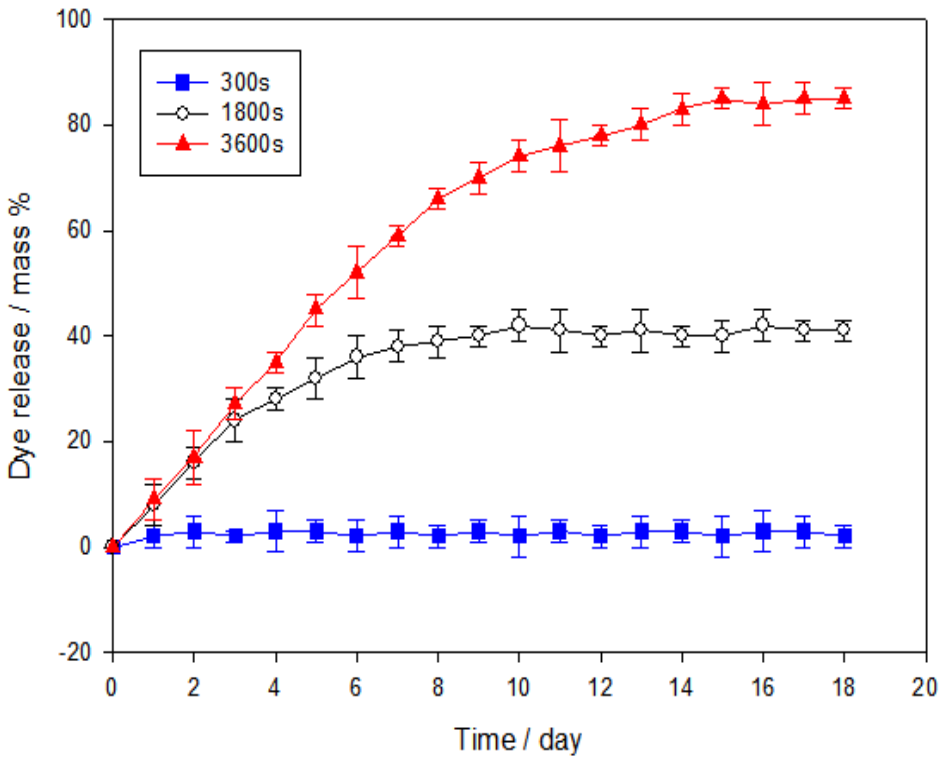

Figure 6.3 Dye release at 37 °C from capsules originally incubated at 45 °C for different times (300, 1800, and 3600s). Error bars represent the standard deviation from three experiments

6.3.2 Effect of temperature

To further quantify the temperature stimulated release characteristics of the PFH capsules, three sets of capsules, containing different amounts of dye were investigated. **Figures 6.4a-c** show the cumulative dye release of the three systems which were allowed to absorb dye at 37, 45 and 57 °C, in each case for 1500s. Therefore the starting

dye contents (mass %) of these capsules were 0, 35 and 72, respectively. In all cases, release experiments were performed at 37, 45 and 57 °C. The results clearly showed that the three systems exhibited sustained release behaviour but, crucially, the dye release rates from these systems were different. At the ambient temperature, the capsules were stable in the medium and therefore possess good storage characteristics.

If the initial incubation temperature was > 37 °C, dye was released at a faster rate. Thus, at 37 °C, the maximum dye content released reaches 72 % in 11 days for the capsules incubated at 57 °C. This is because 72 % dye in the capsules is released by natural diffusion until equilibrium is reached with respect to the dye content in the capsule and medium (Zhao *et al*., 2008). When the temperature of the medium was increased, the dye release rate from the system increased substantially. The released amount reached 72% after 7 days at 45 °C, while at 57 °C, 72% is achieved after 4 days. This difference in release rates is mainly attributed to the fact that PFH is sensitive to the temperature of the medium. At a higher temperature (45 and 57 °C) the PFH in the capsule is active and this can result in enhanced dye release. However, the total amounts released from the three systems are very similar although the release experiments were carried out at different temperatures. Thus, 72 % of the dye was released on incubating at 57 °C, while at 45 °C only 35 % of dye was released. A temperature of 37 °C is not enough to evaporate PFH from the core of the capsules.

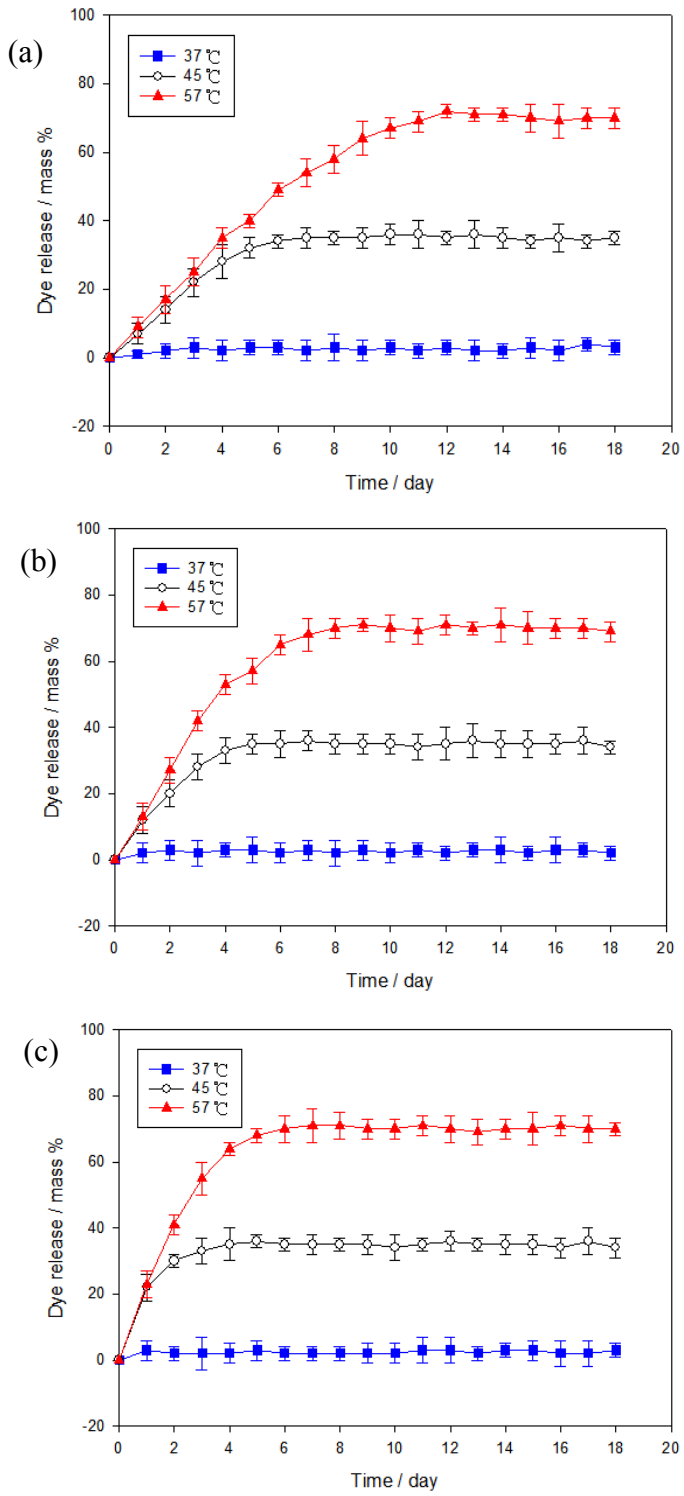

Figure 6.4 Release behaviour of capsules filled with dye at different temperatures (37, 45, and 57 °C) while being subsequently held in the release medium (a: 37 °C, b: 45 °C, c: 57 °C). Error bars represent the standard deviation from three experiments

6.3.3 Stimuli-enhanced release

Experiments were also conducted to investigate the effect of changing the temperature of the release medium. The dye was infused into the capsules by heating at 45 °C for 1500s. Subsequently, the temperature was increased from 37 °C to 57 °C after 2 days to stimulate the PFH for enhanced release and this is crucial in a number of clinical situations (Kim *et al.*, 2006). Herein, the release of the dye from the capsules at different temperature is illustrated in **Figure 6.5**. There is a clear and significant enhancement of dye release on increasing the temperature from 37 to 57 °C, starting with sustained release at 37 °C. At 57 °C the release of dye is strongly temperature-dependent. The temperature increase triggers the liquid to vapour phase transformation of PFH by inducing thermal instability. Consequently, the PFH in the core of the capsules is activated as demonstrated by a fast release of dye at 57 °C (**Figure. 6.5**). However, although the mechanism with respect to a real time stimuli-effect has been demonstrated, the operation temperatures are higher than the normal body temperature, but such a strategy can be useful in medical practice e.g. tumor treatment and stimuli-responsive capsules (Kennedy *et al*., 2003, Berger *et al*., 2009).

6.3.4 Evaluation of surface morphology

The effect of the temperature stimuli on the structure of PMSQ was investigated by comparing the surface morphology of polymer capsules subjected to different temperatures used in this work. After the release of dye molecules, no apparent difference in surface morphology can be observed within the experimental time span, as shown in **Table 6.1**. This was due to PMSQ capsules being collected in distilled water and possessing good mechanical properties and chemical durability (Ye *et al*., 2010). In addition, PFH doesn't change the composition of the shell material because of its

unreactive, immiscible and inert properties. Furthermore, it has been reported that glass-transition temperature of PMSQ polymers is in the range of 80 to120 °C (Huang *et al*., 2003, Seki et al., 2010) and first mass loss of PMSQ can be observed at above 199 °C due to the coupling of the hydroxyl groups with the removal of H_2O (Narisawa et al., 2010), which is far higher than the temperatures used in this research. However, as discussed before PMSQ is stable at 37, 45, 57°C and does not react with the PFH during the loading and the releasing process. Therefore, a new system based on temperature-responsive carriers which enables both stimulus-encapsulation and stimulus-release of a drug offers significant potential benefits for drug delivery applications and the design of stimuli-responsive systems.

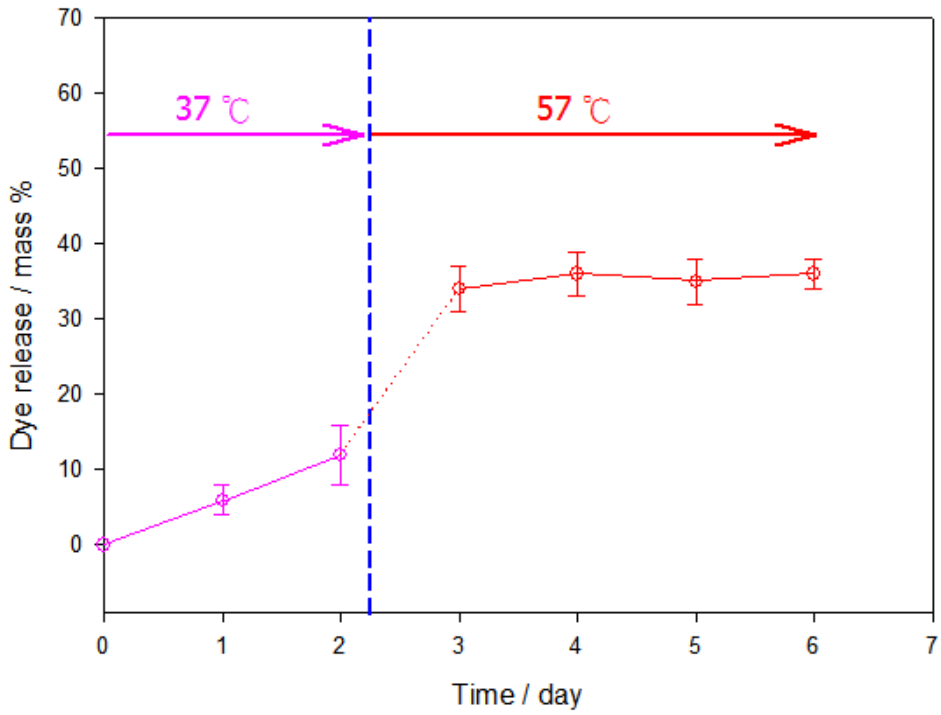

Figure 6.5 Cumulative release of dye from capsules at 37 and 57 °C. Initial incubation was at 45 °C for 1500s. Error bars represent the standard deviation from three experiments

Table 6.1 Microscopic images of polymer carriers subjected to treatment at various temperatures

Temperature	Optical microscopy images	Electron microscope images
37°C	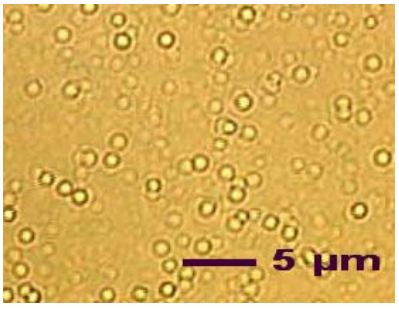	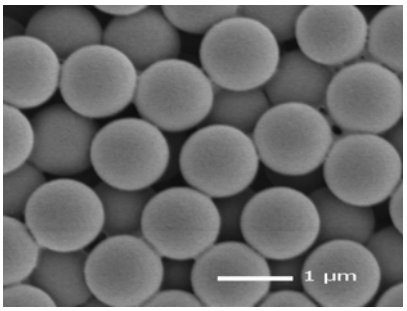
45°C	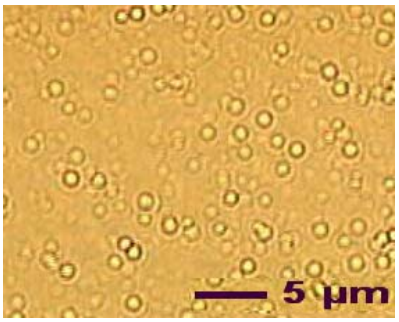	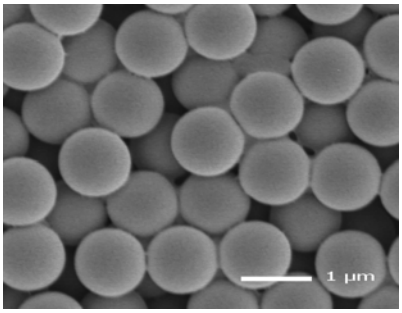
57°C	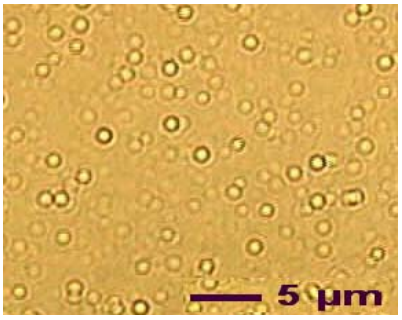	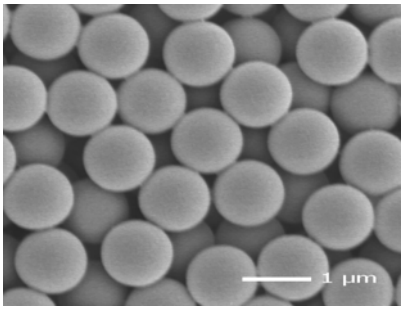

6.4 Ultrasound stimulated drug delivery system

6.4.1 Effect of ultrasound on hollow capsules

Ultrasound can induce physicochemical effects such as surface modification, dispersion, and microannealing in organic and inorganic materials (Magual *et al.*, 2005). Materials of different densities can also exhibit various physiochemical effects when subjected to acoustic waves (Toussirot *et al.*, 2001). In order to fully understand the influence of ultrasound on a hollow capsule made by electrohydrodynamic processing, or more specifically the release rate of the encapsulated dye within the capsule, the suspension was irradiated by ultrasound (20 kHz) for 1 min at duty cycle 60 %.

The release kinetics of dye from hollow capsules with and without exposure to ultrasound is shown in **Figure 6.6**. A possible explanation for the slightly enhanced mass transport is that the hollow carriers were subjected to cavitation and acoustic streaming, where microbubbles in agitated liquids collapse and results in an increase in the surface energy and kinetic energy of the liquid in motion (Fogler and Lund, 1973). As a result, increased liquid velocity and convective mass transport to the diffusion boundary layer of capsules can occur. In addition, it has also been reported that the enhanced mass transport is faster at a high level of agitation in the release medium (Agrawal *et al.*, 1994). Upon introduction of ultrasound, the magnitude of dye release rate was ~3 % higher than that in the absence of ultrasound. These properties of ultrasonic treatment illustrate the necessary conditions for applying ultrasound as a stimulus for remotely controlling the release of dye/drug from loaded capsules.

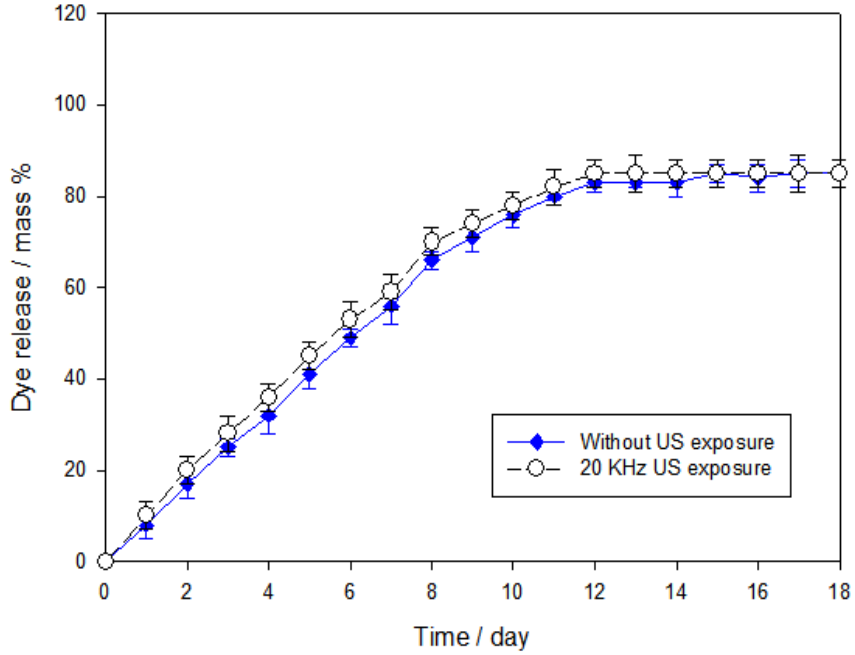

Figure 6.6 Release kinetics of dye from hollow capsule with and without exposed to ultrasound (20 kHz). Error bars represent the standard deviation from three experiments

6.4.2 Effect of ultrasound on hollow capsules with PFH

Once submerged in the encapsulating material solution, the hollow capsules are filled instantly (Im *et al.*, 2005, Zhu *et al.*, 2005). Different amounts of the drug in the hollow capsule can be obtained by controlling the core space of the hollow capsules (Shchukin *et al.*, 2003, Still *et al.*, 2008). To study the effect of ultrasound on the release profile of PFH capsules, samples were prepared by heating the PFH capsules to 45 °C for 1500s to achieve a known amount of encapsulated PFH (~60%) containing dye. The effect of ultrasound on the presence of PFH in the core of the hollow capsules is shown in **Figure 6.7**. The release rate of the hollow capsules under ultrasonic treatment was increased by incorporating PFH. This phenomenon can be attributed to the thermal sensitivity of PFH and disturbance of release medium which leads to a

higher release rate. The fact that the ultrasonic waves propagate in capsules and buffer medium causes their energy to dissipate due to absorption and scattering. The result is release of heat and a temperature elevation in the delivery system. The medium temperature increased from 37 °C to 42 °C during 1 min of ultrasound treatment at duty cycle 60%. As demonstrated in the previous work, an elevated temperature activates the PFH in the capsule and facilitates dye release.

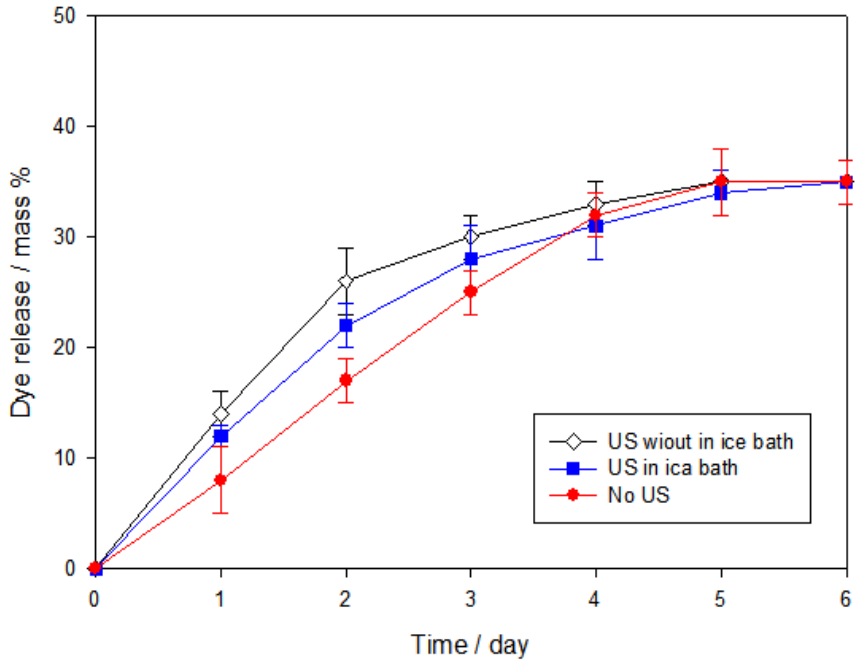

Figure 6.7 The influence of ultrasound on release kinetics of dye from PFH capsules. Error bars represent the standard deviation from three experiments

To verify the effect of temperature elevation on the release of incorporated dye, experiments were performed in an ice-bath during ultrasound treatment. The release rate from PFH capsules decreased under these circumstances, which confirmed the influence of induced temperature and the corresponding release rate. However, the effect of ultrasound on the release rate of drugs incorporated in polymer carriers

showed that cavitation played a significant role (Spieth *et al.*, 2007) and can have a significant influence on the instability of the PFH (Dias *et al.*, 2003). These results suggest that enhanced diffusion by increasing temperature occurred in the core-shell particles with incorporated PFH. Furthermore, thermoacoustic caused by ultrasound treatment could be used for controlled release. Therefore, in the case of the core-shell particles with the PFH molecules, several mechanisms were found to be responsible for the effect of ultrasound-enhanced release. It can be concluded that elevated temperature, cavitation, or mixing effects and a combination of these effects can enhance release dynamics.

6.4.3 Effect of exposure time

Exposure time of ultrasound can be varied greatly from a few second to a few minutes, depending on the material properties of capsules (Cai *et al.*, 2007, Evjen *et al.*, 2011). The density, viscosity, acoustic impedence, and interfacial properties can play a significant role in developing enhanced drug delivery systems with ultrasound treatment. In an attempt to study the influence of exposure time of ultrasound on release rate, the suspensions were subjected to ultrasound for different exposure times: 60, 300, and 600s at a constant duty cycle of 30%. **Figure 6.8** shows the dependence of release rate for different exposure times. The capsules displayed enhancement in the release rate when exposed to ultrasound in the all cases. The carriers showed the stimuli-effect and the release behaviour was altered by the change of the exposure time. Higher ultrasound exposure time caused faster release rates and faster depletion, reaching the values of 9% for 60s, 13% for 300s, and 16% for 600s per day. This may simply be due to ultrasound accelerating permeation and inducing elevated temperature, as a result of the increase in the total energy into the system by increasing exposure time. Therefore, this results in enhanced transport of liquid into the capsule,

exposing more dye for release. In addition, mechanical shear stresses in the liquid jets at a high velocity can cause gas bubbles collapse, and this could also result in enhanced permeation.

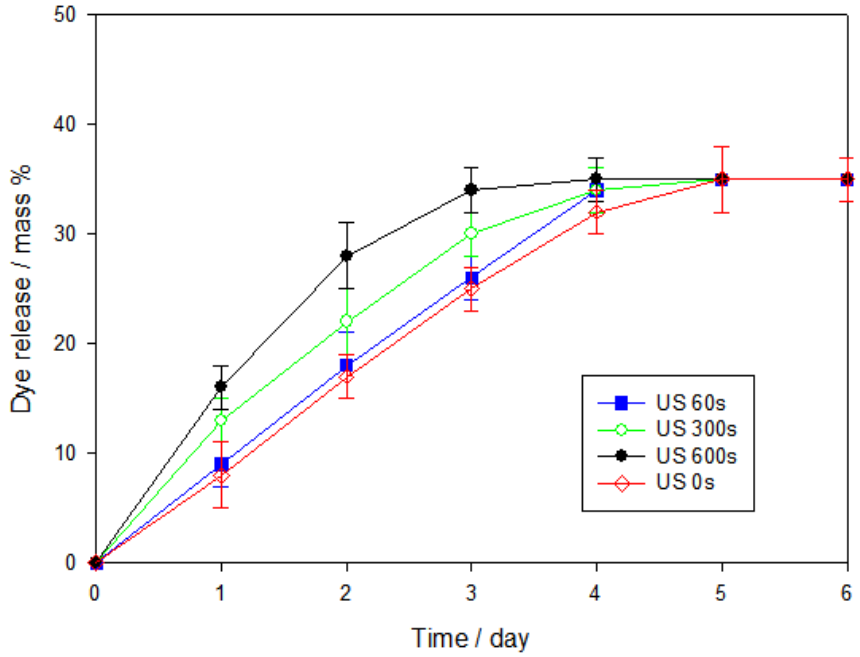

Figure 6.8 Dependence of release enhancement on ultrasound for various time spans. Error bars represent the standard deviation from three experiments

6.4.4 Effect of duty cycle

Duty cycle of ultrasound system is the time that it spends in an active state as a fraction of the total time under consideration. To evaluate the effect of duty cycle on release rate, the PFH capsules were studied at the same ultrasound intensity with duty cycles of 30%, 60% and 90%, while the exposure times were kept at 300s. **Figure 6.9** shows the effect of controlling the duty cycles on the release rates of PFH capsules, suggesting that enhanced dye release occurred when exposing PFH capsules to ultrasound. The use of a higher ultrasound duty cycle caused faster release rates and

faster depletions, reaching the value 13%, 22%, and 30% release per day at duty cycle 30%, 60% and 90% respectively. In addition, the trend of release enhancement induced by controlling the duty cycle is similar to that by increasing the exposure time, thus suggesting that the dependence on duty cycle also plays an important role in determining mass transport. However, from the enhancement point of view, although the release trend and behaviour in the two cases are similar (a long exposure time at a low duty cycle providing an enhancement similar to that induced by a short application of a high duty cycle), the release rate per day can lead to different pharmacokinetic profiles, depending on the control (via the duty cycle or the exposure time). In addition, the effect of ultrasound thermoacoustic effects also leads to different temperature elevations, which results in different release profiles as well. The source of the kinetic effect can be attributed to a convective motion that create circulating transportation at high velocities (>10 m/s) .

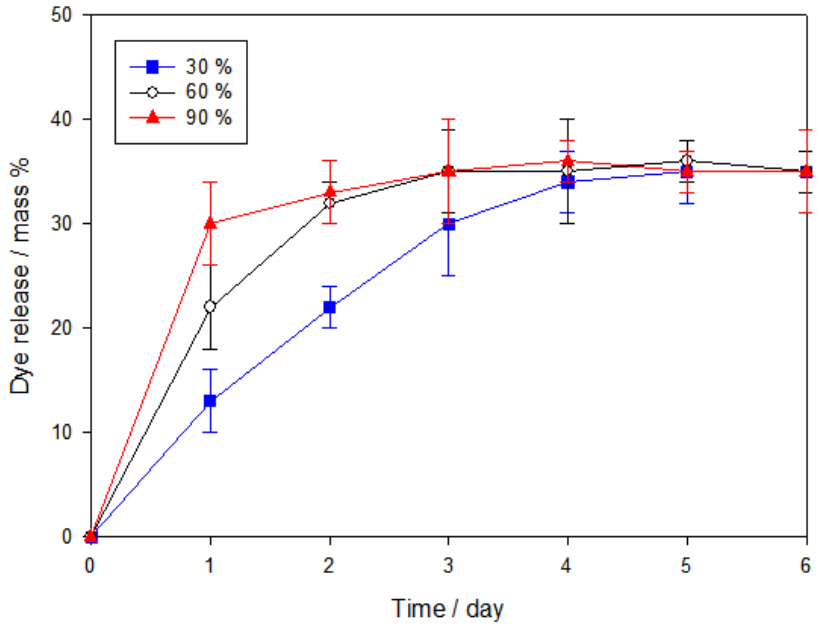

Figure 6.9 Comparison of release rate at duty cycles: 30, 60, and 90%. Error bars represent the standard deviation from three experiments

6.4.5 Effect of ultrasound power

To evaluate the effect of ultrasound power on the release rate, dye-loaded capsules were tested using an ultrasound transducer for 60s (duty cycle 60%). The amplitude of irradiation was increased from output level 2 to output level 6 in the range of 5 W/cm^2 to 26 W/cm^2. The effect of ultrasound power on the release rate is shown in **Figure 6.10**. Faster release rates and faster depletion were observed by applying higher ultrasound power: a low gradual release of ~14 % at amplitude of ~5 W/cm^2 and a higher slope (25 %) above ~10 W/cm^2. Sixty seconds of exposure to ultrasound at 26 W/cm^2 for three consecutive days provided a four-fold enhancement of release. The enhanced effects could be due to vigorous mixing and a higher temperature when the increase of the total energy in the system was performed by changing to a higher output level of ultrasound. The higher mixing effect is thought to be induced by shock waves created during cavitation, which can cause a rapid compression with subsequent expansion of the liquid. In addition, at a higher output level, friction is generated and this causes strain and eventually bond rupture in the medium. This suggests a rapid motion of solvent molecules and elevated medium temperature, resulting in an enhanced release rate.

6.4.6 Effect of PFH content

In order to investigate the effect of ultrasound on different amounts of PFH retained in capsules, samples were heated to 37, 45 and 57 °C for 1500s. *In vitro* dye release of the three systems under ultrasound treatment for 300s (duty cycle 60%) is shown in **Figure 6.11**. For dye content prepared at 37 °C for 1500s, no dye release was observed because 37 °C is not enough to evaporate PFH from the core of the capsules and dye molecules cannot diffuse into the core space in the capsule. However, when higher

incubation temperatures were used more core space for dye encapsulation can be obtained, and the core space can be filled by dye molecules by diffusion. At an incubation temperature of 45 °C (1500s), 35 % of the dye was released after two days. By increasing incubation temperature to 57 °C (1500s), a sustained release can be observed and the encapsulated dye is much higher than that at 45 °C, reaching 72% of the dye after five days. These results suggest that different amounts of PFH in the polymer shell showed no significant effect on release rate under the ultrasound treatment, but this system exhibits the ability to incorporate high or low doses of a dye in the capsule, depending on the PFH content retained in the capsule.

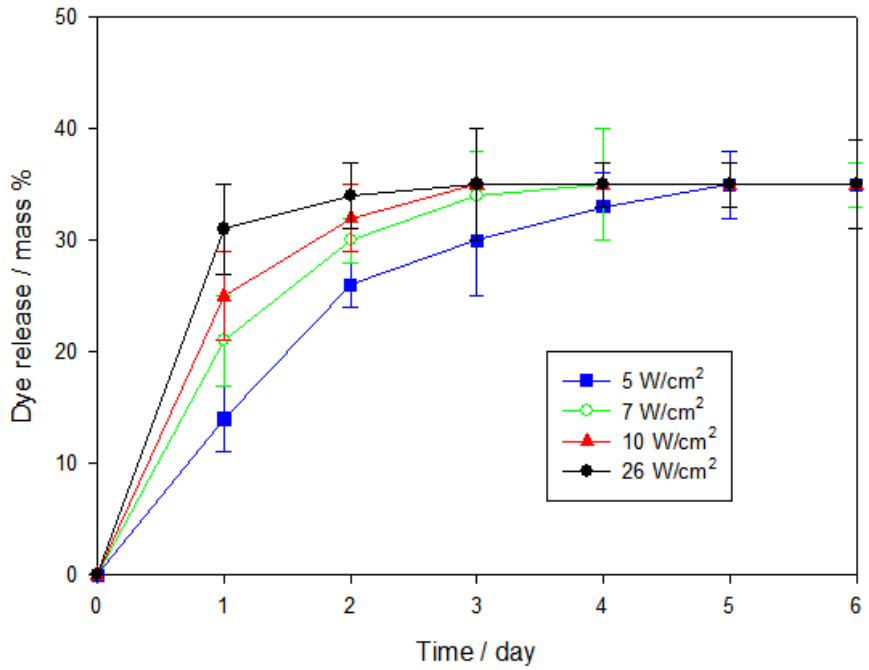

Figure 6.10 The dependence of release rate on ultrasound treatment at various ultrasound intensities while maintaining a constant duty cycle (60 %). Error bars represent the standard deviation from three experiments

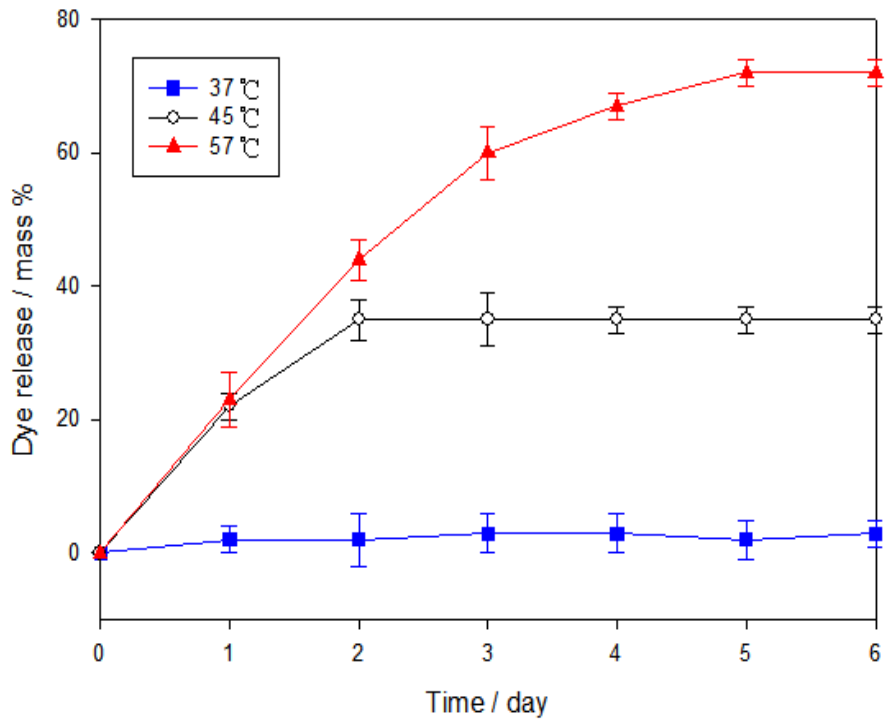

Figure 6.11 Dye released from capsules originally incubated at 37, 45 and 57 °C for 1500s and subjected to ultrasound treatment for 300s and a duty cycle 60%. Error bars represent the standard deviation from three experiments

6.4.7 Stimuli-enhanced release

To study the kinetics of release from the hollow capsules and the regulation effect ultrasound offers, dye was pre-loaded into the interior cavities to trace the dynamical process. The release of encapsulated dye is shown in **Figure 6.12**, showing the behaviour of capsules before and after the exposure to ultrasound. In absence of ultrasound treatment, it can be seen that the initially dye release in the bulk solution remained 8 %. This value contributed to the diffusion of adsorbed dye molecules and the sink. However, it was important that the dye release was steady with time,

indicating that sustained release was achieved from the interior of the devices. After two days, as the capsules were exposured to ultrasound (20 kHz, 60 % duty cycle, 300s), the dye release was significantly increased, indicating a quick release of the encapsulated dye from the capsules (**Figure 6.12**). The real-time response is crucial in a number of clinical situations (Kim *et al.*, 2006) and the reaction can be attributed to three factors: (a) the formation of a core-shell structure with PFH inside the capsule increasing the diffusion of dye by elevating the temperature, (b) higher diffusion due to the additional cavitation and (c) the surface of the capsule is jetted and the release of dye by hydrodynamic activity is enhanced.

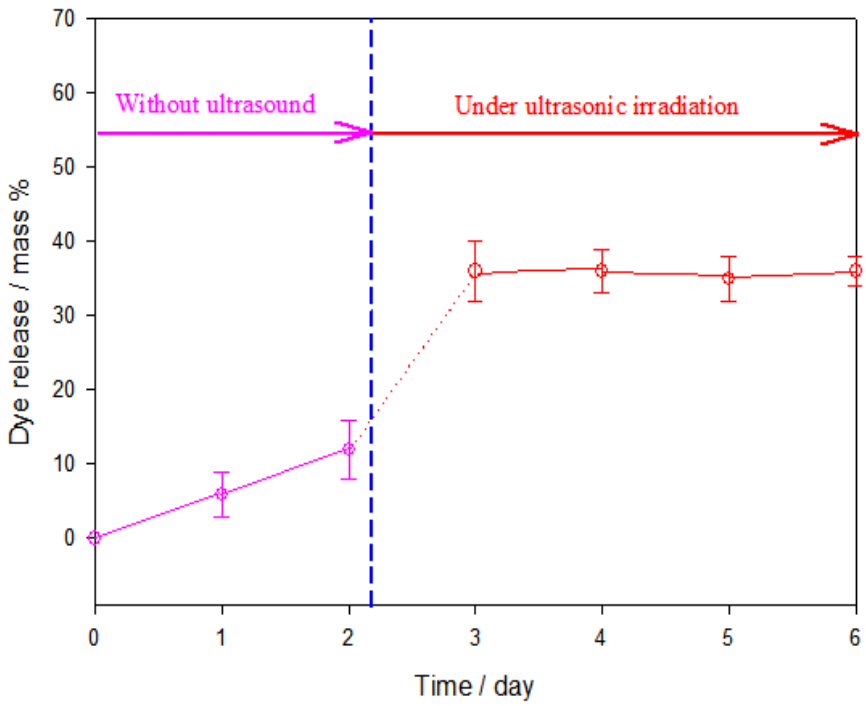

Figure 6.12 Release of dye from capsules without and with ultrasound exposure for 300s at duty cycle 60%. Error bars represent the standard deviation from three experiments

6.4.8 Evaluation of surface morphology

In order to determine whether ultrasound has an influence on the surface morphology of polymeric carriers, the scanning electron micrographs of microspheres from each sample of carriers were examined. **Table 6.2** shows surface morphology of polymer carriers subjected to ultrasound treatment at various conditions. The polymeric capsules prepared by electrohydrodynamic processing are spherical and have smooth external surfaces before ultrasonic treatment, as shown in **Figure 6.1**. However, the influence of the exposure time (60s, 300s, and 600s) and duty cycle (30%, 60%, and 90%) on the capsules integrity showed that they were intact before and after the experiments (**Table 6.2**, symbol A-F). Furthermore, different amounts of PFH in polymer shell showed no significant changes in surface morphology after the same ultrasound treatment (symbol E). This result suggests that although ultrasound can provide enhancement on release rate, ultrasound treatments under these conditions (exposure time and duty cycles) used did not induce significant morphology change and most of the capsules preserved their integrity.

Table 6.2 (symbol H-I) illustrates surface morphology transformation after ultrasonic treatment at different output levels. These capsules have mostly smooth outer surfaces as well, but many macroporous holes were observed on the surface of hollow capsules. These observations are consistent with the work of Aschkenasy *et al.* (2005) suggesting that macrporous surfaces may be obtained by exposing hydrophobic polymeric carriers to ultrasound. In this type of hydrophobic polymers, drug is released by diffusion through pores of ethylene-vinyl acetate copolymer which are created in the polymeric network (Aschkenasy and Kost, 2005).

Lavon and Kost (1998) reported that ultrasound treatments result in large pore size in non-degradable polymer, and similar pore formation was observed after a period release without ultrasound treatment, suggesting ultrasound accelerating phenomena of pore formation (Lavon and Kost, 1998). However, PMSQ capsules showed no significant difference in morphology after a period of release without ultrasound treatment. Based on these results, instead of acceleration by ultrasound, the pore formation in the shell is induced by ultrasound on the polymeric network. This may be attributed to the ladder-like structures with branches in polysilsesquoxanes and under the influence of ultrasound (Ma *et al.*, 2002a), as the ultrasonic waves propagate from the sonicator probe tip, cavitation generates strong shear forces in the surrounding liquid, resulting in a dramatic impact on the integrity of the shell.

In addition, polymeric capsules with an increase in pore size and a crack around the macroporous surface were observed at a higher output level (Symbol I). This suggests that cavitation effects induced by ultrasound play a major role in changing surface morphology. However, it should be noted that if drug molecules were pre-loaded in the cavities of the hollow capsules, they could be released to the sink medium through the pores and via the surface morphology transformation induced by ultrasonic treatment (Symbol H-I). This release pathway was different from the free penetration and diffusion of loaded molecules through the polymeric network in the core-shell systems, implying that release rate of encapsulated drug can be regulated by controlling pore size of the capsules prepared using a higher output level of ultrasound.

Symbol J (**Table 6.2**) shows an SEM image of capsules after exposure to ultrasound at the highest output level. The hollow structures were ruptured and resulted in shell debris when the acoustic pressure was sufficiently high. The collapse of the hollow structure was due to cavitation and acoustic streaming, which have been suggested as a primary cause of ultrasound enhanced collapse of core-shell structures (Shchukin *et al.*, 2006). The process is composed of a series of steps: nucleation or formation of cavitation, bubble growth, and implosive collapse. When high-intensity ultrasound shatter a gas nucleus in solution, ultrasound can lead to rapid growth in pressure and collapse of bubbles, and the nucleus can rapidly expand after the bubbles implode with high velocities, which ultimately leads to the formation of a liquid microjet directed towards the surface. The diameter of the microjet is much smaller than that of the maximum bubble radius and the speed of the liquid microjet can reach 150 m/s, leading to pressure variations in the medium (Benjamin and Ellis, 1966, Lauterborn and Bolle, 1975). At the stage of the collapse of the cavity, radiated friction forces and shock waves generate the stresses on the surface of a polymer chain and/or more possibly within the polymer coil, resulting in bond breaking of the macromolecular chain. Although this leads to a breakup of drug carrier after ultrasound treatment, it also opens up the possibility of using the capsules as drug delivery vehicles, since the capsule content is efficiently released. Skirtach *et al*. (2007) demonstrated ultrasound triggered destruction of polymeric capsules could be used for controlled catalysis from polyelectrolyte capsules (Skirtach *et al.*, 2007). In addition, an approach to destroying capsules completely in suspension for enhanced release of the encapsulated compound was demonstrated by using low frequency ultrasound for remote drug delivery (Shchukin *et al.*, 2006).

Cavitation is a complex phenomena and depends on various parameters, including time, frequency, and intensity etc. Based on these results, the role of factors which affect the ultrasound-enhanced release of dye from the hollow capsules with PFH can be attributed to a different release rate and/or different release mechanism that would occur based on the release kinetics or on the polymer morphology. When ultrasound induces a thermal effect (Singer *et al.*, 1998), the release rate of hollow capsule with PFH was significantly enhanced by an elevated temperature. Upon introduction of a high-intensity ultrasound, a noticeable change in the surface morphology from the macroporous surface to collapse of capsules led to the variable release rates.

It should be noted that the change in morphology of capsules with increasing temperature has been reported before (Prevot *et al.*, 2006). A previous research also revealed that the overall polymer carrier erosion was due to several steps (water diffusion to a labile bond, hydrolysis, and diffusion and dissolution of degradable materials). All steps could be enhanced by an increase of temperature which would lead to differences in release rate. However, PMSQ is a chemically stable polymer and offers pyrolysis to ceramic at 1000 °C. The temperature increase in the experiments would not result in difference in polymer carrier. Therefore, the possible reason for change in morphology might be the effect of ultrasound.

Table 6.2 Surface morphology of the capsules subjected to ultrasound treatment at various conditions (Scale bar: 1μm)

Symbol	Experimental details	SEM images
A	Exposure time: 60s, Duty cycle: 30 % Temperature (°C): 37.7 Intensity (W/cm^2): 0.73	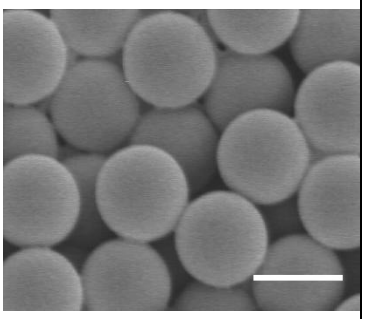
B	Exposure time: 300s, Duty cycle: 30 % Temperature (°C): 40.5 Intensity (W/cm^2): 0.73	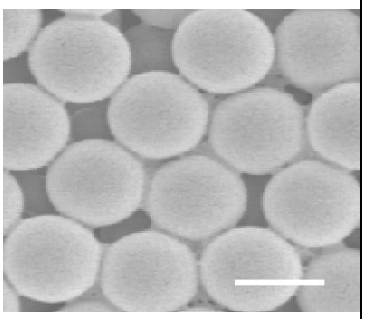
C	Exposure time: 600s, Duty cycle: 30 % Temperature (°C): 44 Intensity (W/cm^2): 0.73	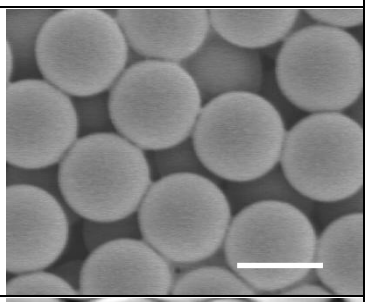
D	Exposure time: 300s, Duty cycle: 30 % Temperature (°C): 40.5 Intensity (W/cm^2): 0.73	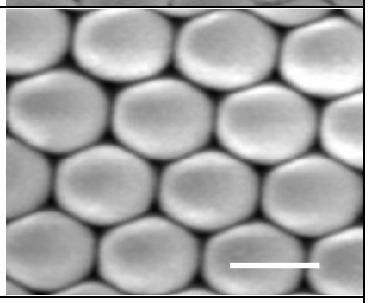
E	Exposure time: 300s, Duty cycle: 60 % Temperature (°C): 58 Intensity (W/cm^2): 4.40	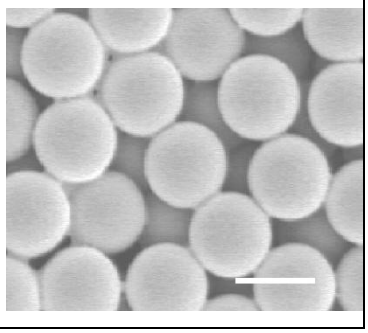

F	Exposure time: 300s, Duty cycle: 90 % Temperature (°C): 72 Intensity (W/cm^2): 7.34	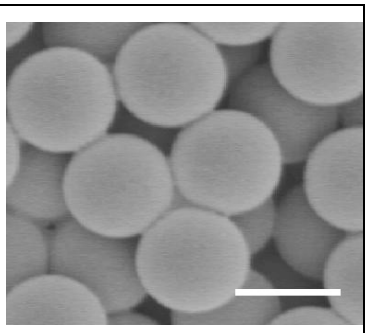
G	Exposure time: 60s, Duty cycle: 60 % Temperature (°C): 42 Intensity (W/cm^2): 5.24	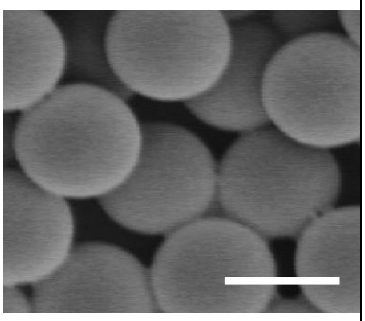
H	Exposure time: 60s, Duty cycle: 60 % Temperature (°C): 44 Intensity (W/cm^2): 7.34	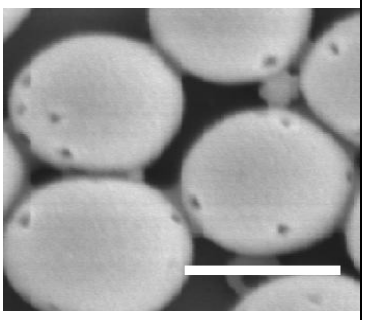
I	Exposure time: 60s, Duty cycle: 60 % Temperature (°C): 47 Intensity (W/cm^2): 10.49	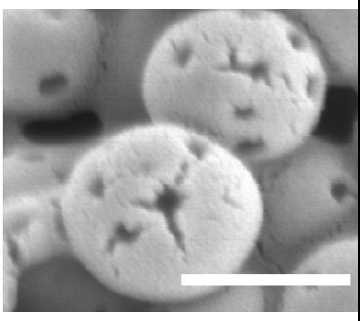
J	Exposure time: 60s, Duty cycle: 60 % Temperature (°C): 62 Intensity (W/cm^2): 26.23	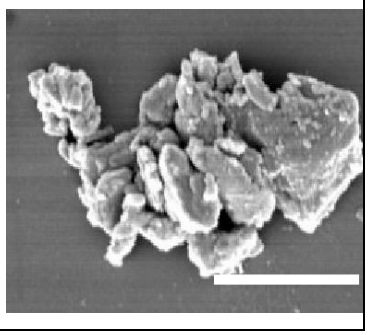

6.5 Applications to drugs

In this work controlled release of Evans blue dye with a molecular weight of 961 has been demonstrated by encapsulating it into a spherical core-shell capsule, where the release rate and profile can be systemically changed. In addition, the real-time enhanced release of the marker can be regulated by temperature and ultrasound. This means that other key therapeutic species with a lower molecular weight (e.g. Ibuprofen 206, Captopril 217, and Aspirin 180) can be encapsulated inside such hollow capsules and released at specific rates, depending on the choice of carrier properties: polymer molecular weight, microsphere size, shell thickness, and processing method. Thus, an attempt was made to evaluate the effect of drug molecular weight on the stimuli enhancing phenomenon, and hollow capsules with PFH were prepared encapsulating different drugs such as aspirin, lactoflavin, and cyanocobalamin, which have a wide range of molecular weights from 180 to 1355, as shown in **Table 6.3**.

Table 6.3 Properties of applied drugs

Drugs	Molecular weight (Da)	Wavelength at maximum UV absorbance (nm)
Aspirin	180	270
Lactoflavin	376	445
Cyanocobalamin	1355	361

6.5.1 Characterization of drugs

Aspirin (Mw: 180), lactoflavin (Mw: 376), and cyanocobalamin (Mw: 1355) were used. Solutions of different concentrations of drugs were directly characterized by UV spectroscopy at the maximum absorption wavelength (**Table 6.3**). **Figure 6.13** shows

the UV absorption spectra of aspirin solution from 250 nm to 320 nm. The concentration of aspirin in the supernatant was determined by UV absorption with reference to the absorption wavelength of 270 nm.

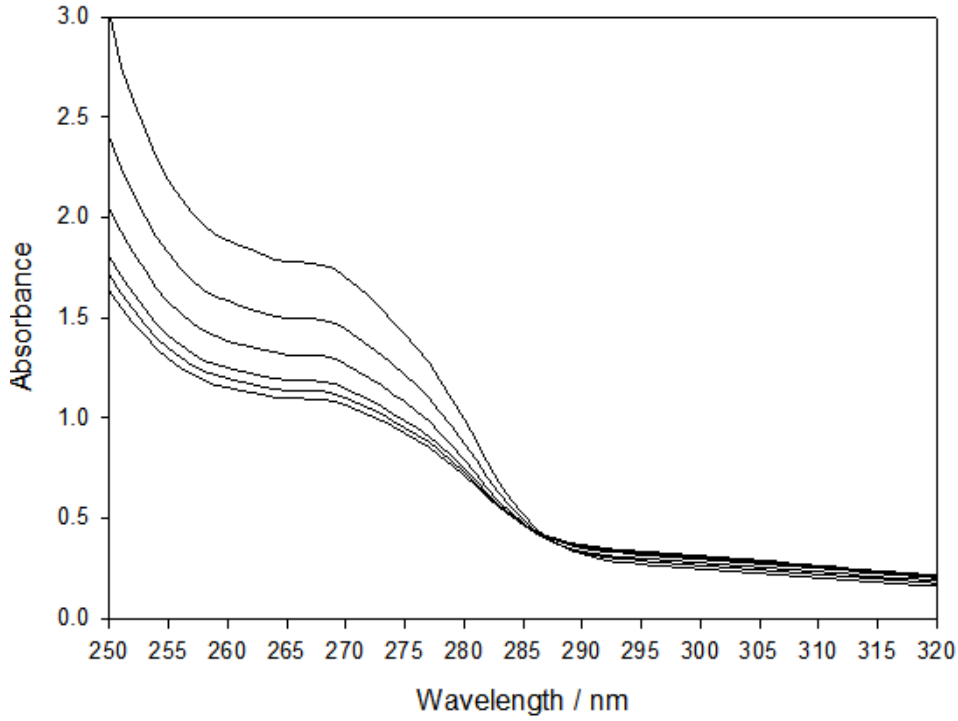

Figure 6.13 The UV-vis absorbance spectra of aspirin with different concentrations (0.1-0.5 mg/ml)

Similarly, solutions of different concentrations of lactoflavin and cyanocobalamin were analysed at the wavelength of 445 nm and 361 nm by UV spectroscopy, respectively. **Figure 6.14** shows the UV absorption spectra of lactoflavin solution from 300 nm to 600 nm, while **Figure 6.15** shows the UV absorption spectra of cyanocobalamin solution in the same range. The calibration curve of lactoflavin and cyanocobalamin were determined by taking maximum absorbance at 445 nm and 361 nm, respectively.

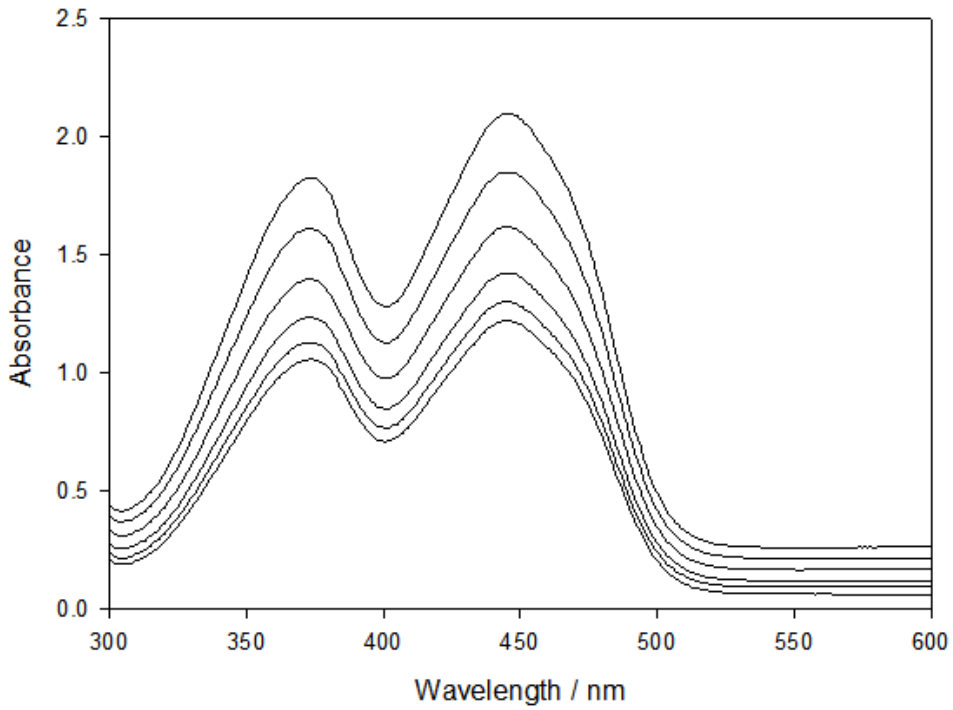

Figure 6.14 The UV-vis absorbance spectra of lactoflavin with different concentrations (0.04-0.1 mg/ml)

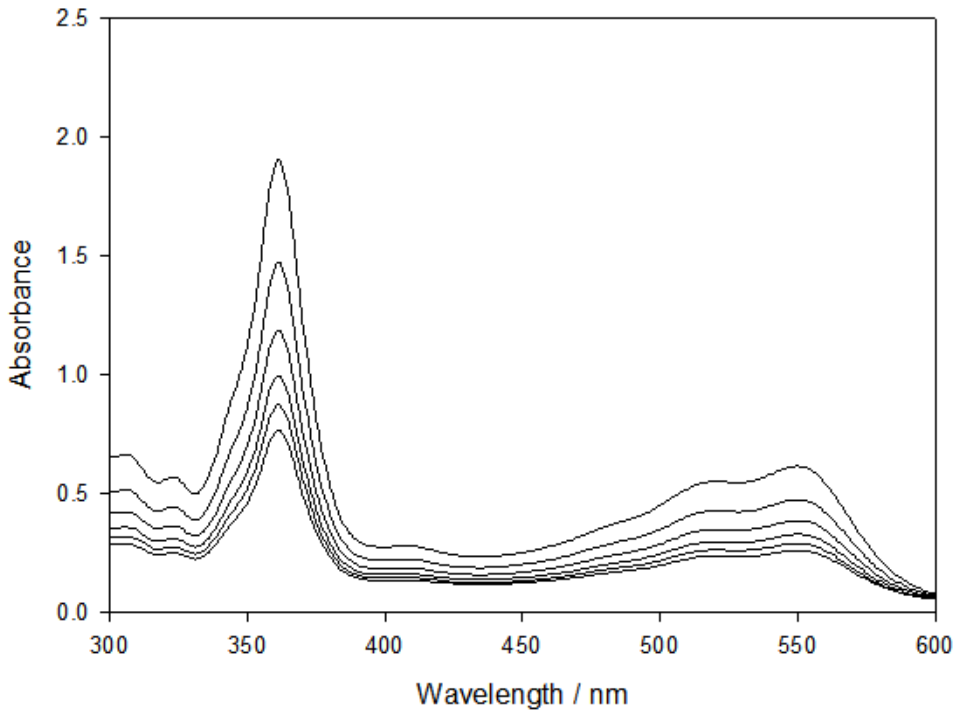

Figure 6.15 The UV-vis absorbance spectra of cyanocobalamin with different concentrations (0.02-0.1 mg/ml)

6.5.2 Stimuli-enhanced release

To investigate the dynamic release of drugs from the hollow capsules and the effect of both stimuli: temperature and ultrasound, drugs were pre-loaded into the interior cavities to trace the dynamic process. **Figure 6.16-18** shows the effect of the incorporated drugs with different molecular weights on the release rates from hollow capsules before and after exposure to the two stimuli. The release behaviour of encapsulated aspirin can be seen in **Figure 6.16**, showing that in absence of stimuli-treatment, the aspirin release in the bulk solution was initially kept at 10 %. This value was contributed to the physical diffusion of drug molecules. After two days, as the capsules were exposured to ultrasound for 300s at a duty cycle 60%, the drug release in the bulk solutions was significantly increased, indicating an enhanced release of the encapsulated aspirin from the capsules (**Figure 6.16**). The quick release rate also can be observed when the capsules were subjected to 57 °C after two days of sustained release.

Figure 6.17 and **Figure 6.18** show the results of similar experiments on lactoflavin and cyanocobalamin, respectively. Without stimuli-treatment, the initial release rate of encapsulated lactoflavin was maintained at 8 %, while cyanocobalamin remained at 5 %, which provided release behaviours as a function of time. As the capsules were subjected to ultrasound and temperature treatment, respectively, after two days sustained release is seen and a much higher cumulative release of drugs was observed, achieving ~20% cumulative release of drug (**Figure 6.17** and **Figure 6.18**). These results confirm that the feasibility of the real-time stimuli-drug delivery system can be achieved, as a function of ultrasound and temperature treatments.

However, it should be noted that the release rates over first two days from each drug were different although they were performed in same drug carriers under the same conditions. The release rate of aspirin was higher than that of cyanocobalamin in the first two days. A possible explanation for this difference might be attributed to the larger molecular weight of cyanocobalamin mass-transport was more limited, therefore, a lower rate of release was achieved compare to the smaller molecules of aspirin. This phenomenon has also been reported whereby small molecules such as ions pass through a permeable layer much easily, while under most conditions, higher molecular weight drugs are more difficult to release (Antipov and Sukhorukov, 2003, Kreft *et al*., 2006). However, the enhancement in the release rate for high molecular weight drugs can be achieved by applying external stimuli such as ultrasound and elevated temperature.

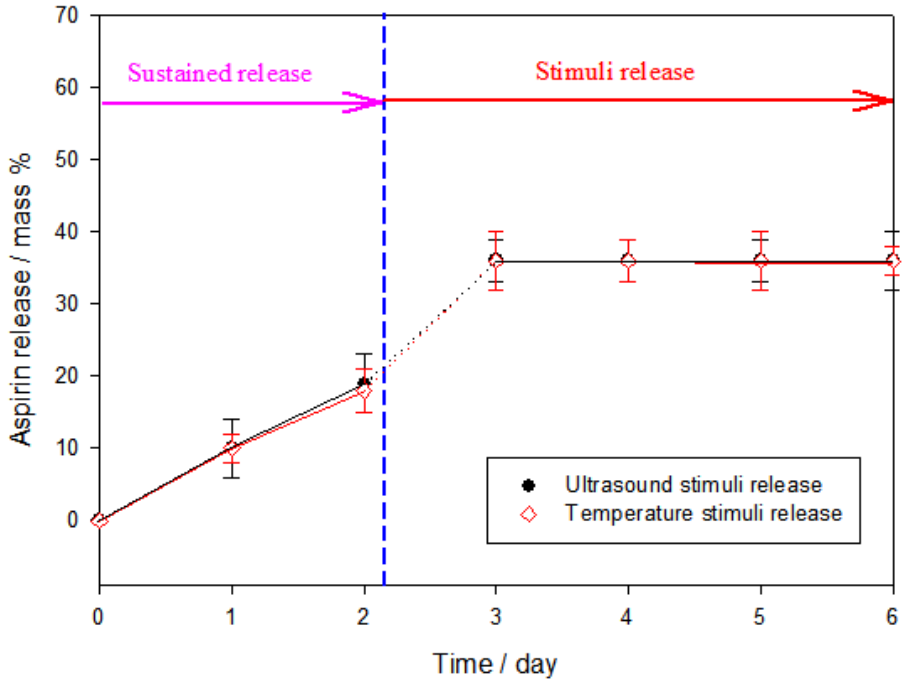

Figure 6.16 Cumulative release of aspirin from capsules without and with stimuli treatment. Error bars represent the standard deviation from three experiments

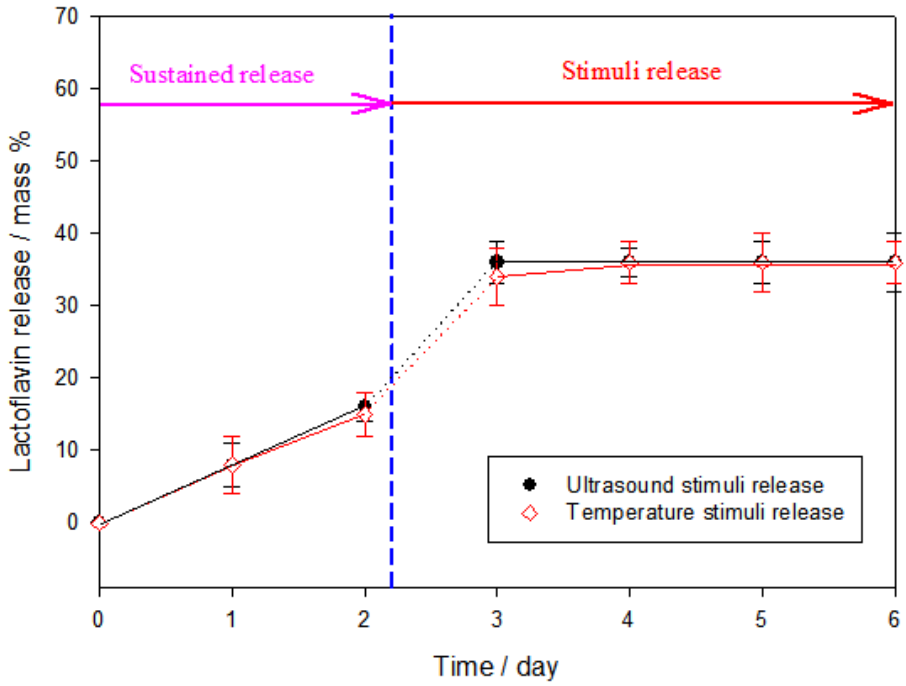

Figure 6.17 Cumulative release of lactoflavin from capsules without and with stimuli treatment. Error bars represent the standard deviation from three experiments

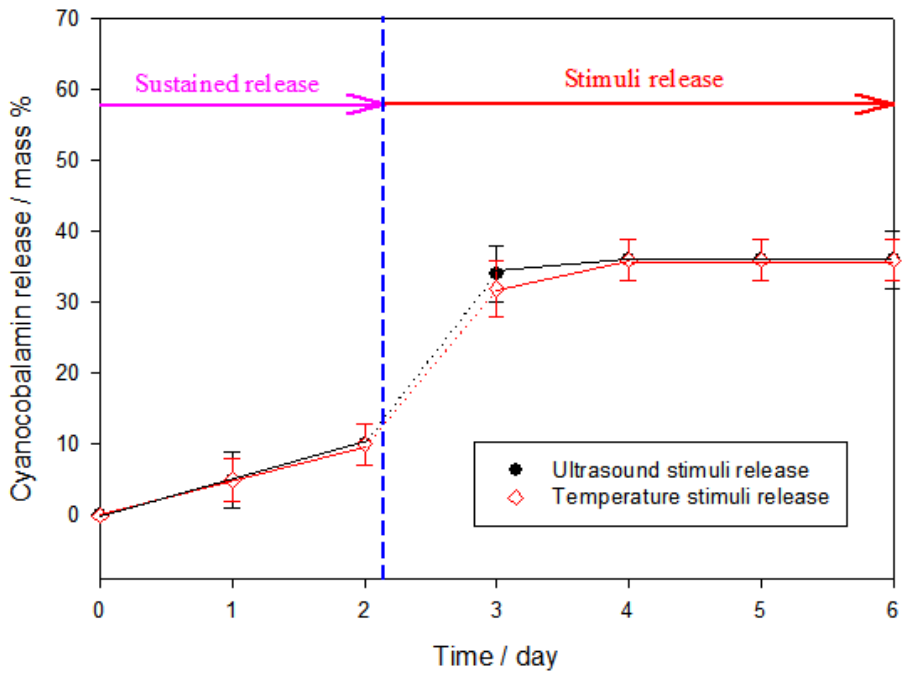

Figure 6.18 Cumulative release of cyanocobalamin from capsules without and with stimuli treatment. Error bars represent the standard deviation from three experiments

6.6 Summary

Delivery systems that provide spatial and temporal control over drug release through extracorporeal stimuli are extremely important in clinical applications. This chapter demonstrates a novel method for stimulated encapsulation and release from polymeric capsules with nanosize shells, containing a volatile liquid core prepared by electrohydrodynamic processing. The system does not require the use of smart polymers but instead relies on a non-toxic, biocompatible, volatile liquid (PFH). When the appropriate temperature was reached, this system exhibited temperature-responsive controllable encapsulation, and therefore offered the ability to incorporate high or low doses of a drug in the capsule. With different applied temperatures, enhanced controlled release with real-time response was also provided.

Ultrasound is another variable that can be specifically exploited in regulating drug release. When exposed to ultrasound the resulting temperature rise causes the liquid core to vaporise, enhancing the drug release from the capsules. This provides a mechanism for the release of encapsulated therapeutic material which can be controlled. The relationship between the release of a drug and the ultrasound intensity, duty cycle, and exposure time were investigated. Cavitation was also observed at high ultrasound intensities and was found to induce pore formation in the shell, offering an alternative pathway for promoting release from the capsules. Hence this work offers potential benefits for drug delivery applications and the design of stimuli-responsive systems.

Chapter 7

Conclusions and Future work

7.1 Conclusions

This research investigates the study of using co-axial electrohydrodynamic atomisation (CEHDA) as a 'one-step' processing method to produce new polymeric drug carriers such as hollow, monoporous hollow capsules. Moreover, a novel concept for stimuli-responsive drug encapsulation, storage and release from polymeric vehicles is demonstrated, using perfluorohexane (PFH) and polymethylsilsesquioxane (PMSQ). The following conclusions have been obtained from the investigations carried out in this thesis.

From the study using co-axial electrohydrodynamic atomisation to produce hollow capsules and their controlled release capabilities:

- The co-axial electrohydrodynamic atomisation process has proven to be a very effective and efficient 'one-step' method of fabricating hollow capsules at ambient temperature compared to conventional techniques which are more time-consuming, require multiple steps and surfactants or additives are heavily involved in the forming process.

- Through control of the processing parameters (e.g. flow rate, working distance, polymer concentration, and applied voltage) a range of hollow capsules has been produced with different mean microsphere diameter and shell thicknesses.

- The mean diameter of the hollow microspheres can be controlled in the range of ~300 nm to ~1000 nm while the corresponding mean shell thickness can be varied from ~40 nm to ~95 nm. The results indicated that the ratio D:t varied with polymer concentration with the largest value of ~10 achieved with a solution containing 18 wt% of the polymer while the smallest value (6.6) was obtained at 36 wt%.

- In the processing study, it was found that the outer PMSQ solution acted as the driving liquid because of its lower electrical relaxation time and higher viscosity compared to the inner liquid (PFH solution). A stable jet was not observed in the absence of the PMSQ solution, this was attributed to the low electrical conductivity of the inner liquid (PFH).

- Irregular microspheres with porous surfaces were generated instead of spherical microspheres at PMSQ flow rate of 200 μl min^{-1} and a PFH flow rate of 150 μl min^{-1}. This suggests that the inner liquid (PFH solution) is unable to be encapsulated by the sufficient driving force of the outer liquid (PMSQ solution) when the flow rate of outer liquid is smaller than a given value (in this case 250 μl min^{-1}).

- A transition from electrohydrodynamic spraying to electrospinning was observed as the polymer concentration was increased to 63 wt%. Hollow microspheres cannot be generated but instead PMSQ fibres encapsulating PFH liquid were obtained.

- It was observed that composite fibres, whose surfaces show both wrinkled and smooth features, consisted of PFH liquid droplets of ~7 μm in diameters encapsulated in ~10 μm diameter PMSQ polymer. This type of structure could potentially be used as a

functional material e.g. for textiles and drug delivery applications.

- It was found that both the polymer and PFH were stable and did not react with each other during the CEHDA processing. The PFH solution provided a volume for shell formation, after which it evaporated, thus providing a superior core-sell structure under ambient conditions. PMSQ showed both physical and chemical stability under experimental conditions used in this research.

- A map of applied voltage vs. flow rate for achieving an electrohydrodynamically stable jet was constructed. It was found that the stable jet can only be achieved when the flow rate and the applied voltage were in a distinctive envelope. With all other parameters fixed, the applied voltage required increased with increasing PMSQ flow rate.

- The capsule shells were found to contain channels (~5nm diameter) with a narrow size distribution, and the majority of the channels were radially aligned and ran through the full thickness of the shell.

- The release characteristics of hollow drug delivery carriers were strongly dependent on the properties of the capsule shell, in particular its thickness and porous structure. It was found that the release rate decreased with increasing shell thickness, and that it became increasingly linear with respect to time.

- Fitting the data to the Higuchi model confirmed that the release mechanism of dye from core to the sink was primarily controlled by Fickian diffusion, and dye molecules in the core space and pore wall did not interact with the PMSQ polymer.

- It has been shown that an increase in the shell thickness, at a fixed outer capsule diameter, caused a reduction of the core volume of hollow PMSQ as well as its surface area, leading to a reduction in the amount of loaded dye (drug) marker.

- Analysis of the release behaviour of different dye (drug) concentrations suggested that varying the characteristics of hollow capsules can be effective in controlling treatment duration and can avoid a high drug release flux. In addition, the release rate from this reservoir-type polymeric delivery device seems less dependent of the drug loading dose as long as the hollow cores can reach the maximum storage capacity and the drug molecules can transport into the hollow cores.

- The effect of medium temperature from 37-57 °C on the release behaviour suggested that under these conditions, no apparent difference in the release rate can be observed, which also follows Fickian diffusion. The channel diameter was found to be similar for all shell thicknesses (~5nm) in the temperature used.

From the study using co-axial electrospraying to produce monoporous hollow capsules and their controlled release capabilities:

- Production of hollow microspheres with a single hole in their shells by co-axial electrohydrodynamic atomisation was successful. This process overcomes several of the key problems associated with existing methods of monoporous microsphere formation including the need for elevated temperatures, multiple processing steps and the use of surfactants and other additives.

- The diameters of the microspheres and of the single surface pore can be controlled by varying the flow rate of the components, working distance, the concentration of the PMSQ solution and the applied voltage in the CEHDA process and the ranges obtained were respectively 275 to 860 nm for the microsphere diameter (D) and 35 to 135 nm for the pore diameter (d).

- The flow rate of the polymer (PMSQ) solution was found to have a greater effect upon the microsphere diameter. This may be attributed to its lower electrical relaxation time which caused it to act as the driving liquid in the process. In contrast, flow rate of PFH solution was found to have a greater effect upon the pore diameter.

- It was observed that the internal structure of monoporous capsule consisted of a single cavity within a polymer shell, which had a varying shell thickness that became lowest in the vicinity of the pore.

- The ratio $\beta = D/d$ was found to be in the range of 3.5 to 12.3. The highest value of β (12.3) was obtained by increasing the applied voltage to ~4 kV while the smallest value of β (3.5) was obtained by increasing the PFH flow rate to ~ 300 μl min^{-1}.

- This investigation has proved that low PMSQ concentrations (18 wt% - 36 wt%) can be used to prepare monoporous micropsheres whilst high PMSQ concentrations (63 wt%) are suitable for preparing functional fibres.

- It was observed that at a critical concentration of 63 wt% PMSQ, electro-spun fibres (diameter of ~10 μm) containing PFH liquid droplets (diameter ~7 μm) were obtained and the cracked open shell presented that the internal cavity of fibres were

previously occupied by PFH.

- It is suggested that the formation of the surface pore is attributed to the properties of PFH such as high evaporability and low electrical conductivity. The creation of the pore in the surface of microsphere may simply be due to the evaporation flux of the PFH solvent and the difference in the driving velocities. Therefore, the formation of monoporous microspheres appears before a complete PMSQ shell forms.

- The parametric applied voltage-flow rate space of the stable jet mode for the preparation of monoporous microspheres at 18 wt%, 27 wt%, and 36 wt% PMSQ concentrations showed that the applied voltage required for the stable jet formation increased with increasing PMSQ flow rate when all other parameters were held constant. Furthermore, when the PMSQ concentration was increased from 18 to 36 wt%, the applied voltage required to achieve the stable jet mode also increased.

- It was found that the dye release rate of the monoporous capsules can be varied by the variation of the pore diameter. Similar diameter monoporous capsules with a larger pore diameter led to a higher release rate of dye and burst release phase while smaller pores exhibited a significantly slower release rate.

- Effect of different diameters of monoporous capsules on the release behaviour has proven that the release is dominated by the diffusion of the dye molecules through the presence of the mono-pore on the hollow capsule, which provides a certain amount of dye to be released to the sink, regardless of the capsule diameter.

- The wide variation in the release behaviour of the dye was studied as a function of

the β value. A β value of 12.3 gave a slower release rate than that of the lowest β value (3.7). In addition, the amount of dye released from the lowest β value (3.7) sample was significantly decreased, which was attributed to the leakage of the dye during sample preparation.

- There was a noticeable difference in the encapsulation rate of the dye molecules for different pore sizes. A large pore on the shell (69 nm) diameter showed a higher encapsulation capacity than that of a small pore size (39 nm). This finding indicated that the existence of the pore on the surfaces of hollow capsules allowed direct loading of drugs. The large pore size provided higher loading capacity because of easier absorption and quicker transport of dye molecules in PMSQ capsules.

- The effect of storage and release of dye on the surface morphology of the capsules suggested that after dye release, there was no apparent difference when compared to the monoporous hollow capsules before dye release, and the pore on each capsule remained intact. The pore size (d) and outer diameter (D) did not change.

From the investigation of stimulated encapsulation, storage and release:

- A new strategy was investigated: How a temperature and ultrasound-responsive drug carrier can be prepared by co-axial electrohydrodynamic processing and stored under ambient conditions and subsequently programmed for controlled drug release without relying on a smart polymer.

- It was found that PFH content retained in the capsule can be controlled by adjusting

incubation times or temperature and therefore provided the ability to incorporate high or low doses of dye (drug) in the capsule. This system exhibited temperature-responsive controllable encapsulation.

- It has been shown that when the temperature of the medium was increased, the release rate of dye from the system increased substantially. This difference in release rate is mainly attributed to the fact that PFH is sensitive to the temperature of the medium. At a higher temperature the PFH in the capsule is active and this can result in enhanced release.

- It was found that the mechanism of real time stimuli-effect can be controlled by increasing the temperature from 37 to 57 °C. In addition, the surface morphology of the capsules is unaltered in this temperatures range.

- Ultrasound assisted "remote-controlled" release of an encapsulated solution can be achieved with the PMSQ-PFH capsules. The release of encapsulated solution can be precisely controlled, and the amount released is a function of power, duty cycle, and time of application of ultrasound.

- It was found that the release rate of encapsulated liquid from the hollow capsules with ultrasound treatment was higher than that without ultrasound.

- This investigation has proved that the influence of ultrasound depends on the presence of PFH in the core of the hollow capsules. Heating induced by absorption of ultrasonic waves was found to be one of the most pronounced effects of ultrasound stimuli-release. Ultrasonic cavitation induced temperature and as a result, causing a

significant instability of the PFH liquid, triggering enhanced release.

- It has been shown that by increasing ultrasound exposure time, release rate and depletion of dye from polymeric capsules can be enhanced. By controlling the duty cycle, hollow capsules with PFH show release enhancement induced in a similar way to that by increasing exposure times, and the release rate per day can lead to different pharmacokinetic profiles.

- It was found that higher ultrasound power resulted in faster release rates and therefore faster depletion. The enhancement of release was four-fold higher than the capsules which were not exposed to ultrasound.

- It was found that different amounts of PFH retained in the polymer shell showed no significant effect on the release rate under the ultrasound treatment, but this system exhibited the ability to incorporate high or low doses of dye in the capsule, depending on the PFH content retained in the capsule. Furthermore, different amounts of PFH in the polymer shell showed no substantial change in the surface morphology under the same ultrasound treatment.

- The influence of the exposure time (60s, 300s, and 600s) and duty cycle (30%, 60%, and 90%) showed that the capsules appears intact before and after the experiments. These results suggested that although ultrasound can provide enhancement on release rate, ultrasound treatments under conditions used do not induce significant morphology change and most of the capsules preserve their integrity after the course of altering exposure time and duty cycles.

- Morphology transformation after ultrasonic treatment by controlling output levels has been observed. Although these capsules have mostly smooth outer surfaces macroporous surfaces with many holes were observed on the surface of hollow capsules. In addition, polymeric capsules with an increased pore size and a crack pore around macroporous surface were observed.

- A collapse of the hollow structures was also observed when high-power output levels of ultrasound were introduced, which offers an alternative pathway to remotely release encapsulated molecules from the hollow capsules.

- The effect of drug molecular weight on the enhanced release from hollow capsules before and after exposure to extracorporeal stimuli was examined. Thus, aspirin, lactoflavin, cyanocobalamin can be encapsulated inside and released under the regulation of a stimulus.

- It was observed that it is easier for aspirin to pass polymeric shell while the high cyanocobalamin are released at a lower release rate than aspirin, which are more mass-transport.

7.2 Future work

Based on the research conducted and the outcome of this research, several aspects of future work are recommended as follows:

- For the investigation of capsule preparation by co-axial electrohydrodynamic processing, the capsule size is directly proportional to infused flow rate of solution. Needles with smaller inner diameter should be used for the investigation of capsule size,

which would enable to work on the lower flow rate regions and hence the capsule size can be scaled down to nano-size.

- The electrohydrodynamic processing set-up should be equipped with a high accuracy electrical current monitor and three dimensional stepping motors. This can provide a real-time record of droplet break-up and accurately control the position between needle exit and ground electrode.

- Hollow microspheres have a vast number of applications ranging from industry to medicine. During this research, PMSQ was used as the driving liquid for the capsule formation using electrohydrodynamic processing. More polymers such as starch, calcium phosphate and other biodegradable molecules should be applied to shell materials to find out the optimum materials for the CEHDA processing and practical applications.

- In the case of replacing PMSQ with a new material, it is essential to investigate the suitability of that material for electrospraying. It will be necessary to experiment with different concentrations of suspensions and plotting a mode map will be required as the conditions for the stable jet will depend on the material. The novel shell material fulfilling these requirements could lead to a new generation of multifunctional capsules.

- In this investigation, whilst PFH was used to form the inner hollow core, it has been observed that the transition from dripping mode to stable jet is independent of the applied voltage. Further work could be done to investigate new suitable liquids with high conductivity in order to observe the effect of the void size and shell thickness of hollow capsules.

- Even if it were possible to produce hollow capsules with sustained release using electrospraying and the release behaviour can be regulated by shell thickness, the mechanical strength of the hollow structures needs to be investigated if they are to be considered for applications where high pressure is required, e.g. insulator.

- In the hollow capsule, reasonable channel sizes in the shell thickness have been observed. Using a solvent with high evaporation rate in the suspension could be investigated as it would increase the channel size and improve the release properties of the hollow capsules.

- The monoporous hollow capsules were prepared at ambient temperature using co-axial electrohydrodynamic processing. Further studies should be carried out by increasing the temperature to study the effect of temperature on CEHDA processing. Solutions will have a lower viscosity when processing is performed at a high temperature. This could be significant in improving the capsule formation and their release characteristics.

- A range of spherical capsules with uniform size-distribution was successfully prepared using CEHDA processing. Although spherical geometries have been preferred as optimal circulating shapes for drug delivery, it is important to further investigate different shapes of capsules e.g. square shape, hexagonal shape and line shape with controllable size.

- It would be beneficial to develop a better understanding of the rheology of the solutions in CEHDA process and control of solution properties might lead to an

important of pore and capsule formation.

- The monoporous hollow capsules used in this investigation can have a pore on their polymeric shell, making the encapsulation efficiency high, but leading to leakage during capsule preparation. Therefore, if pore shaped can be closed after loading the drugs, the packing efficiency would be improved leading to a high encapsulation rate of hollow structures.

- PFH encapsulated in polymer fibres can be obtained at high polymer concentrations. The control over the size of the PFH regions in the polymer fibre could be investigated in detail using co-axial electrohydrodynamic processing, which would enable the production of multi-compartment fibres. Also, the PFH could be replaced with simply a drug, hence enabling co-delivery of drug.

- Further investigations should be carried out to prepare multi-functional drug carriers based on core-shell combinations. Functional multi-layer capsules could be prepared using electrohydrodynamic processing by increasing the number of needles and carefully changing the composition of the solution. These would enable multi-functional drug capsules with multi-compartments such as “particle in particle”, “particle in hollow”, and “hollow in hollow” to meet the therapeutic and diagnostic needs.

- Larger size capsules should be prepared and investigated for even longer sustained release as lower surface area per volume would increase time-periods and might have an advantage in terms of biodistribution and cell-internalization propensity.

- Stimuli-enhanced release of drugs is a relatively new concept in medical therapies because most applications have aimed at a constant release within the therapeutic index of a drug to reduce potential toxic side effects. However, a range of drugs such as aspirin, lactoflavin, and cyanocobalamin has been used to study stimuli-controlled release in this research. Similarly, other asthmatic, and anti-allergic drugs, hormones, insulin and anesthesia could be delivered at certain time intervals.

- PFH liquid has been used as stimulus for enhanced release in this research. The research should move to encapsulating other novel liquids using electrohydrodynamic processing. Functional materials should also be electrosprayed and characterised for novel drug carriers. The optimal processing parameters, including substrate-needle distance, flow rate, polymer concentration and applied voltage, should be investigated in future work.

- Although it was possible to produce a stimuli-drug delivery system using electrohydrodynamic processing, and the release behaviours proved to be regulated by using temperature and ultrasound, drug storage still needs to be improved in the hollow structures if they are to be considered for applications where high load bearing is required.

- The effects of two types of stimulations on stimulating drug release were investigated (e.g. temperature and ultrasound). Similarly, a range of external stimulations (e.g. magnetic, enzyme and optical trigger) could be investigated to observe the effects on the properties such as release behaviour and capsule morphology. The novel combination prepared using this kind of functional materials could lead to a new generation of multi-functional drug carriers.

- Drug enhanced release has been proven with real-time response in this research. However, drug delivery systems with zero release unless triggered should be investigated. This will not only provide effective treatment in cancerous cells, but can avoid the harmful side-effects when chemotherapeutic agents may be administered before reaching tumours.

- The ultrasound stimuli-release system developed has improved release rates. However, a more detailed study needs to follow up this work, investigating effects such as the effects of changing the transducer frequency and the transducer diameter for enhanced release and their effects on the capsule structure, observing any changes in the capsule morphology.

- Ultrasound induced temperature for stimuli-release has been demonstrated. These values were based on the influence on PFH liquids within the polymeric capsules. However, it is expected that the heating of polymeric drug delivery vehicles also occur when surrounded by human tissue. Therefore, further investigation should be carried out with cell culture systems and *in-vivo* to gain further understanding of the capsules behaviour when subjected to stimuli within biological surroundings.

- The influence of the distance between the transducer and the polymer on the temperature should be further investigated with different vials. The temperature in the polymer suspension induced by ultrasound can result in pronounced variation in sink temperature. When the ultrasonic wave has travelled the medium, the intensity of the wave usually decreases with the distance due to the attenuation of sound waves. This effect may result in a change of controlled release and surface morphology.

- By understanding the effects of a range of core-shell structures, it will be possible to further optimise the fabrication process experimentally to produce functionally active multi-layer capsules with more desirable tailored properties, which are capable of responding to the multi-stage triggering.

- The therapeutic window can be increased through targeted stimuli-responsive delivery, which increases the drug's concentration at a diseased site, and releasing or activating the drug only when it reaches the target. Numerous conjugates are used clinically or are being evaluated in trials involving (PEG)-bound camptothecin, poly(l-glutamic acid)-bound, and N-(2-hydroxypropyl)methacrylamide (HPMA) copolymer conjugation as a targeting moiety. The surface of monoporous and hollow capsules could be conjugated, or ligand coated to form targeted drug delivery for tumor treatment, which could reduce the side effects of drugs, and reduce the fluctuation in circulating drug levels.

- Further investigation of biological systems should be carried out. More biological systems should be investigated by electrohydrodynamic processing, as it offers many advantages over others in terms of better control over capsule size and shell thickness and it is a very safe and an economical method.

- Heating induced by therapeutic ultrasound is applied in physiotherapy to relax muscles, as well as in medical applications to increase the blood flow and speed up the healing processes. It would be possible to use drug delivery for applications that could combine physiotherapy and chemotherapy.

- The concept of temperature and ultrasound induced drug delivery can be beneficial for several medical treatments and may enable the development of new and improved therapies. However, to optimise this technology for clinical applications, modelling of the ultrasonic beam behaviour and the associated temperature increase coupled with the induced amount of drug release is required. In addition, safety guidelines with regards to the application of temperature-induced release should be considered to prevent tissue damage.

- It has been shown that the hollow, monoporous and stimulated responsive drug carriers can be successfully formed by using co-axial electrohydrodynamic atomisation process as a very effective and efficient single-step method at ambient temperature for controlled release applications. Further investigations should be carried out to develop a better understanding of the mathematical modelling to complement the experimental results.

- There are a number of clinical situations where such core-shell structure with enhanced release may be desirable. These include the delivery of insulin for patients with diabetes mellitus, gastric acid inhibitors for ulcer control, nitrates for patients with angina pectoris, and cancer chemotherapy.

- Thorough the knowledge of each parameter that influences the release behaviour enables optimisation and improvement of the developed technology. This can be obtained by modelling the drug release as a function of temperature and ultrasound treatment. Integration of this data can further provide a powerful simulation tool that allows the release behaviour to be tuned and designed for a specific medical treatments.

References

Aggarwal, S. (2007) What's fueling the biotech engine? *Nature Biotechnology,* 25**,** 1097-1104.

Agrawal, C., Kennedy, M. & Micallef, D. (1994) The effects of ultrasound irradiation on a biodegradable 50-50% copolymer of polylactic and polyglycolic acids. *Journal of Biomedical Materials Research,* 28**,** 851-859.

Ahmad, Z., Nangrejo, M., Edirisinghe, M., Stride, E., Colombo, P. & Zhang, H. B. (2009) Engineering a material for biomedical applications with electric field assisted processing. *Applied Physics A: Materials Science & Processing,* 97**,** 31-37.

Antipov, A. A. & Sukhorukov, G. B. (2003) Polyelectrolyte multilayer capsules as vehicles with tunable permeability. *Advances in Colloid and Interface Science,* 111**,** 49-61.

Aschkenasy, C. & Kost, J. (2005) On-demand release by ultrasound from osmotically swollen hydrophobic matrices. *Journal of Controlled Release,* 110**,** 58-66.

Babiak, P., Mcova, A. N., Rulısek, L. & Beier, P. (2008) On the miscibility of ethers and perfluorocarbons: An experimental and theoretical study. *Journal of Fluorine Chemistry,* 129**,** 397-401.

Bai, M.-Y., Cheng, Y.-J., Wickline, S. A. & Xia, Y. (2009) Colloidal hollow spheres of conducting polymers with smooth surface and uniform, controllable sizes. *Small,* 5**,** 1747-1752.

Bajpai, A. K., Shukla, S. K., Bhanu, S. & Kankane, S. (2008) Responsive polymers in controlled drug delivery. *Progress in Polymer Science,* 33**,** 1088-1118.

Bawa, P., Pillay, V., Choonara, Y. E. & Toit, L. C. D. (2009) Stimuli-responsive polymers and their applications in drug delivery. *Biomedical Materials,* 4**,** 1-15.

Bekeredjianlow, R., Krolllow, R. D., Fein, E., Tinkov, S., Coester, C., Winter, G., Katuslow, H. A. & Kulaksiz, H. (2007) Ultrasound targeted microbubble destruction increases capillary permeability in hepatomas. *Ultrasound in Medicine & Biology,* 33**,** 1592-1598.

Benjamin, T. & Ellis, A. (1966) The collapse of cavitation bubbles and the pressures thereby produced against solid boundaries. *Philosophical Transactions A,* 260**,** 221-240.

Berger, S., Zhang, H. & Pich, A. (2009) Microgel-based stimuli-responsive capsules. *Advanced Functional Materials,* 19**,** 554-559.

Berkland, C., Pack, D. W. & Kim, K. (2004) Controlling surface nano-structure using flow-limited field-injection electrostatic spraying (FFESS) of poly(d,l-lactide-co-glycolide). *Biomaterials,* 25**,** 5649-5658.

Bertling, J., Blömer, J. & Kümmel, R. (2004) Hollow Microsperes. *Chemical Engineering & Technology,* 27**,** 829-837.

Bischoff, F. (1972) Organic polymer biocompatibility and toxicology. *Clinical Chemistry,* 18**,** 869-894.

Bogart, K. H. A., Dalleska, N. F., Bogart, G. R. & Fisher, E. R. (1995) Plasma enhanced chemical vapor deposition of S_iO_2 using novel alkoxysilane precursors. *Journal of Vacuum Science & Technology A: Vacuum, Surfaces, and Films,* 13**,** 476-480.

Böhmer, M. R., Chlon, C. H. T., Raju, B. I., Chin, C. T., Shevchenko, T. & Klibanov, A. L. (2010) Focused ultrasound and microbubbles for enhanced extravasation. *Journal of Controlled Release,* 148**,** 18-24.

Brodbeck, K. J., Desnoyer, J. R. & Mchugh, A. J. (1999) Phase inversion dynamics of PLGA solutions related to drug delivery Part II. The role of solution thermodynamics and bath-side mass transfer. *Journal of Controlled Release,* 62**,** 333-344.

Bruck, S. D. (1983) Pharmacological basis of controlled drug delivery. *Controlled drug delivery. Basic concepts, vol. I. Boca Raton (FL): CRC Press***,** 1-15.

Cai, K., Luo, Z., Hu, Y., Chen, X., Liao, Y., Yang, L. & Deng, L. (2009) Magnetically triggered reversible controlled drug delivery from microfabricated polymeric multireservoir devices. *Advanced Materials,* 21**,** 4045-4049.

Cai, Y., Pan, H., Xu, X., Hu, Q. & Li, L. (2007) Ultrasonic controlled morphology transformation of hollow calcium phosphate nanospheres: A smart and biocompatible drug release system. *Chemistry of Materials,* 19**,** 3081-3083.

Caruso, F., Caruso, R. A. & Möhwald, H. (1998) Nanoengineering of inorganic and hybrid hollow spheres by colloidal templating. *Science,* 282**,** 1111-1114.

Caruso, F., Yang, W., Trau, D. & Renneberg, R. (2000) Microencapsulation of uncharged low molecular weight organic materials by polyelectrolyte multilayer self-assembly. *Langmuir* 16**,** 8932-8936.

Chen, J.-F., Ding, H.-M., Wang, J.-X. & Shao, L. (2004) Preparation and characterization of porous hollow silica nanoparticles for drug delivery application. *Biomaterials,* 25**,** 723-727.

Chia, S., Urano, J., Tamanoi, F., Dunn, B. & Zink, J. I. (2000) Patterned hexagonal arrays of living cells in sol-gel silica films. *Journal of American Chemical Society,* 122**,** 6488-6489.

Cloupeau, M. & Prunet-Foch, B. (1989) Eletrostatic spraying of liquids in cone-jet mode. *Journal of Electrostatics,* 22**,** 135-139.

Cloupeau, M. & Prunet-Foch, B. (1990) Eletrostatic spraying of liquids: Main functioning modes. *Journal of Electrostatics,* 25**,** 165-184.

Colombo, P. (2008) Engineering porosity in polymer-derived ceramics. *Journal of the European Ceramic Society,* 28**,** 1389-1395.

Couture, O., Bevan, P., Cherin, E., Cheung, K., Burns, P. & Foster, F. (2006) Investigating perfluorohexane particles with high-frequency ultrasound. *Ultrasound in Medicine & Biology,* 32**,** 73-82.

Cui, J., Wang, Y., Postma, A., Hao, J., Hosta-Rigau, L. & Caruso, F. (2010)

Monodisperse polymer capsules: tailoring size, shell thickness, and hydrophobic cargo loading via emulsion templating. *Advanced Functional Materials,* 20**,** 1625-1631.

Daiguji, H., Makuta, T., Kinoshita, H., Oyabu, T. & Takemura, F. (2007) Fabrication of hollow melamine-formaldehyde microcapsules from microbubble templates. *Journal of Physical Chemistry B,* 111**,** 8879-8884.

Das, S., Banerjee, R. & Bellare, J. (2005) Aspirin loaded albumin nanoparticles by coacervation: Implications in drug delivery. *Trends Biomater Artif Organs,* 18**,** 203-212.

Devalapally, H., Shenoy, D., Little, S., Langer, R. & Amiji, M. (2007) Poly(ethylene oxide)-modified poly(beta-amino ester) nanoparticles as a pH-sensitive system for tumor-targeted delivery of hydrophobic drugs: part 3. Therapeutic efficacy and safety studies in ovarian cancer xenograft model. *Cancer Chemotherapy and Pharmacology,* 59**,** 477-484.

Dias, A. M. A., Bonifácio, R. P., Marrucho, I. M., Pádua, A. A. H. & Gomes, M. F. C. (2003) Solubility of oxygen in n-hexane and in n-perfluorohexane: Experimental determination and prediction by molecular simulation. *Physical Chemistry Chemical Physics,* 5**,** 543-549.

Díaz-López, R., Tsapis, N. & Fattal, E. (2010) Liquid perfluorocarbons as contrast agents for ultrasonography and 19F-MRI. *Pharmaceutical Research,* 27**,** 1-16.

Dimasi, J. A., Hansen, R. W. & Grabowski, H. G. (2003) The price of innovation: new estimates of drug development costs. *Journal of Health Economics,* 22**,** 151-185.

Ding, L., Lee, T. & Wang, C.-H. (2005) Fabrication of monodispersed taxol-loaded particles using electrohydrodynamic atomization. *Journal of Controlled Release,* 102**,** 395-413.

Dong, L., Agarwal, A. K., Beebe, D. J. & Jiang, H. (2006) Adaptive liquid microlenses activated by stimuli-responsive hydrogels. *Nature,* 442**,** 551-554.

Dong, W.-F., Ferri, J. K., Adalsteinsson, T., Schnhoff, M., Sukhorukov, G. B. & Mhwald, H. (2005) Influence of shell structure on stability, integrity, and mesh size of polyelectrolyte capsules: Mechanism and strategy for improved preparation. *Chemistry of Materials,* 17**,** 2603-2611.

Dorogotovtsev, V. M. & Akunets, A. A. (1997) Influence of the properties of the furnace atmosphere on microsphere quality. *Fusion Technology,* 31**,** 411-417.

Duncan, R. (2003) The dawning era of polymer therapeutics. *Nature,* 2**,** 347-360.

Eapen, K. C., John, P. J. & Liang, J. C. (1994) Degradatation of a brenched perfluoropolyalkyloether fluid with anhydrous aluminum-chloride. *Macromolecular chemistry and physics,* 195**,** 2887-2903.

Ehrbar, M., Schoenmakers, R., Christen, E. H., Fussenegger, M. & Weber, W. (2008) Drug-sensing hydrogels for the inducible release of biopharmaceuticals. *Nature Materials,* 7**,** 800-804.

Evjen, T. J., Nilssen, E. A., Barnert, S., Schubert, R., Brandl, M. & Fossheim, S. L.

(2011) Ultrasound-mediated destabilization and drug release from liposomes comprising dioleoylphosphatidylethanolamine. *European Journal of Pharmaceutical Sciences,* 42**,** 380-386.

Faisant, N., Akiki, J., Siepmann, F., Benoit, J. P. & Siepmann, J. (2006) Effects of the type of release medium on drug release from PLGA-based microparticles: Experiment and theory. *International Journal of Pharmaceutics,* 314**,** 189-197.

Farook, U., Edirisinghe, M. J., Stride, E. & Colombo, P. (2008) Novel co-axial electrohydrodynamic in-situ preparation of liquid-filled polymer-shell microspheres for biomedical applications. *Journal of Microencapsulation,* 25**,** 241-247.

Fay, B. & Binker, M. (1996) The thermoacoustic effect and its use in ultrasonic power determination. *Ultrasonics,* 34**,** 563-566.

Fisher, K. A., Huddersman, K. D. & Taylor, M. J. (2003) Comparison of micro- and mesoporous inorganic materials in the uptake and release of the drug model fluorescein and its analogues. *Chemistry - A European Journal,* 9**,** 5873-5878.

Fogler, S. & Lund, K. (1973) Acoustically augmented diffusional transport. *Journal of the Acoustical Society of America,* 53**,** 59-64.

Foss, A. C., Goto, T., Morishita, M. & Peppas, N. A. (2004) Development of acrylic-based copolymers for oral insulin delivery. *European Journal of Pharmaceutics and Biopharmaceutics,* 57**,** 163-169.

Ganan-Calvo, A. M. (1999) The electrohydrodynamic atomization of liquids today. *Journal of Aerosol Science,* 30**,** S547-S548.

Ganan-Calvo, A. M., Davila, J. & Barrero, A. (1997) Current and droplet size in the electrospraying of liquids. Scaling laws. *Journal of Aerosol Science,* 28**,** 249-275.

Ganan-Calvo, A. M., Lasheras, J. C., Davila, J. & Barrero, A. (1994) The electrostatic spray emitted from an electrified conical meniscus. *Journal of Aerosol Science,* 25**,** 1121-1142.

Ganta, S., Devalapally, H., Shahiwala, A. & Amiji, M. (2008) A review of stimuli-responsive nanocarriers for drug and gene delivery. *Journal of Controlled Release,* 126**,** 187-204.

Gao, F., Su, Z.-G., Wang, P. & Ma, G.-H. (2009) Double emulsion templated microcapsules with single hollow cavities and thickness-controllable shells. *Langmuir,* 25**,** 3832-3838.

Gao, Z. G., Fain, H. D. & Rapoport, N. (2005) Controlled and targeted tumor chemotherapy by micellar-encapsulated drug and ultrasound. *Journal of Controlled Release,* 102**,** 203-222.

Geest, B. G. D., Sanders, N. N., Sukhorukov, G. B., Demeester, J. & Smedt, S. C. D. (2007) Release mechanisms for polyelectrolyte capsules. *Chemical Society Reviews,* 36**,** 636-649.

Geest, B. G. D., Vandenbroucke, R. E., Guenther, A. M., Sukhorukov, G. B., Hennink, W. E., Sanders, N. N., Demeester, J. & Smedt, S. C. D. (2006) Intracellularly degradable polyelectrolyte microcapsules. *Advanced Materials,* 18**,** 1005-1009.

Giesecke, T. & Hynynen, K. (2003) Ultrasound-mediated cavitation thresholds of liquid perfluorocarbon droplets in vitro. *Ultrasound in Medicine & Biology,* 29**,** 1359-1365.

Gomez, A. & Tang, K. (1994) Charge and fission of droplets in electrostatic sprays. *Physics of Fluids,* 6**,** 404-414.

Grace, J. M. & Marijnissen, J. C. M. (1994) A review of liquid atomization by electrical means. *Journal of Aerosol Science,* 25**,** 1005-1019.

Graham, J. M., Peerson, J. M., Haskell, M. J., Shrestha, R. K., Brown, K. H. & Allen, L. H. (2005) Erythrocyte riboflavin for the detection of riboflavin deficiency in pregnant nepali women. *Clinical Chemistry,* 51**,** 2162-2165.

Grayson, A. C. R., Choi, I. S., Tyler, B. M., Wang, P. P., Brem, H., Cima, M. J. & Langer, R. (2003) Multi-pulse drug delivery from a resorbable polymeric microchip device. *Nature Materials,* 2**,** 767-772.

Greenblatt, D. J. (2006) Pharmacokinetic determinants of hypnotic drug action: The art and science of controlling release. *Sleep Medicine,* 7**,** S10-S14.

Guan, G., Zhang, Z., Wang, Z., Liu, B., Gao, D. & Xie, C. (2007) Single-hole hollow polymer microspheres toward specific high-capacity uptake of target species. *Advanced*

Materials, 19**,** 2370 - 2374.

Gupta, P., Vermani, K. & Garg, S. (2002) Hydrogels: from controlled release to pH-responsive drug delivery. *Drug Discovery Today,* 7**,** 569-579.

Han, J., Song, G. & Guo, R. (2006) A facile solution route for polymeric hollow spheres with controllable size. *Advanced Materials,* 18**,** 3140-3144.

Hartman, R. P. A., Borra, J. P., Brunner, D. J., Marijnissen, J. C. M. & Scarlett, B. (1999a) The evolution of electrohydrodynamic sprays produced in the cone-jet mode, a physical model. *Journal of Electrostatics,* 47**,** 143-170.

Hartman, R. P. A., Brunner, D. J., Camelot, D. M. A., Marijnissen, J. C. M. & Scarlett, B. (1999b) Electrohydrodynamic atomization in the cone-jet mode physical modelling of the liquid cone and jet. *Journal of Aerosol Science,* 30**,** 823-849.

Hartman, R. P. A., Brunner, D. J., Camelot, D. M. A., Marijnissen, J. C. M. & Scarlett, B. (2000) Jet break-up in electrohydrodynamic atomization in the cone-jet mode. *Journal of Aerosol Science,* 30**,** 823-849.

Heller, J. (1987) Use of polymers in controlled release of active agents. In: J.R. Robinson and V.H.L. Lee, Editors, Controlled drug delivery fundamentals and applications (2nd ed), Marcel Dekker, New York. 179-212.

Hest, J. C. M. V. (2009) Materials science: pulsating vesicles. *Nature,* 461**,** 45-47.

Heuschkel, S., Goebel, A. & Neubert, R. H. H. (2007) Microemulsions-modern

colloidal carrier for dermal and transdermal drug delivery. *Journal of Pharmaceutical Sciences,* 97**,** 603 - 631.

Hu, S.-H., Liu, T.-Y., Huang, H.-Y., Liu, D.-M. & Chen, S.-Y. (2008) Magnetic-sensitive silica nanospheres for controlled drug release. *Langmuir,* 24**,** 239-244.

Hu, S., Liu, T., Liu, D. & Chen, S. (2007) Controlled pulsatile drug release from a ferrogel by a high-frequency magnetic field. *Macromolecules,* 40**,** 6786-6788.

Huang, Q. R., Kim, H.-C., Huang, E., Mecerreyes, D., Hedrick, J. L., Volksen, W., Frank, C. W. & Miller, R. D. (2003) Miscibility in organic/Inorganic hybrid nanocomposites suitable for microelectronic applications: Comparison of modulated differential scanning calorimetry and fluorescence spectroscopy macromolecules. *Macromolecules,* 36**,** 7661-7671.

Im, S. H., Jeong, U. & Xia, Y. (2005) Polymer hollow particles with controllable holes in their surfaces. *Nature materials,* 4**,** 671-675.

Itou, N., Masukawa, T., Ozaki, I., Hattori, M. & Kasai, K. (1999) Cross-linked hollow polymer particles by emulsion polymerization. *Colloids and Surfaces,* 153**,** 311-316.

Jaworek, A. & Krupa, A. (1999a) Classification of the modes of EHD spraying. *Journal of Aerosol Science,* 30**,** 873-893.

Jaworek, A. & Krupa, A. (1999b) Jet and drops formation in electrohydrodynamic spraying of liquids: A systematic approach. *Experiment in Fluids,* 27**,** 43-52.

Jayasinghe, S. N. & Edirisinghe, M. J. (2002) Effect of viscosity on the size of relics produced by electrostatic atomization. *Journal of Aerosol Science,* 33**,** 1379-1388.

Jayasinghe, S. N. & Edirisinghe, M. J. (2004) Electrically forced jets and microthreads of high viscosity dielectric liquids. *Journal of Aerosol Science,* 35**,** 233-243.

Jeong, B., Bae, Y. H., Lee, D. S. & Kim, S. W. (1997) Biodegradable block copolymers as injectable drug-delivery systems. *Nature,* 388**,** 860-862.

Jeong, U., Im, S. H., Camargo, P. H. C., Kim, J. H. & Xia, Y. (2007) Microscale fish bowls: A new class of latex particles with hollow interiors and engineered porous structures in their surfaces. *Langmuir,* 23**,** 10968-10975.

Johnston, A. P. R., Mitomo, H., Read, E. S. & Caruso, F. (2006) Compositional and structural engineering of DNA multilayer films. *Langmuir,* 22**,** 3251-3258.

Jones, A. R. & Thong, K. C. (1971) The production of charged monodisperse fuel droplets by electrical dispersion. *Journal of Physics D: Applied Physics,* 4**,** 1159-1166.

Jong, W. H. D. & Borm, P. J. (2008) Drug delivery and nanoparticles: Applications and hazards. *International Journal of Nanomedicine,* 3**,** 133-149.

Jr, J. F. B., Jr, L. H. V., Katchman, A., Eustance, J. W., Kiser, K. M. & Krantz, K. W. (1960) Double chain polymers of phenylsilsequioxane. *Journal of the American Chemical Society,* 82**,** 6194-6195.

Kaneko, Y., Nakamura, S., Sakai, K., Kikuchi, A., Aoyagi, T., Sakurai, Y. & Okano, T.

(1999) Synthesis and swelling-deswelling kinetics of poly(N-isopropylacrylamide) hydrogels grafted with LCST modulated polymers. *Journal of Biomaterials Science,* 10**,** 1079-1091.

Kennedy, J. E., Harr, G. R. & Cranston, D. (2003) High intensity focused ultrasound: surgery of the future? *The British Journal of Radiology,* 76**,** 590-599.

Khan, G. M. & Zhu, J. B. (1999) Studies on drug release kinetics from ibuprofen-carbomer hydrophilic matrix tablets: influence of co-excipients on release rate of the drug. *Journal of Controlled Release,* 57**,** 197-203.

Kim, H.-J., Matsuda, H., Zhou, H. & Honma, I. (2006) Ultrasound-triggered smart drug release from a poly(dimethylsiloxane)-mesoporous silica composite. *Advanced Materials,* 18**,** 3083-3088.

Kim, S., Kim, J.-H., Jeon, O., Kwon, I. C. & Park, K. (2009) Engineered polymers for advanced drug delivery. *European Journal of Pharmaceutics and Biopharmaceutics,* 71**,** 420-430.

Kim, Y. B. & Yoon, K.-S. (2004) A physical method of fabricating hollow polymer spheres directly from oil/water emulsions of solutions of polymers. *Macromolecular Rapid Communications,* 25**,** 1643-1649.

Klouda, L. & Mikos, A. G. (2008) Thermoresponsive hydrogels in biomedical applications. *European Journal of Pharmaceutics and Biopharmaceutics,* 68**,** 34-45.

Kornmann, L., Curfs, D., Hermeling, E., Made, I., Winther, M. & Reneman, R. (2008) Perfluorohexane-loaded macrophages as a novel ultrasound contrast agent: A feasibility study. *Molecular Engineering,* 10**,** 264 -270.

Kortesuo, P., Ahola, M., Karlsson, S., Kangasniemi, I., Yli-Urpo, A. & Kiesvaara, J. (2000) Silica xerogel as an implantable carrier for controlled drug delivery-evaluation of drug distribution and tissue effects after implantation. *Biomaterials,* 21**,** 193-198.

Kost, J., Lenong, K. & Langer, R. (1989) Ultrasound-enhanced polymer degradation and release of incorporated substances. *Applied Biological Sciences,* 86**,** 7663-7666.

Kowalski, A., Vogel, M. & Blankenship, R. M. (1984) Sequential heteropolymer dispersion and a particulate material obtainable therefrom, useful in coating compositions as a thickening and/or opacifying agent. *US Patent. 4427836*.

Kreft, O., Georgieva, R., Bäumler, H., Steup, M., Müller-Röber, B., Sukhorukov, G. B. & Möhwald, H. (2006) Red blood cell templated polyelectrolyte capsules: A novel vehicle for the stable encapsulation of DNA and proteins. *Macromolecular Rapid Communications,* 27**,** 435-440.

Lai, C.-Y., Trewyn, B. G., Jeftinija, D. M., Jeftinija, K., Xu, S., Jeftinija, S. & Lin, V. S.-Y. (2003) A mesoporous silica nanosphere-based carrier system with chemically removable C_dS nanoparticle caps for stimuli-responsive controlled release of neurotransmitters and drug molecules. *Journal of American Chemical Society,* 125**,** 4451-4459.

Langer, R. (1990) New methods of drug delivery. *Science,* 249**,** 1527-1533.

Lauterborn, W. & Bolle, H. (1975) Experimental investigations of cavitation-bubble collapse in the neighbourhood of a solid boundary. *Journal of Fluid Mechanics,* 72**,** 391-399.

Lavon, I. & Kost, J. (1998) Mass transport enhancement by ultrasound in non-degradable polymeric controlled release systems. *Journal of Controlled Release,* 54**,** 1-7.

Lee, E. S., Shin, H. J., Na, K. & Bae, Y. H. (2003) Poly(l-histidine)-PEG block copolymer micelles and pH-induced destabilization. *Journal of Controlled Release,* 90**,** 363-374.

Lehmler, H., Bummer, P. & Jay, M. (1999) Liquid ventilation-a new way to deliver drugs to diseased lungs? *Chemtech,* 29**,** 7-12.

Leong, K. W., Kost, J., Mathiowitz, E. & Langer, R. (1986) Polyanhydrides for controlled release of bioactive agents. *Biomaterials,* 7**,** 364-371.

Li, M.-H. & Keller, P. (2009) Stimuli-responsive polymer vesicles. *Soft Matter,* 5**,** 927-937.

Li, Y., Shi, J., Hua, Z., Chen, H., Ruan, M. & Yan, D. (2003) Hollow spheres of mesoporous aluminosilicate with a three-dimensional pore network and extraordinarily high hydrothermal stability. *Nano Letters,* 3**,** 609-612.

Lin, H.-Y. & Thomas, J. L. (2003) PEG-lipids and oligo(ethylene glycol) surfactants enhance the ultrasonic permeabilizability of liposomes. *Langmuir,* 19**,** 1098-1105.

Lin, H.-Y. & Thomas, J. L. (2004) Factors affecting responsivity of unilamellar liposomes to 20 kHz ultrasound. *Langmuir,* 20**,** 6100-6106.

Liu, J., Lewis, T. & Prausnitz, M. (1998) Non-invasive assessment and control of ultrasound-mediated membrane permeabilization. *Pharmaceutical Research,* 15**,** 918-923.

Liu, Q., Huang, C., Luo, S., Liu, Z. & Liu, B. (2007) Production of micron-sized hollow microspheres by suspension polymerization of St-DEGDA (diethylene glycol diacrylate) with petroleum ether (90-120 °C). *Polymer,* 48**,** 1567-1572.

Liz-Marzán, L. M., Giersig, M. & Mulvaney, P. (1996) Synthesis of nanosized gold-silica core-shell particles. *Langmuir,* 12**,** 4329-4335.

Lopez-Harrera, J., Barrero, A., Lopez, A., Loscertales, I. & Marquez, M. (2003) Coaxial jets generated from electrified taylor cones, scaling laws. *Journal of Aerosol Science,* 34**,** 535-552.

Loscertales, I. G., Barrero, A., Guerrero, I., Cortijo, R., Marquez, M. & Gañán-Calvo, A. M. (2002) Micro/nano encapsulation via electrified coaxial liquid jets. *Science,* 295**,** 1695-1698.

Lu, Z., Prouty, M. D., Guo, Z., Golub, V. O., Kumar, C. S. S. R. & Lvov, Y. M. (2005)

Magnetic switch of permeability for polyelectrolyte microcapsules embedded with Co@Au nanoparticles. *Langmuir,* 21**,** 2042-2050.

Ma, J., Feng, Q. Y., Shi, L. H. & Xu, J. (2002a) Preliminary study on pyrolysis of polymethylsilsesquioxane by FT-IR and XPS. *Chinese Chemical Letters,* 13**,** 75 -78.

Ma, J., Shi, L., Yang, M., Li, B., Liu, H. & Xu, J. (2002b) Synthesis and structure of polymethylsilsesquioxane-clay nanocomposite via in situ intercalative polymerization. *Journal of Applied Polymer Science,* 86**,** 3708-3711.

Magual, A., Horva, T.-S. G. & Masliyah, J. (2005) Acoustic and electroacoustic spectroscopy of water-in-diluted-bitumen emulsions. *Langmuir,* 21**,** 8649-8657.

Mamada, A., Tanaka, T., Kungwatchakun, D. & Irie, M. (1990) Photoinduced phase transition of gels. *Macromolecules,* 23**,** 1517-1519.

Mana, Z., Pellequer, Y. & Lamprecht, A. (2007) Oil-in-oil microencapsulation technique with an external perfluorohexane phase. *International Journal of Pharmaceutics,* 338**,** 231-237.

Marley, E. C., Mackay, E. & Young, G. (2009) Characterisation of vitamin B12 immunoaffinity columns and method development for determination of vitamin B12 in a range of foods, juices and pharmaceutical products using immunoaffinity clean-up and high performance liquid chromatography with UV detection. *Food Additives and Contaminants,* 26**,** 282-288.

Matijevic, E. (1993) Preparation and properties of uniform size colloids. *Chemistry of Materials,* 5**,** 412-426.

Matsusaki, M. & Akashi, M. (2009) Functional multilayered capsules for targeting and local drug delivery. *Expert Opinion on Drug Delivery,* 6**,** 1207-1217.

Meesters, G. M. H., Vercoulen, P. H. W., Marijnissen, J. C. M. & Scarlett, B. (1992) Generation of micron-sized droplets from the Taylor cone. *Journal of Aerosol Science,* 23**,** 37-49.

Mei, F. & Chen, D.-R. (2007) Investigation of compound jet electrospray: Particle encapsulation. *Physics of Fluids,* 19**,** 103303-103310.

Minami, H., Kobayashi, H. & Okubo, M. (2005) Preparation of hollow polymer particles with a sngle hole in the shell by SaPSeP. *Langmuir,* 21**,** 5655-5658.

Moon, G. D. & Jeong, U. (2008) Decoration of the interior surface of hollow spherical silica colloids with Pt nanoparticles. *Chemistry of Materials,* 20**,** 3003-3007.

Mora, J. F. D. L. & Loscertales, I. (1994) The current emitted by highly conduction Taylor cones. *Journal of Fluid Mechanics,* 260**,** 155.

Mutoh, M., Kaieda, S. & Kamimura, K. (1979) Comvergence and disintegration of liquid jets induced by an electrostatic field. *Journal of Applied Physics,* 50**,** 3174-3179.

Nagorynti, V. S. & Bezrukov, V. I. (1980) Droplet emission in an electrostatic field. *Magn Gidrodin USSR,* 16**,** 111.

Nangrejo, M., Ahmad, Z., Stride, E., Edirisinghe, M. & Colombo, P. (2008) Preparation of polymeric and ceramic porous capsules by a novel electrohydrodynamic process. *Pharmaceutical Development and Technology,* 13**,** 425-432.

Narisawa, M., Kado, H., Mabuchi, H. & Kim, Y.-W. (2010) Accelerated ceramization of polymethylsilsesquioxane by aluminum- based filler reductant. *Applied Organometallic Chemistry,* 24**,** 612 - 617.

Nelson, A. (2008) Stimuli-responsive polymers: Engineering interactions. *Nature Materials,* 7**,** 523 - 525.

Nishiyam, N. & Kataoka, K. (2006) Current state, achievements, and future prospects of polymeric micelles as nanocarriers for drug and gene delivery. *Pharmacology & Therapeutics,* 112**,** 630-648.

Okubo, M., Konishi, Y. & Minami, H. (1998) Production of hollow polymer particles by suspension polymerization. *Colloid & Polymer Science,* 276**,** 638-642.

Pancholi, K., Stride, E. & Edirisinghe, M. (2009) In vitro method to characterize diffusion of dye from polymeric particles: a model for drug release. *Langmuir,* 25**,** 10007-10013.

Pareta, R. & Edirisinghe, M. J. (2006) A novel method for the preparation of biodegradable microspheres for protein drug delivery. *Journal of the Royal Society Interface,* 3**,** 573-582.

Peng, X. & Zhang, L. (2005) Surface fabrication of hollow microspheres from N-methylated chitosan coss-linked with gultaraldehyde. *American Chemical Society Journals,* 21**,** 1091-1095.

Peppas, N. A. (1985) Analysis of Fickian and non-Fickian drug release from polymers. *Pharmaceutica acta Helvetiae,* 60**,** 110-111.

Phang, J. S., Marsh, W. A., Barlows, T. G. & Schwartz, H. I. (2004) Determining feeding tube location by gastric and intestinal pH values. *Nutrition in Clinical Practice,* 19**,** 640-644.

Pillai, O. & Panchagnula, R. (2001) Polymers in drug delivery. *Current Opinion in Chemical Biology,* 5**,** 447-451.

Pisani, E., Tsapis, N., Paris, J., Nicolas, V., Cattel, L. & Fattal., E. (2006) Polymeric nano/microcapsules of liquid perfluorocarbons for ultrasonic imaging: Physical characterization. *Langmuir,* 22**,** 4397-4402.

Prestwich, G. D. & Luo, Y. (2001) Novel biomaterials for drug delivery. *Expert Opinion on Therapeutic Patents,* 11**,** 1395-1410.

Prevot, M., Déjugnat, C., Möhwald, H. & Sukhorukov, G. (2006) Behavior of Temperature-Sensitive PNIPAM Confined in Polyelectrolyte Capsules. *ChemPhysChem,* 7**,** 2497-2502.

Putnam, D. (2008) Drug delivery: The heart of the matter. *Nature Materials,* 7**,** 836 -

837.

Qiu, X., Leporatti, S., Donath, E. & Mhwald, H. (2001) Studies on the drug release properties of polysaccharide multilayers encapsulated ibuprofen microparticles. *Langmuir,* 17**,** 5375-5380.

Qiu, Y. & Park, K. (2001) Environment-sensitive hydrogels for drug delivery. *Advanced Drug Delivery Reviews,* 53**,** 321-339.

Rachik, M., Barthes-Biesel, D., Carin, M. & Edwards-Levy, F. (2006) Identification of the elastic properties of an artificial capsule membrane with the compression test: Effect of thickness. *Journal of Colloid and Interface Science,* 301**,** 217-226.

Raghunath, J., Zhang, H., Edirisinghe, M. J., Darbyshire, A., Butler, P. E. & Seifalian, A. M. (2009) A new biodegradable nanocomposite based on polyhedral oligomeric silsesquioxane nanocages: cytocompatibility and investigation into electrohydrodynamic jet fabrication techniques for tissue-engineered scaffolds. *Biotechnology and Applied Biochemistry,* 52**,** 1-8.

Ranade, V. V. & Hollinge, M. A. (1996) Drug delivery systems. *Boca Raton: CRC Press*.

Rathbone, M. J., Cardinal, J. R. & Ogle, C. R. (2000) Mechanisms of drug release from veterinary drug delivery systems, in controlled release veterinary drug delivery: Biological and pharmaceutical considerations, M.J. 246 Rathbone and R. Gurny, Editors. 1st ed. *Elsevier Science: Amsterdam***,** 17-50.

Rayleigh, L. (1878) On the instability of jets. *The Proceedings of the London Mathematical Society,* 10**,** 4-13.

Rayleigh, L. (1879) On the capillary phenomena in jets. *The Proceedings of the Royal Society,* 29**,** 71-97.

Riess, J. (2002) Blood substitutes and other potential biomedical applications of fluorinated colloids. *Journal of Fluorine Chemistry,* 114**,** 119-126.

Riess, J. & Kra, M. (1998) Fluorinated materials for in vivo oxygen transport (blood substitutes), diagnosis and drug delivery. *Biomaterials,* 19**,** 1529-39.

Riess, J. G. (2001) Oxygen carriers (blood substitutes) raison d'Etre, chemistry, and some physiology blut ist ein ganz besondrer saft. *Chemical Reviews,* 101**,** 2797-2919.

Rulison, A. J. & Flagan, R. C. (1994) Electrospray atomization of electrolytic solution. *Journal of Colloid and Interface Science,* 167**,** 135-145.

Rzaev, Z. M. O., Dinçera, S. & Pişkina, E. (2007) Functional copolymers of N-isopropylacrylamide for bioengineering applications. *Progress in Polymer Science,* 32**,** 534-595.

Schroeder, A., Avnir, Y., Weisman, S., Najajreh, Y., Gabizon, A., Talmon, Y., Kost, J. & Barenholz, Y. (2007) Controlling liposomal drug release with low frequency ultrasound: Mechanism and feasibility. *Langmuir,* 23**,** 4019-4025.

Seki, H., Kajiwara, T., Abe, Y. & Gunji, T. (2010) Synthesis and structure of ladder

polymethylsilsesquioxanes from sila-functionalized cyclotetrasiloxanes. *Journal of Organometallic Chemistry,* 650**,** 1363-1369.

Serizawa, T., Kamimura, S., Kawanishi, N. & Akashi, M. (2002) Layer-by-layer assembly of poly(vinyl alcohol) and hydrophobic polymers based on their physical adsorption on surfaces. *Langmuir,* 18**,** 8381-8385.

Shchukin, D. G., Gorin, D. A. & Möhwald, H. (2006) Ultrasonically induced opening of polyelectrolyte microcontainers. *Langmuir,* 22**,** 7400-7404.

Shchukin, D. G., Sukhorukov, G. B. & Hwald, M. H. (2003) Smart inorganic/organic nanocomposite hollow microcapsules. *Angewandte Chemie International Edition,* 115**,** 4610-4613.

Shenoy, D., Little, S., Langer, R. & Amiji, M. (2005) Poly(ethylene oxide)-modified poly(β-amino ester) nanoparticles as a pH-sensitive system for tumor-targeted delivery of hydrophobic drugs: Part 2. in vivo distribution and tumor localization studies. *Pharmaceutical Research,* 22**,** 2107-2114.

Shiga, T. (1997) Deformation and viscoelastic behavior of polymer gels in electric fields. *Advances in Polymer Science,* 134**,** 131-163.

Sill, T. J. & Recum, H. A. V. (2008) Electrospinning: Applications in drug delivery and tissue engineering. *Biomaterials,* 29**,** 1989-2006.

Singer, A., Homan, C., Church, A. & Mcclain, S. (1998) Low-frequency sonophoresis:

Pathologic and thermal effects in dogs. *Academic Emergency Medicine,* 5**,** 35-40.

Sivakumar, S., Bansal, V., Cortez, C., Chong, S.-F., Zelikin, A. N. & Caruso, F. (2009) Degradable, surfactant-free, monodisperse polymer-encapsulated emulsions as anticancer drug carriers. *Advanced Materials,* 21**,** 1820 - 1824.

Skirtach, A. G., Geest, B. G. D., Mamedov, A., Antipov, A. A., Kotove, N. A. & Sukhorukov, G. B. (2007) Ultrasound stimulated release and catalysis using polyelectrolyte multilayer capsules. *Journal of Materials Chemistry* 17**,** 1050-1054.

Smet, M. D., Heijman, E., Langeris, S., Hijnen, N. M. & Grull, H. (2011) Magnetic resonance imaging of high intensity focused ultrasound mediated drug delivery from temperature-sensitive liposomes: An in vivo proof-of-concept study. *Journal of Controlled Release,* 150**,** 102-110.

Smith, D. P. H. (1986) The electrohydrodynamic atomization of liquids. *IEEE Industry Applications Society,* IA-22**,** 527-535.

Song, L., Ge, X., Wang, M., Zhang, Z. & Li, S. (2006) Anionic/Nonionic Mixed Surfactants Templates Preparation of Hollow Polymer Spheres via Emulsion Polymerization. *Journal of Polymer Science Part A: Polymer Chemistry,* 44**,** 2533-2541.

Spieth, P., Knels, L., Kasper, M., Quelhas, A. D., Lupp, A. B., Hübler, M., Neto, A. G., Koch, T. & Abreu, M. G. D. (2007) Effects of vaporized perfluorohexane and partial liquid ventilation on regional distribution of alveolar damage in experimental lung injury. *Intensive Care Medicine,* 33**,** 308-314.

Still, T., Sainidou, R., Retsch, M., U.Jonas, Spahn, P., Hellmann, G. P. & Fytas, G. (2008) The "music" of core-shell spheres and hollow capsules: influence of the architecture on the mechanical properties at the nanoscale. *Nano Letters,* 8**,** 3194-3199.

Stockton, W. B. & Rubner, M. F. (1997) Molecular-level processing of conjugated polymers. 4. Layer-by-layer manipulation of polyaniline via hydrogen-bonding interactions. *Macromolecules,* 30**,** 2717-2725.

Stuart, M. A. C., Huck, W. T. S., Genzer, J., Müller, M., Ober, C., Stamm, M., Sukhorukov, G. B., Szleifer, I., Tsukruk, V. V., Urban, M., Winnik, F., Zauscher, S., Luzinov, I. & Minko, S. (2010) Emerging applications of stimuli-responsive polymer materials. *Nature Materials,* 9**,** 101-113.

Sun, Y., Mayers, B. T. & Xia, Y. (2002) Template-engaged replacement reaction: A one-step approach to the large-scale synthesis of metal nanostructures with hollow interiors. *Nano Letters,* 2**,** 481-485.

Sun, Z., Zussman, E., Yarin, A. L., Wendorff, J. H. & Greiner, A. (2003) Compound core-shell polymer nanofibers by co-electrospinning. *Advanced materials,* 15**,** 1929.

Suzuki, A. & Tanaka, T. (1990) Phase transition in polymer gels induced by visible light. *Nature,* 346**,** 345-347.

Tang, L. & Eaton, J. W. (1995) Inflammatory responses to biomaterials. *American Journal of Clinical Pathology,* 103**,** 466-471.

Taylor, S. (1964) Disintegration of water drops in an electric field. *Mathematical and Physical Sciences*, 383-397.

Toussirot, E., Michel, F. & Wendling, D. (2001) Bone density ultrasound measurements and body composition in early ankylosing spondylitis. *Rheumatology,* 4, 882-888.

Uhrich, K. E., Cannizzaro, S. M., Langer, R. S. & Shakesheff, K. M. (1999) Polymeric systems for controlled drug release. *Chemical Reviews,* 99, 3181-3198.

Ung, T., Liz-Marzán, L. M. & Mulvaney, P. (1998) Controlled method for silica coating of silver colloids: Influence of coating on the rate of chemical reactions. *Langmuir,* 14, 3740-3748.

Vallet-Regi, M., Ra´Mila, A., Real, R. P. D. & Pe´Rez-Pariente, J. (2001) A new property of MCM-41: Drug delivery system. *Chemistry of Materials,* 13, 308-311.

Varde, N. K. & Pack, D. W. (2004) Microspheres for controlled release drug delivery. *Expert Opinion on Biological Therapy,* 4, 35-51.

Vasir, J. K., Tambwekar, K. & Garg, S. (2003) Bioadhesive microspheres as a controlled drug delivery system. *International Journal of Pharmaceutics,* 255, 13-32.

Volodkin, D. V., Larionova, N. I. & Sukhorukov, G. B. (2004) Protein encapsulation via porous $CaCO_3$ microparticles templating. *Biomacromolecules,* 5, 1962-1972.

Wang, A.-J., Lu, Y.-P. & Sun, R.-X. (2007) Recent progress on the fabrication of hollow microspheres. *Materials Science and Engineering: A,* 460-461, 1-6.

Wang, X., Drew, C., Lee, S.-H., Senecal, K. J., Kumar, J. & Samuelson, L. A. (2002) Electrospun nanofibrous membranes for highly sensitive optical sensors. *Nano Letters,* 2**,** 1273-1275.

Wang, Z. J., Qian, L., Wang, X. L., Yang, F. & Yang, X. R. (2008) Construction of hollow DNA/PLL microcapsule as a dual carrier for controlled delivery of DNA and drug. *Colloids and Surfaces A: Physicochemical and Engineering Aspects,* 326**,** 29-36.

Weber, C. (1931) On the breakdown of a fluid jet. *Journal of Mechanics and Applied Mathematics,* 11**,** 136-159.

Wei, B., Wang, S., Song, H., Liu, H., Li, J. & Liu, N. (2006) A review of recent progress in preparation of hollow polymer microspheres. *Petroleum Science,* 6**,** 306-312.

Wilcox, D. L., Berg, M., Bernat, T., Kellerman, D. & Cochran, J. K. (1995) Hollow and solid spheres and microspheres: science and technology associated with their fabrication and application. *Materials Research Society Proceedings, Pittsburgh, PA.***,** 372.

Wilhelm, O., Mädler, L. & Pratsinis, S. E. (2003) Electrospray evaporation and deposition. *Journal of Aerosol Science,* 34**,** 815-836.

Wu, Y., Yu, B., Jackson, A., Zha, W., Lee, L. J. & Wyslouzil, B. E. (2009) Coaxial electrohydrodynamic spraying: a novel one-step technique to prepare oligodeoxynucleotide encapsulated lipoplex nanoparticles. *Molecular Pharmaceutics,* 6**,** 1371-1379.

Xiao, D. S., Yuan, Y. C., Rong, M. Z. & Zhang, M. Q. (2009) Hollow polymeric microcapsules: preparation, characterization and application in holding boron trifluoride diethyl etherate. *Polymer,* 50**,** 560-568.

Xie, J., M.Marijnissen, J. C. & Wang, C.-H. (2006) Microparticles developed by electrohydrodynamic atomization for the local delivery of anticancer drug to treat C6 glioma in vitro. *Biomaterials,* 27**,** 3321-3332.

Xie, J. N., W. J.; Lee, L. Y.; Wang, C.-H (2008) Encapsulation of protein drugs in biodegradable microparticles by co-axial electrospray. *Journal of Colloid and Interface Science,* 317**,** 469-476.

Yang, J., Lee, J., Kang, J., Oh, S. J., Ko, H.-J., Son, J.-H., Lee, K., Suh, J.-S., Huh, Y.-M. & Haam, S. (2009) Smart drug-loaded polymer gold nanoshells for systemic and localized therapy of human epithelial cancer. *Advanced Materials,* 21**,** 4339-4342.

Ye, C., Chen, A., Colombo, P. & Martinez, C. (2010) Ceramic microparticles and capsules via microfluidic processing of a preceramic polymer. *Journal of the Royal Society Interface,* 7**,** S461-S473.

Yin, W. & Yates, M. Z. (2008) Effect of interfacial free energy on the formation of polymer microcapsules by emulsification/freeze-drying. *Langmuir,* 24**,** 701-708.

Young, T.-H. & Chen, L.-W. (1995) Pore formation mechanism of membranes from phase inversion proces. *Desalination,* 103**,** 233-247.

Yow, H. N. & Routh, A. F. (2008) Colloidal buckets formed via internal phase separation. *Soft Matter,* 4**,** 2080-2085.

Zawaneh, P. N., Doody, A. M., Zelikin, A. N. & Putnam, D. (2006) Diblock copolymers based on dihydroxyacetone and ethylene glycol: synthesis, characterization, and nanoparticle formulation. *Biomacromolecules,* 7**,** 3245-3251.

Zeleny, J. (1914) The electrical discharge from liquid points, and a hydrostatic method of measuring the electric intensity at their surfaces. *Physical Review,* 3**,** 69-91.

Zeleny, J. (1915) On the conditions of instability of electrified drops with applications to the electrical discharge from liquid points. *The Proceedings of the Cambridge Philosophy Society,* 18**,** 71-83.

Zelikin, A. N., Li, Q. & Caruso, F. (2006) Degradable Polyelectrolyte Capsules Filled with Oligonucleotide Sequences. *Angewandte Chemie International Edition,* 45**,** 7743-7745.

Zhang, L., Peng, H., Sui, J., Soeller, C., Kilmartin, P. A. & Travas-Sejdic, J. (2009) Self-assembly of poly(o-methoxyaniline) hollow microspheres. *Journal of Physical Chemistry C,* 113**,** 9128-9134.

Zhao, W., Chen, H. & Yongsheng Li, L. L., Meidong Lang, and Jianlin Shi (2008) Uniform rattle-type hollow magnetic mesoporous spheres as drug delivery carriers and their sustained-release property. *Advanced Functional Materials,* 18**,** 2780-2788.

Zhu, Y.-F., Shi, J.-L., Li, Y.-S., Chen, H.-R., Shen, W.-H. & Dong, X.-P. (2005) Hollow mesoporous spheres with cubic pore network as a potential carrier for drug storage and its in vitro release kinetics. *Journal of Material Research,* 20**,** 54-61.

Zhu, Y., Ikoma, T., Hanagata, N. & Kaskel, S. (2009) Rattle-Type Fe3O4@SiO2 hollow mesoporous spheres as carriers for drug delivery. *Small,* 6**,** 471 - 478.

Zhuo, R., Colombo, P., Pantano, C. & Vogler, E. A. (2005) Silicon oxycarbide glasses for blood-contact applications. *Acta Biomaterialia,* 1**,** 583-589.

Zong, X., Ran, S., Kim, K.-S., Fang, D., Hsiao, B. S. & Chu, B. (2003) Structure and morphology changes during in vitro degradation of electrospun poly(glycolide-co-lactide) nanofiber membrane. *Biomacromolecules,* 4**,** 416-423.